Novel Insights into Lipoprotein and Hepatitis C Virus Particles Biogenesis and its Dependency on the Lipid Droplet Protein Perilipin 2

Dissertation

Submitted to the

Department of Chemistry

Faculty of Mathematics, Informatics and Natural Science

University of Hamburg

In fulfillment of the requirements

for the degree of

Doctor of Natural Sciences (Dr. rer. nat.)

by

Susan Lassen

Hamburg, 2017

Contents

Publications, awards and presentations

Publications

Parts of the dissertation are in the manuscript

Perilipin-2 Stimulates Hepatitis C Virus Particle Production by Enhancing Assembly and Stabilizing Apolipoprotein E
Susan Lassen, Cordula Grüttner, Van Nguyen-Dinh, and Eva Herker
in preparation

Awards

2014	Mobility Grant, Heinrich Pette Institute, Hamburg
	Visiting researcher at Mount Sinai School of Medicine, New York
2017	Travel Award
	4th International Symposium on Protein Trafficking in Health and Disease, Hamburg

Presentations

The author presented parts of the dissertation at the following conferences

July 2017	Susan Lassen, Cordula Grüttner, and Eva Herker
	Perilipin-2 Regulates Lipid Droplet Morphology and HCV Replication
	Young Scientist Symposium, Marburg, Germany (oral presentation)
June 2017	Susan Lassen, Cordula Grüttner, and Eva Herker
	Perilipin-2 Regulates Lipid Droplet Morphology and HCV Replication
	4th International Symposium on Protein Trafficking in Health and Disease, Hamburg, Germany (oral and poster)
March 2017	Susan Lassen, Cordula Grüttner, and Eva Herker
	Perilipin-2 Regulates Lipid Droplet Turnover and HCV Replication
	27th Annual Meeting of the Society of Virology, Marburg, Germany (poster)
November 2016	Susan Lassen, Cordula Grüttner, and Eva Herker
	Perilipin-2 Regulates Lipid Droplet Turnover and HCV Replication
	15 th Workshop 'Cell Biology of Viral Infections', Kloster Schöntal, Germany (oral presentation)
November 2016	Susan Lassen, Cordula Grüttner, and Eva Herker
	Imaging of HCV-Infected Cells
	Joint Scientific Retreat, Heinrich Pette Institute, Hamburg, Germany (oral presentation)
October 2016	Susan Lassen, Cordula Grüttner, and Eva Herker
	Perilipin-2 Regulates Lipid Droplet Turnover and HCV Replication
	6th European Congress of Virology, Hamburg, Germany (poster)
March 2016	Susan Lassen, Cordula Grüttner, and Eva Herker
	Perilipin-2 Regulates Lipid Droplet Morphology and HCV Replication
	26th Annual Meeting of the Society of Virology, Münster, Germany (poster)
September 2015	Susan Lassen, Cordula Grüttner, and Eva Herker
	ADRP Regulates Lipid Droplet Morphology and Has a Pivotal Role in the Hepatitis C Life Cycle
	Joint Scientific Retreat, Heinrich Pette Institute, Hamburg, Germany (poster presentation)
October 2014	Susan Lassen, J.V. Perez-Giron, C. Munoz-Fontela and Eva Herker
	Development of a Therapeutic Vaccine Strain Against Hepatitis C
	Joint Scientific Retreat, Heinrich Pette Institute, Hamburg, Germany (poster presentation)

Abbreviations

°C	degree Celsius
μF	microfarad
μg	microgram
μl	microliter
μm	micromolar
3D	three dimensional
aa	amino acids
ACAT	acyl-cholesterol-acyltransferases
ADRP	adipose differentiation related protein
AGPAT	1-acylglycerol-3-phosphate-O-acyltransferase
ALT	alanine aminotransferase
Apo	apolipoprotein
ARF4	ADP-ribosylation factor 4
ASM	acid soluble metabolites
Atg	autophagy gene
ATGL	adipose triglyceride lipase
ATP	adenosine triphosphate
BSA	bovine serum albumin
Bsd	blasticidin S deaminase
BSL	biosafety level
C14orf166	UPF0586 protein C14orf166
CCT	CTP:phosphocholine cytidylyltransferase
CD81	cluster of differentiation 81
CGI-58	comparative gene identification 58
cLD	cytosolic lipid droplets
CLDN1	claudin-1
CO_2	carbon dioxide
CoA	coenzyme A
Con1 SGR	Con1 subgenomic replicon
cPLA2	cytosolic phospholipase A2
CPM	counts per minute
CPT	carnitine palmitoyltransferase
d	day
D	domain
DAA	direct acting antivirals
DC-SIGN	dendritic cell-specific intercellular adhesion molecule 3-grabbing non-integrin
DGAT	diglyceride acyltransferases
DMSO	dimethyl sulfoxide
DNA	deoxyribonucleic acid
DTT	1,4-dithiothreitol
EGFP	enhanced green fluorescent protein
EGFR	epidermal growth factor receptor

ER	endoplasmic reticulum
ESCRT	endosomal-sorting complex required for transport
FC	flow cytometry
FCS	fetal calf serum
FFA	free fatty acid
FFU	focus forming untis
FIT2	fat storage-inducing transmembrane 2 protein
Fluc	Firefly luciferase
FSP27	fat specific protein of 27 kDa
fw	forward
g	gram
GAG	glucosaminoglycan
GAPDH	glyceraldehyde 3-phosphate dehydrogenase
gt	goat
gp	guinea pig
h	hour
HCC	hepatocellular carcinoma
HCV	hepatitic C virus
HDL	high-density lipoprotein
HIV1	human immunodeficiency virus 1
HMM	high molecular mass
HRP	horseradish peroxidase
HSL	hormone-sensitive lipase
HSPG	heparan sulphate proteoglycans
IF	immunofluorescence
IP	immunoprecipitation
IRES	internal ribosomal entry site
JFH1	Japanese Fulminant Hepatitis 1
kb	kilobase pair
kDa	kilodalton
l	liter
LB	Luria-Bertani
LC3	light chain protein 3
LD	lipid droplet
LDL	low-density lipoprotein
LDLR	low-density lipoprotein receptor
LMM	low molecular mass
LPA	lyso-phosphatidic acid
LVP	lipoviroparticle
M	mol/l
MAG	monoglyceride
MCC	Manders' colocalization coefficient
MCS	multiple cloning site
mg	milligram
min	minutes
ml	milliliter
mm	millimetre
mM	millimolar
MMV	multi-membrane vesicle
MnSOD	manganese-dependent superoxide dismutase
MOI	mulplicity of infection

mRNA	messanger ribonucleic acid
ms	mouse
MS	mass spectometry
MTP	microsomal triglyceride transport protein
MTTP	microsomal transfer protein
MW	membranous web
NCR	non-coding regions
NLS	nuclear localization sequence
nm	nanometer
NPC1L1	Niemann-Pick C1 like1
NS	non-structural
nt	nucleotides
o/n	over night
OA	oleic acid
OCLN	occludin
ORF	open reading frame
OXPAT	oxidative tissue–enriched PAT protein
PA	phosphatidic acid
PBS	phosphate-buffered saline
PCR	polymerase chain reaction
PE	phosphatidylethanolamine
PEG	polythylene glycol
PEG-IFNα	pegylated interferon-alpha
PFA	paraformaldehyde
PIC	protease inhibitor cocktail
PLIN	perilipin
pmol	picomol
PMSF	phenylmethysulfonyl fluoride
PPAR	peroxisome proliferator–activated receptor
RAB32	Ras-related protein RAB-32
rb	rabbit
RC	replication complexes
RdRp	RNA-dependent RNA polymerase
rev	reverse
RFP	red fluorescence protein
RIG-I	retinoic acid inducible gene I
RLU	relative light units
RNA	ribonucleic acid
rpm	revolutions per minute
rRNA	ribosomal ribonucleic acid
RT	room temperature
qRT-PCR	quantitiative real-time polymerase chain reaction
SDS	sodium dodecyl sulfate
SDS-PAGE	sodium dodecyl sulfate polyacrylamide gel electrophoresis
SEM	standard error of the mean
shRNA	small hairpin ribonucleic acid
SCARB1	scavenger receptor B1
SVR	sustained virological response
TCID$_{50}$	50% tissue culture infective dose
TEM	transmission electron microscopy

TfR1   transferrin receptor 1
TG   triglyceride
TIP47   tail-interacting protein 47
UTR   untranslated region
v/v   volume/volume
VLDL   very low–density lipoprotein
w/v   weight/volume
WB   western blotting
x g times gravity

Abstract

Hepatitis C virus (HCV) replication depends on the host cell lipid metabolism with lipid droplets serving as putative viral assembly sites. Lipid droplets are cytosolic organelles consisting of a core of neutral lipids such as triglycerides and cholesterol esters, surrounded by an amphipathic phospholipid monolayer and associated proteins. Perilipin-2 (PLIN2) belongs to the perilipin family of lipid droplet–binding proteins and is the major coat protein of lipid droplets in hepatocytes.

In this thesis, the function of PLIN2 on lipid droplet biology and its role in the HCV viral life cycle was investigated. Therefore, shRNA-mediated knockdown experiments were performed to elucidate the molecular function of PLIN2. Silencing of PLIN2 expression had no effect on HCV RNA replication but, in line with the role of lipid droplets in HCV particle assembly, affected the production of infectious viral particles. The reduction in virion production was not caused by a general defect in lipid droplet homeostasis, as the lipid droplet content of the cells and the triglyceride turnover were not affected by PLIN2 knockdown. This was likely due to compensatory functions of PLIN3 that localized to lipid droplets in the absence of PLIN2. However, cells lacking PLIN2 had slightly larger lipid droplets with enhanced lipid droplet–associated lipase activity and displayed a higher β-oxidation capacity, indicating differences in the fatty acid flux. The enhanced lipolysis rate was in line with a recruitment of the adipose triglyceride lipase (ATGL) complex to lipid droplets of PLIN2-knockdown cells. Lipid droplets isolated from HCV-infected PLIN2-knockdown cells displayed a defect in the recruitment of the capsid protein core to lipid droplets, an important step in the HCV assembly process. In line, slightly less high molecular mass core complexes were found in lipid droplet fractions isolated from PLIN2-depleted cells. More strikingly, cells with diminished PLIN2 levels showed reduced protein expression and secretion of apolipoprotein E (ApoE) due to destabilization of the protein. However, the physical properties and functionality of the remaining ApoE protein seemed to be preserved, as the buoyant density, the interaction with NS5A, as well as the subcellular localization of ApoE was unaffected. The reduced availability of ApoE for virion morphogenesis explains the HCV phenotype. This phenotype cannot be compensated by PLIN3. Thus, PLIN2 is as a major host factor involved in egress of host lipoproteins and functional HCV particles.

Zusammenfassung

Die Hepatitis C Virus Replikation ist eng mit dem Lipidmetabolismus der Wirtszellen verknüpft, wobei *Lipid Droplets* als Assemblierungsplattform für die Bildung neuer Viruspartikel dienen. *Lipid Droplets* sind zytosolische Zellorganellen bestehend aus einem Kern aus Neutrallipiden wie Triglyceriden und Cholesterolestern, der von einer amphipathischen einfachen Phospholipidschicht und assoziierten Proteinen umschlossen ist. Perilipin-2 (PLIN2) gehört zu der Perilipin Proteinfamilie der *Lipid Droplet* Bindeproteine und ist das Hauptprotein an *Lipid Droplets* in Hepatozyten.

In dieser Arbeit wurde die Rolle von PLIN2 in der *Lipid Droplet* Biologie und im viralen Lebenszyklus von HCV untersucht. Hierfür wurden shRNA-vermittelte *Knockdown* Experimente durchgeführt, um die Funktion von PLIN2 aufzuklären. Die Herunterregulierung von PLIN2 zeigte keinen Einfluss auf HCV RNA Replikation. Passend zur Rolle der *Lipid Droplets* als Assemblierungsplattform zeigten PLIN2-*knockdown* Zellen jedoch eine Reduktion in der Viruspartikel-Produktion. Dieser Phänotyp basierte aber nicht auf einem generellen Defekt in der *Lipid Droplet* Homöostase, da weder das totale *Lipid Droplet* Volumen noch der Auf- oder Abbau der Triglyceride durch den PLIN2-*knockdown* verändert wurden. Diese Beobachtung ist wahrscheinlich durch eine Kompensation mit PLIN3 zu erklären, das in PLIN2-*knockdown* Zellen zu *Lipid Droplets* lokalisiert. Zellen mit veringerter PLIN2 Protein Expression hatten geringfügig größere *Lipid Droplets*, einhergehend mit einer erhöhten *Lipid Droplet*-assoziierten Lipase Aktivität. Zudem war eine erhöhte β-Oxidationskapazität zu beobachten, was auf einen veränderten Lipidfluss hindeutet. Die erhöhte Lipolyse war einhergehend mit einer Rekrutierung des Adipose-Triglyceride-Lipase (ATGL) Komplex zu *Lipid Droplets* in PLIN2-*knockdown* Zellen. HCV-infizierte PLIN2-*knockdown* Zellen zeigten zudem einen Defekt in der Rekrutierung des Kapsidproteins Core zu den *Lipid Droplets* und in der Bildung von Core-Komplexe mit hoher molekularer Masse in *Lipid Droplet*-Fraktionen. Der größere Phänotyp der PLIN2-*knockdown* Zellen ist die Destabilisierung des Apolipoprotein E (ApoE). Die Zellen weisen eine deutlich verringerte Menge an intra- und extrazellulärem ApoE auf. Die biophysikalischen Eigenschaften und die Funktionalität des verbliebenen ApoE Proteins blieben jedoch unverändert, da weder die Dichte noch die Interaktion mit dem HCV Protein NS5A oder die subzelluläre Lokalisierung von ApoE verändert waren. Die reduzierte Menge an ApoE erklärt den HCV-Phänotyp, da ApoE ein wichtiger Wirtsfaktor für die Virusmorphogenese ist. Dieser Phänotyp kann nicht durch PLIN3 kompensiert werden. Daher ist PLIN2 ein wichtiger Wirtsfaktor für die Biogenese von Lipoproteinen und funktionaler HCV Partikel.

1. Introduction

1.1. Hepatitis C Virus (HCV)

The Hepatitis C virus is a blood borne virus that affects the liver, leading to acute or chronic hepatitis. Worldwide, 110 million people are HCV-antibody positive with 80 million having a chronic viraemic infection. Around 40.000 people die each year due to liver cirrhosis or hepatocellular carcinoma caused by the virus (Gower et al., 2014; WHO, 2017). Transmission occurs mainly via contaminated blood products or by sharing contaminated drug injection needles. Vertical transmission from the HCV positive mother to the unborn child as a route of transmission varies from 5–10% depending on the co-infection of the mother with other viruses such as the human immunodeficiency virus (HIV) (Benova et al., 2014). There are reported cases of sexual transmission, but this route is infrequent and inefficient (Terrault et al., 2013). HCV spreading cannot occur via breast feeding or e.g. by casual skin contacts with an infected patient.

1.2. HCV infection and progression

HCV has a high species tropism only infecting the human or chimpanzee hepatocyte. The acute infection time is around 4–20 weeks, is often asymptomatic and most of the patients are unaware of an infection. In about one third of the newly infected patients, mild symptoms such a nausea and fatigue occur. HCV RNA is detectable to high titers shortly after infection (1–2 weeks) and after several weeks, the serum alanine aminotransferase (ALT), a marker for hepatic damage, increases up to 10-fold before it decreases to normal level and all clinical symptoms disappear (Hoofnagle, 1997). In the first six month of infection around 25% of individuals spontaneously clear the virus (Micallef et al., 2006). This is often accompanied with a strong immune response. The majority of the infected individuals develop a chronic infection, which leads to liver cirrhosis after 20–30 years in about 20% of the cases. Around 5% of these patients develop hepatocellular carcinoma or end stage liver diseases (ESLD) (Seeff, 2009). A chronic infection with HCV is still one of the leading causes for liver transplantation and re-occurrence of the virus after transplantation is observed in almost every patient (Manns et al., 2006). Thus, a clearance of the virus is essential for recovery.

1.3. HCV treatment

One of the first standard treatments for HCV infection was a combination of PEGylated inter-feron α (PEG-IFN) and ribavirin, yielding to a sustained virological response (SVR) in about 50% of the patients (Palumbo, 2011). Unfortunately, this therapy is associated with a wide variety of severe side effects (Dusheiko, 1997; Russo et al., 2003) and made the development of new therapies essential. Since 2011, new therapies are available which are based on direct acting antivirals (DAAs). They show an increased SVR in up to 90% of the patients (Kohli et al., 2015). So far, four different classes of DAAs are available: NS3/4A inhibitors, nucleoside and nucleotide NS5B polymerase inhibitors, non-nucleoside NS5B inhibitors and NS5A inhibitors. All of them impede HCV RNA replication or interfere with the post-translational processing of the RNA (Vermehren et al., 2011). NS5A inhibitors additionally block viral assembly, decreasing viral titers several logs within hours after administration (Guedj et al., 2013). The treatment with DAAs is safer compared to the IFN-based therapy as they have less side effects and the administration time can be reduced from 72 weeks down to 12–24 weeks. Another advantage is the single oral dose per day compared to multiple pills in combination with weekly injections (Kohli et al., 2015; Farnik et al., 2010; Bidell et al., 2016). However, the treatment is extremely cost intensive and the accessibility in high prevalence countries is very low and no vaccine is available.

1.4. HCV prevalence and genotypes

HCV belongs to the flaviviridae family comprising four members. The genus Flavivirus including yellow fever, dengue virus, Zika virus and Japanese encephalitis virus, Pestivirus comprising bovine viral diarrhea- or classical swine fever virus, the newly classified Pegivirus with pegivirus A-K (Smith et al., 2016), and the hepacivirus with Hepatitis C virus as the predominant member next to GBV-B and non-primate hepacivirus (Fernandez-Sanles et al., 2017; Stapleton et al., 2011). HCV was identified in 1989 and its high genetic diversity led to the classification of seven different genotypes (Smith et al., 2014). The different genotypes can vary up to 30–35% in their sequence and within the genotype up to 15%. Genotype 1 is most abundant and accounts for approximately 46.2% of the infections. Genotype 3 is the second most prevalent genotype with approximately 30%. Genotype 2, 4 and 6 are less abundant with 9.1%, 8.3% and 5.4%, respectively. Genotype 5 is even less frequent with only 1% and genotype 7 was isolated from only a few patients in Central America (Messina et al., 2015; Scheel et al., 2013). Figure 1.1 shows the distribution of the different genotypes worldwide.
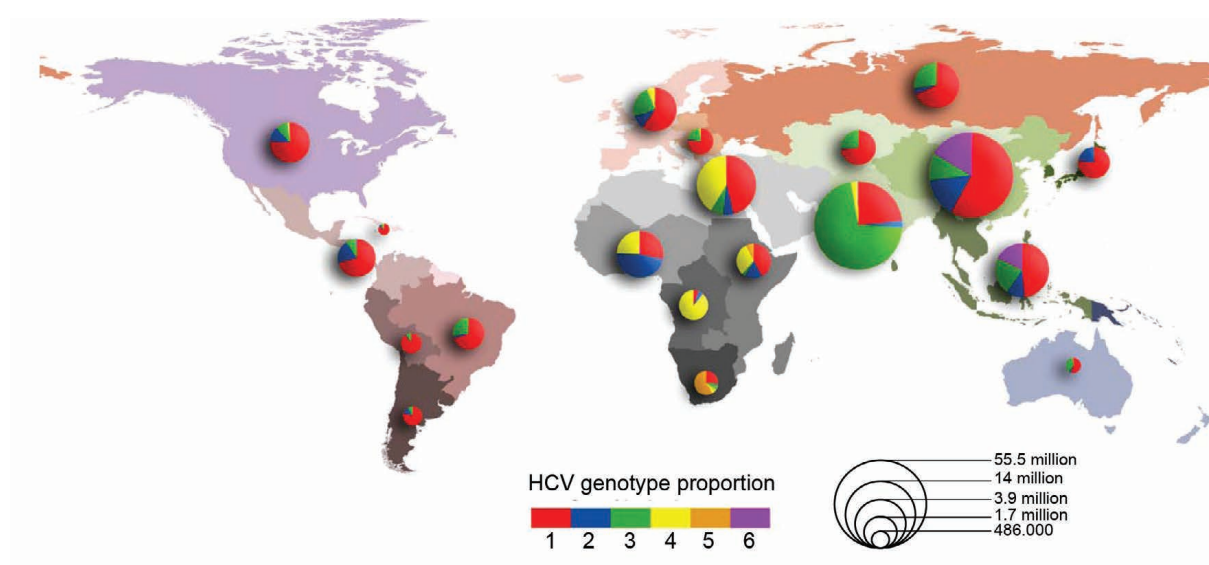
Figure 1.1.: HCV prevalence

The map shows the global distribution and abundance of the six different genotypes. Map is modified from (Messina et al., 2015).

1.5. HCV morphology

HCV is a small enveloped virus with a diameter of approximately 40–75 nm. Electron micro-
scopic analysis revealed a heterogeneous, pleomorphic surface with a dense core presumably
containing the viral RNA (Figure 1.2 a-d) (Catanese et al., 2013; Gastaminza et al., 2010).
The core is surrounded by a lipid bilayer in which the E1 and E2 glycoproteins are embed-
ded. HCV particles have a lower buoyant density (1.03–1.25 g/cm^3) compared to other related
Flaviviruses (1.20–1.23 g/cm^3) but they are found in the same range as serum lipoproteins
(0.95–1.21 g/cm^3) (Catanese et al., 2013; Lindenbach et al., 2013a; Bartenschlager et al.,
2011). This gave the first hint of a connection to lipoproteins (Thomssen et al., 1992). Lipopro-
teins have a core of triglycerides and cholesterol esters and are surrounded by a phospholipid
monolayer. They contain apolipoproteins, which can be exchangeable (like ApoA-I, ApoA-II,
ApoA-IV, ApoC-I-III and ApoE) or non-exchangeable like ApoB-48 and -100. The lipid to pro-
tein ratio determines the buoyant density of the lipoproteins and they are classified into chylomi-
crons, very-low density-, low-density-, or high-density lipoproteins (Ridgway, 2015). A study in
2002 confirmed the association of HCV to lipoproteins, characterizing Hepatitis C virus con-
taining particles of low-and very low densities. These particles are also rich in triglycerides and
this led to the term lipoviroparticle (LVP) (Andre et al., 2002). Later, two models were proposed
explaining the interaction between the LVP and serum lipoproteins: one model suggests a tran-
sient or stable interaction between both (Figure 1.2 f); the other model hypothesizes a hybrid
lipoviroparticle sharing a common membrane (Figure 1.2 g, h).
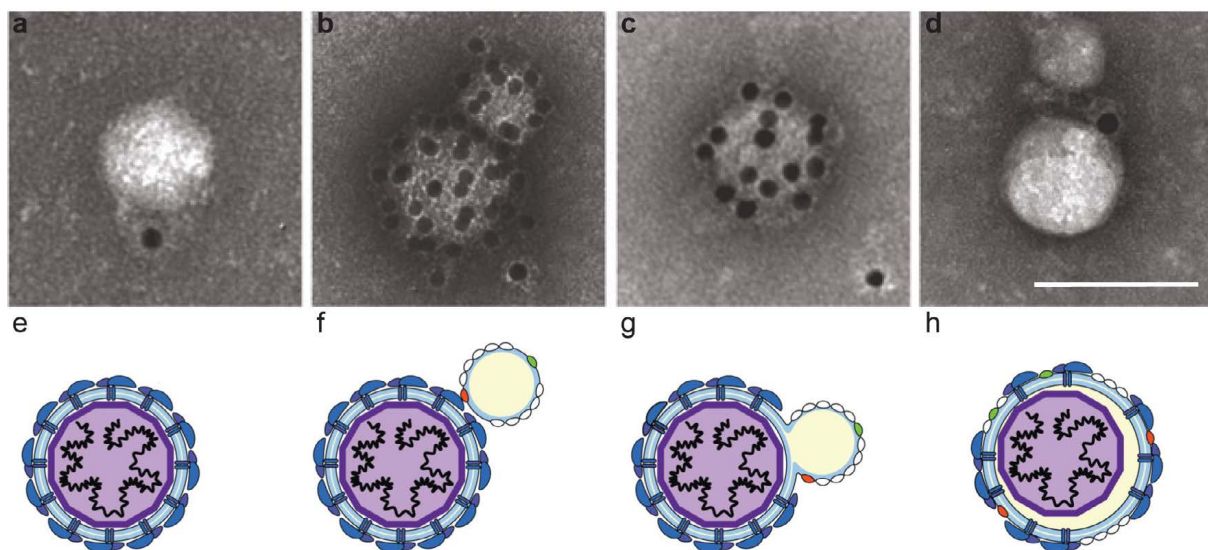
Figure 1.2.: The HCV viral particle

HCV Particles associate with apolipoproteins. (a-d) Electron microscopic images of purified HCV parti-
cles, immunogold-labeled with either (a) HCV-E2 (b) ApoE (c) ApoA-I or (d) ApoB antibodies (scale bar:
100 nm). (e) Schematic picture of an HCV particle. (f) Transient or stable interaction of the HCV particle
with serum lipoprotein. (g, h) Hybrid HCV-lipoporotein particle sharing an envelope membrane. (a-d)
are modified from (Catanese et al., 2013) and (e-h) are modified from (Lindenbach, 2013b).

1.6. HCV life cycle

HCV has a high species and tissue tropism, only infecting human or chimpanzees' hepatocytes. The life cycle can be divided into different steps: entry, fusion and uncoating, RNA replication and translation, assembly, maturation and egress/secretion (Herker et al., 2012). The life cycle of HCV illustrating the different steps is shown in figure 1.3.
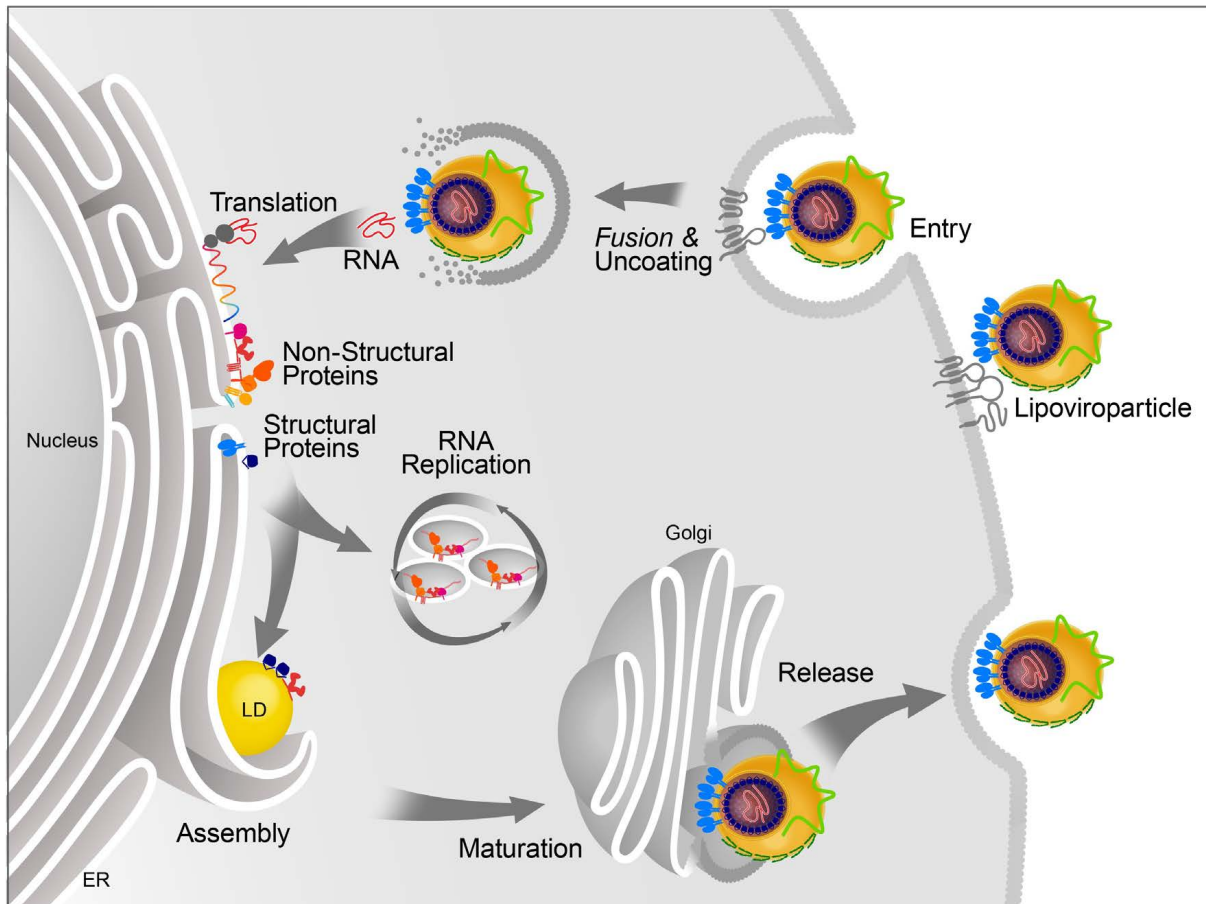
Figure 1.3.: HCV life cycle

HCV attaches to the hepatocyte via different receptors and enters the cell via clathrin-mediated endocytosis. After fusion and uncoating, the viral genome is released. Translation of the polyprotein and processing by viral and host proteases takes places at the ER. RNA replication occurs within the membranous web and assembly takes place at lipid droplets. After maturation, the newly formed virions are secreted in a non-lytic fashion (Illustration kindly provided by Eva Herker and modified from (Herker et al., 2012)).

1.6.1. Viral entry

HCV circulates in the blood as a lipoviroparticle (LVP) and is internalized via receptor-dependent clathrin-mediated endocytosis. The attachment and entry to the cell is a highly orchestrated mechanism (Lindenbach et al., 2013a). First, the virus has to bind to the surface of the cell via the interaction with the low-density-lipoprotein receptor (LDLR) and glycosamino-glycans (GAG). Both can interact with the virion-associated ApoE, thereby supporting the attachment of the virus (Jiang et al., 2012; Germi et al., 2012). Next, the virus binds to the lipoprotein scavenger receptor class B type 1 (SCARB1) by the interaction with ApoE present on the LVP. Then, the receptor binds to the HCV envelope glycoprotein E2 where it is thought to mediate conformational changes of the hypervariable region R1 (HVR1) of E2, thereby facilitating the binding of E2 to the tetraspanin cluster of differentiation 81 (CD81) (Bankwitz, 2014). This surface receptor is ubiquitous expressed and the binding of the LVP to CD81 activates signaling pathways via EGFR, Ras and Rho GTPases (Ding et al., 2014). The activation of Rho GTPases modifies cortical actin filaments and facilitates the lateral membrane movement of the HCV-CD81 complex to the tight junction protein claudin 1 (CLDN1) (Lindenbach et al., 2013a). Occludin (OCLN) is the second tight junction protein involved in the post-attachment steps of the viral entry but its exact role remains unknown (Sourisseau et al., 2013). The transferrin receptor 1 (Trf1), a ubiquitously expressed iron uptake receptor, is important for clathrin-mediated endocytosis. Time-of-addition experiments with inhibitors targeting Trf1 revealed an importance of the receptor post-attachment with CD81 (Martin et al., 2013). The last important factor for the viral entry is Niemann-Pick-C1-like 1 (NPC1L1). This receptor is expressed on the apical and canalicular surface of hepatocytes and is involved in the cholesterol uptake. Inhibition of NPC1L1 by inhibitors or knockdown negatively influences HCV entry (Sainz et al., 2012), but its specific role remains unknown. The HCV-CD81-CLDN1-complex is essential for the viral internalization via clathrin-mediated endocytosis. Following uptake, the complex is transported to early endosomes and the interaction between E2 and CD81 in the low pH environment initiates the fusion of the viral envelope and the endosomal membrane, resulting in the release of the viral genome into the cytoplasm. Subsequently, the (+) ssRNA can be directly translated into viral proteins for the initiation of viral replication (Sharma et al., 2011). Figure 1.4 illustrates the different steps in the entry process.
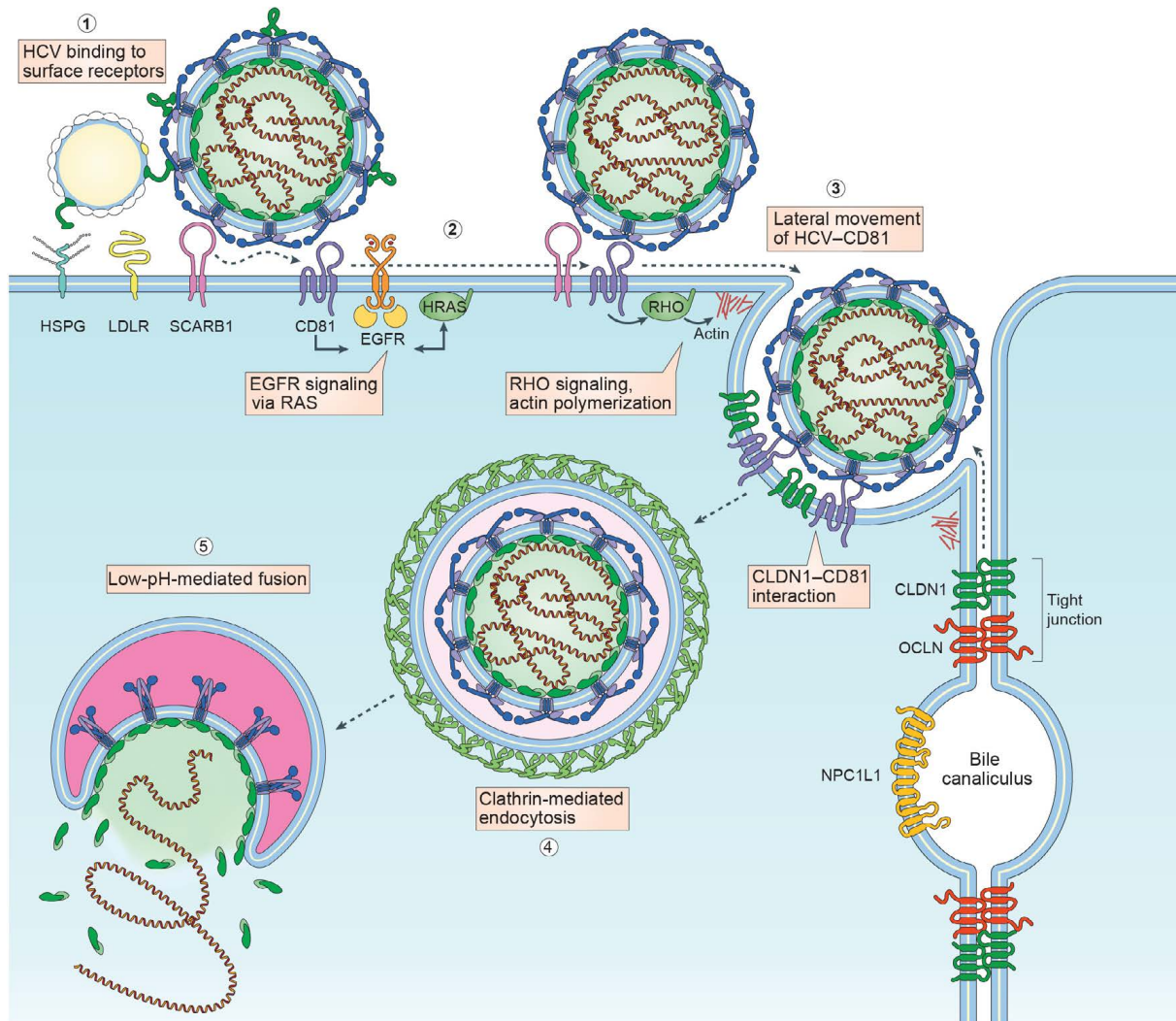
Figure 1.4.: HCV entry process

HCV particles attach to the cell by interaction with several cell surface receptors (1). The LVP-CD81 complex initiates the activation of the signaling pathways via EGFR, Ras and Rho GTPases. (2) HCV-CD81 lateral movement to tight junctions proteins (3) is important for the internalization via clathrin-mediated endocytosis (4). The low pH of the endosomal compartment mediates the fusion and release of the HCV genome (5). Figure modified from (Lindenbach et al., 2013a).

1.6.2. HCV genome and translation

After low pH mediated fusion of the viral envelope, the HCV genome is released into the cytoplasm. The positive-orientated single stranded RNA has a size of 9.6 kb and contains one open reading frame (ORF) flanked by a 5'- and 3'- untranslated region (UTR) (Scheel et al., 2013). The 3'-UTR consists of three parts: a short variable region, a polyuridine/polypyrimidine (polyU/UC) tail and a highly conserved 3'X region (X-tail) with a length of 98 nt (Tanaka et al., 1995). Parts of the 3'X region can bind to parts of the coding sequence of NS5B (5BSL3.2) which is crucial for RNA replication (Friebe et al., 2005). The 5'-UTR harbors an internal ribosomal entry site (IRES) as well as binding sites of the liver-specific micro RNA (miRNA) 122. This complex is essential for viral replication as it protects the HCV RNA from nucleolytic

degradation (Jopling et al., 2005). The IRES then initiates the cap-independent translation of the viral RNA at the ER into one polyprotein. The precursor polyprotein has a length of ~3.000 aa and is co- and post-translationally processed into ten mature viral proteins by viral and host proteases. The three structural proteins as well as the viroporin p7 are cleaved by host signal peptidases between Core/E1, E1/E2, E2/p7 and p7/NS2. The non-structural proteins are processed by the viral proteases: the NS2 cysteine autoprotease cleaves the NS2 protein from NS3 and the NS3/4A serine protease divides all remaining non-structural proteins (NS3, NS4A, NS4B, NS5A and NS5B) (Fields et al., 2007).
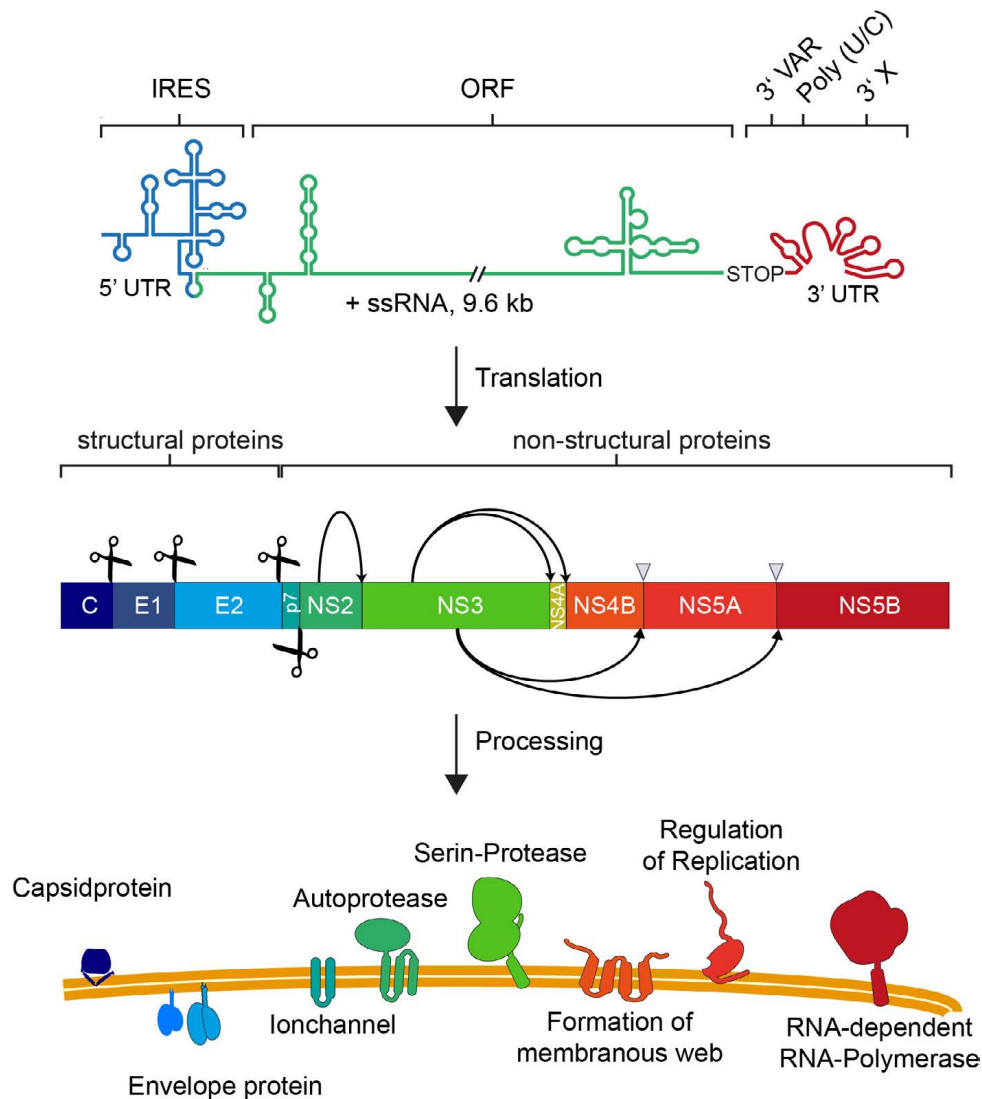
Figure 1.5.: HCV genome organization and polyprotein processing

The HCV genome is flanked by 5'- and 3'- untranslated regions (UTR) (top). The IRES initiates the translation into one polyprotein (middle), which is co- and post-translationally processed into three structural and seven non-structural proteins. Scissors indicate cellular proteases and arrows viral proteases. Modified from (Scheel et al., 2013).

The structural proteins core, E1 and E2 are components of the viral particle and the seven non-structural proteins are involved in the viral replication as well as assembly processes. All viral proteins have distinct functions:

Core protein

The core protein is the first protein processed from the polyprotein by cellular signal peptidases into the precursor core protein with a length of 191 aa. The immature protein has a size of 23 kDa and harbors three domains with different functions (Bartenschlager et al., 2004). The DIII domain of the immature core has a signal sequence important for the trafficking of the nascent protein to the endoplasmic reticulum (ER). At the ER, signal peptide peptidases cleave the E1 signal peptide from the immature core protein resulting in mature 21 kDa core protein. The mature core contains two domains: the highly basic DI, which is located at the N-terminus and the hydrophobic DII located at the C-terminus (McLauchlan et al., 2002; Santolini et al., 1994). DI binds the viral RNA nonspecifically before the protein dimerizes and then forms multimers for nucleocapsid assembly (Santolini et al., 1994). The hydrophobic DII domain is important for binding to membranes of the ER and to the surface of cytosolic lipid droplets (cLDs) (Shavinskaya et al., 2007). The domain harbors two amphipathic helices, which are important for the recruitment to the lipid droplets. Deletion mutation studies in the DII domain have shown that the core protein is rapidly degraded by the proteasome when it is not bound to the surface of lipid droplets (Boulant et al., 2006). In addition, palmitoylation of the conserved cysteine residue has shown to be important for core trafficking as well as for the production of infectious viral particles at cytosolic lipid droplets (Shavinskaya et al., 2007; Majeau et al., 2009). The recruitment process is independent of the HCV genotype, but the strongest accumulation of core on lipid droplets is observed in genotype 3, correlating with high triglyceride levels that are associated with HCV induced liver steatosis (Abid et al., 2005). Beside the main role in capsid assembly, the core protein influences the lipid metabolism, gene transcription, apoptosis and the immune response of the cell (McLauchlan, 2000; Chassey et al., 2008; Kao et al., 2016).

E1 and E2

The glycoproteins E1 (35 kDa) and E2 (70 kDa) are translated into the ER and are cleaved from the polyprotein co-translationally by host signal peptidases. Both are type I transmembrane proteins with a large N-terminal ectodomain residing in the ER lumen and a short C-terminal transmembrane domain anchored in the ER membrane. At the ER, the proteins are heavily glycosylated resulting in non-covalently linked E1-E2 heterodimers. Additional glycosylation and maturation of glycans occurs in the Golgi. The E1-E2 complexes are protease resistant and located on the surface of the viral particle. The glycoproteins are important for the viral entry as they bind to several receptors present on hepatocytes. They are also implicated in the fusion process with endosomal membranes thereby releasing the viral genome (Bartenschlager et al., 2004; Lavie et al., 2006; Voisset et al., 2004; Vieyres et al., 2010).

p7

The viroporin p7 is the first (presumably) non–structural protein released by the cellular signal peptidases. It is a small 7 kDa hydrophobic transmembrane protein with the N- and C-terminus integrated in the ER lumen thereby forming a loop located in the cytoplasm. P7 is important for the late steps of the viral life cycle as it is involved in viral assembly by directly interacting with NS2 (Steinmann et al., 2007; Popescu et al., 2011). In addition, the protein can oligomerize to hexameric and heptameric cation-specific ion channels. It is thought to have an ion channel activity acting as an viroporin to protect the premature virus from acidification during maturation and egress of the virus (Wozniak et al., 2010).

NS2

The NS2 protein has a size of 23 kDa and is a transmembrane (TM) protein with three TMDs in the N-terminus and one cysteine protease domain at the C-terminus. The enzymatic activity of the protease is important for the polyprotein processing at the NS2/3 junction that is the only reported substrate of the enzyme. Interestingly, only the NS2 domain but not the activity is necessary for viral assembly by facilitating the binding of E1/E2, p7 and NS3/4A. Furthermore, the NS2-p7 complex together with NS3/4A is important for the re-localization of the core protein from lipid droplets to assembly sites of the immature virus (Lindenbach et al., 2013a; Popescu et al., 2011).

NS3

The 70 kDa NS3 protein contains N-terminal a serine protease and a RNA helicase/NTPase domain in the C-terminus. For the enzymatic activity, NS3 has to build a non-covalent complex with the small 6 kDa protein NS4A (Morikawa et al., 2011; Kuang et al., 2004).

NS3/4A

The NS3/4A complex is responsible for the processing of the non-structural proteins NS3-NS5B. The NS4A is a transmembrane protein intercalating in the serine protease domain of NS3 thereby anchoring the complex into the ER membrane. This complex is important for RNA replication as well as for the viral assembly (Moradpour et al., 2013). Furthermore, the complex plays an important role in the immune evasion of the virus as it cleaves the mitochondrial antiviral-signaling (MAVS) protein of the mitochondrial and peroxisomal membranes, which, in turn, is then unable to induce innate immunity signaling pathways via the retinoic acid inducible gene I (RIG-I) and melanoma differentiation–associated gene 5 (MDA5) receptors (Li et al., 2005; Cao et al., 2015).

NS4B

The 27 kDa protein is an integral membrane protein with four transmembrane domains and two amphipathic α-helices at the N-terminus. The C-terminus also harbors two amphipathic α-helices and two additional palmitoylation sites. This protein is, together with other NS protein, the main protein responsible for cellular membrane rearrangements called the "membranous web". These cell compartments are described to be the RNA replication site of the virus (Egger et al., 2002).

NS5A

The NS5A protein has a size of 56 kDa at the basal phosphorylated level and 58 kDa when hyperphosphorylated. The protein is composed of three domains: DI contains one amphipathic helix at the N-terminus anchoring the protein into the ER membrane. In addition, DI has a Zn^{2+} binding site and can bind RNA. This domain is responsible for targeting to lipid droplets and both, DI and DII are important for viral RNA replication. However, deletion mutations in DII and DIII had no impact on RNA replication (Appel et al., 2005; Blight et al., 2000). DIII is involved in the assembly process by interacting with the core protein. In addition, immunofluorescence studies revealed a colocalization of NS5A with core on lipid droplets. Taken together, this protein has a dual role; it is important for the regulation of RNA replication and for viral assembly (Moradpour et al., 2013).

NS5B

The last protein of the polyprotein is the 68 kDa NS5B. After posttranslational modification, the hydrophobic C-terminus is integrated into the ER membrane whereas the catalytic domain is facing into the cytosol (Ivashkina et al., 2002). It functions as a RNA-dependent RNA polymerase using the positive RNA strand to synthesize negative RNA. This negative intermediate is then used as a template to generate new positive HCV RNA genomes (Fields et al., 2007). The enzyme has no proof-reading function, leading to the high mutation rate and genomic diversity of the virus (Neumann-Haefelin et al., 2013).

1.6.3. Viral RNA replication, assembly and release

After translation and polyprotein processing, the host cell undergoes enormous cellular membrane rearrangements required for RNA replication. NS4B was the first protein described to induce these alterations. They consist of ER-derived membranes forming single-, double-, and multimembrane vesicles called the membranous web (MW) (Egger et al., 2002; Romero-Brey et al., 2012). Recent studies revealed that also other NS proteins as well as host factors such as the lipid kinase phosphatidylinositol-4-kinase III alpha (PI4KIIIα), contribute to the formation of the MW (Lohmann, 2013). The MW contains the viral genome and (at least) the non-structural proteins NS3/4B-NS5B. Due to their physical properties, these vesicular structures protect the viral RNA from degradation. Interestingly, one replication complex harbors at least one negative RNA strand, two to ten positive RNA strands and up to 1,000 copies of each non-structural protein. Only 5% of the non-structural proteins are protease-resistant in these vesicles and used for full replication activity (Quinkert et al., 2005). The replication complexes are found in close proximity to lipid droplets, which are commonly agreed to be the assembly site of the virus (Herker et al., 2011). The mature core protein traffics to the lipid droplets, a process that is facilitated by the diacylglycerol acetyltransferase (DGAT1) triglyceride-synthesis and MAPK-regulated cytosolic phospholipase A2 (PLA2G4A) activities (Herker et al., 2010; Menzel et al., 2012). The lipid droplet–bound core protein interacts with NS5A, which is enhanced by DGAT1 (Camus et al., 2013). This interaction initiates the first steps in the nucleo-capsid formation (Figure 1.6) (Lindenbach, 2013b). During the assembly process, core has to be retrieved from the lipid droplets and migrates to budding sites of the virus at opposing ER membranes. Alternatively, core that remains at the ER after translation might encapsidate the RNA. However,the exact mechanistic details are still unknown. One possible explanation is an interaction of the core protein with the clathrin adaptor protein complex 2 (AP2M1), thereby releasing core from the lipid droplets (Neveu et al., 2012). Live cell imaging analysis showed that the core protein traffics to and is recruited from the lipid droplets along microtubules (Counihan et al., 2011). Another key player in the retrieval process of core from the lipid droplets is the p7-NS2 interaction with the NS3/4A complex. NS2 interaction with p7 is also important for the recruitment of the other NS proteins to the assembly site. In addition, NS2 is associated with the formation of protein-protein interaction of p7, NS3 and NS5A with E1 and E2 (Popescu et al., 2011). The insertion of the glycoproteins into the envelope of the virion takes place during budding into the ER lumen. The endosomal sorting complex required for transport (ESCRT) pathway supports the budding and/or post-assembly process (Ariumi et al., 2011). After the budding event, the E1 and E2 glycoproteins are post-translationally modified with high mannose and complex N-linked glycans, indicating that the virus is released via the secretory pathway through the Golgi. This modification of high mannose glycans to complex glycans is known to occur only in the Golgi. In addition, the released virus shares high similarity with lipoproteins indicating the same secretory route (Vieyres et al., 2010; Syed et al., 2017). An electron microscopic analysis of immunoprecipitated COPII vesicles revealed a colocalization of HCV particles and apolipoproteins in these compartments of the Golgi (Syed et al., 2017). Furthermore, ApoE has been

shown to be important for the maturation of viral particles. Knockdown experiments revealed a strong defect in the production of infectious viral particles. In detail, envelopment of the viral particles into membranes is independent of ApoE but ApoE plays an important role in the maturation step of the virions prior to the release (Lee et al., 2014; Hueging et al., 2014). Additionally, downregulation of ApoB as well as inhibition of the microsomal transfer protein (MTP), involved in the lipid transport of the ER lumen, leads to a reduction of released infectious viral particles (Gastaminza et al., 2008). Noteworthy, Huh7-derived cell lines are not able to produce fully lipidated ApoB resembling rather LDLs than VLDLs (Meex et al., 2011). In infection studies, they secrete predominately HCV particles which are ApoB-negative (Bartenschlager et al., 2011). Therefore, the formation of infectious HCV particles in Huh7-derived cells depends on ApoE but not on ApoB secretion (Jiang et al., 2009).
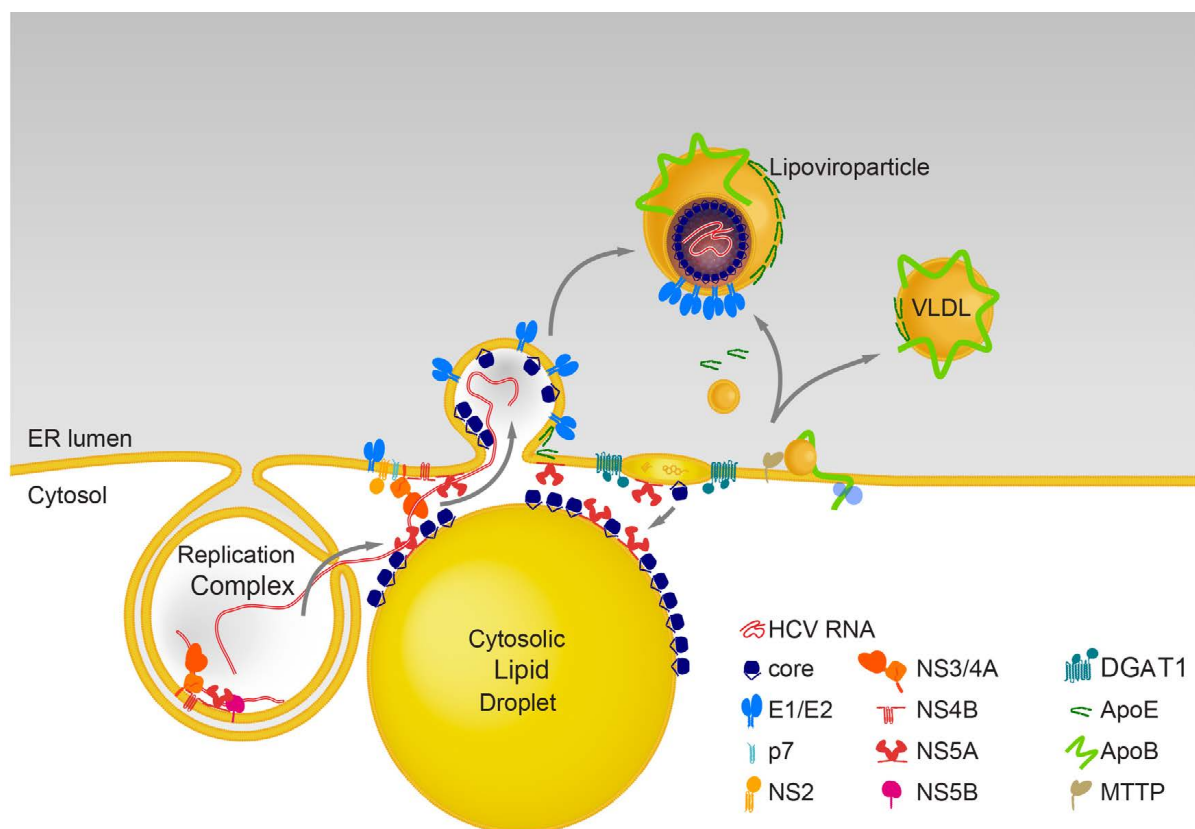
Figure 1.6.: Assembly and maturation

The replication complexes (RC) are in close proximity to lipid droplets (LDs). Recruitment of the RC to the lipid droplets is mediated by PLIN3 and the viral proteins core and NS5A. After retrieval of core from the lipid droplets, NS2 facilitates the assembly process by interaction with other NS proteins. During the budding event into the ER lumen, the glycoproteins E1/E2 are integrated into the envelope of the viral particle. Then, the particle matures to a lipoviroparticle and is released out of the cell via secretory pathways (Illustration kindly provided by Eva Herker) (Herker et al., 2011).

1.7. Lipid droplets

Lipid droplets are cytosolic organelles with a neutral core of triglycerides, sterol esters and retinyl esters surrounded by an amphipathic phospholipid monolayer (Figure 1.7) (Farese et al., 2009). On the surface, several proteins are located e.g. proteins of the perilipin (PLIN) and proteins involved in the breakdown machinery of the droplets. Lipid droplets are found in every tissue but vary in size (20 nm to 100 μm) (Long et al., 2012; Fujimoto et al., 2011). Lipid droplets are important for the lipid metabolism, energy homeostasis and lipid signaling of the cell. Abnormal accumulation of lipid droplets is observed in various diseases such as obesity, atherosclerosis and liver steatosis (Greenberg et al., 2011). A dysfunction of the lipid metabolism has also been reported to contribute to neurodegenerative disorders such as Huntington's disease and Parkinson (Martinez-Vicente et al., 2010; Cole et al., 2002). The Hepatitis C virus is the best studied virus using lipid droplets as assembly sites, but other viruses such as Dengue virus and the Rotavirus are also known to hijack lipid droplets for their own viral life cycle (Herker et al., 2012).
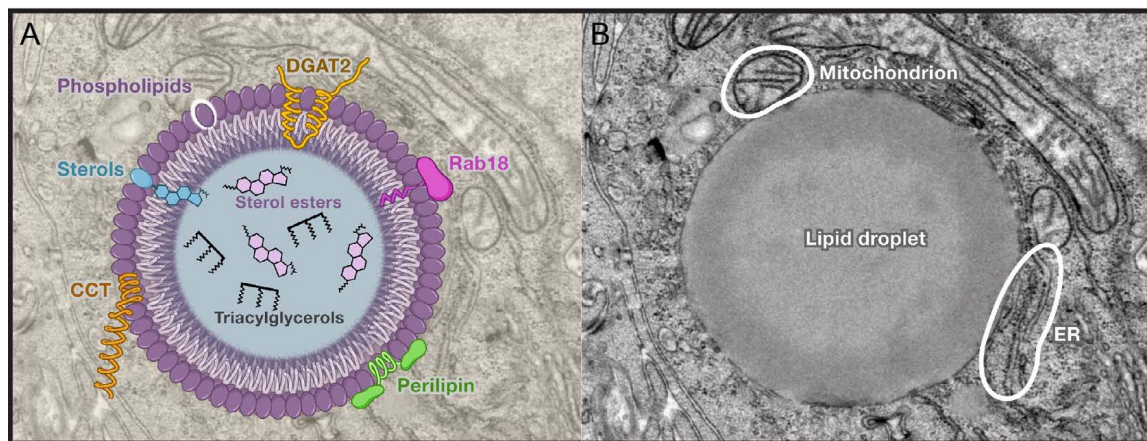
Figure 1.7.: Lipid droplet

(A) Scheme of a lipid droplet containing neutral lipids (sterol esters and triglycerides) and associated proteins embedded in the amphipathic phospholipid monolayer. (B) Electron microscope picture of a lipid droplet of a hepatoma cell in close proximity to the ER and mitochondria (Farese et al., 2009).

1.7.1. Lipid droplet biogenesis

Lipid droplets contain neutral lipids which are synthesized within the ER by two different pathways: the glycerol-3-phosphate pathway or the monoacylglycerol pathway (Wilfling et al., 2014b; Walther et al., 2017; Welte, 2015). In the glycerol-3-phosphate pathway, the *de novo* synthesis of triglycerides is a four steps process mediated by enzymes located permanently or transiently at the ER. First, glycerol-3-phosphate is acylated by the addition of one fatty acid chain into lysophosphatidic acid (LPA or 1-acylglycerol-3-phosphate) catalyzed by glycerol-phosphate acyltransferase (GPAT) (Figure 1.8A). Through a second acylation step catalyzed by the acylglycerol-phosphate acyltransferase (AGPAT), phosphatidic acid (PA) is generated. PA is then dephosphorylated into diglyceride (DAG), which is used as a substrate by the enzymes diacylglycerol acyltransferase 1 and 2 (DGAT1 and DGAT2). They catalyze the last

addition of a fatty acyl chain to form triglycerides (TGs) (Figure 1.8 A). In the monoacylglycerol pathway monoglycerides are converted to diglycerides by monoglyceride acyltransferase (MGAT), which are further processed to triglycerides by the DGAT enzymes. The generation of triglycerides via the monoacylglycerol pathway is more abundant in intestinal enterocytes and adipocytes than in the liver (Walther et al., 2017; Pol et al., 2014). The synthesis of sterol esters is catalyzed by acyl-CoA:cholesterol acyltransferase (ACAT). Depending on the cell type and the physiological conditions, sterol esters or triglycerides are dominating the lipid droplet core (Wilfling et al., 2014b). Several studies have shown that the triglycerides within the bilayer of the ER membrane can exist in a dispersed form and after a certain threshold (3–10 mol%) the triglycerides tend to form an oil lens (Wilfling et al., 2014b; Walther et al., 2017; Duelund et al., 2013; King et al., 1994). Successive growth of the oil lens leads to the formation of nascent lipid droplets, which start to bud out of the ER. The process of lipid growth is thought to be mediated by different proteins such as fat storage-inducing transmembrane (FIT) 2 and PLIN3. PLIN3 is found on the surface of small lipid droplets and thought to have a stabilization function (Choudhary et al., 2015; Londos et al., 2005). FIT2 is an ER-associated protein and is proposed to have a function in lipid partitioning. In the budding event of lipid droplets, proteins such as seipin play an important role. Seipin resides in the ER and several studies indicate a role for seipin in the initial steps of lipid droplet formation and a regulatory role of the protein composition of lipid droplets (Walther et al., 2017; Wang et al., 2016). The last step in lipid droplet biogenesis is the growth and expansion of smaller droplets. Therefore, the phospholipids are removed from the droplets via the ARF1 and COP-I/coatamer protein complex. This leads to enhanced surface tension and enzymes for triglycerides synthesis such as DGAT2 localize to the surface for lipid droplets growth. During this process, the lipid droplets interact with the ER thereby building a "membrane bridge" (Wilfling et al., 2014a). Lipid droplet expansion can also occur via permeation and coalescence or fusion. In case of the permeation process, the triglycerides of a small lipid droplet are transferred to a larger droplet. In adipocytes the protein Fsp27 mediates this process (Gong et al., 2011). In the coalescence process, two or more droplets fuse due to limited amounts of phospholipids in the surface membrane of lipid droplets resulting in high surface tension (Thiam et al., 2013). However, other proteins located in the cytoplasm are also able to traffic to the droplets under those conditions. For instance, The CTP:phophocholine cytidylyltransferase (CCT) 1 protein traffics to the "naked" lipid droplet and activates the local synthesis of phospholipids to generate a membrane necessary for the expansion of the droplet (Figure 1.8 B) (Martin et al., 2006; Krahmer et al., 2011). Proteins involved in the lipid droplet homeostasis like proteins of the perilipin (PLIN) family and proteins involved in the breakdown of lipid droplets are found on the surface of the mature droplet. Some, but not all, lipid droplets stay connected to the ER. They are associated with other organelles such as the mitochondria, lysosomes and endosomes indicating that the droplets are also involved in other cellular processes such as fatty acid signaling and lipid trafficking (Barbosa et al., 2015). To date four different types of lipid droplets are known to exist: cytosolic lipid droplets (cLD), the apoB-containing lipid droplets (VLDL and its precursors), the luminal

apoB-free lipid droplets and nuclear lipid droplets. Cytosolic lipid droplets are the largest and best characterized type whereas the nuclear lipid droplets represent the latest and smallest group (Uzbekov et al., 2013; Wang et al., 2007).

Figure 1.8.: Lipid droplet synthesis

(A) Scheme of triglyceride synthesis via the glycerol-3-phosphate pathway. (B) Lipid droplet formation. Triglycerides accumulate between the ER leaflets forming a lens before they either bud of the ER or stay connected (modified from (Wilfling et al., 2014b) (C) 3D SIM image of Huh7.5 cells carrying the RFP-NLS-IPS reporter. Left panel shows the RFP expressing mitochondria. In the middle panel are lipid droplets visualized with Bodipy495/503. Right channel is an overlay of both panels. Scale bar 2 μm.

1.7.2. Breakdown of lipid droplets

The cell breaks down lipid droplets under catabolic conditions such as starvation and for the generation of membranes. The triglycerides inside the lipid droplets can be hydrolyzed by two different pathways: either by lipolysis or by autophagy (Figure 1.9) (Singh et al., 2012; Zechner et al., 2017). Lipolysis is a three steps process initiated by the activation of the lipase adipose triglyceride lipase (ATGL) and its co-factor comparative gene identification-58 (CGI-58). Under basal conditions CGI-58 is bound to PLIN1, the first member of the PLIN family. During lipolysis, PLIN1 is phosphorylated, releasing CGI-58, which in turn activates ATGL. In addition, ATGL can be phosphorylated by cyclic AMP (cAMP) activated protein kinase K (PKA) upon β-adrenergic stimulation (Miyoshi et al., 2007; Meyers et al., 2017). The triglycerides are then hydrolyzed by ATGL to diglycerides and one free fatty acid (FFA). The resulting diglycerides are further processed to monoglycerides by the hormone-sensitive lipase (HSL). The last step involves the enzyme monoglyceride lipase (MAG) releasing the last free fatty acid (Figure 1.9 A, B). This pathway has been intensively studied in adipocytes and there approximately 90% of the triglycerides are hydrolyzed by ATGL and HSL (Schweiger et al., 2006). Even though ATGL is

expressed in almost every tissue, the expression levels vary indicating that other lipases might be involved. PLIN1 expression in non-adipocytes is low and PLIN5 replaces its function in ATGL-mediated triglyceride hydrolysis in muscle (Zierler et al., 2014; Fagerberg et al., 2014). However, the expression levels of PLIN5 are also low in hepatocytes leading to the speculation that other PLINs might be involved in the regulation of triglyceride breakdown inside the liver. Indeed, overexpression of PLIN2 in hepatoma cells has been shown to inhibit ATGL activity (Listenberger et al., 2007). Moreover, ATGL deficient mice develop hepatic steatosis without an altered VLDL production, indicating that other lipases are involved in the breakdown machinery (Bell et al., 2008; Wu et al., 2011). The other pathway resulting in the breakdown of lipid droplets is macrolipophagy. During this process lipid droplets, or at least parts, are sequestered into double-membrane vesicles called autophagosomes, which fuse with lysosomes to form autolysosomes (Singh et al., 2009; Zechner et al., 2017). Lysosomal acid lipases inside the lysosomes then hydrolyze the triglycerides to free fatty acids (Figure 1.9 B) (Singh et al., 2009). Macrolipophagy is a stepwise process, where first the autophagy gene (Atg) 7 localizes to the surface of lipid droplets enabling the conjugation of Atg12 to Atg5. In addition, it facilitates the lipidation of light chain protein (LC) 3 with phosphatidylethanolamine (PE) through a covalent bond, resulting in LC3-II. Interestingly, PLIN2 and PLIN3 are substrates for degradation via chaperone-mediated autophagy, a prerequisite for both macrolipophagy and lipolysis (Kaushik et al., 2015).
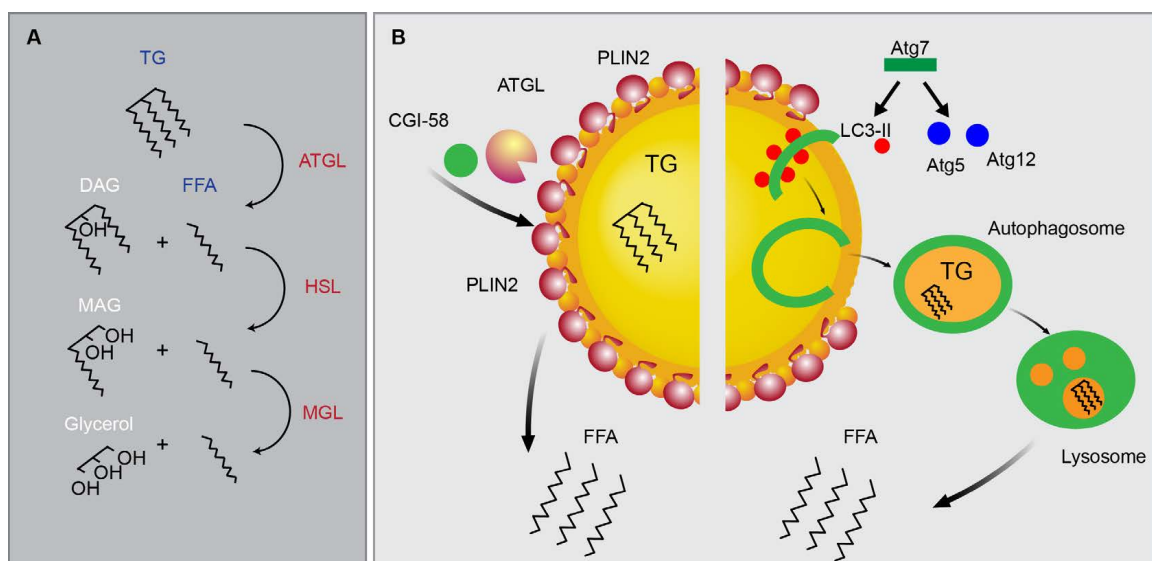
Figure 1.9.: Breakdown of lipid droplets

(A) Breakdown of triglycerides via lipolysis in three steps. TG, triglycerides; DAG, diglycerides; MAG, monoglycerol; ATGL, adipocyte triglyceride lipase; HSL, hormone stimulated lipase; MGL, monoglyceride lipase (Eichmann et al., 2012). (B) Scheme of the lipid droplet breakdown via lipolysis (left) and autophagy (right). FFA, free fatty acid; CGI-58, comparative gene identification 58; LC3, light chain protein 3; Atg, autophagy gene (model based on (Singh et al., 2012))

1.8. Mitochondrial β-oxidation

Free fatty acids released from triglycerides by macrolipophagy or lipolysis are used for cell sig-
naling and VLDL synthesis, or for mitochondrial β-oxidation for energy demands (Quiroga et al.,
2012). Small free fatty acids (<12 carbon chains) can pass the mitochondrial membrane with-
out the help of cargo or transport helpers. Fatty acids with a chain length over 12 carbon atoms
have to be activated by long-chain acyl-CoA synthetases which reside at the outer membrane
of the mitochondria (Yan et al., 2015). The activated fatty acid is then either oxidized by a four
steps process to acetyl-CoA and acyl-CoA (Figure 1.10) (Da Poian et al., 2010), or is esterified
into triglycerides as described in the glycerol-3-phosphate pathway (Figure 1.8 A). But prior
β-oxidation, the activated fatty acid serves as a substrate for carnitine palmitoyltransferase I
(CPT-I), an enzyme generating acyl-carnitine from acyl-CoA. The acyl-carnitine is then shut-
tled to the inner mitochondria membrane by carnitine:acylcarnitine translocase. At the inner
mitochondrial membrane, CPT-II catalyzes the reverse reaction and generates acyl-CoA from
acyl-carnitine by esterification. Next, the β-oxidation process is initiated (Figure 1.10). During
this process, the acyl-CoA is shortened by two carbon atoms, giving rise to acetyl-CoA. The
shortened acyl-CoA is able to re-enter the β-oxidation procedure. This cycle is repeated for
fatty acids with an even number of C-atoms until only acetyl-CoA is left. In the case of an
uneven number of C-atoms, acetyl-CoA and propionyl-CoA are the last products generated.
During each β-oxidation cycle the flavin adenine dinucleotide ($FADH_2$) and nicotinamin ade-
nine (NADH) are generated. The electrons from the $FADH_2$ and NADH are transferred in the
respiratory chain thereby generating a proton-motive gradient which is then used to produce
energy in form of ATP. In addition, the resulting acetyl-CoA of each β-oxidation cycle enters the
citric acid cycle where it is oxidized. During this process one additional ATP is generated con-
cominant with additonal NADH and $FADH_2$, which are again used for the production of ATP. The
rate-limiting step of β-oxidation is the availability of carnitine, which can be either endogenously
synthesized or ingested from exogenous sources. Further, malonyl-CoA, which is involved in
the synthesis of long-chain fatty acids from acyl-CoA, can hinder β-oxidation by inhibiting the
activity of CPT-I and promoting the generation of fatty acids. If the cell is under energy de-
mands, the malonyl-CoA level drops thereby promoting β-oxidation to generate energy. In the
liver, acyl-CoA can be further processed to ketone bodies, which serve as an energy source
for other tissues if glucose levels are low. Ketone bodies are circulating in the blood, supplying
organs that are either unable to or only inefficiently generate energy from fatty acids such as
the brain (Ridgway, 2015; Laffel, 1999). Along with the mitochondria as the major organelle for
β-oxidation, peroxisomes are also capable to shorten fatty acids for energy production, but this
degradation is less efficient (Wanders et al., 2001).
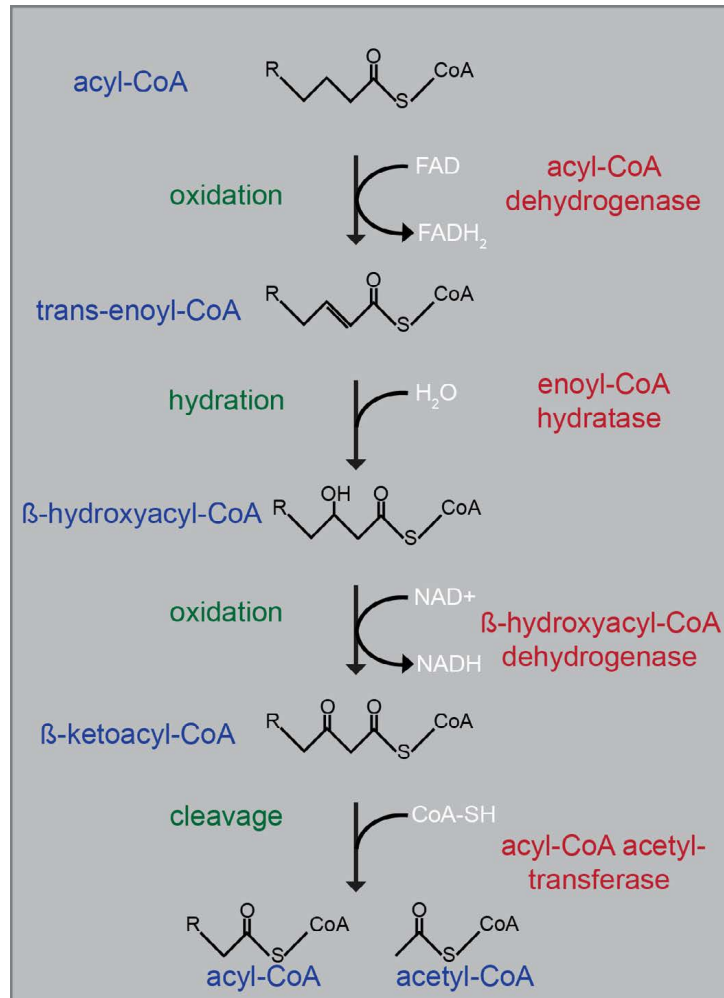
Figure 1.10.: β-oxidation of free fatty acids

The β-oxidation process by four enzymatic steps to degrade acyl-Co thereby shortening the fatty acids by two carbon atoms, liberating acetyl-CoA and reducing NAD and FAD to NADH and FADH$_2$, respectively. The shortened acyl-CoA re-enters the β-oxidation process. Modified from (Da Poian et al., 2010).

1.9. Perilipin family

On the surface of lipid droplets several proteins are embedded, which are involved in the homeostasis of the droplet. The major coat proteins belong to the perilipin (PLIN) family comprising five family members that have been recently renamed (Table 1.1, modified from (Kimmel et al., 2010)).

Table 1.1.: Nomenclature for the PLIN family members

Human Symbol	Approved Name	Aliases	LD binding
PLIN1	perilipin 1	perilipin, PERI, PLIN	constitutively
PLIN2	perilipin 2	ADRP, ADFP, adipophilin	constitutively
PLIN3	perilipin 3	TIP47, PP17, M6PRBP1	exchangeable
PLIN4	perilipin 4	S3-12	exchangeable
PLIN5	perilipin 5	PAT1, LSDP5, OXPAT, MLDP	exchangeable

PLIN proteins are synthesized at free ribosomes and either bind constitutively to lipid droplets or can be exchanged between the cytoplasm and lipid droplets (Londos et al., 1999; Brasaemle et al., 1997; Wolins et al., 2003; Yamaguchi et al., 2006). The PLIN proteins differ in their tissue distribution (Figure 1.12) as well as in expression levels and in the interaction with other proteins. PLIN1-3 have a conserved PAT domain, which was named after the aliases perilipin A, Adrp and Tip47 (Lu et al., 2001). Blast analysis revealed PLIN5 as the fifth protein sharing this domain (Kimmel et al., 2010). This domain is located at the N-terminus followed by a conserved 11-mer repeat of helices in all PLIN members, but with different loci and sequence (Figure 1.11). How the PLIN proteins target to the surface of lipid droplets is still under debate. It is suggested that the 11-mer repeat is involved in the binding to lipid droplets and not the PAT domain as earlier studies have proposed (Rowe et al., 2016). The 11-mer repeat is proposed to form amphipathic α-helices that can anchor the protein into the phospholipid monolayer of lipid droplets (Bussell et al., 2003). Indeed, fluorescence resonance energy transfer (FRET)-analysis of PLIN2 and lipids located in the monolayer revealed a close physical association as well as involvement in lipolysis of the lipid droplet (Najt et al., 2014; McIntosh et al., 2012). However, the different PLINs favor different lipid droplet sizes as well as lipid droplet lipid compositions: in adipocytes, small droplets are mainly coated with PLIN3 and 4 and PLIN1 and 2 are found on larger lipid droplets (Wolins et al., 2005). Triglyceride-rich lipid droplets are often associated with PLIN1 and 5, whereas PLIN2 and 3 prefer triglyceride- and cholesterol ester-containing lipid droplets. PLIN4 is found on cholesterol-rich lipid droplets (Okumura, 2011). However, the expression of the different PLINs varies depending on the tissue (Figure 1.12).
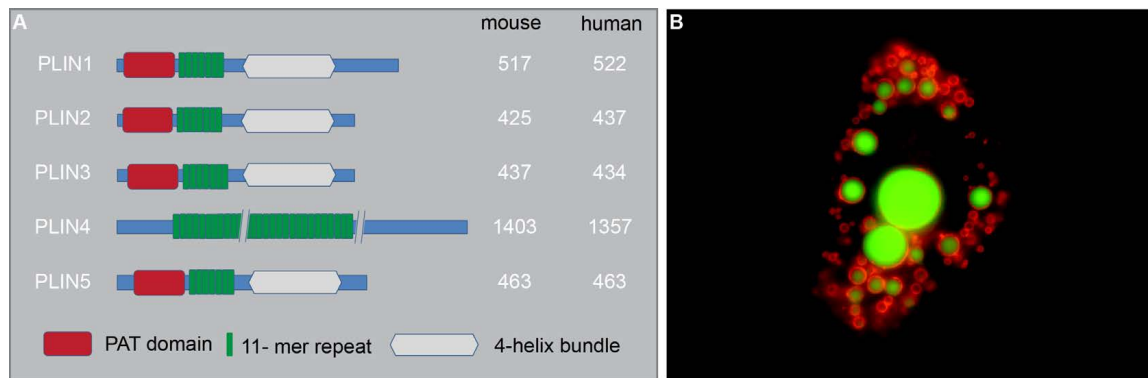
Figure 1.11.: Simplified sequence structure of the PLIN family and colocalization of PLIN1 with lipid droplets
(A) Schematic sequence homology of the different PLIN proteins is illustrated. Numbers of the amino acids of the different PLIN proteins in mouse and human are shown. PLIN1-3 and 5 share a conserved PAT domain as well as the 4-helix bundle (modified from (Itabe et al., 2017)). (B) Confocal microscope picture of lipid droplets in a 3T3-L1 adipocyte. Cells were fixed with paraformaldehyde, permeabilized and immunostained against PLIN1 (red). Lipid droplets were visualized using Bodipy495/503 (cyan). PLIN1 form a ring-link structure around the lipid droplets (modified from (Cohen et al., 2004)).

1.9.1. Perilipin 1 (PLIN1)

Perilipin-1 (PLIN1) is the best investigated protein of the PLIN family and has four different isoforms, A-D, all sharing a common N-terminal region, but differing in the C-terminal region (Lu et al., 2001; Bickel et al., 2009). It shares 40% sequence homology with PLIN2 at the N-terminus and 20% sequence identity at the C-terminus with PLIN2 (Londos et al., 2005). PLIN1 is constitutively bound to lipid droplets and is rapidly degraded through the proteasome if unbound (Takahashi et al., 2016; Xu et al., 2005). The most abundant isoform in adipocytes is perilipin A and is known to be the main regulator of lipolysis by serving as the major cAMP-dependent protein kinase substrate. It has the ability to act as an inhibitor for lipase activity under basal conditions by shielding lipid droplets from cytosolic lipases. Upon stress situations like energy deficits, catecholamine binds to adrenergic receptors, initiating the production of cAMP, which in turn activates PKA. PKA phosphorylates PLIN1 at PKA consensus sites leading to protein rearrangements on the surface of the lipid droplet as described in 1.7.2 resulting in the breakdown of lipid droplets (Brasaemle et al., 2008). PLIN1 is highly expressed in adipocytes and only present at low levels in the liver but the expression increases in steatotic liver stages (Straub et al., 2008).

1.9.2. Perilipin 2 (PLIN2)

The second protein constitutively bound to lipid droplets is PLIN2. Like PLIN1, it is degraded via the ubiquitin pathway in the cytoplasm if not bound to lipid droplets (Takahashi et al., 2016; Xu et al., 2005). It shares a sequence homology with PLIN3 in the first 100 amino residues and 40% at the C-terminus (Londos et al., 2005). PLIN2 is the major lipid droplet coating protein with high expression levels in the liver and has been considered as a reliable marker for lipid droplets (Fujimoto et al., 2004; Mak et al., 2008; Conte et al., 2016). Supporting a role in lipid homeostasis, the hepatic triglyceride content in PLIN2^{-/-} mice is reduced up to 60% (Chang et

al., 2006; Tsai et al., 2017). Interestingly, these mice did not show an impaired VLDL secretion, most likely due to enhanced MTP levels, leading to an increase in ApoB synthesis (Chang et al., 2006). In contrast, mice treated with a PLIN2-antisense oligonucleotide (ASO) showed an impaired VLDL secretion in the absence of PLIN2 (Varela et al., 2008; Imai et al., 2012). However, further studies are needed to clarify the exact underlying mechanism of PLIN2 in VLDL synthesis. Even though PLIN3 is recruited to lipid droplets in PLIN2$^{-/-}$ mice, PLIN3 cannot compensate all functions of PLIN2 (Libby et al., 2016). In cells overexpressing PLIN2, the triglyceride levels are elevated, which is concomitant with a reduced association of the lipolytic pathway marker ATGL to lipid droplets. This subsequently leads to an in impaired lipolysis supporting an interaction between ATGL and PLIN2 (Listenberger et al., 2007; Kaushik et al., 2015). PLIN2 expression is upregulated upon lipid loading of the cells as well as in chemical-induced ER stress situations (Chen et al., 2017). In addition, PLIN2 as well as PLIN3 are substrates for the chaperone-mediated autophagy, a pre-requisite for the lipid droplet degradation via lipolysis as well as macrolipophagy (Kaushik et al., 2015). Taken together, PLIN2 is involved in the lipid droplet stability and lipid accumulation.

1.9.3. Perilipin 3 (PLIN3)

Perilipin 3 (PLIN3) is ubiquitous expressed and found in the cytoplasm and on lipid droplets. It shares a high sequence similarity to PLIN2 (Wolins et al., 2001) and crystal structure analysis revealed a high similarity to the N-terminal lipid-binding domain of ApoE (Hickenbottom et al., 2004). Both, ApoE and PLIN3 harbor a α/β domain and four amphipathic α-helices at the C-terminus, which resembles the LDL receptor binding domain of the apolipoproteins (Hickenbottom et al., 2004). PLIN3 was first described as an intracellular trafficking protein due to its ability to bind to mannose 6-phosphate receptors (MPR) cytoplasmic domains. MPRs are involved in the transport of lysosomal hydrolases from the Golgi to the endosomes and back (Diaz et al., 1998; Kornfeld, 1992). Several studies have demonstrated a direct connection between PLIN3 and the endosomal transport machinery (Burguete et al., 2005; Ganley et al., 2004). This contradicts with immunofluorescence studies which could not identify any colocalization to MPR or other marker proteins involved in the endocytic pathway nor its synthesis, whereas a colocalization to lipid droplets was demonstrated (Bulankina et al., 2009). Even though PLIN3 knockdown experiments showed a decreased lipid droplet biogenesis, its expression level does not correlate with the amount of lipid droplets or hepatic steatosis like PLIN2 (Straub et al., 2008; Bulankina et al., 2009). In addition, PLIN3 has been described as a pro-viral host factor in HCV infection by interacting with the HCV-NS5A protein and knockdown studies of PLIN3 showed an impaired viral RNA replication (Vogt et al., 2013).

1.9.4. Perilipin 4 (PLIN4)

PLIN4 is an exchangeable lipid droplet–binding protein with the lowest sequence homology to any other PLIN protein and lacks the PAT domain as well as the α-helix bundle. It is most abundant in adipocytes but the function of PLIN4 remains unknown.

1.9.5. Perilipin 5 (PLIN5)

The last and newest member of the PLIN family is PLIN5, mainly expressed in oxidative tissue such as the heart, liver and skeletal muscle. It is an exchangeable lipid droplet–binding protein but it has also been found in the cytoplasm, where it associates with the mitochondria in cardiac muscle cells. PLIN5 can be stimulated by peroxisome proliferator-activated receptors (PPARs) and by fasting (Wolins et al., 2006; Bosma et al., 2012a). PLIN5, like PLIN1, is a target for PKA thereby stimulating lipolysis (Wang et al., 2011). In PLIN5 overexpressing AML12 cells, a mouse liver cell line established from transgenic mice expressing the human TGF-α, the triglyceride content increases and the lipolysis decreases. However, PLIN5 knockout mice showed controversial results. They all lack cardiac lipid droplets upon prolonged fasting and showed increased β-oxidation, but triglyceride levels in the liver range from no phenotype, elevated hepatic triglyceride level to reduced triglyceride levels (Mason et al., 2014; Kuramoto et al., 2012).
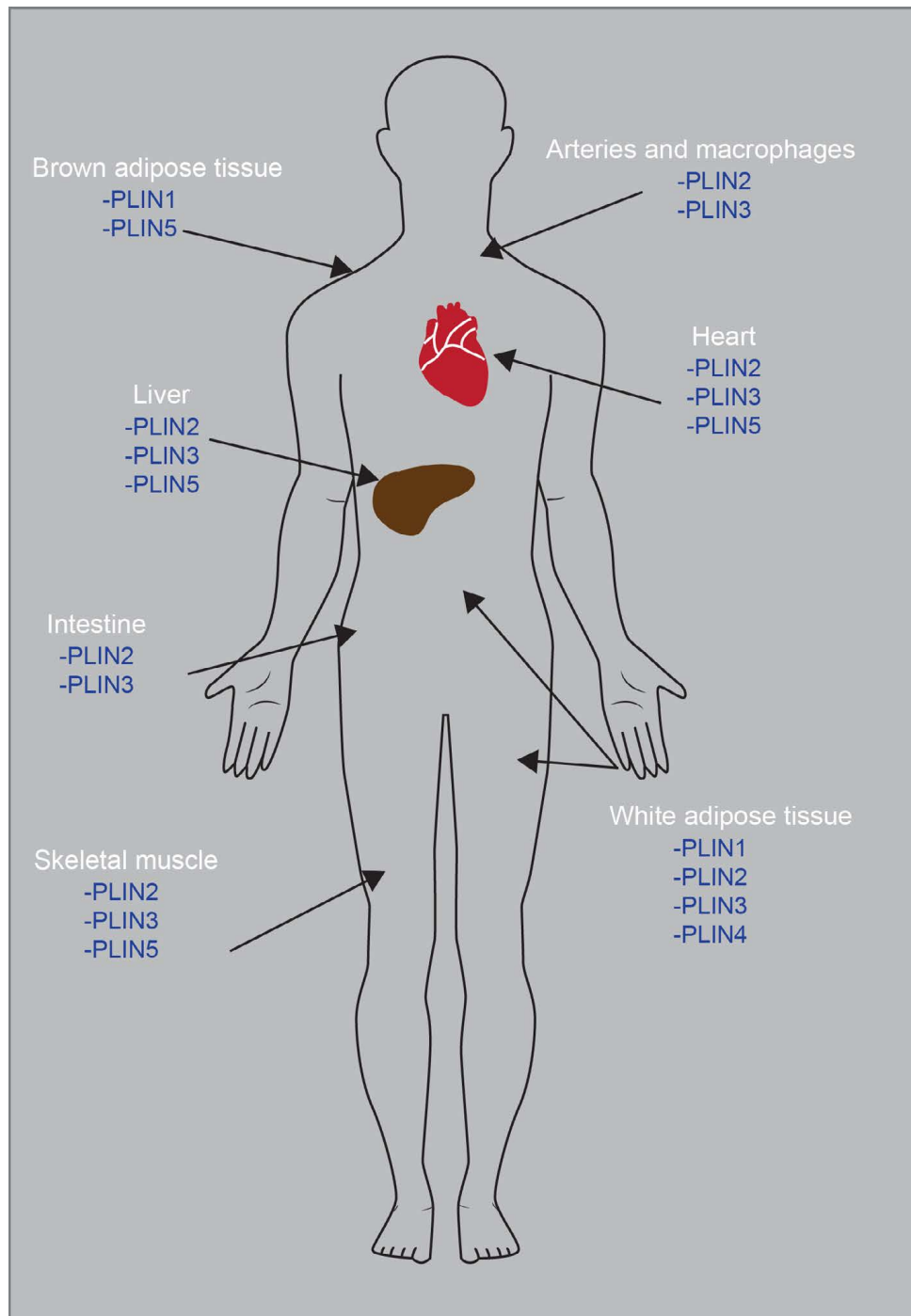
Figure 1.12.: Distribution of the PLIN proteins in the body

2. Aim of the dissertation

The Hepatitis C virus was identified in 1989 but the first first fully infectious cell culture model was established only in 2005. Since then, major advance has been made in understanding virus replication and virus-host interactions. However, the late steps of the life cycle, virion morphogenesis and release, are still poorly understood. Lipid droplets are hijacked by HCV for these late steps as the virus utilizes them as assembly platforms for viral particles. Lipid droplets are cytosolic storage organelles for lipids (and proteins) with several lipid droplet–associated proteins embedded in the surface of the surrounding phospholipid monolayer. The perilipin protein family (PLIN1-5) belongs to the lipid droplet–associated proteins and all of them are involved in regulating lipid droplet homeostasis. A functional role of the facultative lipid droplet–binding protein PLIN3 in HCV replication has already been investigated, revealing a dependence of HCV RNA replication on PLIN3 expression. On a molecular level, PLIN3 interacts with the non-structural protein NS5A of HCV and thereby mediates a tight association of RNA replication complexes with lipid-rich cell fractions. However, in hepatocytes the major coat protein of lipid droplets is PLIN2. Therefore, the aim of this thesis was to investigate in molecular detail the role of PLIN2 in regulating lipid droplet homeostasis and lipid metabolic processes and its putative impact on HCV infection.

3. Results

3.1. PLIN2 is required for HCV replication

3.1.1. Validation of the downregulation of PLIN2

Lipid droplets are cellular organelles essential for HCV infection as they are serving as putative assembly sites (Herker et al., 2011). In the hepatocytes and hepatoma cells permissive for HCV, PLIN2 is the major lipid droplet–coating protein (Fujimoto et al., 2004; Conte et al., 2016). To investigate if the protein itself or the lipid droplet homeostasis regulated by PLIN2 is required for HCV replication, knockdown experiments were performed. Therefore, lentiviral particles encoding a small hairpin RNA (shRNA) targeting PLIN2 or a non-targeting (NT) RNA were generated. This lentiviral vector additionally carries the fluorescence marker mCherry, enabling to monitor the transduction efficiency via flow cytometry. For all cell culture experiments in this study the human hepatoma cell line Huh7.5 was used (Figure 3.1A). The knockdown efficacy was validated on mRNA as well as on protein levels (Figure 3.1B, C). qRT-PCR analysis revealed a significant downregulation of *PLIN2* mRNA expression of almost 75%. In addition, western blot analysis showed that the protein was almost abolished at day five post transduction (dpT) and stably reduced for at least 15 days post transduction when compared to control. To exclude any cytotoxic side effects of the downregulation, the viability of the knockdown cells was investigated. As shown in figure 3.1D, silencing of PLIN2 had no influence on cell viability.
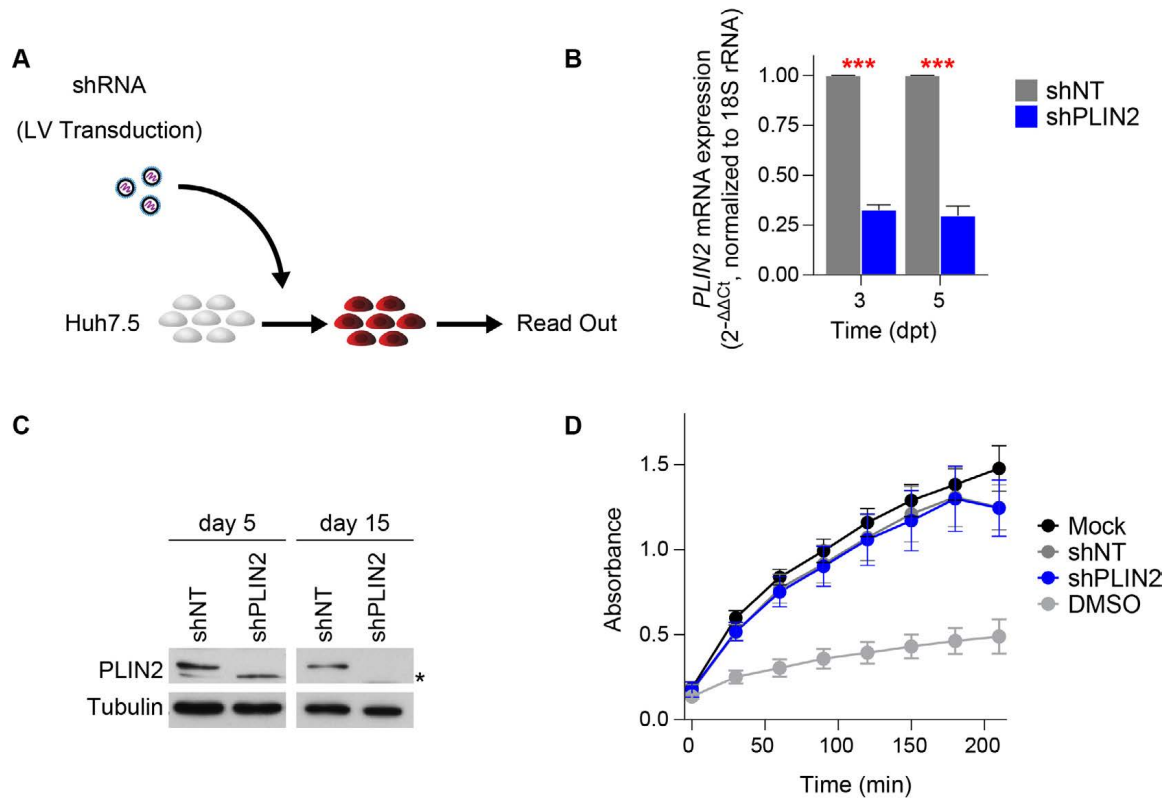
Figure 3.1.: Generation of PLIN2-knockdown cells

(A) Experimental set up to investigate PLIN2 knockdown efficacy and cell viability. (B) Knockdown efficacy on mRNA level was measured by qRT-PCR three and five days post transduction. Shown are the $2^{-\Delta\Delta Ct}$ values relative to shNT control and normalized to 18S rRNA (Mean $\pm$ SEM, n = 6-7, **$p <$ 0.001) (C) The knockdown efficacy on protein level was measured five and 15 days post transduction via western blotting. Tubulin served as a loading control. Asterik marks unspecific band. (D) The viability of mock and lentivirus transduced cells was determined using the CellTiter 96 AQueous One Solution assay five days post transduction. Cells treated with 5% DMSO served as a negative (dead) control. The amount of produced formazan was measured by the absorbance at 490 nm over the time (Mean $\pm$ SEM, n = 5-6).

3.1.2. Viral spreading is impaired in cell lacking PLIN2

Next, the shNT- and shPLIN2-transduced cells were infected with an HCV Jc1 reporter strain carrying an EGFP fluorescent reporter in between a duplicated NS5AB cleavage site (Jc1$^{NS5AB\text{-}EGFP}$) (Figure 3.2 A). This construct enables to measure the viral spreading via flow cytometry (Webster et al., 2013). Spreading efficiency was monitored two, four, and six days after infection with an MOI of 0.01 or 0.001 (Figure 3.2 B). The shPLIN2-transduced cells showed a significant reduced viral spreading compared to shNT control. This phenotype was more prominent in cells infected with the lower MOI. Due to the experimental variances, the significance was only reached when normalized to control (Figure 3.2 C).
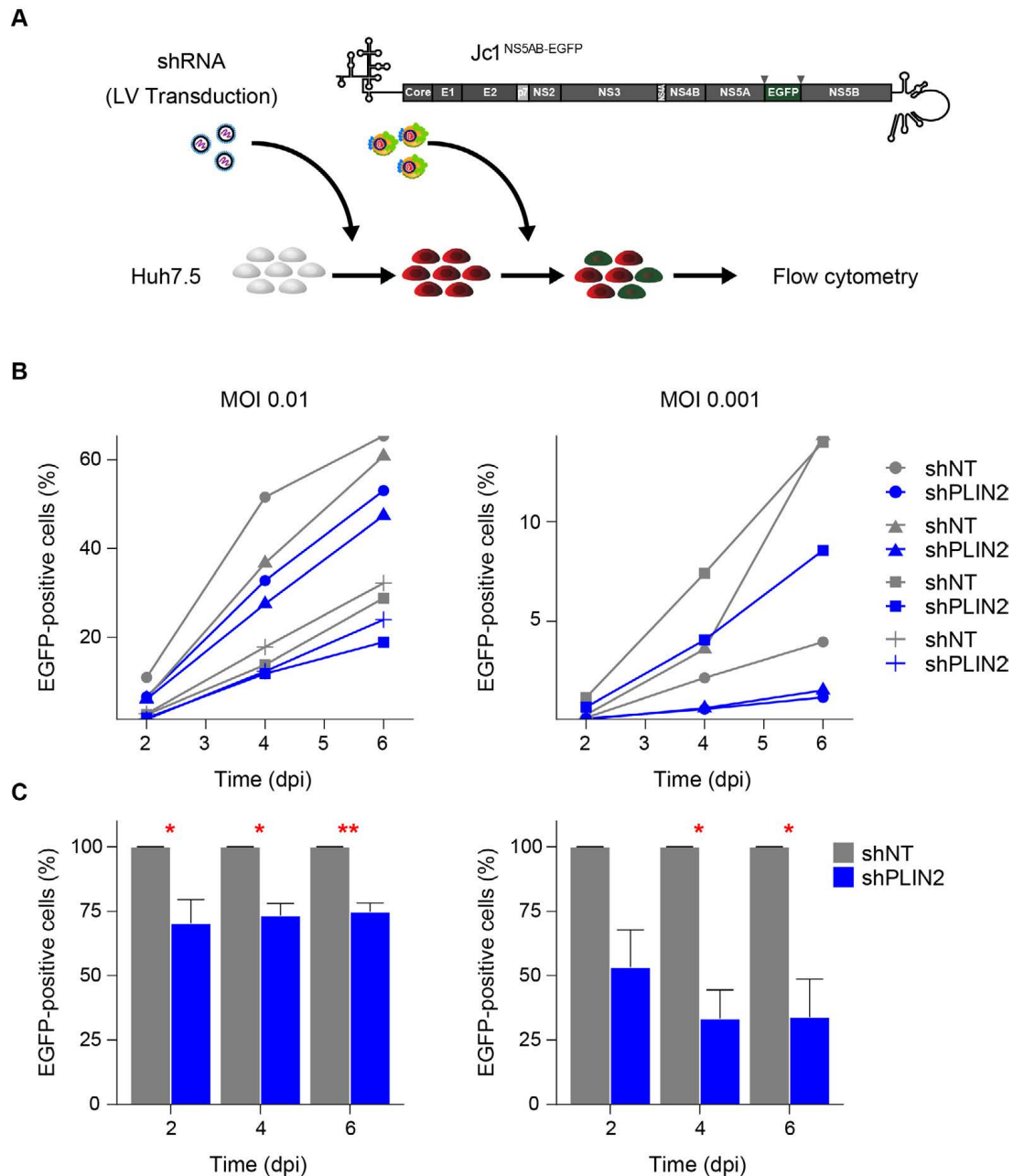
Figure 3.2.: Depletion of PLIN2 strongly reduced viral spreading

(A) Scheme of the experimental set up. Huh7.5 cells were transduced with lentiviral particles and infected with Jc1[NS5AB-EGFP] three days post transduction. Viral spreading was monitored by flow cytometry two, four, and six days post infection. (B) The shNT- and shPLIN2-transduced cells were infected with Jc1[NS5AB-EGFP] with an MOI of 0.01 or 0.001. The cells were harvested and fixed with 2% paraformaldehyde at the indicated time point. Viral spreading was measured by detecting the EGFP signal by flow cytometry. Shown is the amount of EGFP-positive cells gated on the mCherry-positive, live, single-cell population. (C) Results of B are shown as % of shNT control (Mean $\pm$ SEM, n = 3-4 *$p < 0.05$, **$p < 0.01$).

3.1.3. HCV entry factors are unaffected by PLIN2-knockdown

PLIN2 expression has been previously linked to expression of occludin, one of the HCV receptors essential for HCV entry (Branche et al., 2016). To investigate if the reduced viral spreading is due to an impaired HCV entry process, the expression of different surface receptors involved in virus entry was analyzed via western blot or by flow cytometry (Figure 3.3). First, the protein levels of the surface receptors CLDN1, OCLN and SCARB1 in uninfected and HCV-infected were analyzed. As shown in chapter 3.1.2, the viral spreading of the shPLIN2-transduced cells was impaired. To exclude an impact of the different viral spreading rates of the virus between the shNT- and shPLIN2-transduced cells, which might influence the expression of the surface receptors, Huh7.5 cells were first infected with Jc1$^{NS5AB-EGFP}$. The infection rate was determined by monitoring the EGFP expression marker by flow cytometry. In all performed experiments, the cells were over 80% HCV-positive before the knockdown was introduced. No major differences in the protein levels of CLDN1, OCLN or SCARB1 were detectable by western blot analysis, neither in the HCV-infected nor in the uninfected cells (Figure 3.3 A). To analyze the expression of the surface marker CD81, western blot analysis should either be performed under non-reducing conditions or by surface staining following analysis by flow cytometry (Fritzsching et al., 2002). In addition, the LDL receptor could not be detected by western blotting. Therefore, the expression of the receptor was also analyzed by surface staining. This was performed without the use of enzymes for detachment of the cells to avoid the digest of the entry receptors on the surface of the cells (Guevin et al., 2009) (Figure 3.3 B). Non-transduced Huh7.5 cells only stained with the secondary antibody were clearly separated from the shNT- and shPLIN2-transduced cells which were stained with the specific antibody and the secondary antibody. No major differences between the two lentiviral transduced cell populations were observed (Figure 3.3 B). These results show that the expression of HCV entry factors is not influenced by the PLIN2-knockdown, indicating that the entry process is not dependent on PLIN2.
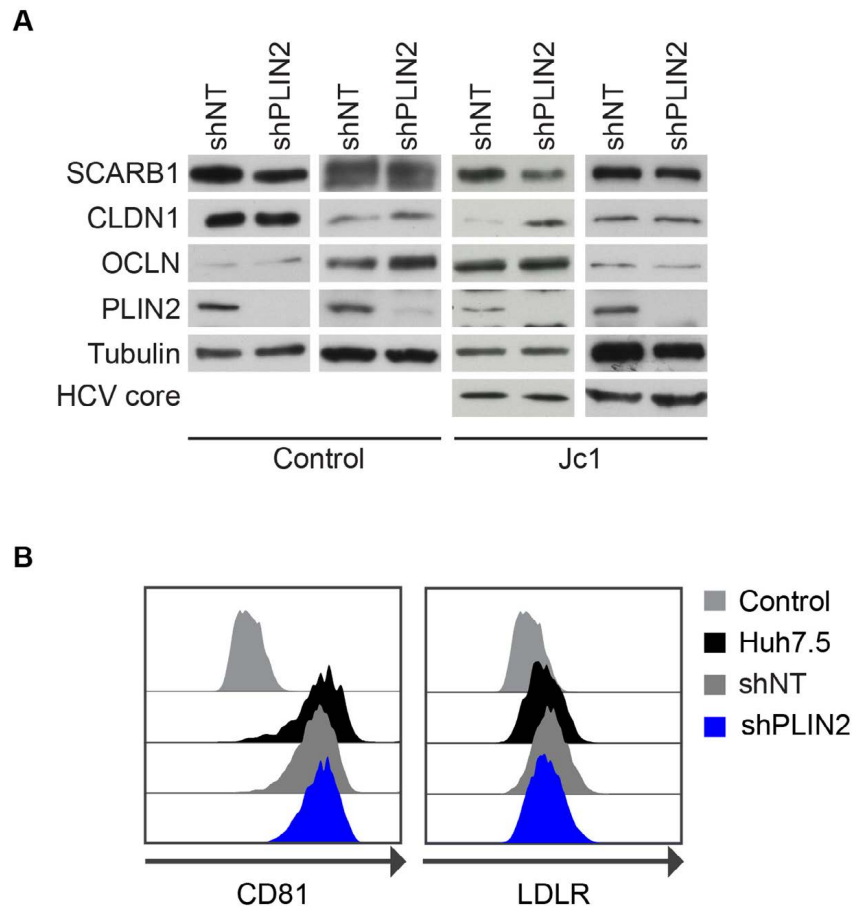
Figure 3.3.: PLIN2 does not influence the expression of HCV entry factors

(A) Two representative western blots of PLIN2-depleted and control cells. Lysates of uninfected and HCV-infected cells were analyzed for the expression of the surface receptors SCARB1, CLDN1 and OCLN. Knockdown was determined using an antibody specific for PLIN2. HCV infection was verified using an antibody detecting the HCV core protein. (B) Flow cytometry analysis of uninfected but transduced Huh7.5 cells stained with antibodies detecting CD81 and the LDL receptor. Staining with a secondary antibody alone served as control for unspecific binding of the secondary antibody (light grey).

3.1.4. HCV RNA replication is independent of PLIN2

Next, HCV RNA replication was investigated by transfecting the shPLIN2- and the shNT-transduced cells with a subgenomic bicistronic HCV replicon (genotype 1b, Con1 SGR) carrying a neomycin resistance gene (Choi et al., 2004). The Con1 SGR cells were cultured in media containing 1 mg/ml G418 for 2–3 weeks followed by crystal violet staining of the HCV replication competent colonies. The PLIN2-depleted cells had slightly less surviving colonies compared to the control cells (Figure 3.4 B). As the Con1 SGR assay lacks an internal transfection control and needs long-term cultivation, a second reporter was used to further investigate RNA replication. This replicon system harbors a luciferase in between a duplicated NS5AB cleavage site and does not harbor the envelope proteins E1 and E2 (Jc1$^{\Delta E1E2NS5AB\text{-}Luc}$) (Figure 3.4 C). By carrying the firefly luciferase, this reporter enables to normalize to the transfection efficiency and to measure RNA replication at early time points after electroporation. The shPLIN2-transduced cells showed a reduced HCV RNA replication capability at the first time point post transfection when compared to control. However, two and three days after electroporation, the luciferase activity of the PLIN2-silenced and control cells was only slightly and non-significantly reduced, indicating that HCV RNA replication is generally independent of the PLIN2 expression.
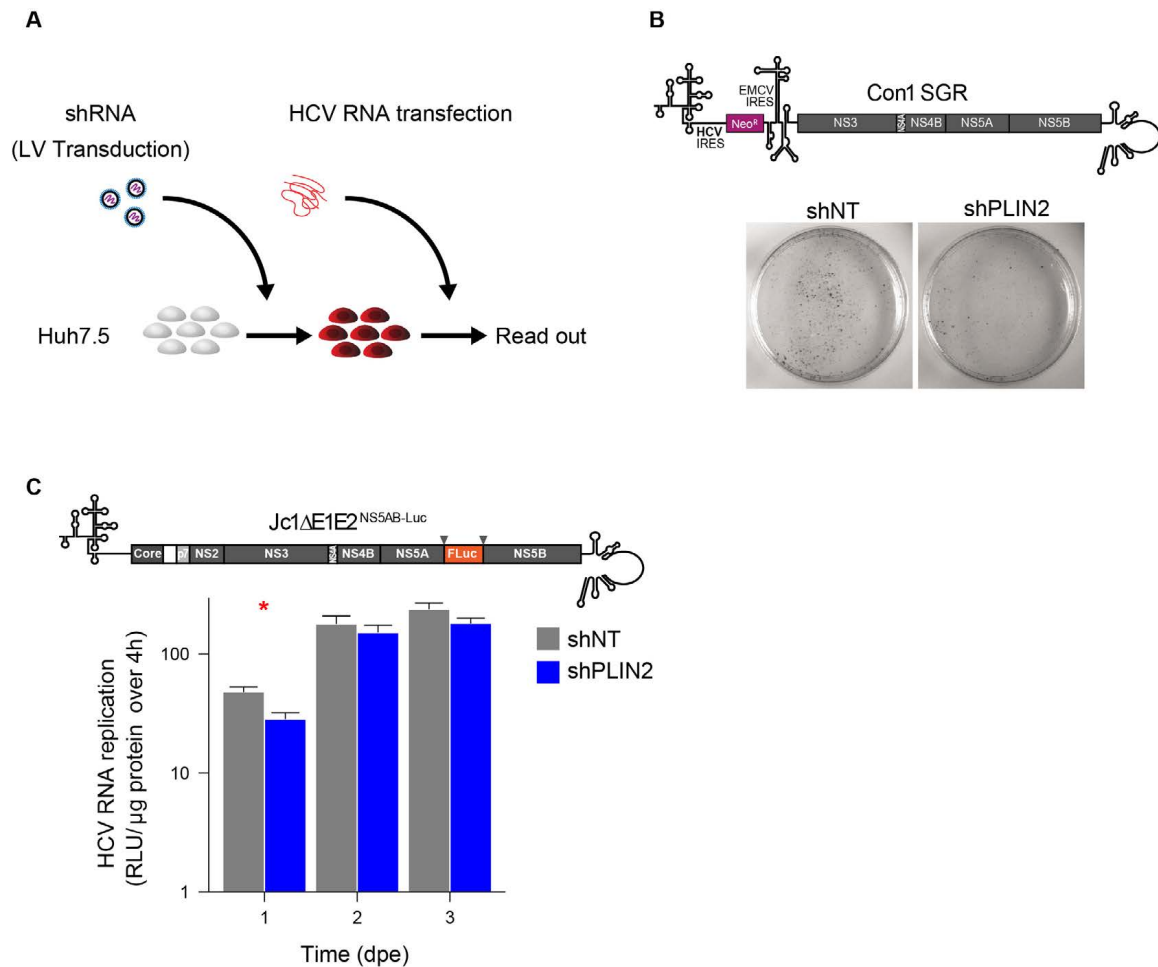
Figure 3.4.: HCV RNA replication is only slightly impaired in shPLIN2-transduced cells

(A) Scheme of the experimental set up. (B) shNT- and shPLIN2-transduced cells were transfected with *in vitro* transcribed Con1 SGR RNA carrying a neomycin resistance gene. The Con1 SGR cells were kept under selective pressure for 2–3 weeks followed by crystal violet staining of the replication competent colonies. (C) shNT- and shPLIN2-transduced cells were electroporated with Jc1$^{\Delta E1E2NS5AB-Luc}$ RNA. Luciferase activity (relative light units, RLU) was measured at the indicated time points, normalized to protein level and is shown as fold change over the 4 h time point (Mean $\pm$ SEM, n = 3, *$p < 0.05$).

To investigate if the RNA translation into viral proteins is impaired in cells lacking PLIN2, naïve Huh7.5 cells were first infected with Jc1$^{NS5AB-EGFP}$. The infection rate was determined by monitoring the EGFP expression marker by flow cytometry. After an infection rate above 80%, the knockdown was introduced. Five days post transduction the cells were harvested and analyzed for the protein expression of the HCV capsid protein core protein and NS5A by western blotting (Figure 3.5). As for the RNA replication, no major differences in HCV RNA translation were observed in the PLIN2-depleted cells compared to the control cells.
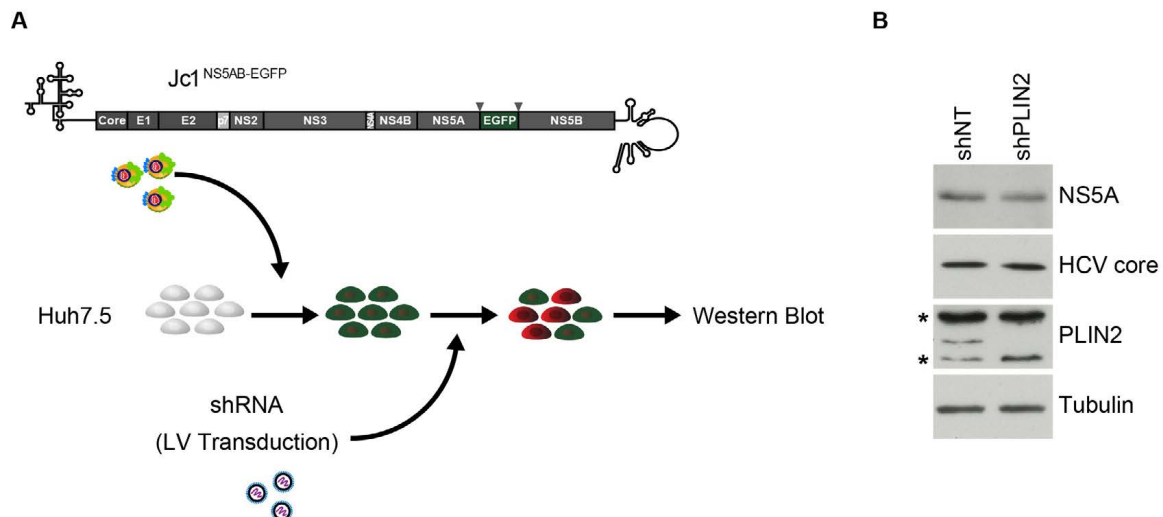
Figure 3.5.: HCV RNA translation into protein is independent of PLIN2

(A) Scheme of the experiment. Naïve Huh7.5 cells were infected with Jc1$^{NS5AB-EGFP}$ before the cells were transduced with lentiviral particles targeting PLIN2 or shNT control. Five days post transduction, the cells were harvested and used for the analysis of viral protein expression by western blotting. (B) Shown is one representative western blot. Cell lysates were analyzed by using antibodies detecting PLIN2, HCV core and NS5A. Tubulin served as a loading control. Asterisks mark unspecific bands.

3.1.5. PLIN2 is required for the production of infectious viral particles

To investigate whether the decreased spreading is due to an impaired virion production, shPLIN2- and shNT-transduced cells were electroporated with *in vitro* transcribed Jc1$^{NS5AB-EGFP}$ RNA. Three days post transfection, equal transfection rates were verified by detecting the expressed EGFP reporter signal via flow cytometry. Afterwards, the cells were seeded at the same density in 6-well plates and the supernatant was harvested after two, four, and six days (Figure 3.6 A). The viral RNA was isolated and the secreted HCV genome copy number was measured by qRT-PCR. Indeed, the HCV copy number was significantly decreased in cells lacking PLIN2 at day four and six post transfection (Figure 3.6 B). In line with the reduced HCV copy number, the core protein secretion was severely impaired in shPLIN2-transduced cells measured by ELISA in parallel to the viral RNA analysis (Figure 3.6 C). As the HCV copy number does not reflect the infectivity of the released virions into the supernatant (Lindenbach et al., 2005) and viral particles that are secreted can vary regarding their infectivity (Gastaminza et al., 2010), the infectivity of the supernatant was determined by measuring the 50% tissue culture infective dose (TCID$_{50}$) by limiting dilution on Huh7.5-RFP-NLS-IPS reporter cells (Figure 3.6 D-E). As expected, approximately only 1 out of 1000 HCV genome RNAs was infectious in the control cell line, which is comparable to what others measured (Keum et al., 2012). In line with the observed reduced HCV copy number and the reduced amount of the capsid protein core, the infectivity of the supernatant of the shPLIN2-transduced cells was significantly reduced compared to the control cells.
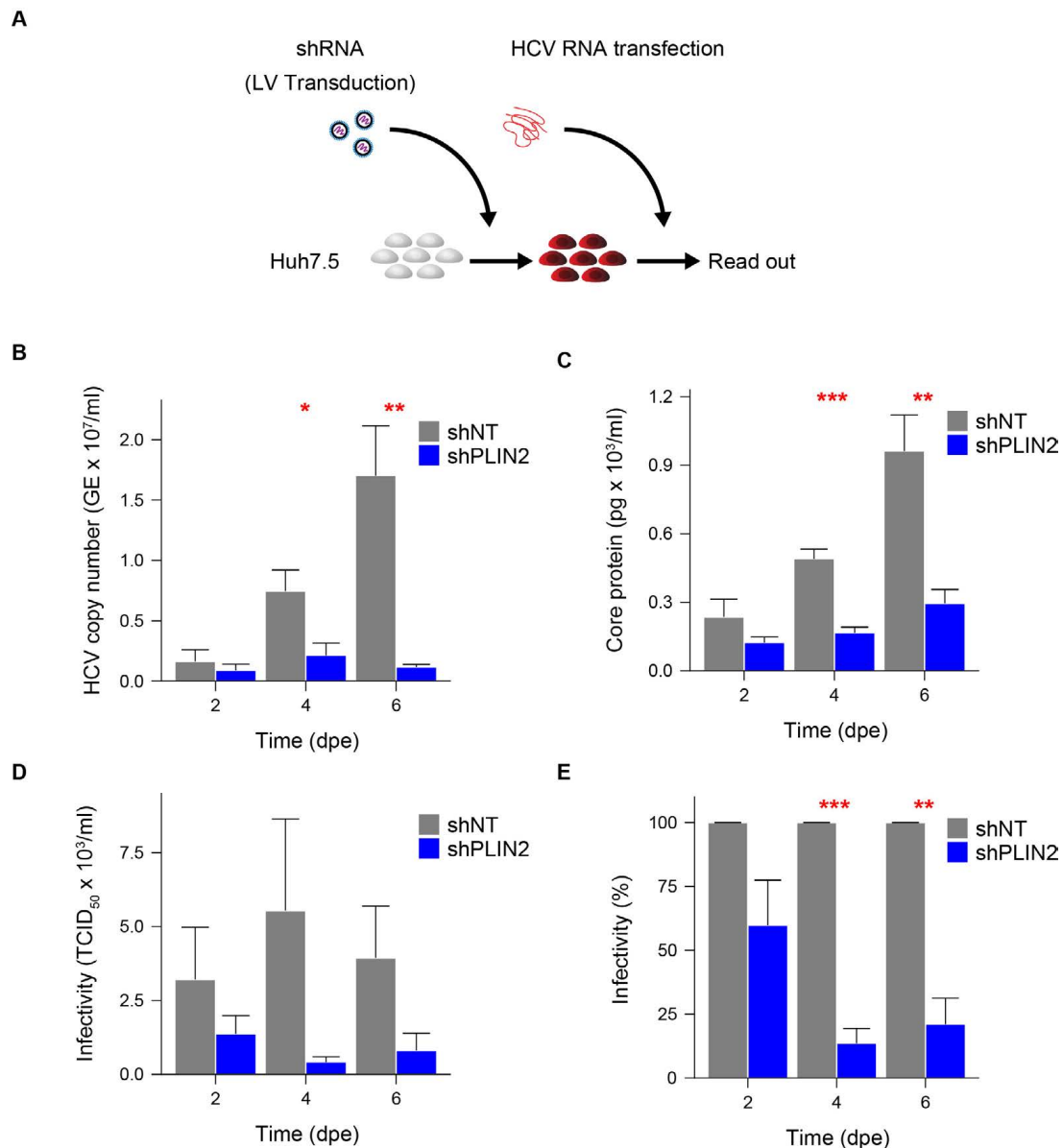
Figure 3.6.: PLIN2 is important for the production of infectious viral particles

(A) Scheme of the experiments. Huh7.5 cells were transduced with lentiviral particles targeting PLIN2 or shNT control. After stable integration, the cells were electroporated with *in vitro* transcribed HCV RNA (Jc1[NS5AB-EGFP]). Equal transfection rates were verified by flow cytometry. The supernatant was harvested at the indicated time points and analyzed for the HCV copy number, secretion of capsid protein core and for the infectivity of the supernatant. (B-E) Extracellular HCV RNA was isolated and (B) HCV copy number (GE/genome equivalents) was determined by qRT-PCR at indicated time points (Mean $\pm$ SEM, n = 5-8, $*p < 0.05$, $**p < 0.01$). (C) The secretion of the HCV core protein was measured by ELISA (Mean $\pm$ SEM, n = 4-6, $**p < 0.01$, $***p < 0.001$). (D, E) To determine the infectivity of extracellular viral particles, TCID$_{50}$ measurements by limiting dilution titration on Huh7.5-RFP-NLS-IPS reporter cells were performed. Shown are the absolute values and the percent of control at the indicated time points (Mean $\pm$ SEM, n = 5, $**p < 0.01$, $***p < 0.001$).

3.2. PLIN2 regulates lipid droplet homeostasis

3.2.1. PLIN2 knockdown slightly alters lipid droplet morphology

Lipid droplets are putative HCV assembly sites (Herker et al., 2012). Inhibition studies as well as knockdown studies of enzymes involved in the lipid droplet biogenesis clearly demonstrate the importance of these organelles for the production of infectious viral particles (Miyanari et al., 2007; Liefhebber et al., 2014). In addition, a previous study has shown that PLIN2 protein expression is upregulated after HCV infection (Branche et al., 2016). The morphology of lipid droplets seemed to be dependent on the expression of PLIN2 as the size as well as the lipid droplet number per cell increased in cells overexpressing PLIN2 (Imamura et al., 2002; Branche et al., 2016). Therefore, the morphology of lipid droplets in cells lacking PLIN2 was investigated by 3D confocal microscopy studies (Figure 3.7). For these experiments, the Huh7.5-RFP-NLS-IPS reporter cell line was used to distinguish between HCV-infected and uninfected cells. The RFP-NLS-IPS fusion protein is located at the mitochondria as the C-terminal IPS fragment harbors a mitochondrial localization sequence as well as the NS3/4A recognition site. Upon infection, the HCV N3/4A protease cleaves IPS. Due to the NLS sequence fused to RFP, the protein translocates to the nucleus (Jones et al., 2010). This reporter cell line was transduced with shNT- or shPLIN2-lentiviral particles carrying a puromycin resistance gene for selection of successfully transduced cells. The cells were treated with 1.5 μg/ml puromycin and after one week of selection, the knockdown was verified by western blotting (Figure 3.7 A). One publication has shown that PLIN2 is replaced on lipid droplets upon HCV infection (Boulant et al., 2008). Therefore, to investigate if HCV infection changes the lipid droplet morphology, the reporter cells were transduced with lentiviral particles targeting PLIN2 or control and one to three days post transduction, the cells were infected with Jc1$^{Flag-E2}$. Uninfected shPLIN2-transduced or control cells carrying the reporter were cultured in parallel. Then, the uninfected and HCV-infected of either PLIN2-depleted or control cells were mixed and were seeded on μ-dishes. The next day the cells were fixed for confocal microscopy. The lipid droplets of the cells were visualized with Bodipy493/503 and z-stacks were recorded to determine the lipid droplet volumes as well as lipid droplet number per cell by using the 3D object counter function of Fiji (Figure 3.7 B, C). The quantification of the lipid droplet volume revealed a significant increase of the size of lipid droplets in cells lacking PLIN2 compared to control. However, the magnitude of the increase was rather small: the median lipid droplet volume was only slightly increased ($\sim$18% or 0.015 μm^3) in cells silenced of PLIN2. In contrast, the number of lipid droplets was significantly decreased in shPLIN2-transduced cells. The infection with the HCV virus did not lead to an increase in the lipid droplet volume of both, the shPLIN2- and shNT-transduced cells. However, the lipid droplets of the shPLIN2-depleted cells were still larger in size. This effect was again significant but the change was fairly small ($\sim$11% or 0.0099 μm^3). The number of lipid droplets per cells and the total lipid droplet volume of the shPLIN2-transduced cells was similar to the infected shNT-transduced cells. Taken together, silencing of PLIN2 had only a minor effect on the lipid droplet morphology, leading to slightly increased median lipid droplet

volumes which is independent of an HCV infection.
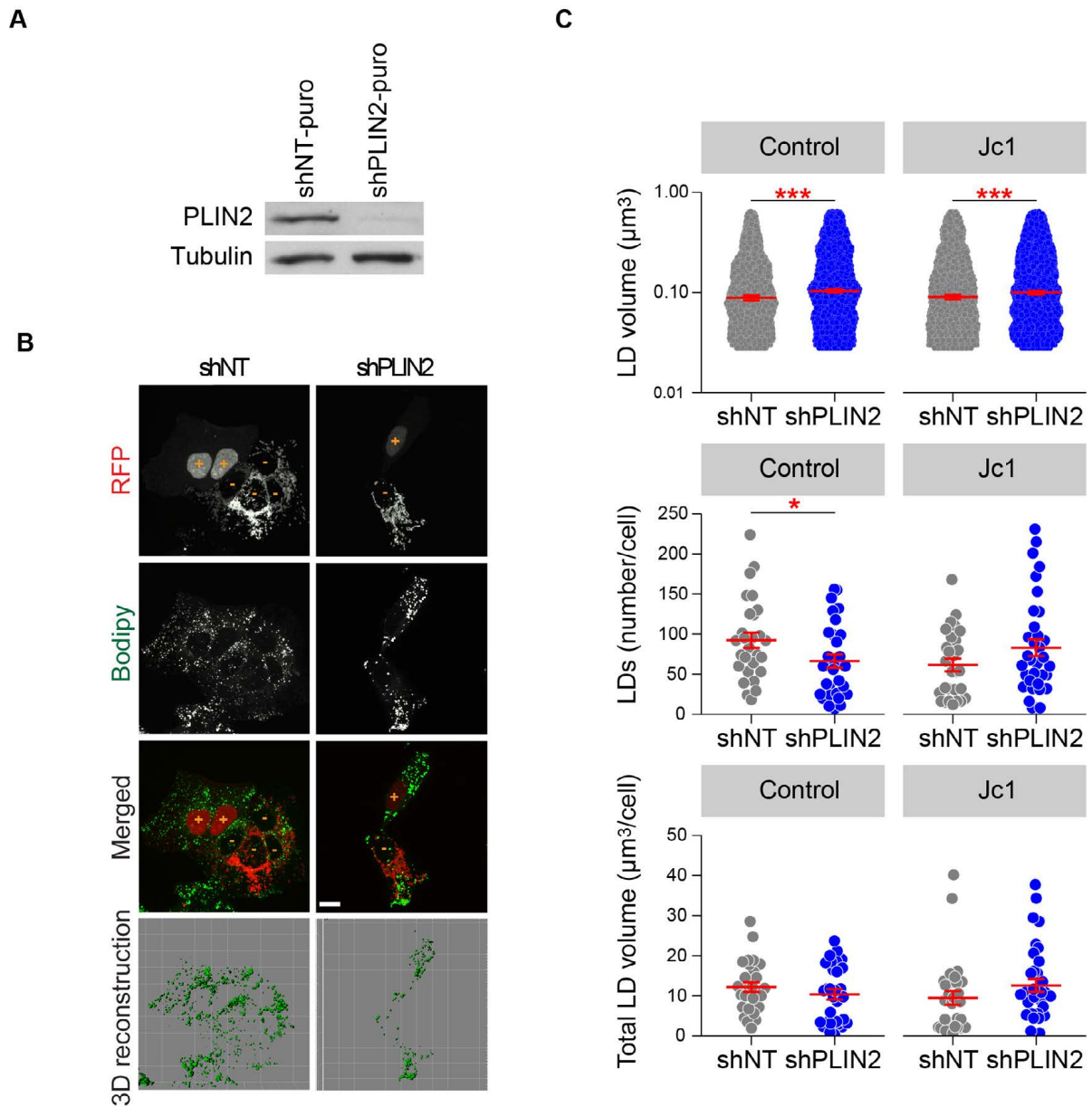
Figure 3.7.: PLIN2 changes the morphology of lipid droplets

(A) Western blot analysis to verify the knockdown of PLIN2 in Huh7.5 cells. Cells transduced with a lentivirus carrying the shRNAs and a selection marker were analyzed with an antibody detecting PLIN2. (B) Representative pictures of shNT- and shPLIN2-transduced cells. The Huh7.5-RFP-NLS-IPS reporter cell line was used to distinguish between HCV-infected (+) and uninfected cells (-). The RFP protein is located at the mitochondria in uninfected cells. Upon infection, the HCV N3/4A protease cleaves RPF-NLS from IPS and RFP-NLS translocates to the nucleus (Jones et al., 2010). The reporter was co-transduced with a lentivirus carrying shRNAs targeting either PLIN2 or control. Cells were fixed and the lipid droplets were stained with Bodipy493/503. Z-stacks were recorded on a spinning disk confocal microscope and a 3D image was constructed using Imaris Bitplane software. Scale bar 10 μm (C) The lipid droplet number and volume of three independent experiments were determined using the 3D objects function of Fiji (Mean $\pm$ SEM, number of cells = 28-34, $*p < 0.05$, $***p < 0.001$).

A major component of lipid droplets in hepatocytes are triglycerides (Fujimoto and Parton 2011) and a change in the lipid droplet morphology might be accompanied by alterations in triglyceride content. Therefore, and to confirm the microscopic analysis, the triglyceride levels of the shNT- and shPLIN2-transduced cells were analyzed. Cells were seeded at the same density in a 6-well plate, and after 24 h total lipids were extracted using the Bligh and Dyer method. The triglyceride concentrations were determined using the infinity triglyceride reagent revealing a slight but non significant reduction of the triglyceride content in the cells lacking PLIN2 compared to control (Figure 3.8).
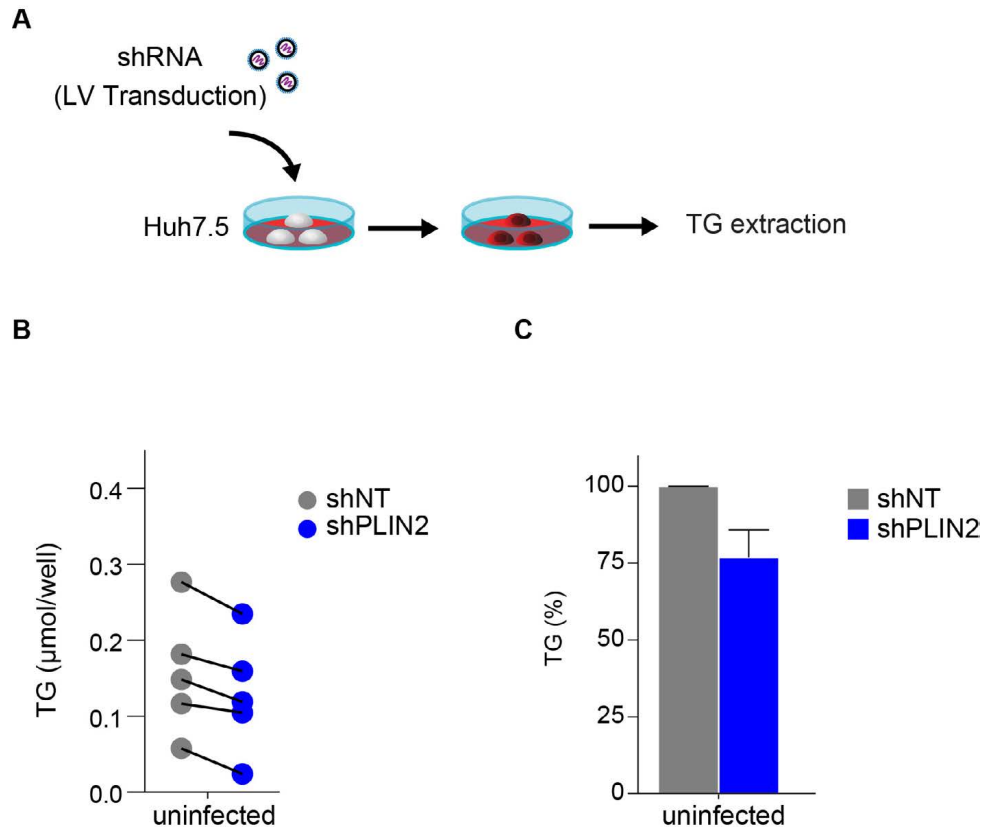
Figure 3.8.: Intracellular triglyceride levels are independent of PLIN2

(A) Scheme of the experiment. Five to six days post transduction with lentiviral particles targeting PLIN2 or control, the cells were seeded in a 6-well plate. One to two days later, the triglycerides were extracted using Bligh and Dyer method. The triglycerides level were measured using the infinity triglyceride reagent. (B) The amounts of triglycerides are shown in absolute values. The line demonstrates corresponding values of independent experiments. (C) Shown are the values as percent of control (Mean $\pm$ SEM, n = 5).

To examine if cells lacking PLIN2 are impaired in lipid droplet biogenesis following loading with fatty acids, uninfected shRNA-expressing Huh7.5 cells were cultured in media supplemented with oleate. This time, cells were transduced with shRNAs carrying a fluorescence marker to monitor the transduction efficiency by flow cytometry. Then, the cells were treated with oleate prior to microscopic analysis described above. As expected, the lipid droplet volume, lipid droplet number and the total lipid droplet volume per cell was increased upon oleate supplementation. This was observed in the PLIN2-depleted cells as well as in the control cells. Again, the lipid droplet volume of the PLIN2-silenced cells was significantly increased when compared

to control cells, both in cultures treated with or without oleate (Figure 3.9). However, the lipid droplet numbers and the total lipid droplet volumes per cell were similar between the shNT- and shPLIN2-transduced cells.
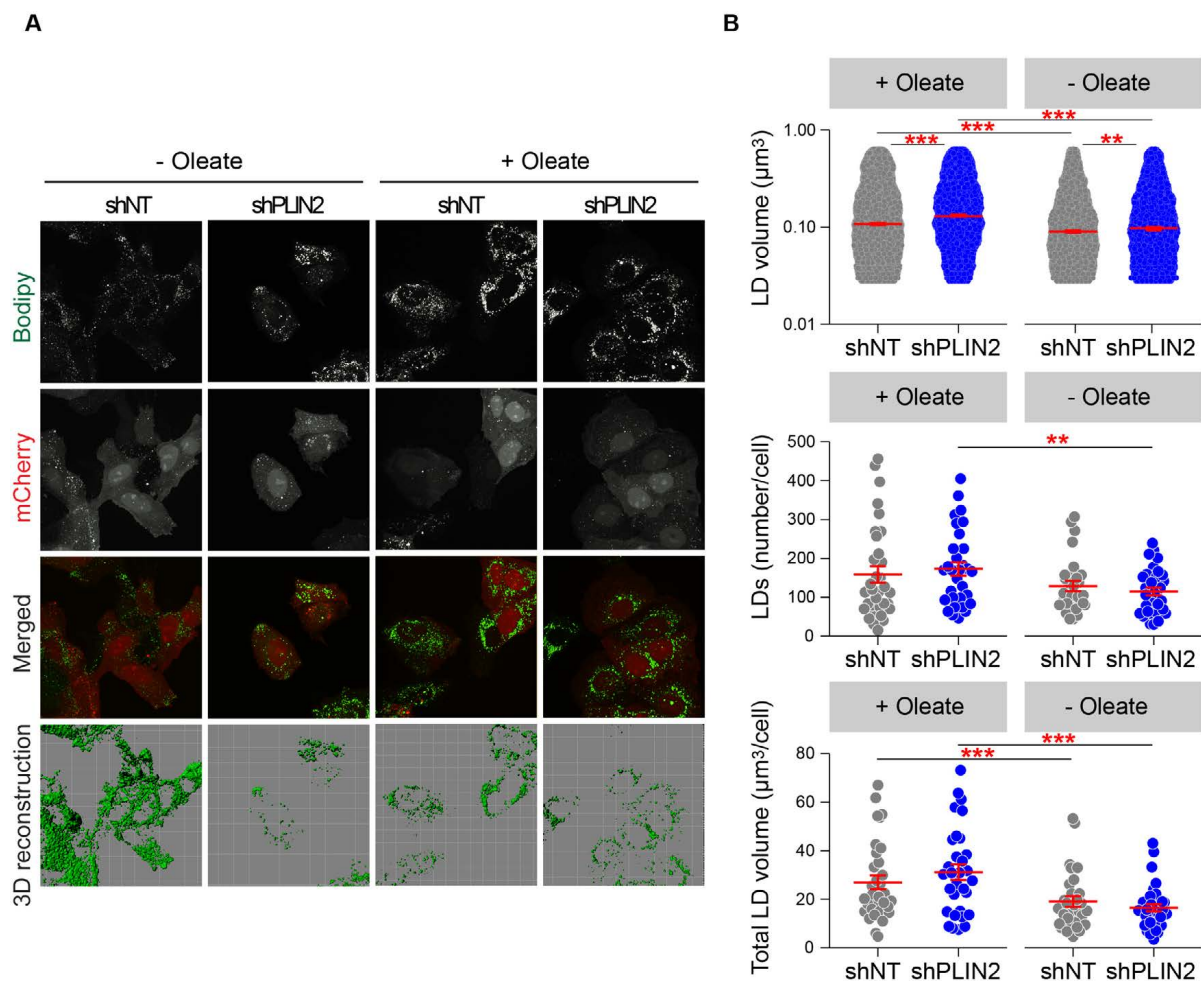
Figure 3.9.: Oleate treatment changes the morphology of shNT- and PLIN2-depleted cells in a similar manner

(A) Huh7.5 cells were transduced with a lentivirus carrying shRNAs targeting either PLIN2 or control. The cells were fixed and the lipid droplets were stained with Bodipy493/503. Z-stacks were recorded on a spinning disk confocal microscope. The 3D image was constructed using Imaris Bitplane software. Scale bar 10 μm. (B) The lipid droplet number and volume of two independent experiments was determined using the 3D object counter function of Fiji (Mean $\pm$ SEM, number of cells = 30-34).

Additionally, the intracellular levels of triglycerides of the oleate-treated PLIN2-depleted and control cells were determined. The lipid extraction and the measurement of the triglyceride levels was performed as described above. The triglyceride levels were increased in both, the shNT- and shPLIN2-transduced cells (compared to Figure 3.8). Interestingly, the cells lacking PLIN2 showed a significant reduction of ~30% triglycerides after oleate supplementation in the cell culture media compared to the oleate-treated control cells (Figure 3.10). Due to the experimental variances, the significance was only reached when normalized to control. The reduced triglycerides levels contrast with the microscopic analysis where no major changes were observed. This is likely due to the high variances in the lipid droplet content (volume and numbers) which reflects the natural biological variances from cell to cell. To obtain more robust results from microscopy, many more cells have to be analyzed. However, this result indicates a

reduced capacity to esterify oleate into triglycerides in the shPLIN2-transduced cells.
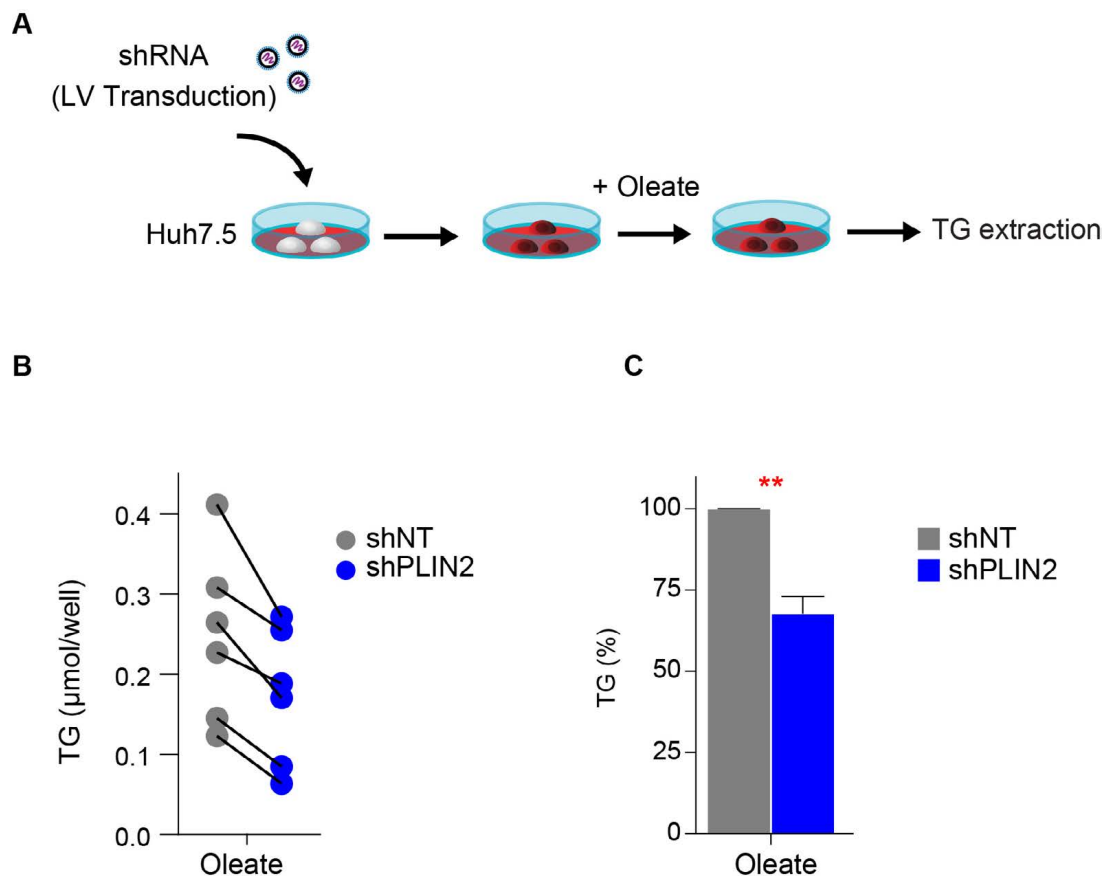
Figure 3.10.: PLIN2-knockdown cells have a reduced capacity to store oleate in triglycerides

(A) Scheme of the experiment. Five to six days post transduction with lentiviral particles targeting PLIN2 or control, the cells were seeded in a 6-well plate. The days before extraction, the cell culture medium was supplemented with oleate. Then, the triglycerides were extracted using Bligh and Dyer method. The triglycerides level were measured using the infinity triglyceride reagent. (B) The amounts of triglycerides are shown in absolute values. The line demonstrates corresponding values of independent experiments. (C) Shown are the values as percent of control (Mean $\pm$ SEM, n = 6).

3.2.2. Mitochondrial β-oxidation capacity is increased after PLIN2 depletion

To investigate if PLIN2-knockdown cells have enhanced maximal β-oxidation rates that might compensate the reduced capacity to esterify supplemented fatty acids, an assay to measure β-oxidation capacity with ^{14}C-labeled palmitate was performed. During β-oxidation the supplemented palmitate is oxidized by multiple steps to acyl-CoA in the mitochondria. Acyl-CoA then enters the TCA cycle, thereby generating NADH and FADH$_2$, which then is used by the oxidative phosphorylation pathway to generate multiple ATPs. The shNT- and shPLIN2-transduced cells were incubated with ^{14}C-labeled palmitate in the presence of carnitine to direct the palmitate towards β-oxidation. The production of ^{14}CO$_2$ as well as ^{14}C-containing acid soluble metabolites (ASM) was measured. To analyze the magnitude of esterification of free fatty acids with diglycerides, the cells were additionally treated with a DGAT1 inhibitor (Figure 3.11 A). This inhibitor blocks the final step of triglyceride biosynthesis by DGAT1. It is assumed that DGAT1 and not DGAT2 is the predominant enzyme catalyzing esterification of exogenous fatty acids in the liver

(Villanueva et al., 2009). Thus, the shNT-and shPLIN2-transduced cells were seeded in 6-well plate at the same density and the night before the assay was performed, the cells were treated with the DGAT1 inhibitor. Then, the cells were incubated with radiolabeled palmitic acid for 3 h before the supernatant was harvested for the analysis of the production of radioactive CO_2 and acid soluble metabolites (ASM). The amount of the released CO_2 as well as the ASMs of the shNT-transduced cells treated with the inhibitor was similar to the CO_2 and ASM without the treatment with the DGAT1 inhibitor. This indicates that under the experimental conditions used in this study, the supplemented palmitate is not incorporated into triglycerides but undergoes β-oxidation (Figure 3.11 B). Intriguingly, cells depleted for PLIN2 had significantly increased maximal levels of β-oxidation compared to control cells, both in presence or absence of DGAT1 inhibition.
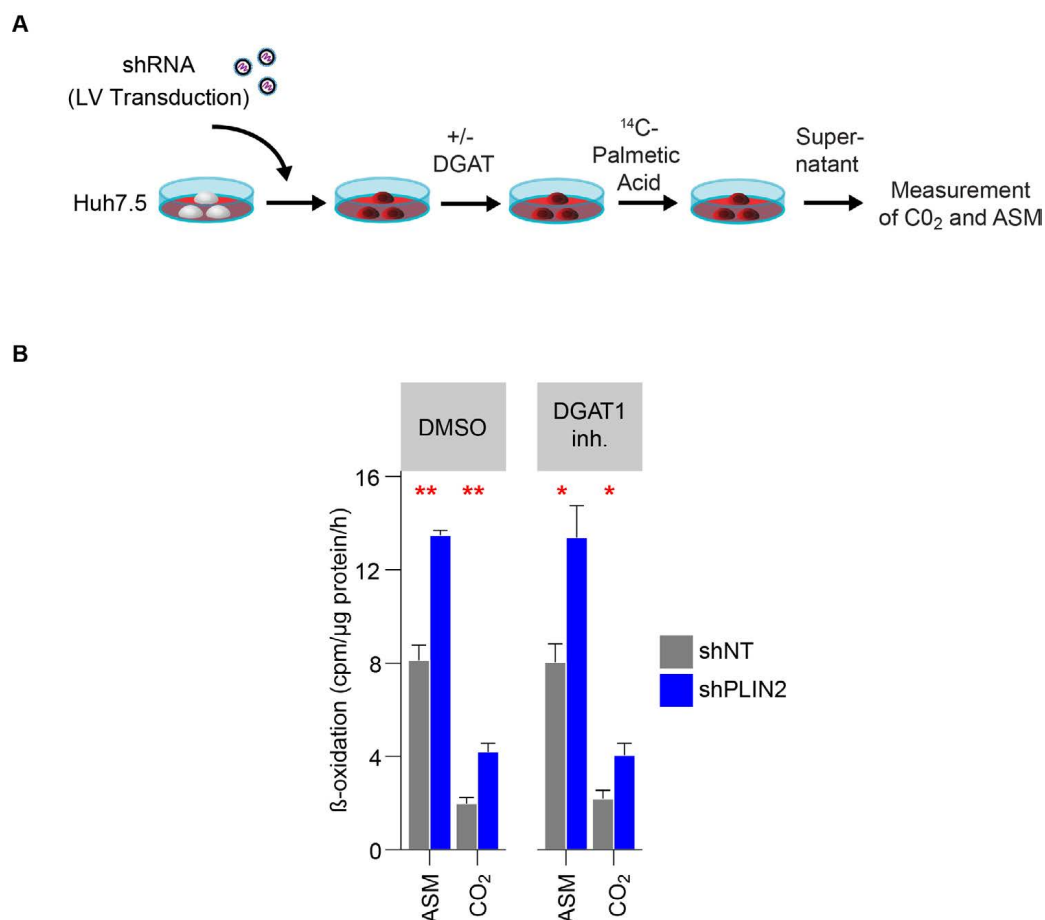
Figure 3.11.: The β-oxidation rate is higher in cells lacking PLIN2 independent of the treatment with DGAT1 inhibitor

(A) Scheme to measure the mitochondrial β-oxidation capacity. Naïve Huh7.5 cells were transduced with lentivirus targeting PLIN2 or control. After stable integration, the cells were seeded in a 6-well plate. The night before the assay was performed, the cells were treated with a DGAT1 inhibitor or DMSO control. The next day the cells were incubated with radiolabeled palmitic acid for 3 h before the supernatant was harvested for the analysis of the production of radioactive CO_2 and acid soluble metabolites (ASM). (B) Shown are the counts per minute (CPM) normalized to mg protein (Mean $\pm$ SEM, n = 4, *$p < 0.05$, **$p < 0.01$).

To investigate if PLIN2-knockdown cells harbor more mitochondria, which might explain the higher β-mitochondrial rates, or if the mitochondria have an increased β-oxidation capacity, western blot analysis of uninfected and HCV-infected cells transduced with lentivirus targeting PLIN2 or control were performed (Figure 3.12 A). However, no major differences in the expression level of the mitochondrial marker MnSOD were observed between the PLIN2-depleted and control cells, neither in the HCV-infected nor in the uninfected cells. This indicates that the shPLIN2-transduced cells harbor mitochondria with an increased β-oxidation capacity (Figure 3.12 B).

A

B
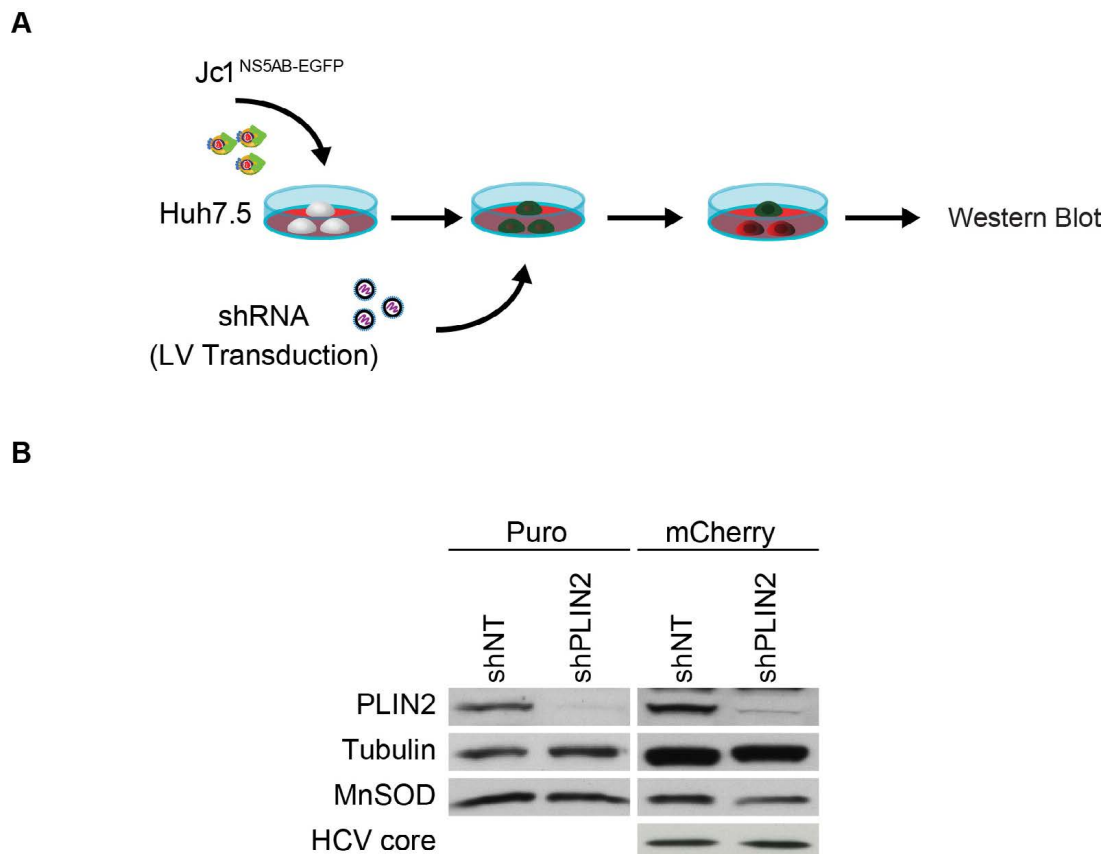
Figure 3.12.: PLIN2-depleted cells do not harbor more mitochondria

(A) Scheme of the experiment. HCV-infected or uninfected cells were transduced with lentiviral particles targeting PLIN2 or control. Cells were either transfected with a lentivirus harboring the puromycin resistance gene or a mCherry marker. The cells carrying the mCherry marker were harvested eight days post transduction for western blotting. Cells harboring the selection marker were cultured in medium containing 1.5 μ/ml puromycin and after one week of the selection, the cells were harvested for western blotting to analyze the expression level of the mitochondrial marker MnSOD. (B) Representative western blot of cells transduced with the lentivirus harboring the puromycin resistance gene or the mCherry marker. The same western blot of the cells transduced with the lentivirus harboring the puromycin resistance gene is shown in figure 3.7 Antibodies detecting PLIN2, MnSOD or HCV core were used. Tubulin served as a loading control.

Nevertheless, it has been shown that an HCV infection negatively affects the function of mitochondria and thereby reduces β-oxidation rates (Amako et al., 2015). To address the question if expression of core protein influenced the fatty acid oxidation in this cell culture system and might counteract the loss of PLIN2, the mitochondrial β-oxidation in cells expressing core of two

different genotypes was analyzed. Therefore, the Huh7.5 cells were transduced with lentiviral particles expressing the core protein or with lentiviral particles of the respective empty vector control. Then, the knockdown of PLIN2 was introduced by a second lentiviral transduction (Figure 3.13 A). Next, the cells were analyzed as described above. Again, the production of the ASM and the amount of the released $^{14}CO_2$ was higher in the empty vector transduced shPLIN2-transduced cells when compared to the empty vector control cells. In addition, the β-oxidation rate was unaffected by core-expression, neither in the shNT-expressing cells nor in the PLIN2-depleted cells. The shPLIN2-transduced cells still showed enhanced β-oxidation capacity in a similar manner, independent of core expression (Figure 3.13 B-C). Taken together, downregulation of PLIN2 increases β-oxidation capacity of cells and this phenotype is not reversible by the expression of the capsid protein core.
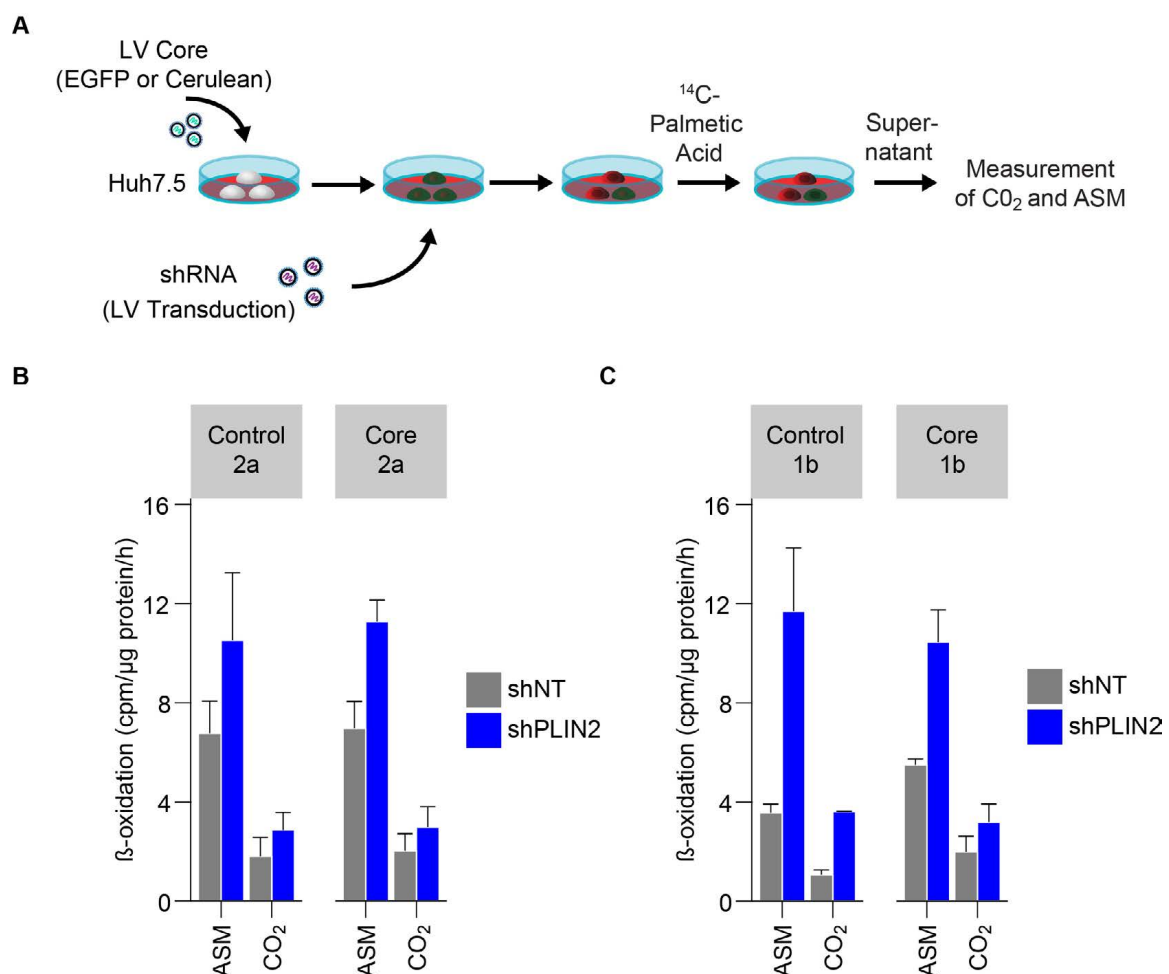
Figure 3.13.: The mitochondrial β-oxidation capacity is increased in PLIN2-depleted cells

(A) Scheme to measure the mitochondrial β-oxidation capacity. Naïve Huh7.5 cells or core-expressing cells (genotype 1b or 2a) were transduced with lentivirus targeting PLIN2 or control. After stable integration, the cells were treated with radiolabeled palmitic acid for 3 h before the supernatant was harvested for the analysis of the production of radioactive CO_2 and acid soluble metabolites (ASM). (B-C) The production of radioactive CO_2 and acid soluble metabolites (ASM) of transduced cells with or without an additional core protein expression was measured. Shown are the counts per minute (CPM) normalized to mg protein (Mean $\pm$ SEM, n = 2).

3.2.3. The triglyceride turnover rates in Jc1-infected cells are dependent of PLIN2 protein levels

Afterwards, the influence of the enhanced β-oxidation capacity on the triglyceride metabolism was investigated by performing pulse-chase experiments. Therefore, shNT- and shPLIN2-transduced cells seeded at the same density in a 6-well plate were pulsed with oleate and chased in serum-free media containing the acyl-CoA synthase inhibitor triacsin C to prevent re-esterification of the released free fatty acids. This allowed measuring only triglyceride degradation (Figure 3.14 A). Of note, triacsin c does not inhibit β-oxidation capacity of cells (Muoio et al., 2000). The triglyceride content stored in the cells as well as the amount of released free fatty acids into the supernatant was measured at different time points during the chase. In uninfected cells, a steady decrease in triglyceride levels and a steady increase of the released free fatty acids during the chase independent of PLIN2 expression was observed (Figure 3.14 B). Former studies have shown that the HCV capsid protein core is capable to stabilize triglycerides and thus decrease lipid droplet turnover (Harris et al., 2011). Indeed, in HCV-infected cells a stabilization of the triglyceride turnover rates were observed, but only in the shNT-transduced cells (Figure 3.14B). This result indicates that the triglyceride turnover rates in Jc1-infected cells are dependent of PLIN2 expression. Remarkably, the amount of free fatty acids in the supernatant did not show differences between PLIN2-knockdown and control cells during the chase, neither in the uninfected cells nor in the infected cells indicating that the released fatty acids are likely used for β-oxidation.

A

B
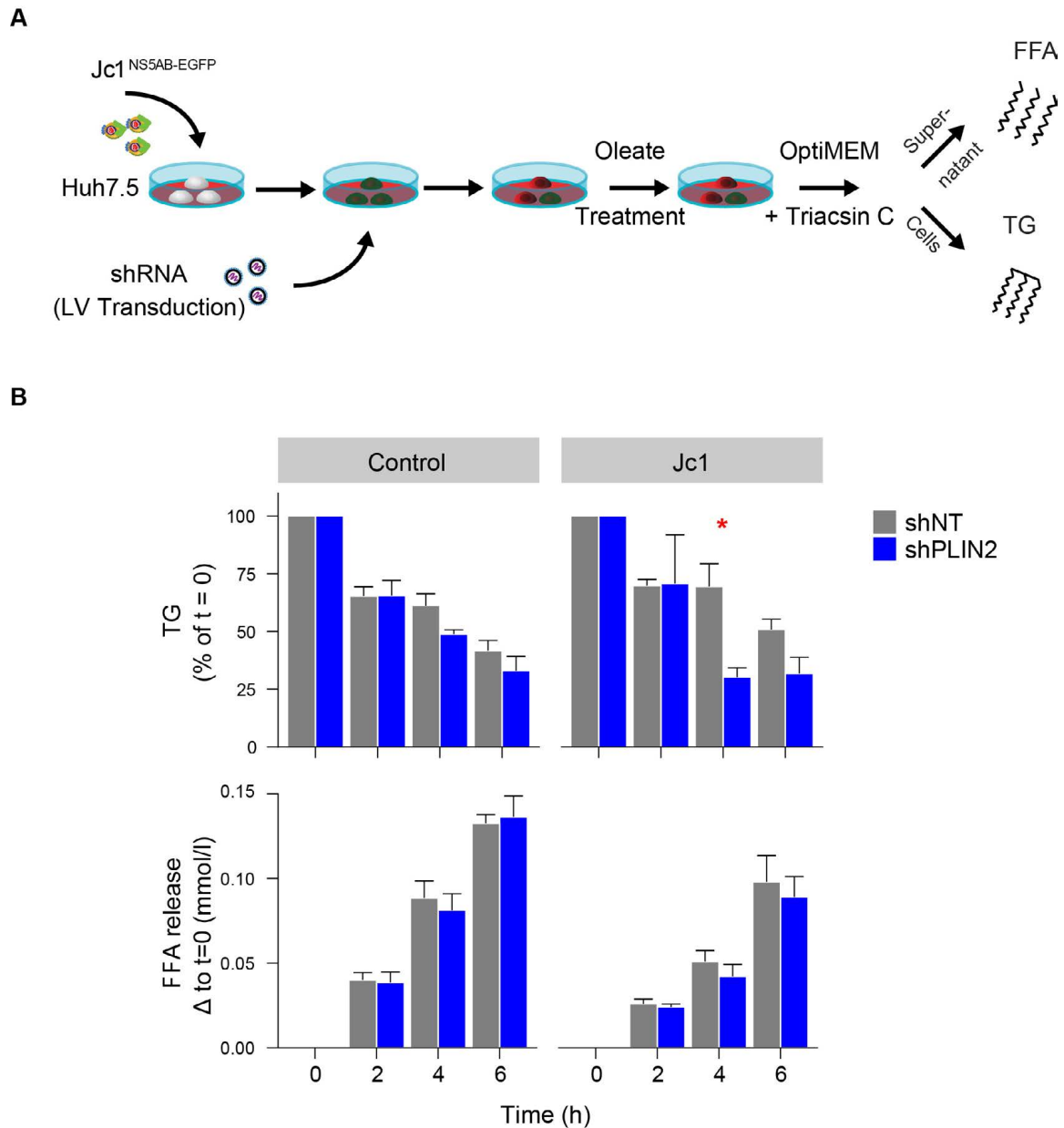
Figure 3.14.: The triglyceride turnover rates are higher in Jc1-infected shPLIN2-expressing cells

(A) Scheme of the experimental set up to measure the triglyceride turnover of HCV-infected and un-infected cells. The cells were treated with 100 μM oleate overnight and the next day the media was changed to OptiMEM containing 10 μM of the inhibitor triacsin C and 2% fatty acid-free BSA. (B) The supernatant and the cells were harvested at the time points indicated. The lipids were extracted by the Bligh and Dyer method and analyzed for the triglyceride content. The triglycerides levels were measured using the infinity triglyceride reagent. The supernatant of the cells was harvested to measure the amount of the released free fatty acids (FFAs) using the NEFA-HR kit. Triglyceride reduction and the release of FFAs were normalized to t = 0 (Mean $\pm$ SEM, n = 3-4, *$p < 0.05$).

3.2.4. Lipid droplet–associated protein levels increase at lipid droplets in PLIN2-knockdown cells

Lipid droplets are decorated with several proteins, for instance with lipid droplet–associated proteins of the PLIN family. In the liver, PLIN2 is the major lipid droplet–coating protein of the PLIN family (Fujimoto et al., 2004). Furthermore, it has been shown that downregulation of PLIN2 influences the protein levels and/or subcellular localization of other PLIN family members (Bell et al., 2008). Therefore, the impact of the knockdown of PLIN2 on the lipid droplet protein composition and on mRNA expression was investigated (Figure 3.15 A). First, the cells were transduced with lentiviral particles targeting PLIN2 or control and were harvested three and five days post transduction for the analysis of the mRNA expression levels of *PLIN1-3* by qRT-PCR analysis. Expression of the different *PLIN* genes is depicted as $2^{-\Delta Ct}$ compared to 18S rRNA to illustrate the different expression levels. *PLIN1* was significantly upregulated in shPLIN2-transduced cells compared to control cells. And as expected, the $2^{-\Delta Ct}$ values of *PLIN2* were significantly reduced in the PLIN2-depleted cells verifying the successful downregulation of *PLIN2* on mRNA level. The $2^{-\Delta Ct}$ values of PLIN3 were similar in shPLIN2- and shNT-transduced cells indicating that this gene is not affected by the downregulation of *PLIN2*. Even though the *PLIN1* expression levels were significantly elevated in PLIN2-silenced cells, the $2^{-\Delta Ct}$ values of *PLIN1* are very low compared to *PLIN3* and *PLIN2*, confirming that *PLIN1* is not well expressed in the hepatoma cell line Huh 7.5 (Figure 3.15 B). Afterwards, the translation into the protein and the protein composition of lipid droplets was analyzed by western blotting. Therefore, lipid droplets were isolated by sucrose-density centrifugation of post-nuclear supernatants from Huh7.5 cells lacking PLIN2 and control cells. The lipid droplet fractions as well as the input fractions were analyzed for protein levels of PLIN2 and PLIN3 as well as other lipid droplet–associated proteins by western blotting. Usually PLIN2 serves as a loading control for isolated lipid droplets. However, in these experiments PLIN2 was downregulated and could not be used as loading control. Consequently, silver staining was performed to verify equal protein amounts loaded on the SDS-PAGE prior to western blot analysis (Figure 3.15 C). In the post-nuclear fraction, similar PLIN3 protein levels were detected. In contrast, PLIN3 protein levels were enhanced in the lipid droplet fraction isolated from PLIN2-knockdown cells. As the mRNA expression was unchanged upon downregulation of PLIN2, this result indicates a recruitment of PLIN3 to lipid droplets rather than an upregulation of the protein. PLIN proteins are important for the regulation of the cellular lipid metabolism and are involved in the breakdown of triglycerides stored in lipid droplets into free fatty acids and glycerol. The breakdown can occur via two different pathways, either by lipolysis or by autophagy (Welte, 2015). Therefore, the level of LC3 as a marker for autophagy and the protein amounts of ATGL and CGI-58 were analyzed as markers for lipolysis. All three markers were used to analyze the cell homogenate and the purified lipid droplet fraction of the transduced Huh7.5 cells. In the input fraction, the lipase complex ATGL and CGI-58 as well as the autophagy marker LC3 were expressed to a similar level in PLIN2-depleted and control cells. In the lipid droplet fractions, the lipase complex was detectable but only LC3-I of the autophagy marker and not the PE-conjugated LC3-II. This re-

sult indicates that the lipid droplets are hydrolyzed via lipolysis in Huh7.5 cells. Interestingly, the protein levels of ATGL as well as CGI-58 in the lipid droplet fraction of the shPLIN2-transduced cells were increased, although the variability between different experiments was too high to reach significance (Figure 3.15 C). These results suggest a correlation between the protein amounts of PLIN2 on lipid droplets and the recruitment of the ATGL/CGI-58 complex to lipid droplets.
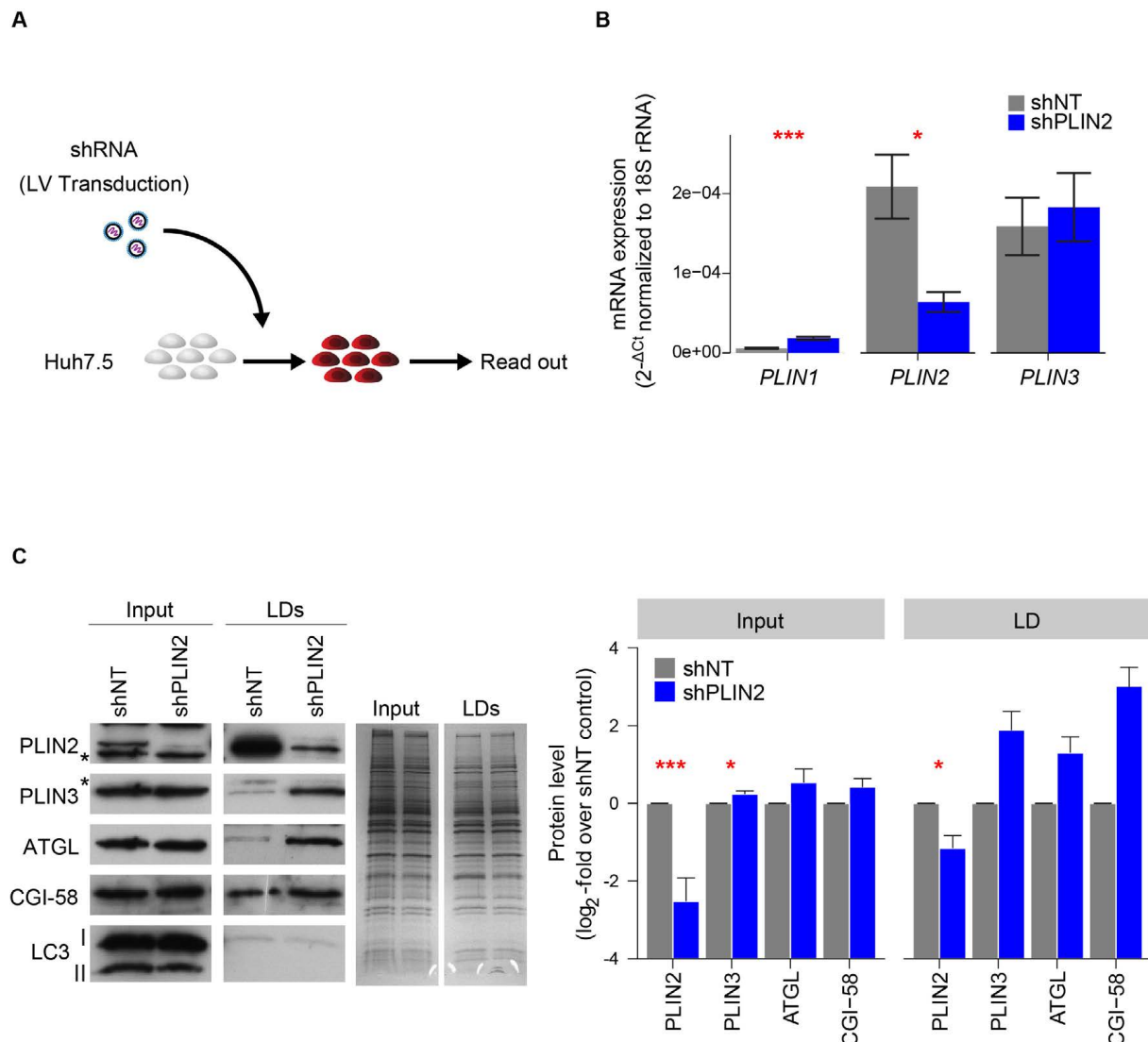
Figure 3.15.: Knockdown of PLIN2 alters the lipid droplet protein composition

(A) Naïve Huh7.5 cells were transduced with lentiviral particles targeting PLIN2 or control (shNT). Cells were harvested for the analysis of the mRNA expression levels or for the isolation of lipid droplets. (B) Five days post transduction, cells were harvested and analyzed by qRT-PCR. Shown are the $2^{-\Delta Ct}$ values to illustrate the differences in expression levels between the different PLIN genes, normalized to 18S rRNA (Mean $\pm$ SEM, n = 6-7, $***p < 0.001$). (C) Lipid droplets were isolated by sucrose-density gradient centrifugation. The post-nuclear (input) as well as the lipid droplet (LD) fraction was analyzed. To verify equal protein amounts loaded on the gels, silver staining was performed. 0.5 μg of each fraction was loaded on a SDS-PAGE and stained with silver nitrate. The input and lipid droplet fractions were analyzed by western blotting using LC3, ATGL, PLIN3, CGI58, and PLIN2 antibodies. Asteriks mark unspecific bands. Band intensities of the input and lipid droplet fractions were quantified using the densitometric quantification function of Fiji (Mean $\pm$ SEM, n = 5-7, $*p < 0.05$, $**p < 0.01$).

3.2.5. Local lipolysis rate is enhanced in lipid droplets fractions of PLIN2-knockdown cells

To investigate if the increased levels of the lipid droplet–localized lipase complex ATGL/CGI-58 enhances the local lipolysis rate, lipid droplets of shNT- and shPLIN2-transduced cells were isolated by sucrose-density gradient centrifugation and used for *in vitro* self-digestion experiments. Therefore, the triglyceride levels of the isolated lipid droplets were measured and equal amounts of triglycerides were incubated in the presence of fatty acid-free bovine serum albumin to increase triglyceride breakdown. After a 1 h incubation at 37 °C, the lipid droplets were solubilized with triton X-100 and the amount of released free fatty acids was determined (Figure 3.16 A). Indeed, following the incubation, higher amounts of free fatty acids were detected in lipid droplet fractions isolated from PLIN2-depleted cells compared to lipid droplets isolated from control cells (Figure 3.16, B). Lipid droplets are known to be putative assembly sites of HCV with the capsid protein core located on the surface of lipid droplets after HCV infection (Herker et al., 2012). In addition, previous studies have shown that the HCV core protein interferes with the ATGL/CGI-58 complex at lipid droplets thereby reducing the triglyceride turnover in the cells (Camus et al., 2014). To explore if the capsid protein core inhibits the enzymatic function of the ATGL/CGI-58 complex and therefore counteracts the enhanced lipolytic activity in PLIN2-knockdown cells, an overexpression of the core protein via lentiviral gene transfer was performed. Huh7.5 cells were transduced with lentivirus with the empty vector or expressing the core protein of two different genotypes (2a (JFH1) and 1b (Con1)) before the PLIN2-knockdown or the control was introduced. As observed before, lipid droplet isolated of shPLIN2-empty vector transduced cells had slightly enhanced lipolytic activity (Figure 3.16 C). In contrast, the core protein of both genotypes present on the lipid droplets stabilized the local lipolysis rate in PLIN2-depleted cells. Of note, expressing both the core protein and the shRNAs from lentiviral constructs negatively affected the amounts of triglycerides that were recovered from a given number of cells.
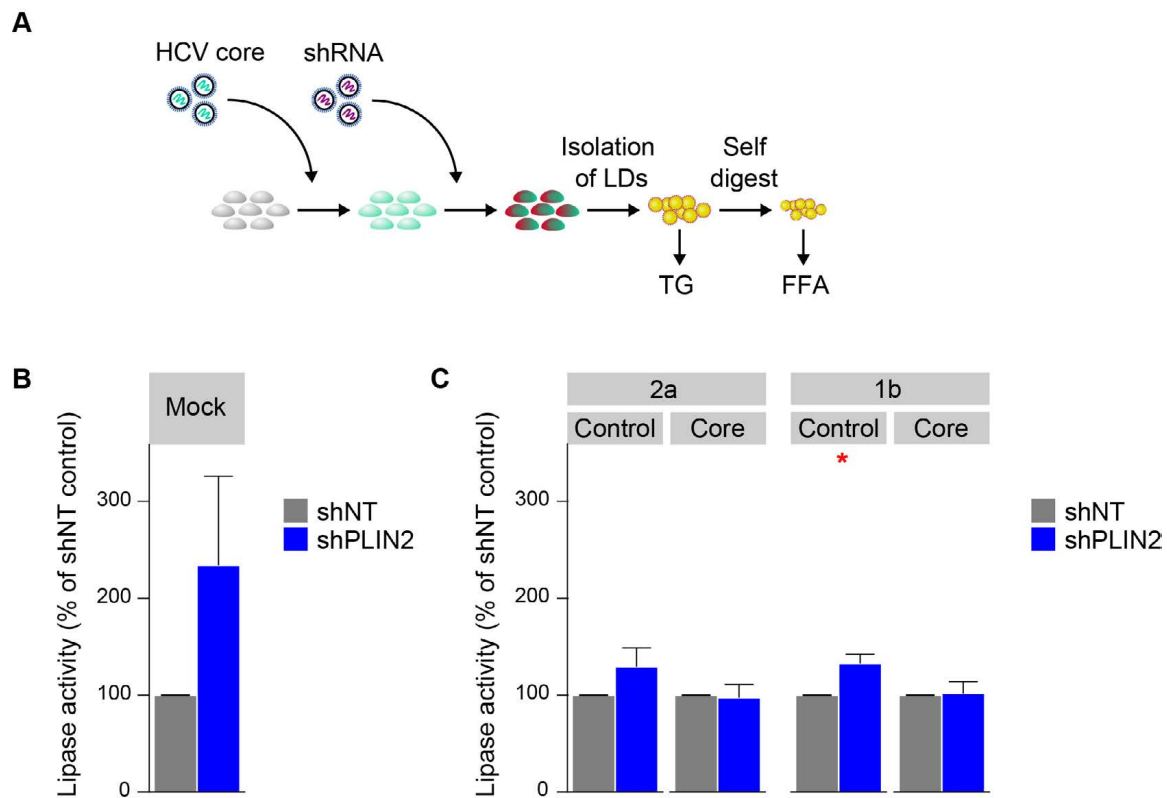
Figure 3.16.: Local lipolysis is enhanced on lipid droplets isolated from PLIN2-depleted cells

(A) Experimental procedure to analyze the local lipolysis rate of isolated lipid droplets of core or non-core expressing cells. Lipid droplets were isolated by sucrose-density gradient centrifugation, analyzed for their triglyceride levels, equalized to the same triglyceride levels and used for *in-vitro* self-digestion at 37 °C for 1 h before the release of free fatty acids (FFAs) was measured. (B) Lipid droplet–associated lipase activity of shPLIN2-transduced cells normalized to control is shown (Mean $\pm$ SEM, n = 6). (C) Lipid droplet–associated lipase activity of core and non-core expressing PLIN2-silenced cells normalized to control is shown (Mean $\pm$ SEM, n = 3-5, *$p < 0.05$)

To investigate if the core overexpression is able to block the recruitment of the lipase complex ATGL/CGI-58 to lipid droplets in PLIN2-depleted cells (Figure 3.15 C), the protein composition of the lipid droplets isolated for the determination of the local lipolysis rate was investigated by western blotting. First, a core gt2a (JFH1) lentiviral overexpression construct that shows comparable core expression as HCV Jc1 infected cells was analyzed. Again, silver staining of the SDS-PAGE gel was performed prior to western blotting to verify equal protein amounts loaded on the gel. As for single-lentivirus transduced cells, the input of the shNT- and shPLIN2 and core or empty vector transduced cells (the same samples that were probed for lipid droplet–associated lipase activity) showed no major differences in the expression level of PLIN3 as well as the lipase complex (Figure 3.17). Surprisingly, the protein profile of the lipid droplets isolated from the PLIN2-depleted cells transduced with the empty vector control showed no increase of PLIN3 or the ATGL/CGI-58 complex while the lipid droplet fraction isolated from the core (gt 2a) -expressing cells showed an increase for PLIN3 and the ATGL/CGI-58 complex as observed before for cells just transduced with lentiviral shRNAs (Figure 3.15 C). For the experiments performed with genotype 1b construct, a construct where core is expressed under a strong EF1α promoter and reaches expression levels higher than in HCV-infected cells, no

major changes were observed for all analyzed proteins of the input and lipid droplet fractions. But taken together, the core protein does not seem block the recruitment of the ATGL/CGI-58 to the lipid droplets in cells depleted from PLIN2. Finally, to verify the expression of the core protein and its trafficking to lipid droplets, an antibody detecting core was used. The protein expression level of the core protein was similar in the input fractions for PLIN2-knockdown and control cells indicating similar transduction efficiencies. Surprisingly, the core protein from gt2a was almost completely absent from lipid droplets isolated of PLIN2-knockdown cells while gt1b core that is highly expressed localized to lipid droplets even in the absence of PLIN2 (Figure 3.18). Thus, even though all other lipid droplet–associated proteins preferentially show higher levels in lipid droplets fractions from PLIN2-silenced cells, HCV core is either not affected or even less present. The differential effect between the experiments performed with gt1b vs gt2a constructs could be due to the different genotypes or expression levels of the two constructs.
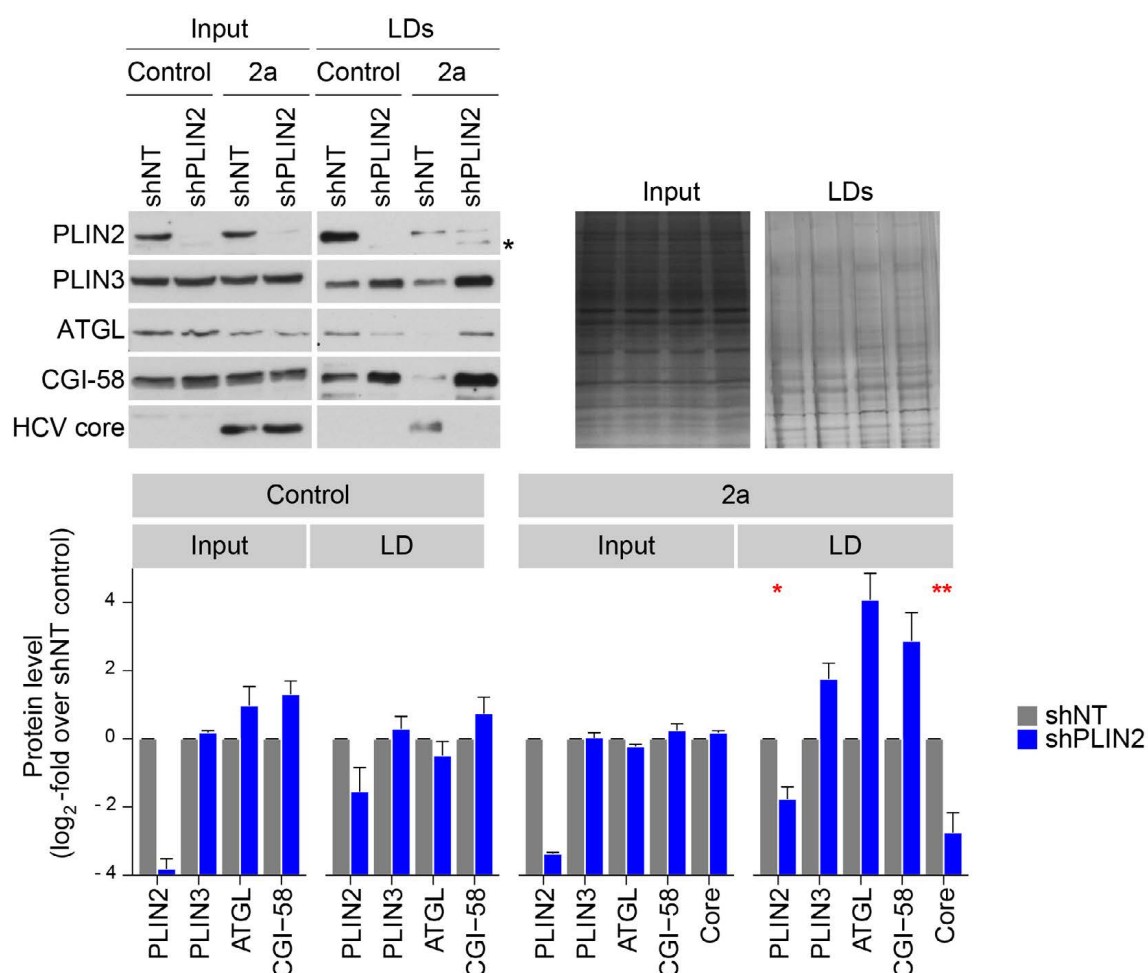
Figure 3.17.: Protein composition of cells lacking PLIN2 and expressing core gt2a

Lipid droplets were isolated by sucrose-density gradient centrifugation from empty vector control and core-expressing (gt2a) Huh7.5 cells transduced with lentiviral shRNAs targeting PLIN2 or non-targeting. The post-nuclear (input) as well as the lipid droplet fractions were analyzed by SDS-PAGE and western blotting. To verify equal protein amounts loaded on the gels, silver staining was performed. 0.5 μg of each fraction was loaded on a SDS-PAGE and stained with Ag-Nitrate. The input and lipid droplet fractions were analyzed by western blotting using PLIN2, PLIN3, ATGL, CGI58 and HCV core antibodies. Asterisks marks unspecific band. Band intensities of the input and lipid droplet fractions were quantified using the densitometric quantification function of Fiji (Mean $\pm$ SEM, n = 2-3, $p < 0.05$, *$p < 0.01$, for n = 2 no significances were determined).
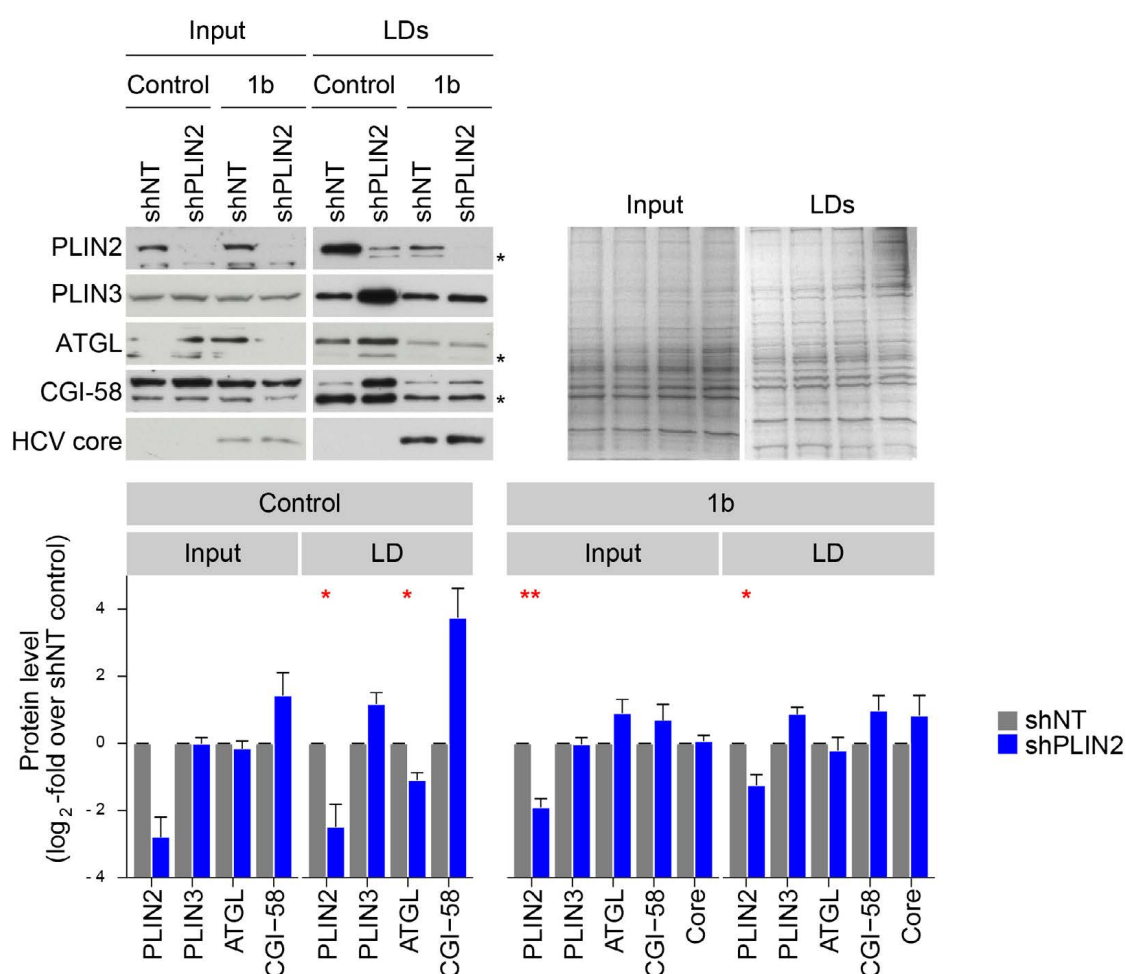
Figure 3.18.: Protein composition of cells lacking PLIN2 and expressing core gt1b

Lipid droplets were isolated by sucrose-density gradient centrifugation from empty vector control and core-expressing (gt1b) Huh7.5 cells transduced with lentiviral shRNAs targeting PLIN2 or non-targeting. The post-nuclear (input) as well as the lipid droplet fractions were analyzed by SDS-PAGE and western blotting. To verify equal protein amounts loaded on the gels, silver staining was performed. 0.5 μg of each fraction was loaded on a SDS-PAGE and stained with Ag-Nitrate. The input and lipid droplet fractions were analyzed by western blotting using PLIN2, PLIN3, ATGL, CGI58 and HCV core antibodies. Asterisks mark unspecific bands. Band intensities of the input and lipid droplet fractions were quantified using the densitometric quantification function of Fiji (Mean $\pm$ SEM, n = 2-5, $p < 0.05$, *$p < 0.01$, for n = 2 no significances were determined).

3.3. PLIN2 is involved in the trafficking of HCV proteins to lipid droplets

The reduction of the core protein in lipid droplet fractions (Figure 3.17) indicated a defect in the trafficking of HCV proteins to lipid droplets. Lipid droplets are known to play an important role in the HCV life cycle and different HCV proteins, such as core and NS5A are recruited to lipid droplets upon infection (Miyanari et al., 2007). However, it is unknown whether the PLIN2-knockdown affects the amount of HCV proteins on lipid droplets during infection. Therefore, the post-nuclear fractions as well as isolated lipid droplet fractions of HCV-infected shPLIN2- and shNT-transduced cells were analyzed. First, Huh7.5 cells were infected with Jc1$^{\text{EGFP-NS5AB}}$. Then, after they were at least 80% positive for HCV infection, the knockdown of PLIN2 was introduced. Lipid droplets were isolated by sucrose-density gradient centrifugations of post-nuclear supernatant as described before. Equal protein amounts loaded on the SDS-PAGE were confirmed by silver staining of the gel before the protein levels were analyzed by western blotting. Antibodies detecting PLIN2 and PLIN3 as well as the antibodies recognizing ATGL/CGI-58 complex were used. In addition, the protein levels of HCV core were analyzed. The input fraction showed a similar protein expression profile for all analyzed proteins between the shNT- and shPLIN2-transduced cells. No major changes were observed for PLIN3 or for the ATGL/CGI-58 complex. The protein level of the capsid protein core was similar in PLIN2-silenced and control cells indicating similar infection rates. The lipid droplet fraction isolated from the PLIN2-depleted cells showed an increase of lipid droplet–associated proteins PLIN3, ATGL and slight increase for CGI-58 (Figure 3.19). This is in line with the results obtained for lipid droplet fraction isolated from the cells expressing the core protein of genotype 2a (Figure 3.17) and with the uninfected cells (Figure 3.15 C). But, more strikingly, only ∼25% of the core protein was detectable in isolated lipid droplets of HCV-infected PLIN2-knockdown cells compared to lipid droplets isolated from the HCV-infected shNT-transduced cells (Figure 3.19). This phenotype is in line with the reduced protein levels of the core protein in the isolated lipid droplet fraction from the shPLIN2-transduced cells expressing the core protein of the genotype 2a (Figure 3.17), which is the same gt as the Jc1 strain used for infection experiments. These results indicate a strong trafficking defect of the HCV protein to the lipid droplets in the absence of PLIN2.
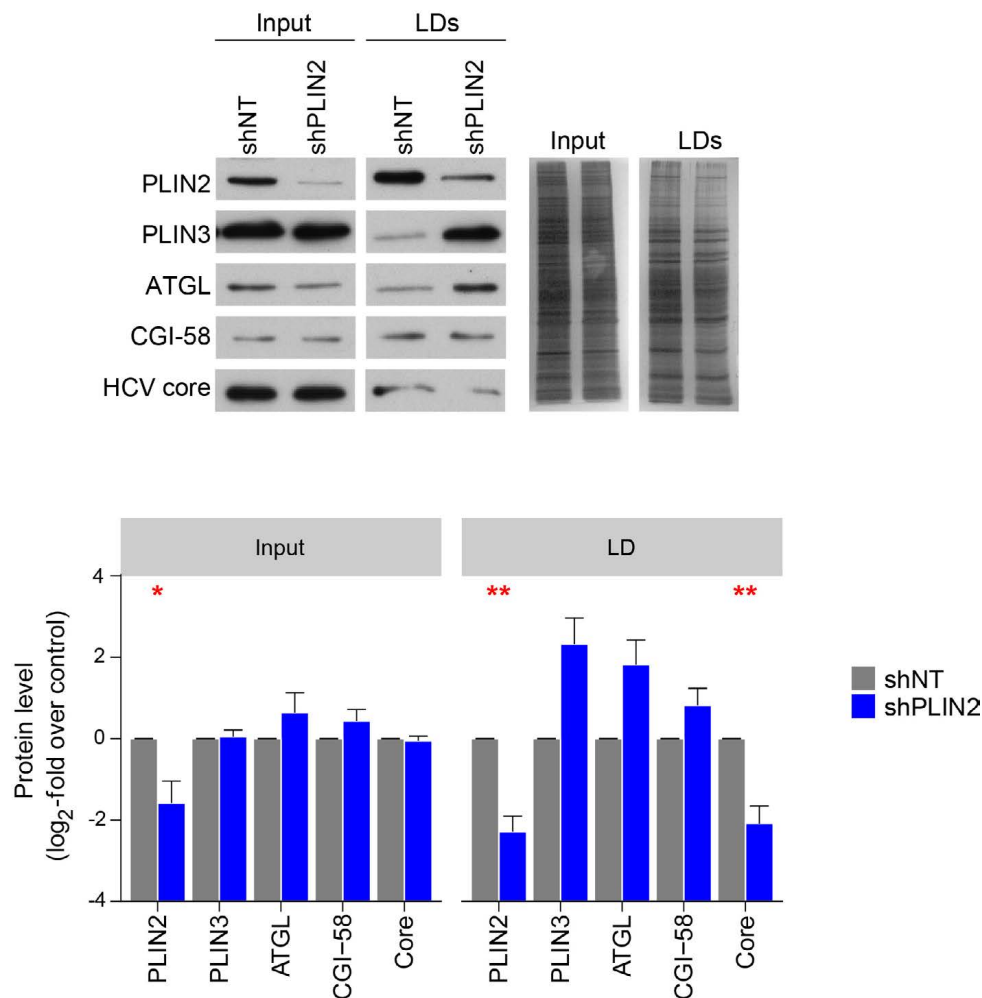
Figure 3.19.: The trafficking of the capsid protein core is dependent on PLIN2

Lipid droplets were isolated by sucrose-density gradient centrifugation from infected Huh7.5 cells transduced with lentiviral shRNA targeting PLIN2 or non-targeting control. The post-nuclear fraction (input) as well as the lipid droplet fraction was analyzed. To verify equal protein amounts loaded on the gels, silver staining was performed. 0.5 μg of each fraction was loaded on a SDS-PAGE and stained with Ag-Nitrate. (A) The input and lipid droplet fractions were analyzed by western blotting and analyzed with antibodies detecting PLIN3, ATGL, CGI-58, PLIN2 and HCV core. Band intensities of the input and lipid droplet fractions were quantified using the densitometric quantification function of Fiji (Mean $\pm$ SEM, n = 4-7, $p < 0.05$, *$p < 0.01$).

3.4. Assembly of core complexes, but not envelopment of core is mediated by PLIN2

PLIN2 expression is required for trafficking of the core protein to lipid droplets, a step critical for virion morphogenesis. To investigate the next steps in virion assembly, the formation of high molecular core complexes was analyzed. Therefore, shNT- and shPLIN2-transduced cells were transfected with Jc1$^{\text{NS5AB-EGFP}}$ RNA. Three days post transfection, the cells were harvested and lysed under native conditions and subjected to 2D blue native PAGE to analyze the formation of core complexes ranging from low-molecular-weight (LMM) to high-molecular-weight (HMM) (Gentzsch et al., 2013) (Figure 3.20 A). The formation was investigated early after transduction (5 days) and 2.5 weeks post transduction. However, no differences in the core

complex formation of HMM and LMM in whole cell lysates of shPLIN2- and shNT-transduced cells were detectable. This was also independent of the duration of the lentiviral transduction (Figure 3.20 B).

A

B
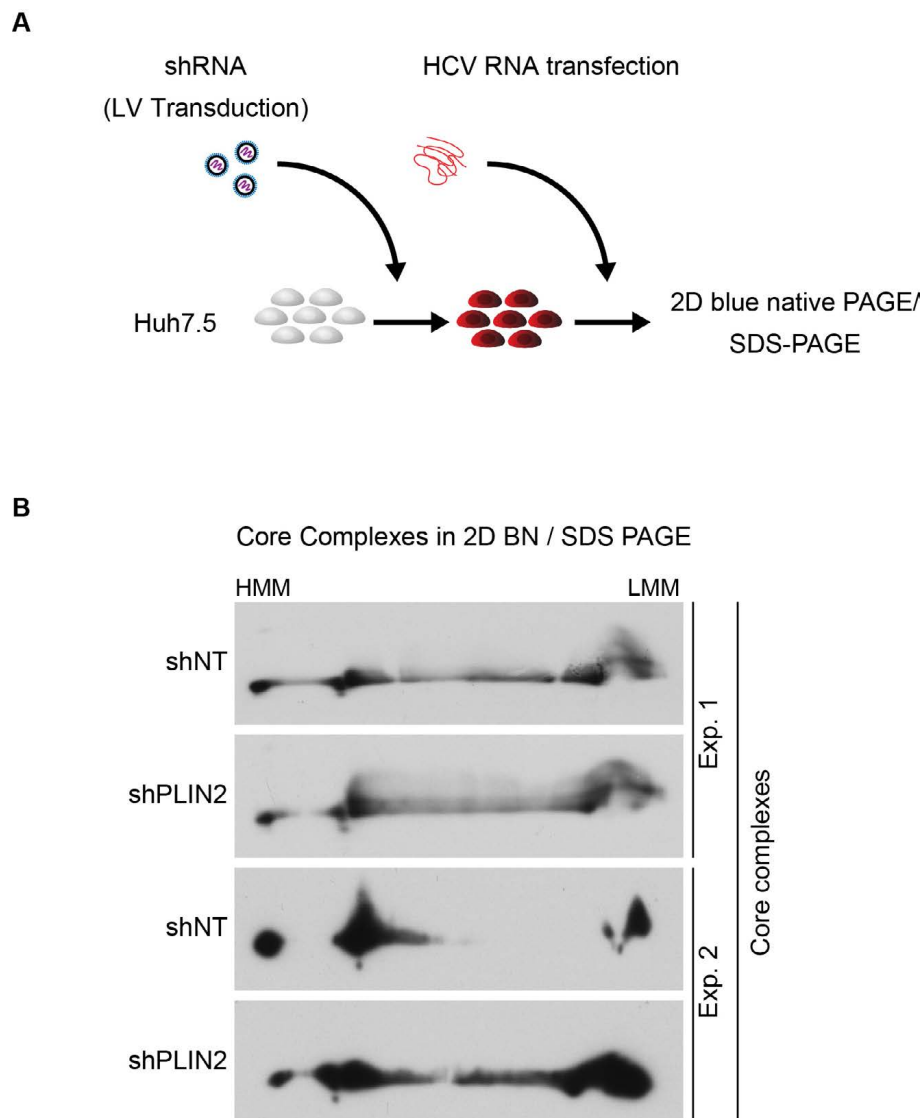
Figure 3.20.: The core complex distribution in whole cell lysates is similar in shNT- and shPLIN2-transduced cells

(A) Scheme of the experiment to analyze the formation of high molecular mass (HMM) and low molecular mass (LMM) core complexes in PLIN2-knockdown and control cells. The cells were transduced with lentiviral particles targeting PLIN2 or control. For experiment 1, the cells were transfected with Jc1[NS5AB-EGFP] RNA five days post transduction. For experiment 2, the cells were transduced for 20 days before the cells were transfected with Jc1[NS5AB-EGFP]. Three days post transfection, the cells were lysed under native conditions before the formation of HMM and LMM core complexes were analyzed by 2D blue native SDS-PAGE followed by western blotting. (B) Representative western blots of two individual experiments of PLIN2-depleted and control cells are shown. In experiment 1 the cells were transduced with the lentiviral particles for five days and in experiment 2 the cells were 2.5 weeks transduced before the cells were electroporated with Jc1[NS5AB-EGFP] RNA. An antibody specific for the HCV core protein was used to detect the distribution of the core complexes.

The next step for the virus after the formation of core complexes is thought to be the envelopment of the core protein into membranes. Thus, the envelopment of the core protein into membranes was analyzed by protease protection assays. This assay allows the distinction between membrane-protected and -unprotected proteins. The enveloped core is resistant against proteinase K treatment in contrast to the non-membrane protected NS5A, which served as a negative control. Therefore, shPLIN2- and shNT-transduced cells were transfected with Jc1$^{NS5AB-EGFP}$ and two days later, equal transfection rates were determined by flow cytometry. Three days post transfection, the cells were harvested and subjected to five freeze and thaw cycles. The cell lysates were divided in three portions and were either left untreated, treated with proteinase K or permeabilized with triton X-100 prior to proteolytic treatment. Triton X-100 disrupts all membranes and served as a positive control. Indeed, the core protein but not NS5A was detected in samples treated with proteinase K only. However, no differences in core protein levels of proteinase K treated shNT- or shPLIN2-transduced cell lysates were detectable (Figure 3.21).
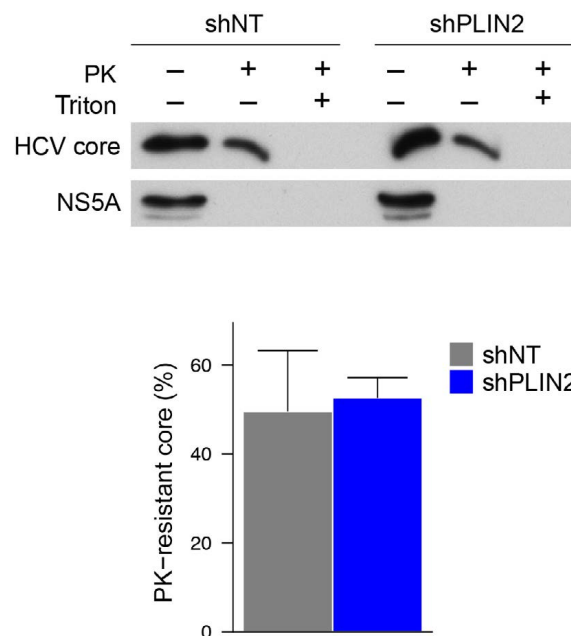
Figure 3.21.: The envelopment of the core protein is independent of PLIN2

Huh7.5 cells were transduced with lentiviral particles targeting PLIN2 or control. Three days post transduction, the cells were electroporated with HCV Jc1 RNA (Jc1$^{NS5AB-EGFP}$) and lysed under native conditions three days post electroporation. The samples were divided in three equal portions and either left untreated, treated with proteinase K or permeabilized with triton X-100 prior to proteolytic treatment. Samples were analyzed by western blotting. Shown is one representative western blot. Quantification of core levels as the percentage of core protected (+PK) compared to untreated control (Mean $\pm$ SEM, n = 3).

However, core complex formation may differ in regard of cellular compartments. After translation and maturation, core traffics from the ER to lipid droplets, which are known HCV assembly platforms, and then assembles at opposing ER membranes to bud into the ER. Therefore, it was of interest to analyze these two. Differential centrifugation of cell lysates was used to obtain the ER-containing microsomal as well as the lipid droplet fraction (Figure 3.22 A). To verify equal protein amounts loaded on the SDS-PAGE, silver-staining of the different samples and fractions was performed (Figure 3.22 B) prior to the 2D blue native PAGE analysis of the purified lipid droplet and ER fractions. The purity and enrichment of the different compartments was confirmed via western blotting (Figure 3.22 C). Consistent with the cell lysate, the formation of HMM as well as LMM core complexes were detectable in both fractions isolated from the control cells. However, the formation of HMM core complexes was enhanced in the microsomal fraction compared to the lipid droplet fraction. Interestingly, the HMM core complex formation was slightly delayed in both fractions isolated from cells lacking PLIN2 leading to the conclusion that PLIN2 or sufficient core protein levels at lipid droplets are necessary for the HCV core protein to multimerize into HMM complexes (Figure 3.22 D). Therefore, the delay observed in isolated cell fraction might not be sufficient to be detected in whole cell lysate under steady state conditions. This might be due to lower levels of core located at or close to lipid droplets. However, the slightly lower formation of the core complexes cannot explain the significant difference in virus production observed in PLIN2-knockdown as compared to control cells.
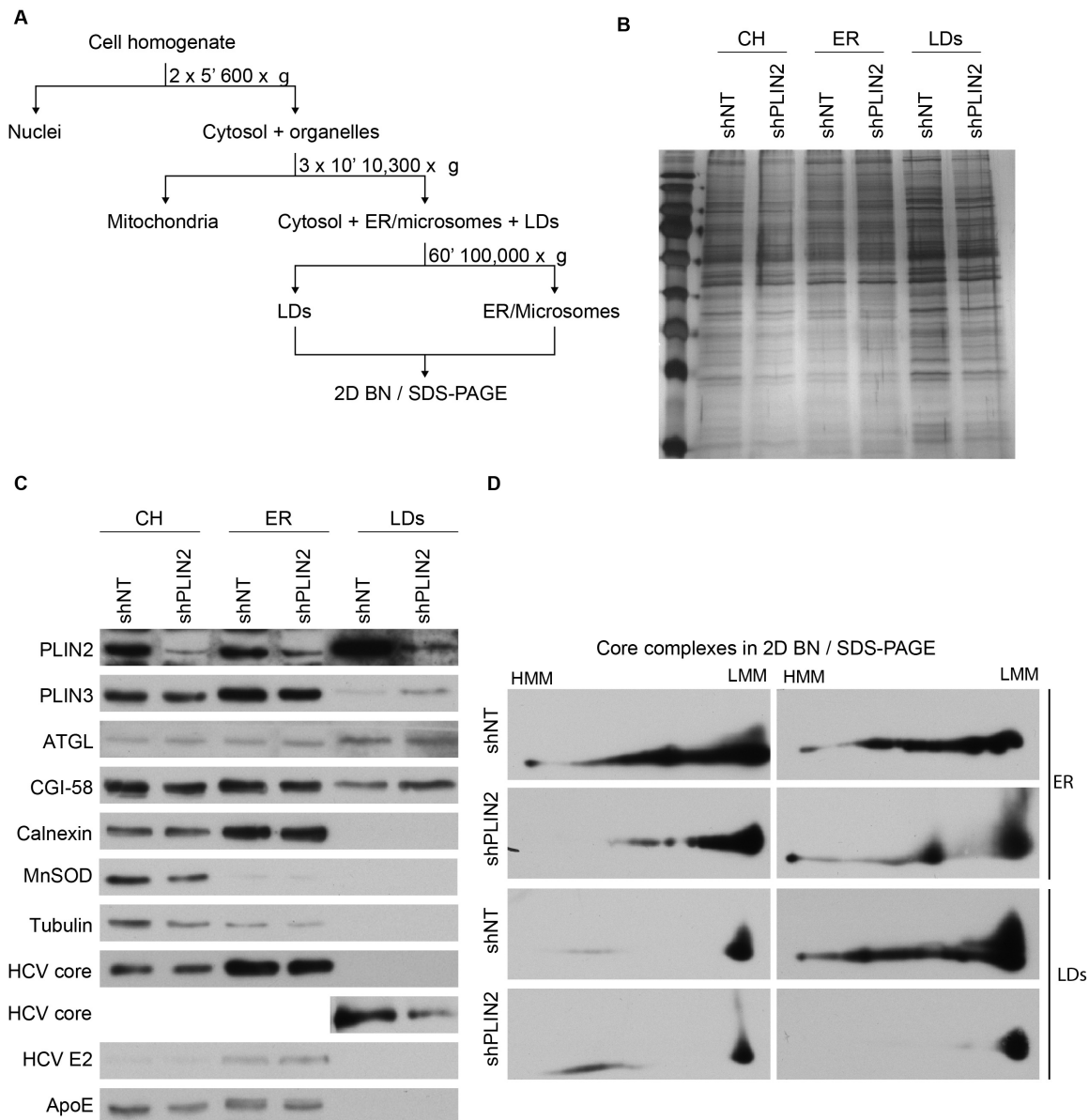
Figure 3.22.: The core complex formation is slightly delayed in fractions isolated from shPLIN2-transduced cells

(A) Scheme of the purification protocol to obtain the different cell compartments of cells infected with Jc1[NS5AB-EGFP]. The cells were transduced with lentiviral particles targeting PLIN2 or control. Eight days post transduction, the different fractions were used for 2D BN / SDS-PAGE and western blot analysis of the formation of core complexes and for analysis of the purity of the different compartments. (B) To verify equal protein amounts loaded on the gels, silver staining was performed. 0.5 μg of each fraction was loaded on a SDS-PAGE and stained with silver nitrate. (C) A representative western blot of the cell compartments is shown. Different antibodies were used to verify the enrichment of cell compartments and to show HCV infection. (D) Cell compartments obtained in (A) were lysed under native conditions and analyzed by 2D blue native PAGE followed by SDS-PAGE and western blotting. An antibody recognizing the HCV core protein was used to detect the formation of core complexes. Shown is the distribution of core in high molecular weight (HMM) and low molecular weight (LMM) complexes of the ER and lipid droplet fraction purified from shNT- and shPLIN2-transduced cells.

3.5. ApoE metabolism is dependent on PLIN2

The HCV assembly and maturation overlaps with parts of the lipoprotein biogenesis and se-
cretion. Furthermore, the infectivity of HCV viral particles depends on their density and their
association with apolipoproteins such as ApoE and, in vivo, ApoB (Bartenschlager et al., 2011).
Lipoprotein secretion starts with the co-translational lipidation of ApoB to form a very low-
density lipoprotein (VLDL) precursor and the formation of luminal lipid droplets through ac-
cumulation of triglycerides in the ER lumen. The translation of ApoE starts at the ER and the
nascent protein is translated into the ER lumen. The formation of mature VLDLs likely occurs
during secretion via the Golgi. The amount of available neutral lipids is rate limiting for the
lipidation of VLDL precursors, which are degraded by the proteasome if not fully lipidated, as
well as for the formation of luminal lipid droplets (Lehner et al., 2012). The results obtained
so far indicate that downregulation of PLIN2 slightly alters the lipid droplet morphology and
local lipolysis rates and thereby affects the cellular triglyceride metabolism. To investigate if
those alteration affect luminal lipid metabolism and lipoprotein assembly and secretion, ApoB
synthesis and, in greater detail, the ApoE metabolism was investigated next. Of note, the cell
lines used for all the studies, the HCV-permissive Huh7-drived hepatoma cells, display defects
in ApoB lipidation and secretion, limiting their usefulness for studying ApoB metabolism (Meex
et al., 2011).

3.5.1. PLIN2 does not influence the density of ApoE

ApoE is an exchangeable protein of VLDLs. To investigate if lipidation of ApoE is altered in
PLIN2-knockdown cells, an iodixanol density gradient was used. This gradient allows sep-
arating particles based on their buoyant density (Figure 3.23 A). In order to investigate the
density profile of the released lipoproteins of shNT- and shPLIN2-transduced cells, the cells
were seeded at the same density in a 10 cm^2 dish and incubated with OptiMEM the day be-
fore the supernatant was harvested. Then, the supernatant was concentrated and applied on
a linear iodixanol gradient. Equal amounts of the supernatant from the PLIN2-depleted and
control cells, which were not applied on the gradient, were also investigated and referred as
input control. After centrifugation, fractions of the gradient were harvested from the bottom
to the top and analyzed for their buoyant density as well as for the protein levels of ApoE by
western blotting. The detection of the ApoE protein of the different fractions and of the input
of the shNT- and shPLIN2-transduced cells was performed simultaneously. The ApoE protein
peaked in the same fractions of the PLIN2-silenced and control cells (Figure 3.23 B). When the
relative signal intensity of the ApoE signal of the different fraction was calculated and plotted
against the buoyant density of the different fractions, the distribution of the extracellular ApoE
of the shNT- and PLIN2-transduced cells within the gradient was almost identical (Figure 3.23
C). This indicates that the released ApoE proteins are lipidated in a similar manner and thus
the particles have the same physical properties. However, the protein amount of the secreted
ApoE of the PLIN2 lacking cells seemed to be reduced when compared to control. Therefore,

the synthesis of ApoE and ApoB was analyzed in more detail.

A
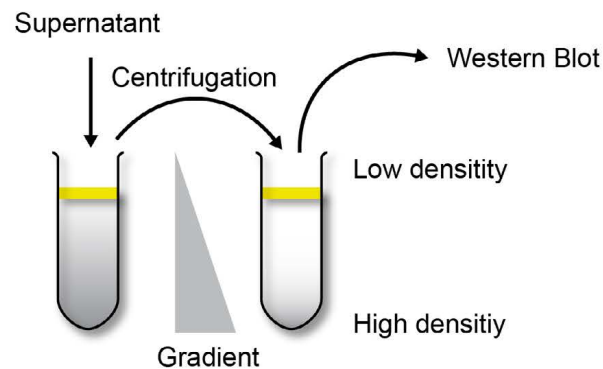
B
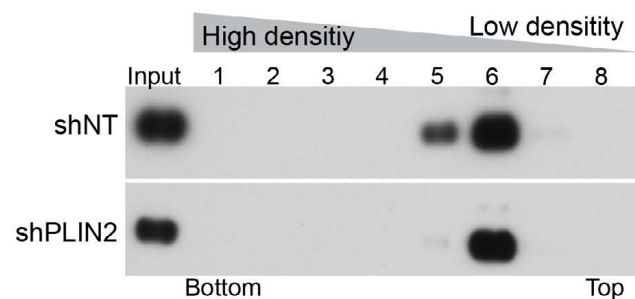
C
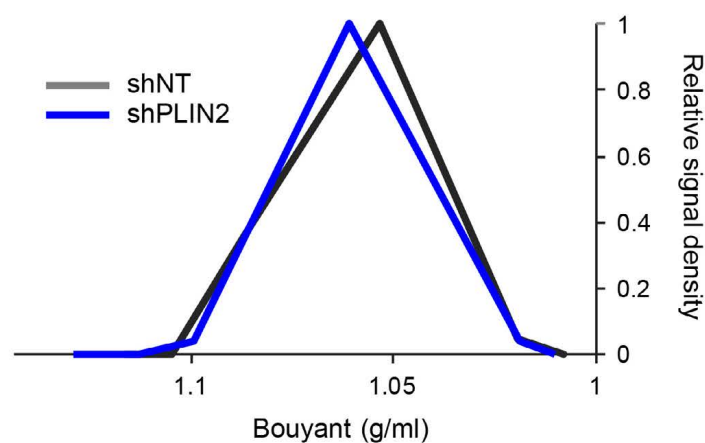
Figure 3.23.: The density of the secreted ApoE is independent of PLIN2 expression

(A) Scheme of the experimental procedure. The cell supernatant was loaded on a 6–40% linear iodixanol gradient. After 16 h of high-speed centrifugation, fractions from the bottom to the top were harvested and analyzed for the ApoE levels and the buoyant density. (B) Representative western blot of the input and the upper eight fractions is shown. The distribution of the extracellular ApoE of the shNT- and PLIN2-transduced cells within the gradient is shown. An antibody specific for ApoE was used. (C) Band intensities of the western blot in (B) were determined using the densitometric function of Fiji. The relative signal density was blotted against the buoyant density of the different fractions.

3.5.2. PLIN2-knockdown destabilizes ApoE

As the results indicate that the cells lacking PLIN2 secrete less ApoE, the protein levels of ApoE and ApoB were analyzed in more detail. Therefore, Huh7.5 cells were transduced with lentivirus targeting PLIN2 or control and were seeded in a 6-well plate at the same density. The day before the cells were harvested for western blot analysis, the media was changed to the same volume of OptiMEM to avoid cross reactivity of the antibody detecting ApoB with the serum proteins. The intra- and extracellular protein levels of ApoB were not affected by PLIN2-knockdown (Figure 3.24 A). In contrast, the ApoE levels were significantly reduced in the cell lysate as well as in the supernatant of cells depleted of PLIN2. To investigate if this effect is similar in the context of an HCV infection, Huh7.5 cells were infected with Jc1$^{\text{NS5AB-EGFP}}$ and the infection rate was determined by monitoring the EGFP expression marker by flow cytometry. The knockdown of PLIN2 was introduced when the cells were over 80% positive for EGFP. A reduction of extra- and intracellular ApoE was observed in HCV-infected shPLIN2-transduced cells, whereas no differences were observed for the expression levels of ApoB. Unfortunately, ApoB could not be detected in the supernatant of the HCV-infected cells (Figure 3.24 A). To investigate if the reduction of the protein levels of ApoE is due to a downregulation of the mRNA expression levels, qRT-PCR of HCV-infected as well as uninfected cells was performed. The mRNA expression levels of *ApoE* and *B* were analyzed three and five days post transduction with the lentiviral particles. However, no major changes in the mRNA expression levels of *ApoE* and *B* were observed between the uninfected PLIN2-knockdown and control cells. The mRNA expression levels of *ApoB* in the HCV-infected PLIN2-silenced cells were similar to the infected control cells at both time points. The *ApoE* expression levels were not affected in the PLIN2-depleted cells at the first-time point, but on day five post transduction. There, the mRNA levels of *ApoE* were significantly lower in cells lacking PLIN2; however, the expression level of *ApoE* was only reduced to ~80% when compared to control (Figure 3.24 B). Taken together, the protein translation as well as the mRNA expression of ApoB is independent of PLIN2. In contrast, the secretion and translation of ApoE is strongly impaired in cells lacking PLIN2 which cannot be explained with the slight reduction on mRNA expression level in the infected cells. These results indicate that the protein expression and secretion of ApoE is dependent on the expression levels of PLIN2.
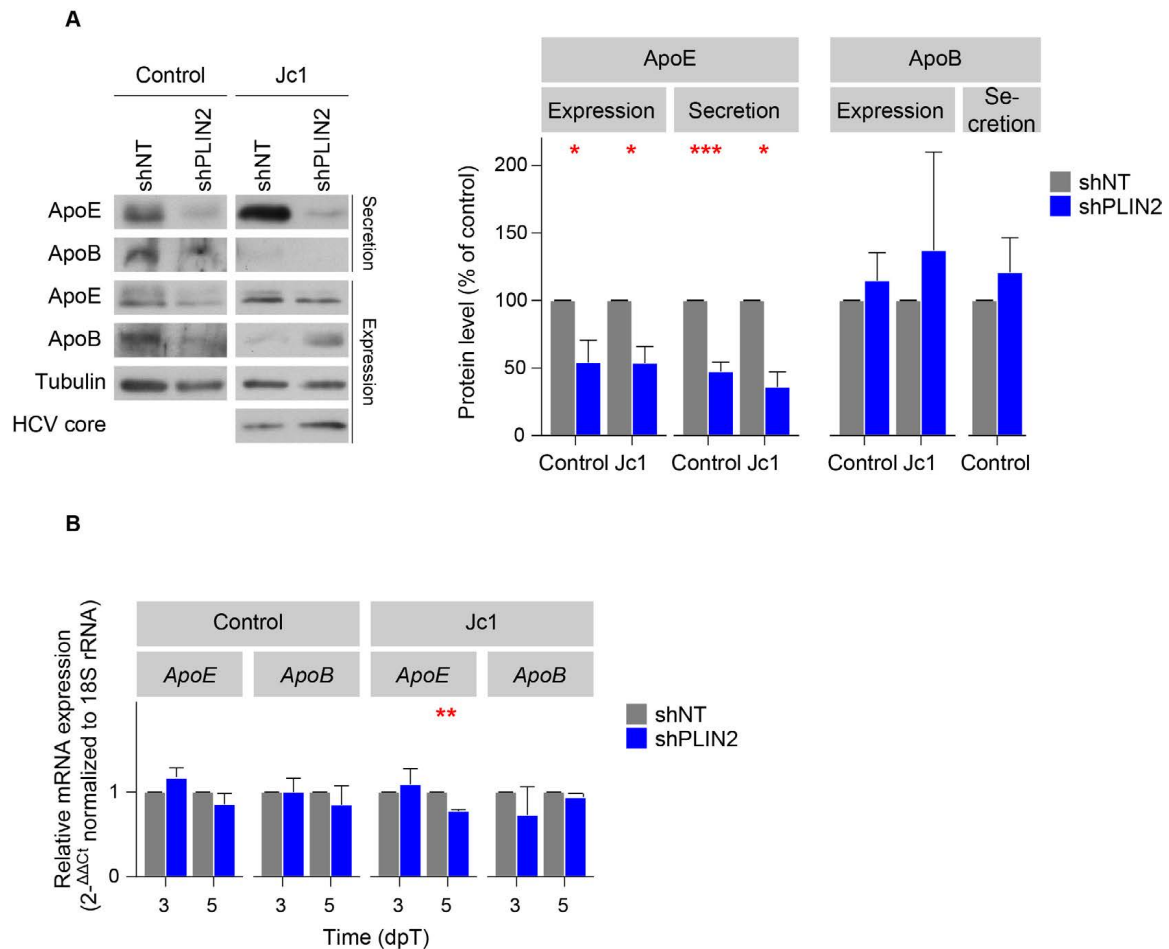
Figure 3.24.: PLIN2-knockdown destabilizes ApoE

(A) A representative western blot of uninfected and HCV-infected shNT- and shPLIN2-transduced cells is shown. The supernatant and the cell lysates were analyzed by western blotting using ApoE, ApoB and HCV core antibodies. Tubulin served as a loading control. The band intensities were quantified and normalized to shNT-transduced cells (Mean $\pm$ SEM, n = 3-5, $p < 0.05$, $**p < 0.001$). (B) *ApoE* and *ApoB* mRNA expression levels of uninfected and Jc1$^{NS5AB-EGFP}$ infected cells were analyzed by qRT-PCR. Shown are $2^{-\triangle\triangle Ct}$ values relative to shNT-transduced and normalized to 18S rRNA (Mean $\pm$ SEM, n = 3-5).

3.5.3. Lysosomal degradation of ApoE is enhanced in shPLIN2-transduced cells

As the ApoE mRNA expression was almost unchanged but protein levels reduced following downregulation of PLIN2, the degradation process of ApoE was investigated. Therefore, the proteasomal and the lysosomal degradation pathways were studied by using the proteasomal inhibitor MG132 and the lysosomal inhibitors leupeptin, chloroquine and ammonium chloride (NH_4Cl), respectively. Thus, the cells were transduced with lentiviral particles targeting PLIN2 or control and five days post transduction, the cells were seeded in a 6-well plate at the same density. Then, the cells were treated overnight with MG132 and at least 6 h with the lysosomal inhibitors before the cells were harvested. The intracellular ApoE levels were analyzed by SDS-PAGE followed by western blotting (Figure 3.25 A). The inhibitor MG132 was not able to maintain the ApoE protein levels in cells depleted of PLIN2 as they were reduced similarly to the untreated cells. By using the lysosomal inhibitors leupeptin, chloroquine or NH_4Cl, the ApoE levels in the PLIN2-knockdown cells were restored to levels similar to the shNT-transduced cells indicating a rescue of the ApoE protein. The quantification of the band intensity further supported the rescue of the ApoE protein with the treatment of the lysosomal inhibitors (Figure 3.25 B). To study if HCV-infection interferes with the lysosomal degradation of ApoE in the shPLIN2-transduced cells, Huh7.5 cells were infected with Jc1[NS5AB-EGFP] before the PLIN2-knockdown was introduced and analyzed for the degradation as described before. Again, treatment with MG132 was not able to stabilize ApoE in the HCV-infected cells lacking PLIN2 whereas all the lysosomal inhibitors were able to restore ApoE protein levels (Figure 3.25). Taken together, the degradation of ApoE is independent of HCV infection and enhanced PLIN2-silenced cells. This process can be inhibited by blocking the lysosomal degradation pathway.
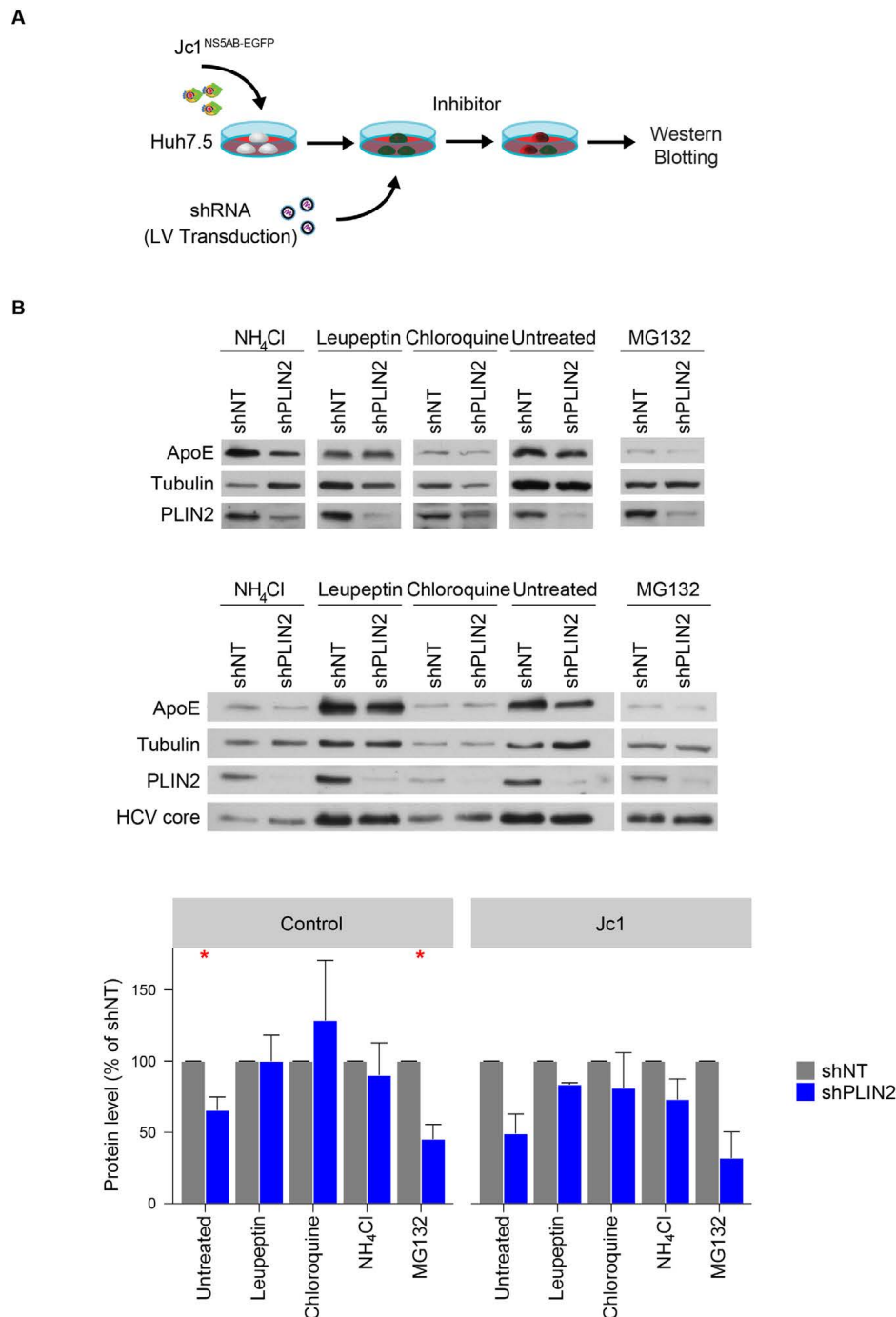
Figure 3.25.: Lysosomal degradation of ApoE is enhanced in cells lacking PLIN2

(A) Scheme of the experiment to analyze ApoE degradation. Naïve Huh7.5 or Jc1[NS5AB-EGFP] infected cells were transduced with lentiviral particles targeting PLIN2 or control. After stable integration, the cells were treated with inhibitors targeting the proteasomal (2 μg/ml MG132) or lysosomal (100 μg/ml leupeptin, 200 μM Chloroquine or 10 mM NH$_4$Cl) pathways before the cell lysates were analyzed by western blotting (B). Representative western blots of transduced cells treated with either MG132 or lysosomal inhibitors are shown. Antibodies detecting PLIN2 and ApoE were used. Infection was verified by using an antibody detecting the HCV core protein. Quantification of band intensities using the densitometric function of Fiji is shown (Mean $\pm$ SEM, n = 2-5, $p < 0.05$, for n = 2 no significances were determined).

3.5.4. Overexpression of shRNA-resistant PLIN2 recues the shPLIN2-mediated effect on ApoE

To validate the reliability of the results obtained, rescue experiments were performed. Therefore, different lentiviral plasmids were generated: a plasmid expressing the wildtype PLIN2 and two plasmids expressing PLIN2 with a silent mutation which cannot be recognized by the shRNA targeting PLIN2. One of the variants was N-terminal tagged with HA thus allowing to distinguish between endogenously and exogenously expressed PLIN2. First, the cell viability was tested to exclude any cytotoxic side effects. Therefore, lentiviral construct for the overexpression of the two PLIN2 mutants and the wildtype as well as an empty control were transduced into the Huh7.5 cell line three days before the knockdown of PLIN2 was introduced. Neither the knockdown of PLIN2 nor the overexpression of the wildtype PLIN2 or the silencing-resistant variants had any impact on the cell viability (Figure 3.26).
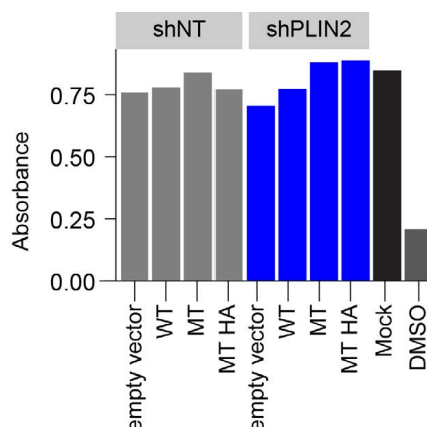
Figure 3.26.: The viability of cells is not affected by the overexpression of PLIN2

The viability of mock and lentivirus-transduced cells was determined using the CellTiter96 AQueous One Solution assay. As a negative (dead) control served cells treated with 5% DMSO. The amount of produced formazan was measured by the absorbance at 490 nm after 60 min. One representative experiment is shown.

Then, the transfection efficacy as well as the correct localization of the overexpressed PLIN2 was monitored by immunofluorescence microscopy. Therefore, the cells were seeded on coverslips, fixed with 2% paraformaldehyde and stained with antibodies detecting PLIN2 or with Bodipy650/665 to visualize the lipid droplets. As expected, the PLIN2-depleted cells transduced with the wildtype PLIN2 or with the empty vector were negative for the PLIN2 staining verifying a successful downregulation of the protein. In contrast, in all (empty vector and PLIN2 overexpressing) shNT-transduced cells, PLIN2 was detected around the lipid droplets. When the PLIN2-depleted cells were transduced with the two silencing-resistant variants, PLIN2 was detectable and localized to the lipid droplets. As almost every cell was PLIN2-positive, the transduction efficacy was almost 100% in these cells (Figure 3.27).
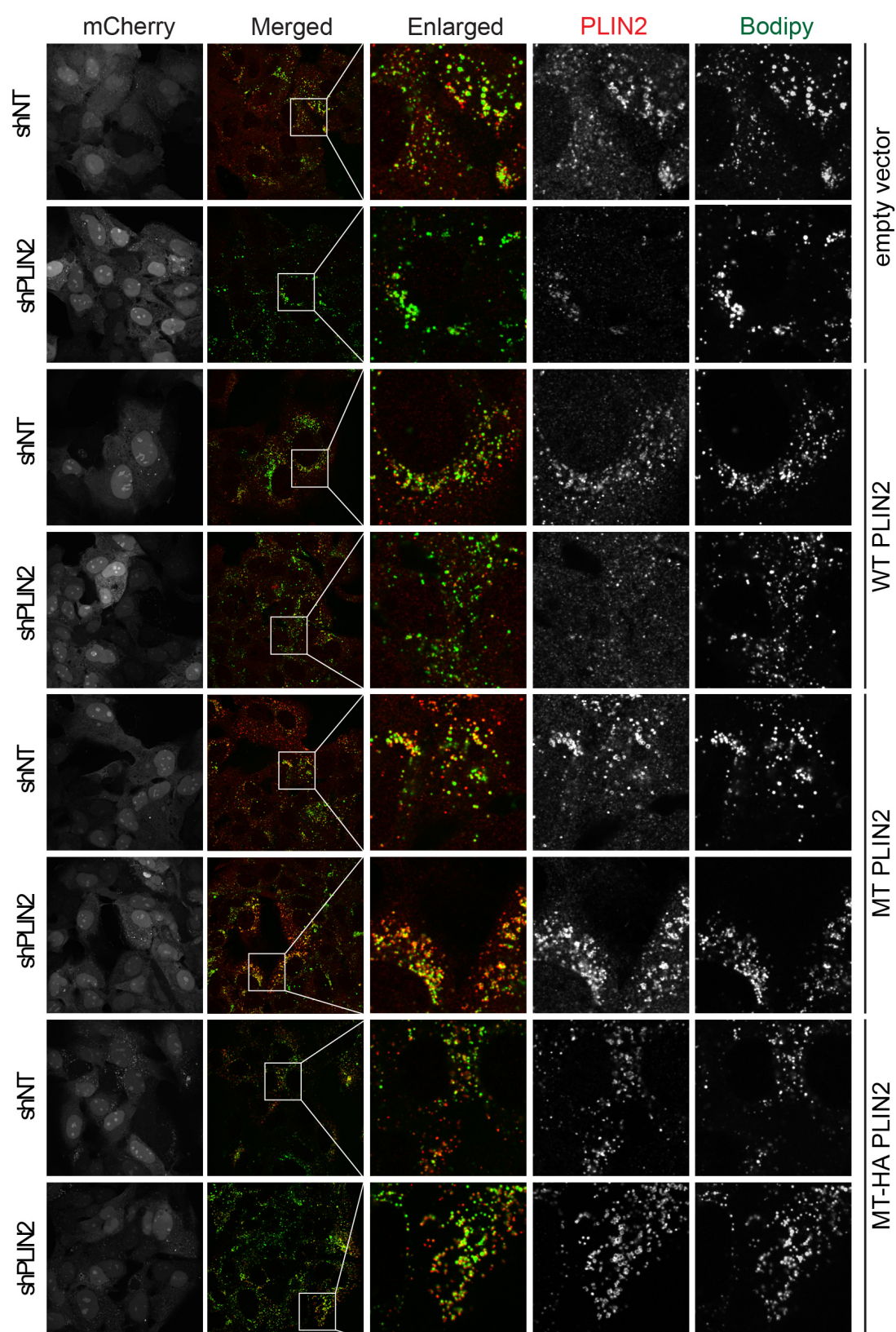
Figure 3.27.: Immunofluorescence study revealed a proper localization of the sh-resistent PLIN2

Immunofluorescence studies of PLIN2-depleted and control cells transduced with the indicated constructs. Cells were stained with an antibody detecting PLIN2 and with Bodipy650/665 to visualize lipid droplets. The first panel shows the mCherry transduced cells. The second shows a merged image of PLIN2 in red and lipid droplets in green. In the third panel is an enlarged part of the merged panel shown. The last two panels show the respective single channel of the merged panel in black and white.

To verify that the PLIN2 protein is indeed restored, western blot analysis was performed. Antibodies recognizing PLIN2 and HA were used. As expected, the cells transduced with the empty vector or the wildtype PLIN2 were not resistant against the shRNA targeting PLIN2 as the protein was not detectable by western blotting compared to the cells transduced with the non-targeting control. In contrast, the PLIN2-knockdown cells expressing the silencing-resistant PLIN2 (with and without the HA-tag) had similar PLIN2 proteins levels compared to the shNT-transduced cells indicating a successful rescue of the PLIN2 on protein level. As one mutant carried an HA-tag, the exogenous expressed PLIN2 could also be distinguished from the endogenous PLIN2. Interestingly, shNT-transduced cells overexpressing PLIN2 had similar PLIN2 protein levels compared to the shNT-transduced cells transduced with the empty vector control (Figure 3.28). This indicates that the cells have a limited capacity for PLIN2 protein levels located at the lipid droplet surface and PLIN2 that is not bound to lipid droplets is rapidly degraded (Kaushik et al., 2015; Kaushik et al., 2016). To test whether the ApoE phenotype could also be restored, an antibody detecting ApoE was used. Indeed, the ApoE levels of the PLIN2 mutants transduced with shPLIN2 were similar to the control cells. These experiments underlined that the PLIN2 phenotype observed in this thesis are specific for PLIN2 and not due to side effects mediated by the knockdown.
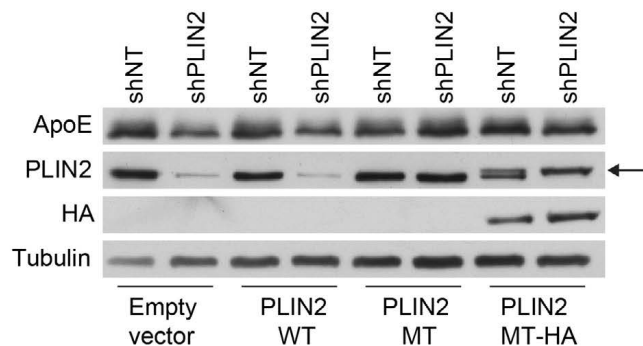
Figure 3.28.: Overexpression of PLIN2 recues the shPLIN2-mediated destabilization of ApoE

Representative western blot of shNT-and shPLIN2-transduced cells overexpression wildtype (WT) or shRNA-resistant mutants of PLIN2 (MT). Cells were lysed and analyzed by SDS-PAGE followed by western blotting. Antibodies detecting PLIN2, HA and ApoE were used. Tubulin served as a loading control. Arrow marks HA-tagged-PLIN2.

3.5.5. Subcellular localization of ApoE is not influenced by PLIN2

HCV infection changes the subcellular localization of ApoE (Rosch et al., 2016). To analyze whether the reduced ApoE levels affect the subcellular localization pattern of the protein in the shPLIN2-transduced cells compared to control cells in response to HCV infection, immunofluorescence studies were performed. Therefore, uninfected cells and cells infected with Jc1$^{Flag-E2}$ were transduced with lentiviral particles targeting PLIN2 or control. To distinguish between infected and uninfected cells, the RFP-NLS-IPS HCV reporter was used. The cells were seeded on coverslips and fixed with 2% paraformaldehyde prior to the staining with antibodies detecting ApoE and the Golgi marker GM130. The quantification of the colocalization between ApoE and the Golgi was performed by determining the Manders' colocalization coefficient. The analysis of the immunofluorescence showed less signal of ApoE in the uninfected PLIN2-knockdown cells, which is in line with the reduced ApoE levels in the cell lysate (Figure 3.24). By determining the Manders' colocalization coefficient, a significantly higher colocalization between ApoE and the Golgi was observed in uninfected shNT-transduced cells as compared to HCV-infected cells, similar to what was observed previously (Rosch et al., 2016)(Figure 3.29). Strikingly, a reduction of the colocalization between ApoE and the Golgi was also observed in the HCV-infected PLIN2-depleted cells when compared to the uninfected PLIN2-knockdown cells indicating that the subcellular localization of the remaining ApoE is not affect by the downregulation of PLIN2. The difference in ApoE expression levels in shNT- compared to shPLIN2-expressing cells makes it difficult to compare the subcellular localization between those cells.
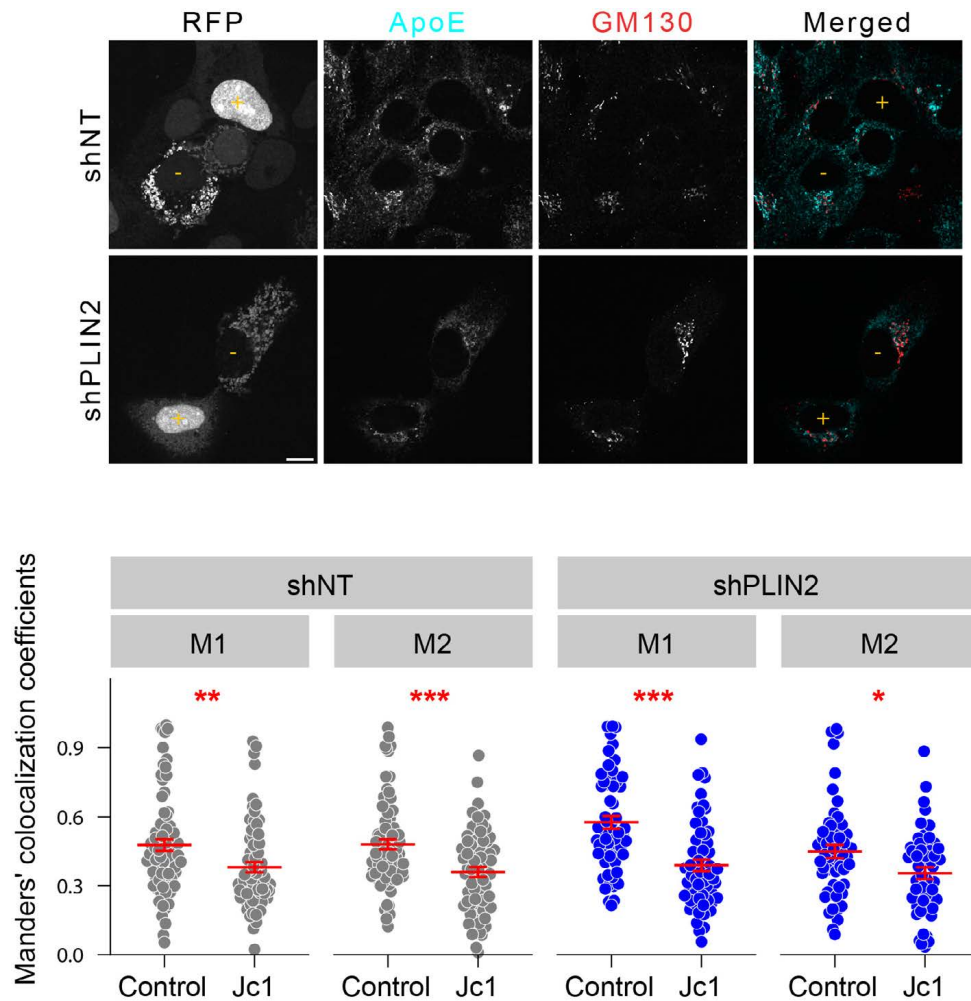
Figure 3.29.: Subcellular localization of ApoE is not influenced by PLIN2

Immunofluorescence studies of cells infected with HCV Jc1[Flag-E2] and uninfected cells to investigate Golgi and ApoE colocalization. Cells were fixed and stained with antibodies detecting ApoE and GM130. Shown are representative single channels and an overlay of all channels (Scale bar 10 μm). The Manders' colocalization coefficient was quantified using Coloc2 in Fiji. Each dot represents one cell. M1 measures the colocalization between the ApoE and the GM130 signal and M2 measures the signal of GM130 to ApoE. At least 18 cells of each construct and infection were analyzed. Data represent three independent experiments. In one experiment Flag-E2 was used to detect HCV-infected cells by staining with Flag antibodies instead of using the HCV-reporter cell line (Mean $\pm$ SEM, number of cells = 57-77, $p < 0.05$, *$p < 0.01$, **$p < 0.001$).

3.5.6. Interaction of the remaining ApoE with E2 is independent of PLIN2 expression

ApoE localization is altered in HCV-infected cells and it has been shown that annexin A3 expression mediates the re-localization of ApoE and its interaction with the viral E2 protein (Rosch et al., 2016). Therefore, the interaction of the remaining ApoE present in PLIN2-knockdown cells with the HCV envelope protein E2 was investigated by co-immunoprecipitation experiments using a HCV Jc1$^{\text{Flag-E2-NS5AB-EGFP}}$ construct that expresses Flag-tagged E2. Cells lacking PLIN2 and control were transfected with *in vitro* transcribed HCV Jc1$^{\text{Flag-E2-NS5AB-EGFP}}$ or HCV Jc1$^{\text{NS5AB-EGFP}}$ RNA without a tag which served as a negative control. After verification of equal transfection rates, Flag-E2 was pulled down and probed for co-immunoprecipitation of ApoE (Figure 3.30). In the input, the ApoE levels were again lower in the shPLIN2-transduced cells. However, ApoE was also detected in both pull-down samples but to lesser extent in the PLIN2-knockdown samples. Interestingly, the amount of ApoE interacting with E2 was similar between shPLIN2- and shNT-transduced samples. No interaction between E2 and ApoE were observed in the shPLIN2- and shNT-transduced cells transfected with the untagged Jc1$^{\text{NS5AB-EGFP}}$ RNA confirming the specificity of the ApoE-FLAG-E2 interaction observed for the cells transfected with Jc1$^{\text{Flag-E2-NS5AB-EGFP}}$ RNA. These results highlight that ApoE, which is still present in PLIN2-depleted cells, fully supports the formation and secretion of infectious particles.

A

shRNA
(LV Transduction)

HCV RNA transfection

Huh7.5 → → Read out

B

| | Jc1 | | Jc1 Flag-E2 | |
| | shNT | shPLIN2 | shNT | shPLIN2 | |

ApoE — IP: Flag
Flag-E2

ApoE — Input
Flag-E2
Tubulin
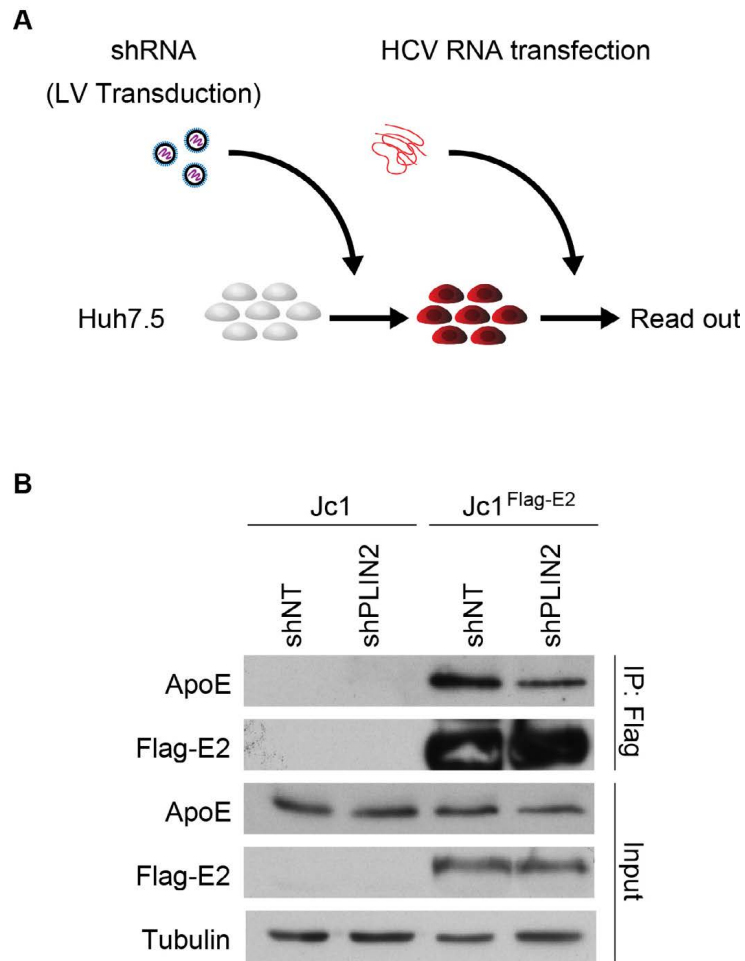
Figure 3.30.: Co-immunoprecipitation study of the remaining ApoE reveals an intact interaction of ApoE with the envelope protein E2 in PLIN2-depleted cells

Cells were transduced with lentiviral particles targeting PLIN2 or control before transfection with *in vitro* transcribed Jc1 Flag-E2-NS5AB-EGFP or Jc1 NS5AB-EGFP RNA. After verification of equal transfection rates, the cells were harvested and subjected to Flag specific co-immunoprecipitation and analyzed by western blotting using antibodies detecting ApoE and Flag-E2. Tubulin served as a loading control.

3.5.7. The specific infectivity is not altered in particles released from shPLIN2-transduced cells

The specific infectivity of HCV particles is variable and depends on the lipidation of the lipoviroparticles as well as their association with ApoE. However, when the specific infectivity was determined by dividing the number of infectious particles in the supernatant by the HCV copy number or by the amount of the secreted core protein, no major changed were observed (Figure 3.31). These results clearly revealed that PLIN2 is necessary to produce infectious viral particles but that the remaining virions released into the supernatant have similar infectivity properties as virions in the supernatant of the control. Of note, the high error bars are due to experimental variances.
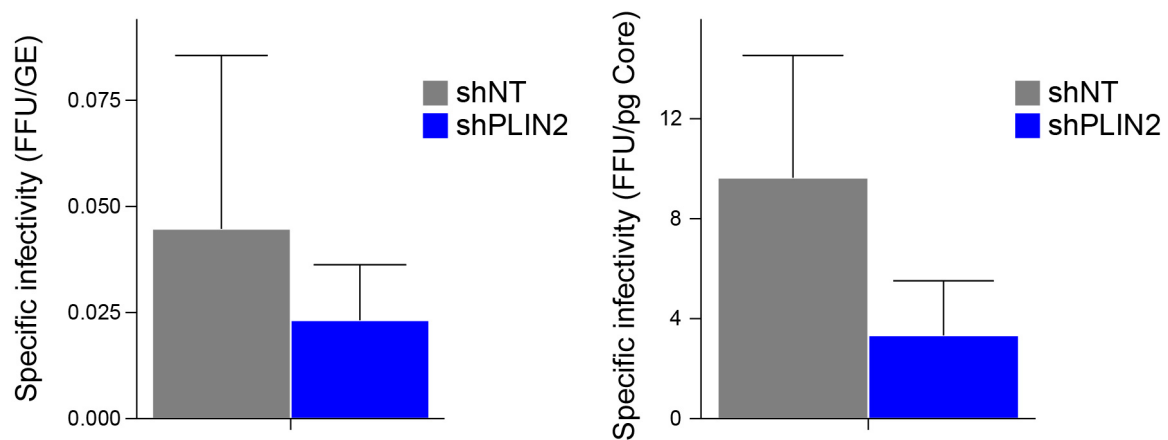
Figure 3.31.: The specific infectivity of the supernatant is similar for shNT- and shPLIN2-transduced cells

The specific infectivity was calculated by dividing the number of focus forming units (FFU) of the supernatant by the HCV copy number or by the amount of the secreted core protein in the supernatant six days post transfection (Mean $\pm$ SEM, n = 5).

4. Discussion

4.1. PLIN2 is required for HCV replication

Lipid droplets are important cellular organelles for the Hepatitis C virus and are thought to represent the putative virion assembly sites (Herker et al., 2012). The impact of PLIN3, a lipid droplet–associated protein of the PLIN family, on the HCV viral life cycle has already been described: PLIN3 plays an important role in HCV replication by interacting with NS5A to enable a close association of the membranous web with lipid droplets (Vogt et al., 2013; Ploen et al., 2013a; Ploen et al., 2013b). In addition, the interaction of PLIN3 with Rab9 is required for HCV trafficking and release (Ploen et al., 2013a). However, PLIN3 does not affect lipid droplet morphology as the size of lipid droplets remained unchanged after PLIN3 downregulation (Bell et al., 2008). The function of PLIN2, the most abundant protein of the PLIN family on lipid droplets in hepatocytes, and its role in HCV replication is poorly understood. Therefore, the impact of the downregulation of PLIN2 on HCV infection and on lipid droplet biology was investigated. The results obtained during this thesis revealed an impaired HCV viral spreading in cells lacking PLIN2, implicating a pro-viral function of the protein. This contradicts a publication describing that the downregulation of PLIN2 had no effect on the HCV viral life cycle (Branche et al., 2016). This discrepancy is likely due to the different experimental set ups. Branche *et al* used the small interference (si) RNA technology leading to a transient downregulation of the PLIN2 protein of only ∼30%. In this study, the small hairpin (sh) RNA technology was used. Lentiviral delivery of shRNAs led to a stable reduction of over 70% on mRNA level and an almost complete absence of the protein. Branche *et al* additionally showed that an overexpression of PLIN2 induced an upregulation of the entry factor occludin, which consequently led to higher HCV infection rates. The attachment and entry to the target cells are the first steps in the HCV viral life cycle, a highly-orchestrated mechanism (Lindenbach et al., 2013a). This process involves several host factors like such as the LDL receptor, SCARB1, CD81 and the tight junction transmembrane proteins occludin and claudin. In this study, the expression levels of the entry factors were unchanged in HCV-infected and uninfected shPLIN2-transduced cells compared to control cells, indicating that the observed defect in viral spreading is not due to impaired entry process of the virus. In addition, overexpression of PLIN2 did not change total PLIN2 protein levels. All publications that used overexpression constructs of PLIN2 in cell lines reported an increased level of *PLIN2* mRNA but did not validate the increased expression on protein level or showed only a week overexpression of the protein (Branche et al., 2016; Imamura et al., 2002; Sapiro et al., 2009; McIntosh et al., 2012). The results presented here indicate that the cellular levels of PLIN2 are tightly controlled and excess PLIN2 protein is readily degraded. The subsequent

step in the HCV viral entry process is the internalization via clathrin-mediated endocytosis. Following uptake, fusion and uncoating the genome is released into the cytoplasm. Then, the viral RNA replicates in cellular membrane rearrangements called the membranous web. As mentioned above, PLIN3 has already been shown to be important for HCV RNA replication (Ploen et al., 2013a; Vogt et al., 2013). In two different experimental systems used in this study, no major differences in the viral RNA replication capacity between the PLIN2-depleted and control cells were observed, leading to the conclusion that RNA replication is independent of PLIN2. In addition, the translation of viral proteins was also not affected by the downregulation of PLIN2, as similar protein levels of the capsid protein core and NS5A in the HCV-infected cell lacking PLIN2 and in HCV-infected control cells were observed. Further, this indicates a different function of PLIN2 for the HCV viral life cycle compared to PLIN3. The next step after RNA replication and translation is the assembly process of the virus. The assembly process is thought to start either at the lipid droplet surface or at ER membranes opposing lipid droplets, which are in close proximity to the replication complexes (Bartenschlager et al., 2011). However, due to technical limitations, the late steps of the life cycle are poorly understood so far. Nevertheless, in both assembly models, the capsid protein core accumulates on the surface of lipid droplets as a pre-requisite for viral assembly. PLIN2-knockdown cells secreted less viral HCV RNA genomes and less amounts of the capsid protein core. The HCV copy number and the amount of secreted protein core does not reflect the infectivity of the released virions, consequently, the infectivity of the supernatant was determined by measuring $TCID_{50}$ (Lindenbach et al., 2005). Indeed, the infectivity of the supernatant of the PLIN2-silenced cells was significantly reduced compared to the control cells. These results indicate a defect rather in the late steps of the viral life cycle.

4.2. PLIN2 is largely dispensable for lipid droplet homeostasis

The assembly process of virions likely takes place at ER membranes in close proximity to lipid droplets. Lipid droplet homeostasis is regulated by several proteins including proteins from the PLIN protein family. Initially, the effect on the lipid droplet morphology upon depletion of PLIN2 was investigated. Even though the average lipid droplet volume was significantly increased in shPLIN2-transduced cells, the increase was only minor. Previously, the HCV core protein has been shown to displace PLIN2 from the surface of lipid droplets upon HCV infection (Boulant et al., 2008). Here, the lipid droplet volume of HCV-infected PLIN2-depleted cells was still enhanced compared to the HCV-infected control cells. HCV infection itself had no impact on the average lipid droplet as well as the total lipid droplet volume per cell. These results are in line with studies in which PLIN2 was downregulated by siRNA transfection and with studies of fibroblasts isolated from PLIN2-knockout mice. Here, no major changes in the lipid droplet morphology (size and number) of cells lacking PLIN2 were observed. Interestingly, only the simultaneous downregulation of PLIN2 and PLIN3 resulted in a massive alteration of the lipid droplet morphology, with decreased numbers and volumes of lipid droplets (Branche et al., 2016; Bell et al., 2008; Sztalryd et al., 2006).

The microscopic analysis described here revealed no major changes in the total lipid droplet volume of the uninfected PLIN2-transduced cells when compared to control. However, the amounts of triglycerides stored in the lipid droplets of PLIN2-silenced cells were slightly reduced compared to the control cells. A reduction of triglycerides has also been reported for PLIN2$^{-/-}$ mice and mice treated with PLIN2-antisense oligonucleotide (ASO) (Tsai et al., 2017; Imai et al., 2012; Varela et al., 2008). There, all mice showed an even stronger reduction in the hepatic triglyceride content of up to 60%. In the study presented here, the effect of PLIN2 knockdown of a hepatoma cell line (Huh7.5) was investigated and the reduction was only minor. But of course other mechanisms that regulate the lipid metabolism in whole animals are lacking. Of note, the slight reduction of the triglyceride content observed for cells lacking PLIN2 was not detected by microscopic analysis. This is likely due to high variances in the lipid droplet content (volume and numbers) which reflects the natural biological variances from cell to cell. To obtain more robust results from microscopy, many more cells have to be analyzed.

Interestingly, lipid loading of PLIN2-depleted cells revealed a significantly reduced capacity to esterify fatty acids to triglycerides stored in lipid droplets as the triglyceride levels were lower in the oleate-treated cells lacking PLIN2 compared to the oleate-treated control cells. These results are in line with studies of isolated myotubes from PLIN2$^{-/-}$ mice (Bosma et al., 2012; Feng et al., 2017). As observed for the non-oleate-treated cells, the average lipid droplet volume was slightly, but significantly increased in the oleate-treated PLIN2-silenced cells compared to the oleate-treated control cells. The total lipid droplet volumes between the oleate-treated shNT-and PLIN2-transduced cells were similar as observed for the non-oleate treated cells. However, the oleate-treated cells lacking PLIN2 have the same total lipid droplet volume but less triglyceride levels when compared to the oleate-treated control cells. As mentioned above, the microscopic analysis has high variances and to reach significance more data have to be

generated. On the other hand, the triglyceride levels were not normalized to the amount of total protein as after lipid isolation using Bligh and Dyer the solubilization of proteins was incomplete and therefore protein measurements varied too much. Even though the cell proliferation rate seemed not to be affected by the knockdown of PLIN2, slight differences in the cell density at the end of the experiment cannot be excluded. Therefore, and to verify the result, a different extraction protocol or simultaneous measurement of protein content in a duplicated well should be used that would allow for normalization of the triglyceride levels to the protein levels of the samples. Still, the results obtained in this study indicate that cells lacking PLIN2 have a reduced capacity to esterify the supplemented fatty acids into triglycerides. Supporting this hypothesis, the shPLIN2-transduced cells showed higher maximal mitochondrial β-oxidation rates. This might be a result of preventing lipotoxicity in response to the excess amounts of fatty acid loading as a consequence of a diminished capacity to esterify fatty acids into triglycerides. Of note, the cells were treated with carnitine to force mitochondrial β-oxidation. Thus, these experiments reflect the capacity of the cells to oxidize exogenous free fatty acid sources. In contrast, as observed for the oleate-treated cells lacking PLIN2, these cells have a diminished capacity to esterify exogenous fatty acids into triglycerides.

The HCV capsid protein core has been shown to localize to lipid droplets and to mitochondria (Schwer et al., 2004). Two independent HCV-infection studies revealed a dysfunction of mitochondria, leading to diminished mitochondrial β-oxidation (Amako et al., 2015; Sato et al., 2013). In addition, it has been shown that the expression of the HCV core protein in transgenic mice induces the activation of peroxisome proliferator-activated receptors α (PPARα), a transcription factor regulating the lipid metabolism of cells. Persistent activation of PPARα leads to the breakdown of the outer mitochondrial membrane, resulting in the loss-of-function of mitochondrial β-oxidation (Tanaka et al., 2008). In this study, no impact on the mitochondrial β-oxidation due to the expression of the HCV core protein of two different genotypes was observed. Cells lacking PLIN2 still showed enhanced β-oxidation in a similar manner as non-core expressing cells, indicating that the capsid protein core itself cannot inhibit the fatty acid oxidation in this cell culture model. As described above, treatment of the cells with carnitine as a driver for mitochondrial β-oxidation reflects the maximal capacity of cells to oxidize exogenous free fatty acids and might not reflect the effect of HCV core protein on basal (not carnitine fueled) β-oxidation. In addition, protein levels of the mitochondrial marker MnSOD were similar in cells lacking PLIN2 compared to control, which was independent of an HCV-infection. Therefore, the higher β-oxidation capacity is not due to higher amounts of mitochondria in the PLIN2-knockdown cells.

4.3. HCV-infected cells have lower triglyceride turnover rates dependent on PLIN2 expression levels

Triglycerides stored in lipid droplets are hydrolyzed into free fatty acids under circumstances such as energy demands (Quiroga et al., 2012). As β-oxidation capacity was enhanced in PLIN2-depleted cells, it was tested if triglyceride turnover was affected. Of note, triglyceride flux can be altered even in the absence of effects on total lipid droplet volumes. Therefore, cells were cultured in oleate-supplemented media before the media was changed and they were treated with triacsin C. This inhibitor prevents the re-esterification of free fatty acids without affecting the β-oxidation capacity of cells (Muoio et al., 2000). Both, shNT- and shPLIN2-transduced cells displayed the same steady reduction of triglycerides concomitant with an increased release of free fatty acids into the supernatant. As PLIN2-silenced cells have a lower capacity to esterify supplemented fatty acids into triglycerides, the triglyceride levels at the beginning of the experiments were not equal. Therefore, the triglyceride levels were normalized to the amounts of triglycerides at the beginning of the experiments but no differences in triglyceride reduction rates between the PLIN2-depleted and control cells were observed. Previously, the HCV core protein has been shown to inhibit the ATGL-mediated lipid mobilization, thereby stabilizing the triglyceride content of cells (Camus et al., 2014; Harris et al., 2011). In this study, HCV-infected cells expressing PLIN2 had lower triglyceride turnover rates than HCV-infected cells lacking PLIN2 indicating that the HCV core-mediated stabilization of triglycerides is partially dependent on the expression of PLIN2. The release of the free fatty acids was similar of the shNT- and shPLIN2-transduced cells, in uninfected as well as in HCV-infected cells. This was unexpected as the triglyceride reduction rate of the HCV-infected PLIN2-depleted cells was higher compared to the HCV-infected control cells. The released free fatty acids might directly be used for β-oxidation in the PLIN2-silenced cells and are not released into the supernatant. Of note, one limitation of the experimental set up was that measurement of the released free fatty acids was close to the limit of detection. To summarize, the results obtain in this study indicate that the triglyceride turnover is at least partially dependent on PLIN2 but only in the instance of an HCV-infection.

4.4. Lipid droplet protein composition is altered in shPLIN2-transduced cells affecting the local lipolysis rate

The PLIN2 protein is the main protein associated with the surface of lipid droplets in hepatocytes. Downregulation of the PLIN2 protein could have led to the formation of supersized lipid droplets due to instability of the surface membrane of the lipid droplets that would lead to fusion of the droplets. Nonetheless, the knockdown of the PLIN2 protein had only a minor effect on the lipid droplet morphology as the volume of the lipid droplets were only slightly increased. To analyze whether other proteins might compensate for the loss of PLIN2, the lipid droplet protein composition was analyzed. First, mRNA analysis of whole cells lysates was performed

revealing a significant increase of *PLIN1*. In contrast, the mRNA levels of *PLIN3* remained un-changed. However, and as expected, *PLIN1* was not well expressed in the hepatoma cell line Huh7.5 used in this study compared to the mRNA expression levels of *PLIN3* and *PLIN2*. The total protein amount of PLIN3 was unchanged, whereas PLIN3 was highly enriched on lipid droplets of PLIN2-depleted cells. This finding fits well with studies in mouse liver cells where the knockdown was delivered by siRNA transfection and in immortalized fibroblasts isolated from PLIN2-knockout mice (Bell et al., 2008; Sztalryd et al., 2006). In these studies, PLIN3 was also recruited to lipid droplets in cells lacking PLIN2, but without changes of the total protein amount of PLIN3.

PLIN proteins are involved in stabilizing lipid droplets. However, proteins involved in breakdown of lipid droplets are also localizing to the surface of lipid droplets such as the lipase ATGL and LC3, a commonly used marker for autophagy. These proteins are involved in the breakdown of triglycerides stored in lipid droplets. The analysis of the protein composition of isolated lipid droplets demonstrated a preferred breakdown via lipolysis. The autophagy marker LC3-II was not detected on lipid droplets isolated either from shNT-transduced cells or from PLIN2-depleted cells. In contrast, the lipolysis complex ATGL/CGI-58 was detected both on isolated lipid droplets of shNT-expressing and PLIN2-silenced cells. Interestingly, an enrichment of this complex was found on lipid droplets isolated from PLIN2-depleted cells compared to the control. This result was also observed in lipid droplet fractions isolated from HCV-infected shNT- and shPLIN2-transduced cells, with an enrichment of PLIN3 and the ATGL complex on lipid droplets after PLIN2 knockdown. These results are in line with studies of lipid droplets isolated from mouse livers. There, the autophagy marker LC3-II was only detectable when the mice where kept under starvation conditions (Singh et al., 2009), leading to the conclusion that the breakdown via the lipolysis route is preferred but hydrolysis of the lipid droplets via the autophagy pathway can be induced under circumstances such as starvation (Dong et al., 2011; Singh et al., 2009; Tsai et al., 2017).

Unexpectedly, the protein profile of the lipid droplets isolated from the PLIN2-depleted cells transduced with the empty vector control used for the core gt2a expression showed no increase of PLIN3 or the ATGL/CGI-58 complex. However, lipid droplets isolated from the empty vector control used for the gt1b-expressing cells again revealed an increase of CGI-58 and PLIN3. As the number of cells had to be increased for the isolation of the lipid droplets in these ex-periments, a contamination with membranes might explain the similar protein levels observed for the lipid droplets isolated from PLIN2-depleted and control cells transduced with the empty vector control used for gt2a. Additionally, the variability between different experiments using two lentiviral constructs in combination with the lower amount of lipid droplets recovered from cells make is difficult to interpret the experiments. However, is has been shown that the core protein recruits the ATGL/CGI-58 complex to lipid droplets (Camus et al., 2014). In the core (gt1b)-expressing cells, none of the investigated proteins were elevated, neither in the input fraction nor in the isolated lipid droplet fractions. In contrast, lipid droplet fractions isolated from the core (gt2a)-expressing cells showed an increase for PLIN3 and the ATGL/CGI-58 complex

as observed before for cells transduced with lentiviral shRNAs only. Unfortunately, it was not possible to evaluate if the core protein with the gt2a is able to block the recruitment of the ATGL/CGI-58 complex to lipid droplets as no increase was observed for the cells transduced with the empty control. Overall, the results obtained here indicate that the recruitment of the ATGL/CGI-58 complex to lipid droplets cannot be blocked by the expression of the core protein. Supporting the hypothesis, an increase of the lipase complex and PLIN3 was observed for uninfected and HCV-infected cells isolated from PLIN2-depleted cells. Therefore, an HCV infection cannot block the recruitment of the ATGL/CGI-58 complex to the lipid droplets isolated from PLIN2-depleted cells.

More strikingly, the core protein levels of the isolated droplets from the HCV-infected shPLIN2-transduced cells showed a strong reduction when compared to HCV-infected control cells. The reduction of the core protein was also observed in the lipid droplet fractions of the shPLIN2-transduced cells expressing the core protein of the gt2a but not for gt1b. The lipid droplet–binding domain of core is similar in these two genotypes (Shavinskaya et al., 2007) and therefore does not explain the differences in the core trafficking to the droplets. More likely, variances in the expression levels of the core protein, might explain the differential outcomes for the two constructs. The expression of core protein from the genotype 1b is under the control of the EF1α promoter and the core protein of genotype 2a is driven by the SFFV promoter. The EF1α and the SFFV are both constitutive promoters driving the ectopic expression of the gene of interest. However, the expression levels of the inserted gene varies dependent on the promoter strength and the used cell line (Gautam et al., 2016). The expression of the core protein under the control of the strong EF1α promoter is higher compared to the SFFV driven expression and reaches levels higher than in HCV-infected cells. Therefore, the differences observed for the core trafficking of the gt1b and gt2a are likely due to different expression levels.

A recent study has shown that inhibition of cytosolic phospholipase A2 (PLA2G4A) leads to a trafficking defect of core protein to the surface of lipid droplets (Menzel et al., 2012). This enzyme cleaves off the fatty acid at the second C atom of certain phospholipids, releasing arachidonic acid thereby influencing membrane fluidity. However, in that study, a defect in the envelopment of viral particles into membrane was also found. Additionally, they observed an intracellular accumulation of the capsid protein, whereas the core protein levels in this study were almost unchanged. Neither an accumulation nor an envelopment defect of the capsid protein core into membranes was found in this study. A functional defect in the activity of the PLA2G4A enzyme in PLIN2-knockdown cells is therefore unlikely. Another important enzyme involved in the trafficking of core protein to lipid droplets is the diacylglycerol O-acyltransferase 1 (DGAT1). This enzyme is important in the final step of triglyceride biosynthesis. It is assumed that DGAT1 and not DGAT2 is the predominant enzyme catalyzing esterification of exogenous fatty acids in the liver (Villanueva et al., 2009). Inhibition of DGAT1 or expression of an inactive mutant leads to a defect in the localization of core and the NS5A protein to lipid droplets (Camus et al., 2013; Herker et al., 2010). However, it is unclear yet if DGAT1 only affects core trafficking to lipid droplets or might have additional effects on assembly, maturation, and release of virions.

A reduced DGAT1 activity caused by the downregulation of PLIN2 might explain the trafficking defect. Unfortunately, no reliable cell-based assays to measure DGAT1 enzymatic activity and distinguish it from DGAT2 are available.

The reduced amount of the capsid protein core at the lipid droplets might be also explained by an alteration of the surface of lipid droplets. Lipid droplets are surrounded by an amphipathic phospholipid monolayer (Tauchi-Sato et al., 2002). Changes of the phospholipid monolayer might influence the binding capacity and/or stability of core protein at lipid droplets, either directly or by changing interaction partners. It has been shown recently that the lipidomic and proteomic profile of lipid droplets changes upon HCV infection supporting the very dynamic lipid and protein composition of lipid droplets (Hofmann et al., unpublished) (Rosch et al., 2016). Additionally, the HCV core protein has two α-helices in the D2 domain separated by a short hydrophobic loop domain enabling to interact with phospholipids on the lipid droplet surface (Boulant et al., 2006). However, if the capsid protein core and NS5A, the other HCV protein found on the surface of lipid droplets upon infection, directly bind to the lipids or to other surface proteins of lipid droplets is still unknown (Shi et al., 2002). Moreover, overexpression studies of PLIN2 highlighted, that not only cellular neutral lipids are increasing, but also that the phospholipid composition of lipid droplets is changing. Altering the phospholipid monolayer influences the binding capacity of proteins associated with the surface of lipid droplets (McIntosh et al., 2012). However, it is almost impossible to separate lipid droplets completely from ER and other lipid droplet–connected organelles such as mitochondria (Gao et al., 2015). Therefore, the changes observed in that study might not only reflect altered phospholipid composition of lipid droplets but also altered lipid droplet membrane contact sites. To summarize, it is likely that membrane alterations of the lipid droplet monolayer in combination with alterations of lipid droplet membrane contacts sites and protein composition led to the stabilization/trafficking defect of the core protein to the lipid droplet surface.

As a recruitment of the lipolysis complex ATGL/CGI-58 to the surface of lipid droplets was observed, the lipid droplet–associated triglyceride hydrolysis rate was investigated. Indeed, the lipid droplet turnover rates were increased in lipid droplets isolated from PLIN2-silenced cells. The core protein localizes to lipid droplets upon HCV infection and therefore, an influence of core protein overexpression on the local lipolysis was analyzed. Lipid droplets isolated from core-expressing shPLIN2-transduced cells had similar local lipolysis rates compared to core-expressing shNT-transduced cells indicating a stabilization effect of core on lipid droplets of PLIN2-depleted cells. Even though no stabilization effect on the triglyceride turnover rates in HCV-infected PLIN2-knockdown cells was observed, the reduced core levels observed for the gt2a seem to be sufficient to alter the local lipolysis of lipid droplets isolated from shPLIN2-transduced cells. This is in line with previous experiments where core-expressing cells displayed increased ATGL-complex levels in isolated lipid droplet fractions but the local triglyceride hydrolysis rate was lower indicating that core can block ATGL activity at lipid droplets (Camus et al., 2014).

4.5. Effect of PLIN2-depletion on core multimerization, virion assembly and envelopment

The results obtained in this study revealed the importance of PLIN2 for trafficking of the HCV capsid protein core to lipid droplets. The next step in virion morphogenesis is the multimerization of core to higher molecular mass complexes (Bartenschlager et al., 2011). The analysis of whole cell lysates of shNT- and shPLIN2-transduced cells revealed no major changes in the formation of core complexes, indicating that lipid droplet localization of core is not strictly required for its multimerization. By isolating the cell compartments implicated in HCV capsid assembly, microsomal fractions and lipid droplets, by differential centrifugation, the formation of HMM core complexes was analyzed in more detail. Interestingly, the formation of HMM core complexes was observed in the lipid droplet and in the microsomal fraction. As expected, the HMM core complexes were more prominent in the microsomal fraction. Only a slight reduction in the formation of the core complexes was observed in both cell compartments isolated from shPLIN2-transduced cells. Of note, in those experiments the same amount of protein was loaded on the 2D blue native PAGE, but not equal amounts of the core protein. Intracellular core protein levels of whole cell lysate were equal regardless of PLIN2 expression, whereas a defect in the localization of the core protein to lipid droplets was observed in PLIN2-knockdown cells. Therefore, the different amounts of core protein loaded on the gels might be mistaken as a slight reduction of the formation of the complexes. To verify the results, the concentration of core protein should be first determined by ELISA. Then, the same amount of core protein should be used for the analysis of the core complex formation.

Nevertheless, in protease-protection assays, the envelopment of core protein by membranes was not dependent on PLIN2 expression, arguing that lipid droplet localization is dispensable for core to be protected by membranes. However, this assay is not very sensitive and might be dependent on the expression level of the analyzed protein. A previous study showed that ectopically expressed core protein is protected by membranes even without co-expression of the viral glycoproteins E1 and E2 (Ai et al., 2009). This is surprising and contrasts with another study revealing that E1 and E2 glycoproteins are required for envelopment of core and for protecting it from proteolytic digestion (Gentzsch et al., 2013). These discrepancies might be partially explained by the different experimental systems used. The ectopically expressed core protein has some alterations regarding its physical properties: it localized to a denser fraction in density gradients than core from JFH1- or Jc1-transfected cells. Additionally, in cell fractionation experiments, it co-sedimented with the plasma membrane and is more evenly distributed along the ER/late endosome and the small vesicles fractions. In contrast, core protein produced from JFH1- or Jc1-transfected cells fractionated in very distinct peaks, was less distributed and almost no protein was detectable in the small vesicle fraction (Ai et al., 2009). A more recent study investigated the impact of the ApoE on the production of viral particles. Downregulation of ApoE strongly impaired the virion production without affecting the encapsidation process of viral particles (Lee et al., 2014). The knockdown of ApoE led to an impaired secretion of the

core protein, but did not alter the intracellular amounts. This is similar to the core phenotype observed in this study. The intracellular core levels were not impaired but the core protein secretion was reduced. To summarize, PLIN2 protein expression is dispensable for the core envelopment into membranes.

4.6. ApoE metabolism is dependent on PLIN2 expression

The infectivity of HCV particles is dependent on their density and their association with apolipoproteins such as ApoE (Bartenschlager et al., 2011). Lipoprotein secretion starts with co-translational lipidation of ApoB, formation of luminal lipid droplets, as well as translation of ApoE into the ER lumen (Lehner et al., 2012). The formation of mature very low-density lipoproteins (VLDLs) likely occurs during secretion via the Golgi. The amount of neutral lipids is rate-limiting for the lipidation of VLDL precursors as well as for the formation of luminal lipid droplets (Lehner et al., 2012). The HCV-permissive Huh7-derived hepatoma cell line used in this study displays defects in the VLDL metabolism as it produces VLDLs that are less lipidated and they secrete ApoB and E independently. Thus, the formation of infectious HCV particles in Huh7-derived cells depends on ApoE but not ApoB secretion (Jiang et al., 2009).

Intracellular and secreted ApoE protein levels were significantly lower in PLIN2-knockdown cells compared to controls. The analysis of the mRNA levels indicated that the gene transcription of *ApoE* was not influenced by the downregulation of PLIN2. Previously, ApoE has been shown to be degraded via the lysosomal pathway in HepG2 cells and in macrophages (Deng et al., 1995; Ye et al., 1993). As cellular ApoE levels were lower in PLIN2-silenced cells, enhanced degradation via lysosomes was investigated. Intriguingly, by treating the cells with lysosomal inhibitors, but not with proteasomal inhibitors, the intracellular ApoE levels in PLIN2-depleted cells were completely restored. One gold standard to validate knockdown studies are rescue experiments. These experiments restore the expression of the downregulated protein using shRNA-resistant constructs. In the experiments performed here, PLIN2 protein levels were restored to control levels and ectopically expressed PLIN2 displayed proper localization surrounding lipid droplets. Strikingly, ApoE levels were also rescued verifying the validity and specificity of the results obtained with the downregulation of PLIN2. In a recent study, accumulation of ApoB, induced by treatment with a proteasomal and lysosomal inhibitor, led to tight association of ApoB-containing ER membranes with lipid droplets, indicating a defect in the budding event of lipid droplets from the ER (Ohsaki et al., 2008). These lipid droplets have an additional ER-derived membrane where lipidated ApoB accumulates, which in turn disturbs lipid droplet scission. Interestingly, by immunofluorescence studies no colocalization of PLIN2 with these ApoB-containing membranes was observed. In contrast, ApoB and PLIN2 located to opposing semicircles around lipid droplets and PLIN2 was located where ApoB was not present. By overexpression of PLIN2, this phenotype was almost abolished whereas the downregulation of PLIN2 seemed to augment the accumulation of ApoB and membranes around lipid droplets. A defect in ER membrane lipid droplet interaction concomitant with membrane alterations around

lipid droplets might explain the ApoE phenotype in PLIN2-deficient cells where ApoE cannot associate with lipids and is degraded and not available for the production of infectious viral particles.

PLIN2-depleted cells displayed a severe defect in ApoE metabolism independently of HCV infection. ApoE is an important host factor for HCV replication as it is crucial for assembly and maturation of viral particles (Jiang et al., 2012; Chang et al., 2007; Jiang et al., 2009; Lee et al., 2014). Interestingly, the reduced ApoE levels in PLIN2-silenced cells had no impact on the physical properties of the remaining ApoE, as the secreted ApoE had the same buoyant density as the ApoE protein released from the shNT-transduced cells, indicating proper lipidation. Further, the colocalization between ApoE and the Golgi was abolished in HCV-infected cells lacking PLIN2 similar to HCV-infected controls, a phenotype which has been reported recently for HCV-infected cells (Rosch et al., 2016). Moreover, the remaining ApoE protein was sufficient to produce a decreased amount of infectious viral particles. The buoyant density of released viral particles determines their specific infectivity. Viral particles released from PLIN2-depleted cells had the same specific infectivity as viral particles released from shNT-transduced cells. In addition, the residual ApoE still interacted with Flag-tagged E2 underscoring that the remaining ApoE functions in HCV maturation. As mentioned above, ApoE is crucial for the production of infectious viral particles and the diminished amount of ApoE due to the lack of PLIN2 consequently lead to a reduction of HCV particle production. Therefore, the diminished level of ApoE is the main reason for the impaired HCV replication in the cells that were silenced of PLIN2.

4.7. Conclusion and working model

The results obtained during this study demonstrated that a fully functional host lipid metabolism is essential for the Hepatitis C virus and confirmed the vital role of lipid droplets in HCV particle production. PLIN2, the major lipid droplet–binding protein in hepatocytes, was identified as an important host protein for the late steps of virion morphogenesis as the production of infectious viral particles is impaired in cells lacking PLIN2 expression. This is likely due to a defect in the ApoE metabolism caused by PLIN2 knockdown. PLIN2-depleted cells showed an enhanced lysosomal degradation of ApoE although the exact molecular mechanism is still unknown. ApoE is a crucial host factor for HCV infection, important for assembly and maturation of newly synthesized virions. Consequently, the lower amount of ApoE in PLIN2-silenced cells led to impaired HCV particle production. In addition, this study provided the first evidence that PLIN2 is crucial for the formation of ApoE-containing VLDLs, most likely by providing triglycerides for VLDL maturation. This indicates that cytosolic lipid droplets are functionally connected to VLDL secretion via PLIN2 and that HCV targets lipid droplets to exploit this pathway. Therefore, PLIN2 is as a major host factor involved in egress of host lipoproteins and functional and infectious HCV particles (Figure 4.1).
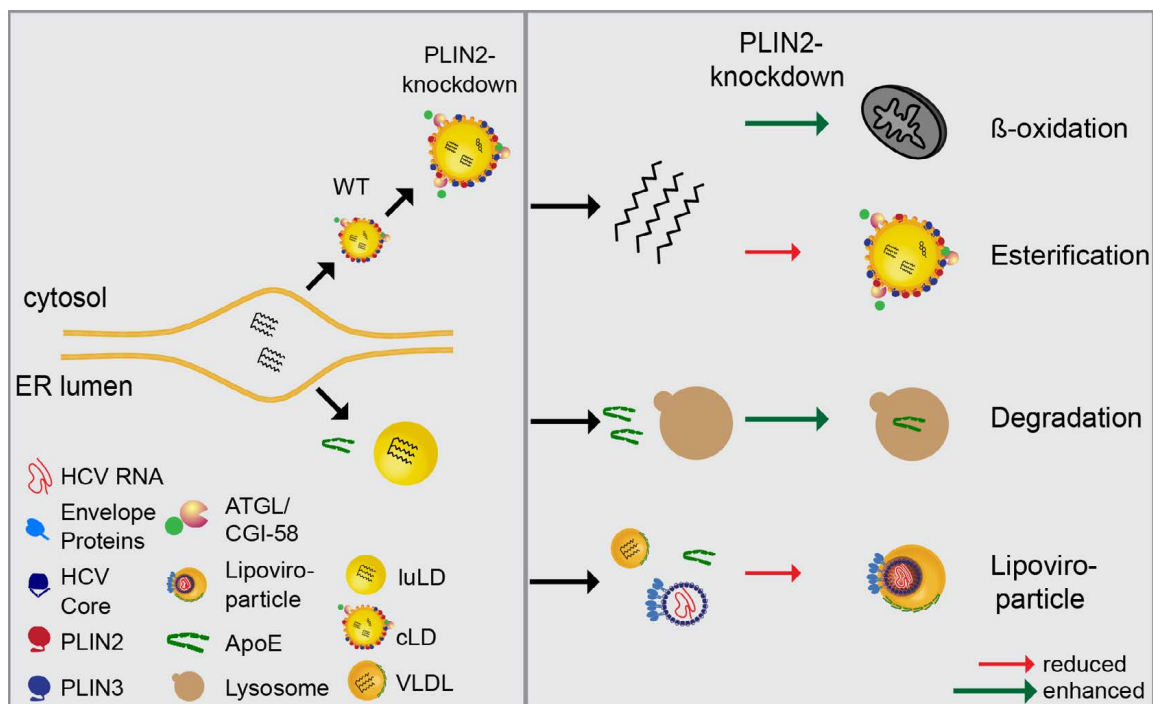
Figure 4.1.: Working model
Triglycerides accumulate within the ER bilayer and bud out of the ER either to the cytosolic side or to the ER lumen, thereby forming cytosolic lipid droplets (cLD) or luminal lipid droplets (luLD), respectively. PLIN2-knockdown cells have larger cytosolic lipid droplets with an enrichment of PLIN3 and the lipase complex ATGL/CGI-58 at the surface of the lipid droplets compared to wildtype (WT) lipid droplets. These lipid droplets have an enhanced local lipolysis rate and the PLIN2-depleted cells have a defect in the esterification of exogenous fatty acids sources concomitant with an increased β-oxidation capacity. Lysosomal ApoE degradation is increased in PLIN2-knockdown cells likely due to a defect in either ApoE lipidation or fusion of luminal lipid droplets with ApoE resulting in a defect in VLDL synthesis and secretion. As a consequence HCV particles cannot assemble to lipoviroparticles, thereby leading to a defect in mature infectious HCV particle production.

4.8. Future Aspects

One important experiment to validate the phenotype observed for the impaired production of infectious viral particles is the rescue of the PLIN2 protein expression followed by infection studies such as viral spreading infection assays or the investigation of the production of infectious viral particles. In preliminary experiments, the initial infection rates were not equal and the treatment of the cells with the required high amounts of lentiviral particles reduced the HCV-permissiveness to an extend that made the experiments inconclusive. However, a defect in the cell viability was excluded as no cytotoxic side effects were observed. To overcome the transduction with lentiviral particles introducing the knockdown and the overexpression, one could generate PLIN2 knockout cell lines using the CRISPR/Cas9 technology. This technique allows the investigation of the complete silencing of the gene. The impact on HCV replication could be verified and in addition, overexpression of PLIN2 could be introduced by lentiviral delivery and the rescue could be analyzed by spreading infection assays and/or the production of infectious viral particles.

To verify that the defect in the HCV-particle production is only due to the diminished ApoE levels in the PLIN2-depleted cells, one could treat the cells with exogenously produced ApoE. For instance, C-terminal tagged ApoE produced in Huh7-derived cells could be purified by sepharose beads. The purified apolipoprotein could be incubated with cells of HCV-infected shPLIN2- and shNT-transduced cells prior to the analysis of the infectivity of the virions in the supernatant. This would also allow tracking the exogenous ApoE via immunofluorescence staining of the C-terminal tag.

Electron microscopy (EM) studies could further provide insight how the lipid droplet morphology and interaction with other organelles is affected. One study has shown that triglycerides from PLIN2-depleted mice accumulate in the microsomal fraction (Chang et al., 2006). EM studies would allow analyzing membrane alterations of and around lipid droplets induced by the downregulation of PLIN2. A recent report has shown that a defect in the ApoB processing leads to membrane alterations of lipid droplets (Ohsaki et al., 2008). It would be of great interest if the ApoE reduction induced by the PLIN2 knockdown leads to a similar phenotype of the lipid droplets.

Thin layer chromatography (TLC) analysis of cells and purified lipid droplets would allow deciphering the lipid composition of PLIN2-silenced cells. Even though isolated lipid droplets might still harbor proteins and membranes from other cell compartments, the direct comparison with lipid droplets isolated from control cells might help to further elucidate why the HCV core protein is unable to traffic to the surface to lipid droplets and if the phospholipid composition is altered. The core protein needs a hydrophobic environment to anchor into the surface with its D2 domain in plane. Alteration in the phospholipid composition might change the physical properties necessary for the core protein to bind to the surface. Moreover, mass spectrometry of the isolated lipid droplets would further allow the analysis different lipid species and classes. A new emerging technique combining the spatial localization with metabolic analysis is called TOF-SIMS; time-of-flight secondary-ion-mass-spectrometry technique. This technique allows the *in*

situ characterization of the lipid droplet composition without the need of the lipid extraction of the sample of interest (Daemen et al., 2016) and enables the identification and localization of unknown surface molecules.

Alternatively, direct lipid droplet–core interaction studies could be performed. Therefore, isolated lipid droplets from shNT- and shPLIN2-transduced cells could be incubated with isolated and purified core protein. The production of the core protein in E. *coli* is difficult as the protein is insoluble if expressed as immature protein. To circumvent this, the protein could be *in vitro* transcripted/translated in reticulocyte cell lysates from a DNA template. Translation should be done in the presence of exogenous membranes such as canine pancreatic microsomal membranes. In addition, an inhibitor of the signal peptide peptidase necessary for the processing of immature core protein to mature core protein could be used to generate a protein that is not able to localize to lipid droplets. Then, the different proteins can be used for core–lipid droplet interaction studies. Lipid droplet could be incubated with the different core variants, washed to remove the unbound core proteins, and analyzed by SDS-PAGE followed by western blotting to analyze whether the core protein was able to bind physically to lipid droplets without the help of enzymes involved in the trafficking of the core protein to the lipid droplets.

HCV core protein cannot traffic to lipid droplets in cells lacking PLIN2. The other protein located on the surface of lipid droplets upon HCV infection is NS5A. Like core, NS5A requires DGAT1 activity to traffic to lipid droplets but then recruits PLIN3 for HCV RNA replication (Camus et al., 2013; Vogt et al., 2013). In this study, an enhanced recruitment of PLIN3 to lipid droplets in PLIN2-deficient cells was observed. It is therefore of great interest to analyze if NS5A is more abundant on lipid droplets isolated from HCV-infected shPLIN2-transduced cells or if they have also a defect in the trafficking to lipid droplets as observed for the capsid protein core.

The binding of PLIN2 to lipid droplet has been intensively studied suggesting that the 11mer repeat at the N-terminus forming amphipathic α-helices can anchor the protein into the phospholipid monolayer of lipid droplets (Bussell et al., 2003). However, direct binding partners of PLIN2 have not been identified yet. One approach to identify interaction partner and elucidate the mechanism of ApoE stabilization would be the conventional co-immunoprecitation. The lentiviral construct expressing PLIN2 with an N-terminal HA-tag generated in this study could be used to pull down the PLIN2 protein by HA-specific immunoprecipitation. Then, specific antibodies can be used to probe for specific interaction partners. In addition, the purified sample can be used for the analysis by mass spectrometry (MS). To enhance the purity of the samples, a second tag such as the His-tag or Flag-tag could be used in addition to the HA-tag and the sample can be enriched by a second immunoprecipitation. This methods is called tandem affinity purification (TAP) (Gregan et al., 2007). After purification, the sample can be the further analyzed by western blotting and /or MS. However, one disadvantage of this system is that weak or transient interactions might be lost and membrane-bound proteins tend to be rather sticky. To overcome these limitations, two recently published methods could be employed: The proximity labeling methods biotin identification (BioID) and the engineered ascorbate peroxidase (APEX). These two methods are suitable to identify physiologically relevant protein-protein interactions

in the living cells. For BioID the modified biotin ligase BirA is fused to the protein of interest. Cells overexpressing the protein are cultured in medium containing biotin and the biotin ligase biotinylates all proteins that are in close proximity to the protein of interest. The radius of the biotinylated proteins is within 20–30 nm, therefore, it also identifies weak and/or transient interaction partners. The biotinylated proteins can be easily isolated and analyzed by MS (Roux et al., 2013). When using the APEX technology, the protein of interest is fused to APEX. The cells expressing the fusion protein are incubated with biotin-phenol prior to treatment with H_2O_2. APEX uses H_2O_2 to catalyze the oxidation of biotin-phenol. The short-lived biotin-phenoxyl radical is highly reactive and biotinylates proximate proteins. The reaction is stopped using a quencher and the cells can be harvested and enriched by immunoprecipitation using streptavidin beads. Then, the proteins can be isolated and analyzed by MS. The spatial resolution using this method is below 20 nm (Chu et al., 2017; Hung et al., 2016). Both methods allow the investigation of protein binding partners in close proximity in living cells and as the cells can be lysed under harsh denaturing conditions, unspecific interactions of sticky hydrophobic proteins are minimized. Finding interaction partners of PLIN2 would help to understand its role in the HCV assembly process as well as its role in the lipoprotein metabolism of ApoE.

5. Material

5.1. Bacteria

Table 5.1.: Bacterial strains

Bacterial strain	Genotype	Company
DH5α^{TM}	F$^-$ Φ80lacZΔM15 Δ(lacZYA-argF) U169 recA1 endA1 hsdR17(rk$^-$, mk$^+$) phoA supE44 thi-1 gyrA96 relA1 $\lambda$$^-$	ThermoFisher Bioscience, Darmstadt
Stbl2^{TM}	F- mcrA Δ(mcrBC-hsdRMS-mrr) recA1 endA1lon gyrA96 thi supE44 relA1 λ- Δ(lac-proAB)	ThermoFisher Bioscience, Darmstadt

Table 5.2.: Bacterial media

Name	Components	Quantity
LB-medium	Trypton	10g
	Yeast extract	5g
	NaCl	10g
	5N NaOH	200μl
	dH$_2$O	ad 1l

The medium was autoclaved and supplemented with 100 μg/ml ampicillin if needed.

Name	Components	Quantity
LB-agar	Trypton	10g
	Yeast extract	5g
	NaCl	10g
	5N NaOH	200μl
	Agar bacteriology grade	15g
	dH$_2$O	ad 1l

The LB-agar was autoclaved and cooled to approximately 60 °C before 100 μg/ml ampicillin was supplemented. The LB-agar was poured into sterile petri dishes.

5.2. Eukaryotic cell lines

All cell lines were cultured under standard cell culture conditions at 37 °C and 5% CO_2.

5.2.1. HEK239T

HEK293T is a human embryonic kidney cell line stably expressing the large T antigen supporting the replication of plasmids carrying the SV40 origin of replication (DuBridge et al., 1987). Cells were obtained from the American Type Culture Collection.

5.2.2. Huh7 and Huh7.5 cell lines

The Huh7 cell line is a hepatocellular carcinoma cell line from a liver tumor of a 57-year-old patient (Nakabayashi et al., 1982). The Huh7 cell line was transduced with an HCV replicon and cured by interferon treatment resulting in the highly permissive cell line Huh7.5 (Blight et al., 2000). The cell line was kindly provided by Charles M. Rice.

5.2.3. Huh7.5-RFP-NLS-IPS cell line

Huh7.5 cells were transduced with lentiviral particles expressing RFP-NLS-IPS (Jones et al., 2010). The red fluorescence protein (RFP) is fused to an SV40 nuclear localization sequence (NLS) and to the mitochondrial targeting sequence as well as the HCV NS3/4A cleavage site of the IPS-1/MAVS protein. In uninfected cells, the RFP-NLS-IPS is localized at the mitochondria and in infected cells the IPS-1 is cleaved by the NS3/4A proteases of the HCV virus and the RFP-NLS is translocated to the nucleus. This cell based reporter system allows to monitor HCV infection.

Table 5.3.: Cell culture media and supplements

Name	Components	Concentration
DMEM	Dulbecco's modified eagle medium (High glucose, no glutamine)	
	Fetal bovine calf serum (FCS)	10% (v/v)
	GlutaMAX 100x	1% (v/v)
	Penicillin/Streptomycin 100x	1% (v/v)
Freezing medium	DMSO	10% (v/v)
	Fetal bovine calf serum (FCS)	90% (v/v)
Cytomix	Potassium phosphate buffer (pH 7.6)	10 mM
	KCl	120 mM
	$MgCl_2$	5 mM
	HEPES	25 mM
	$CaCl_2$	0.15 mM
	dH_2O	
	adjust pH 7.6 with 1 N KOH	
	sterile filtered (0.22 μm filter)	
	ATP	2 mM
	Glutathione	5 mM
	added before transfection	
1 M Potassium phosphate buffer	1 M $KH_2 PO_4$	19% (v/v)
	1 M K_2HPO_4	81% (v/v)
	adjust pH 7.4	
2x HBS	NaCl	275 mM
	KCl	10 mM
	Na_2PO_4	1.4 mM
	HEPES	42 mM
	Glucose	11 mM
	adjust pH 7.05	
Chloroquine	Chloroquine diphosphate	25 mM
	dH_2O	
Polybrene	Polybrene	4 mg/ml
	PBS	
Trypsin-EDTA	Trypsin-EDTA	0.05%

5.3. Plasmids

Table 5.4.: HCV plasmids

Number	Plasmid	Description	Source and Reference
HH14	pBR322 Jc1$^{\text{Flag-E2 NS5AB-EGFP}}$	Jc1 (J6 (1-846) JFH1 chimera) expressing a Flag-tagged E2 and an EGFP flanked by the duplicated NS5A and NS5B cleavage site	Sarah Hofmann, PCR to generate the FLAG-E2 construct as decribed in (Merz et al., 2011)
HH21	pBR322 Jc1$^{\text{Flag-E2}}$	Jc1 expressing a Flag-tagged E2	Katrin Rösch (Eggert et al., 2014)
HH38	pCMV6-XL4	Plasmid encoding PLIN2	Origene
HH166	pUC-HCV replicon	Con1 bicistronic subgenomic replicon carrying a neomycin resistance gene in the first cistron followed by an EMCV IRES and NS3-NS5B of HCV Con1	James Ou (Choi et al., 2004)
HH337	pBR322 Jc1ΔE1E2$^{\text{NS5AB-FLuc}}$	Jc1 replicon, the E1/E2 genes from amino acids 313-567 of the Jc1 polyprotein is deleted	this thesis
pMO977	pBR322 Jc1$^{\text{NS5AB-EGFP}}$	Jc1 EGFP flanked by the duplicated NS5A and NS5B cleavage site in the Jc1	Brian Webster (Webster et al., 2013)
pMO981	pBR322 Jc1$^{\text{NS5AB-BSD}}$	Jc1 with a selection markers in between a duplicated NS5A-NS5B cleavage site	Brian Webster (Webster et al., 2013)
pMO983	pBR322 Jc1$^{\text{NS5AB-Fluc}}$	Jc1, firefly luciferase flanked by the duplicated NS5A and NS5B cleavage site in the Jc1	Brian Webster (Webster et al., 2013)

Table 5.5.: Lentiviral plasmids

Number	Plasmid	Description	Source and Reference
HH71	pSicoR-MS1	Backbone for shRNA constructs encoding mCherry	Matt Spindler (Wissing et al., 2011)
HH98	Trip-RFP-NLS-IPS	HCV reporter, upon infection the RFP-NLS is cleaved by NS3/4A from the mitochondria and translocates to the nucleus	Charles M. Rice (Jones et al., 2010)
HH106	LeGO-iCer2	Lentiviral vector with an SFFV promotor followed by an IRES the cerulean expression	Boris Fehse (Weber et al., 2008)
HH116	pSicoR-PLIN2	pSicoR carrying PLIN2 shRNA	this thesis
HH230	pSicoR-NT	pSicoR carrying non-targeting (NT) shRNA	Anja Schöbel, shNT sequence from (Neufeldt et al., 2013)
HH231	pSicoR-puro-NT	pSicoR carrying non-targeting (NT) shRNA	Anja Schöbel, shNT sequence from (Neufeldt et al., 2013)
HH245	LeGO-iCer2 expressing Flag tagged core (2a)	Lentiviral vector expressing core (HCV gt 2a) under the control of an SFFV promotor followed by an IRES for cerulean expression	Kathrin Rösch (Rosch et al., 2016)
HH315	pSicoR-puro-PLIN2	pSicoR carrying PLIN2 shRNA	this thesis
pMO86	pCMV ΔR8.91	Lentiviral packaging plasmid	(Naldini et al., 1996)
pMO87	pMD.G	VSV-G envelope glycoprotein	(Naldini et al., 1996)
pMO155	pHR' eGFP	Lentiviral vector, an IRES of ECMV is driving the EGFP expression	(Herker et al., 2010)
pMO160	pHR' Core eGFP	Lentiviral vector, expressing core (HCV gt 1b) under the control of an EF1a promoter, followed by an IRES of ECMV driving the EGFP expression	(Herker et al., 2010)

5.4. Oligonucleotides

Table 5.6.: Cloning primers to exchange mCherry against puromycin resistance gene of the pSicoR plasmid and to generate the PLIN2 overexpressing constructs

Primer	Sequence 5'-3'
Puro fw	ATGCTAGCGCTACCGGTCGCCACCATGACCGAGTAC-AAGCCCACGGTG
Puro rev	GAGAATTCTTAGGCACCGGGCTTG
PLIN2 fw	CTGTGACCGGCGCCTACGATGGCATCCGTTGCAGTT
PLIN2 HA fw	CTGTGACCGGCGCCTACGGCCACCATGTACCCATAC-GATGTTCCAGATTACGCTATGGCATCCGTTGCAG
PLIN2 overlap rev	AGGTATTGGCAACTGCAATCTGTGGTTCCAGC
PLIN2 overlap fw	GCAGTTGCCAATACCTATGCCT
PLIN2 rev	TAGGTCCCTCGACGAATTTTAATGAGTTTTATGC

Oligonucleotides were purchased from Sigma-Aldrich, Taufkirchen

Table 5.7.: shRNA primer

Gene	Primer	Sequence 5'-3'
PLIN2	PLIN2 fw	TGCTAGAGCCGCAAATTGCATTCAAGAGA-TGCAATTTGCGGCTCTAGCTTTTTTC
	PLIN2 rev	TCGAGAAAAAAGCTAGAGCCGCAAATTGC-ATCTCTTGAATGCAATTTGCGGCTCTAGCA
NT	shNT fw	TGCGCGATAGCGCTAATAATTTTCAAGAG-AAATTATTAGCGCTATCGCGCTTTTTTC
	shNT rev	TCGAGAAAAAAGCGCGATAGCGCTAATAA-TTTCTCTTGAAAATTATTAGCGCTATCGCGCA

Oligonucleotides were purchased from Sigma-Aldrich, Taufkirchen

Table 5.8.: qRT-PCR primer

Gene	Primer	Sequence 5'-3'	Harvard primer bank ID or reference
PLIN1	PLIN1 fw	TGTGCAATGCCTATGAGAAGG	223718195c1
	PLIN1 rev	AGGGCGGGGATCTTTTCCT	
PLIN2	PLIN2 fw	ATGGCATCCGTTGCAGTTGAT	327199305c1
	PLIN2 rev	GGACATGAGGTCATACGTGGAG	
PLIN3	PLIN3 fw	TATGCCTCCACCAAGGAGAG	255958305c1
	PLIN3 rev	ATTCGCTGGCTGATGCAATCT	
18S rRNA	18S rRNA fw	GTAACCCGTTGAACCCCATT	
	18S rRNA rev	CCATCCAATCGGTAGTAGCG	
JFH1	JFH1 fw	CGGGAGAGCCATAGTGG	(Herker et al., 2010)
	JFH1 rev	AGTACCACAAGGCCTTTCG	
β-Actin	β-Actin fw	CATGTACGTTGCTATCCAGGC	
	β-Actin rev	CCATCCAATCGGTAGTAGCG	
ApoE	ApoE fw	GTTGCTGGTCACATTCCTGG	48762938c1
	ApoE rev	GCAGGTAATCCCAAAAGCGAC	
ApoB	ApoB fw	TGCTCCACTCACTTTACCGTC	105990531c1
	ApoB rev	TAGCGTCCAGTGTGTACTGAC	

The qPCR-primer mix contains 10 μM forward primer and 10 μM reverse primer diluted in nuclease-free H_2O. Oligonucleotides were purchased from Sigma-Aldrich, Taufkirchen

5.5. DNA and protein standards

Table 5.9.: DNA and protein standards

Application	Ladder	Company
DNA	GeneRuler DNA Ladder Mix	Fermentas, Darmstadt
Protein	PageRuler Prestained (10-170 kDa)	Fermentas, Darmstadt
	Spectra Muticolor HighRange Proteinladder (40-300 kDa)	Thermofisher Bioscience, Darmstadt

5.6. Solvents and buffer

5.6.1. Agarose gel eletrophoresis

Table 5.10.: Buffer and chemicals for gel electrophoresis

Name	Components	Final concentration
Agarose gel	Agarose	0.7–1.5% (w/v)
	EtBr	1 μg/ml
	1x TAE buffer	
10x TAE buffer	Tris base	2 M
	Acetic acid	5.71% (v/v)
	EDTA (pH 8)	50 mM
	dH$_2$O	

5.6.2. Lysis buffer

Table 5.11.: Lysis buffer

Lysis Buffer	Component	Final concentration
RIPA	Tris-HCl (pH 7.4)	50 mM
	EDTA	1 mM
	NaCl	150 mM
	NP-40	0.01
	Na-Desoxycholat	0.005
	SDS	0.001
	dH$_2$O	
Native PAGE buffer	Aminocaproic acid	0.75 mM
	Tris-Bis	50 mM
	pH 7	
NP40 lysis buffer	Tris-HCl (pH 7.4)	50 mM
	NaCl	150 mM
	NP-40	1%
	1x PIC	

Either the protease inhibitor cocktail (PIC) or the protease inhibitors leupeptin (20 μg/ml), antipain (2 μg/ml) and pepstatin (1 μg/ml) were added directly before use.

5.6.3. SDS-PAGE and western blotting

Table 5.12.: SDS-PAGE and western blotting

Name	Component	Final concentration
6x Lämmli buffer	Tris-HCl (pH 6.8)	375 mM
	Glycerol	25.8% (v/v)
	SDS	12.3% (w/v)
	Bromophenol blue	600 μg/ml
	β-Mercaptoethanol	6% (v/v)
	dH$_2$O	
10x Running buffer	Tris base	3.02% (w/v)
	Glycine	18.8% (w/v)
	SDS	1% (w/v)
	dH$_2$O	
10x Native PAGE running buffer	Tris base	3.03% (w/v)
	Glycine	14.4% (w/v)
	dH$_2$O	
	10x Blotting buffer	10% (v/v)
	Methanol	20% (v/v)
	dH$_2$O	
20x TBS-T	Tris base	200 mM
	NaCl	3 M
	Tween 20	1% (v/v)
	dH$_2$O	
	adjust to pH 7.4	
Blocking buffer	Nonfat dried milk powder	5% (w/v)
	1x TBS-T	

5.6.4. 2D blue native PAGE

Table 5.13.: Buffer used for 2 D blue native PAGE

Name	Component	Final concentration
Coomassie blue dye	Coomassie blue G	5%
	Aminocaproic acid	0.5 M
2x non-reducing sample buffer	Tris-HCl, pH 6.8	62.5 M
	Glycerol	25%
	Bromophenol blue	0.002%
2x SDS sample buffer	Tris-HCl, pH 6.8	150 mM
	SDS	1.2%
	Glycerol	30%
	Bromophenol blue	0.002%
	β-mercaptoethanol	15%
1x running buffer	Tris Base	25mM
	Glycine	192 mM

5.6.5. Silver staining

Table 5.14.: Silver staining

Name	Component	Final concentration
Fixation solution	Methanol	50% (v/v)
	Acetic acid	12% (v/v)
	Formaldehyde	0.0185% (v/v)
	dH_2O	
Wash solution	Methanol	50% (v/v)
	dH_2O	
Pretreatment solution	$Na_2S_2O_3$	0.02% (w/v)
Impregnate solution	Formaldehyde	0.0278% (v/v)
	dH_2O	
Developing solution	Na_2CO_3	6% (w/v)
	Formaldehyde	0.0185% (w/v)
	$Na_2S_2O_3$	0.0004% (w/v)
	dH_2O	
Stopping solution	Methanol	50% (v/v)
	Acetic acid	12% (v/v)
	dH_2O	

5.6.6. Buffer for lipid droplet isolation

Table 5.15.: Buffer used for lipid droplet isolation

Name	Component	Final concentration
Sucrose buffer	Sucrose	0.25 M
	EDTA	1 mM
	DTT	1 mM
	pH 7	
Potassium phosphate	Potassium phosphate	0.1 M
	KCl	100 mM
	EDTA	1 mM

Add protease inhibitor coktail (PIC) and 1mM PMSF or 1 μg/ml pepstain A, 2 μg/ml antipain and 20 μg/ml leupeptin directly before use

5.6.7. Iodixanol density gradient

Table 5.16.: Density gradient

Solution	Component	Quantity
40% Iodixanol	60% Optiprep	16 ml
	0.1 M EDTA (pH 7.6)	0.34 ml
	1.5 M Tris-HCl (pH 6.8)	0.34 ml
	0.25 M Sucrose	0.34 ml
6% Iodixanol	60% Optiprep	1.7 ml
	0.1 M EDTA (pH 7.6)	0.34 ml
	1.5 M Tris-HCl (pH 6.8)	0.34 ml
	0.25 M Sucrose	14.6 ml

Gradients were prepared with a gradient mixer

5.6.8. Buffer for annealing of primers

Table 5.17.: Annealing buffer

Component	Concentration
K-acetate	200 mM
HEPES pH 7.4	60 mM
Mg-acetate	4 mM

5.6.9. Other standard buffer and solutions

Table 5.18.: 18 Other standard buffer and solutions

Name	Component	Final concentration
BSA	Bovine serum albumin, FFA free	10% (w/v)
	dH_2O	
Crystal violet	Crystal violet	0.5% (w/v)
	Methanol	20%
Mowiol	Tris-HCl, pH 8.5	0.2 M
	Mowiol 4-88	12% (w/v)
	Glycerol	30%
Triton X-100	Triton	0.1%
	in PBS	
PFA	Paraformaldehyde	16% (w/v)
	in PBS	
Proteinase K buffer	Tris-HCl, pH 8	50 mM
	CaCl2	10 mM
	DTT	1 mM
IF Blocking solution	Bovine serum albumin	5%
	Fish skin gelatin	1%
	Tris	50 mM

5.7. Antibodies and dyes

Table 5.19.: Antibodies used for immunofluorescence (IF), flow cytometry (FC) and western blotting (WB)

Antigen/clone	species	Dilution	Company	Catalogue no
ApoB	rb	1:1000 WB	Abcam, Cambrige (UK)	ab31992
ApoE	rb	1:1000 WB, 1:100 IF	Abcam, Cambrige (UK)	ab52607
ATGL	rb	1:1000 WB	Cell Signaling, Leiden (NL)	2138S
Calnexin	goat	1:1000 WB	Santa Cruz Biotechnology, Heidelberg	sc-6465
CD81	ms	1:1000 WB, 1:100 FC		(Fritzsching et al., 2002)
CGI-58	rb	1:1000 WB	Abcam, Cambrige (UK)	ab73551
Claudin1	rb	1:1000 WB	Abnova, Walnut (USA)	H00009076-MO1
HCV Core	rb	1:250 WB, 1:25 IF	Santa Cruz Biotechnology, Heidelberg	sc-57800
HCV E2, AP-33	ms	1:2000 WB, 1:100 IF	Genentech Inc., San Francisco (USA)	AP-33
Flag	ms	1:1000 WB, 1:100 IF	Sigma-Aldrich Chemie GmbH, Taufkirchen	F1804-200UG
Flag	rb	1:1000 WB, 1:100 IF	Sigma-Aldrich Chemie GmbH, Taufkirchen	F7425-.2MG
Flag-agarose	ms	IP: 20 μl/ sample	Sigma-Aldrich Chemie GmbH, Taufkirchen	A2220-1ML
GM130	goat	IF: 1:25	Santa Cruz Biotechnology, Heidelberg	sc-16268
HA	rb	1:1000 WB, 1:100 IF	Sigma-Aldrich Chemie GmbH, Taufkirchen	H6908-100UL
LC3I/II	rb	1:1000 WB	Cell Signaling, Leiden (NL)	D11
LDL	ms	1:20 FC	Santa Cruz Biotechnology, Heidelberg	sc-18823
MnSOD	rb	1:1000 WB	Enzo Life Science, Farmingdale (USA)	ADI-SOD-110-F
NS5A, 2F6/G11	ms	1:1000 WB, 1:100 IF	IBT-GmbH, Reutlingen	HCM-131-5
Occludin	ms	1:1000 WB	Life Technologies, Darmstadt	33-1500
PLIN2	rb	1:1000 WB, 1:100 IF	Abcam, Cambrige (UK)	ab52355
PLIN2	gt	1:125 IF	PROGEN Biotechnik GmbH, Heidelberg	AP125
PLIN3	rb	1:1000 WB	Abcam, Cambrige (UK)	ab47639
PLIN5	rb	1:1000 WB	Biozol GmbH, Eching	ABN-PAB12542-100
SR-B1	rb	1:100 FC	Novus Biologicals, Littleton	NB400-104
Tubulin	ms	1:2000 WB	Sigma-Aldrich Chemie GmbH, Taufkirchen	T6074

Table 5.20.: Secondary antibodies

Name	Dilution	Company
Peroxidase-AffiniPure goat anti-mouse IgG (H+L)	1:10,000 WB	JacksonImmunoResearch Laboratories, Suffolk (UK)
Peroxidase-AffiniPure goat anti-rabbit IgG (H+L)	1:10,000 WB	JacksonImmunoResearch Laboratories, Suffolk (UK)
Peroxidase-AffiniPure donkey anti-goat IgG (H+L)	1:10,000 WB	JacksonImmunoResearch Laboratories, Suffolk (UK)
Alexa Fluor 488 donkey anti-mouse IgG (H+L)	1:1,500 IF	Life Technologies, Darmstadt
Alexa Fluor 488 donkey anti-mouse IgG (H+L)	1:1,500 IF	Life Technologies, Darmstadt
Alexa Fluor 488 donkey anti-rabbit IgG (H+L)	1:1,500 IF	Life Technologies, Darmstadt
Alexa Fluor 555 donkey anti-mouse IgG (H+L)	1:1,500 IF	Life Technologies, Darmstadt
Alexa Fluor 555 donkey anti-rabbit IgG (H+L)	1:1,500 IF	Life Technologies, Darmstadt
Alexa Fluor 647 donkey anti-goat IgG (H+L)	1:1,500 IF	Life Technologies, Darmstadt

Table 5.21.: Dyes

Dye	Concentration	Company
Bodipy 493/503	1 μg/ml	Life technologies, Darmstadt
Bodipy 650/665	50 ng/ml	Life technologies, Darmstadt
Coomassie Blue G	0.5% (w/v)	Sigma-Aldrich Chemie GmbH, Taufkirchen
Crystal violet		Geyer Th. GmbH & CO. KG, Renningen
Hoechst	2 μg/ml	Sigma-Aldrich GmbH, Taufkirchen

5.8. Enzymes

All restriction endonucleases were purchased from New England Biolabs GmbH and used with buffers according to manufacturer's instructions.

Table 5.22.: Other enzymes

Name	Company
Alkaline phosphatase, Calf Intestinal (CIP)	New England Biolabs GmbH, Ipswich (USA)
Maxima SYBR Green/Rox qPCR Master Mix	Life Technologies, Darmstadt
Phusion High-Fidelity DNA Polymerase	ThermoFisher Bioscience, Darmstadt
Proteinase K	Life Technologies, Darmstadt
Super Script III Reverse Transcriptase	ThermoFisher Bioscience, Darmstadt
T4 DNA ligase	ThermoFisher Bioscience, Darmstadt
T4 Polynucleotide kinase	New England Biolabs GmbH, Ipswich (USA)
Taq DNA polymerase	ThermoFisher Bioscience, Darmstadt
T4 DNA polymerase, LIC qualified	Novagen, Madison (USA)

5.9. Inhibitors

Table 5.23.: Inhibitors

Name	Company
Antipain	Sigma-Aldrich Chemie GmbH, Taufkirchen
DGAT1	Santa Cruz, Heidelberg
Leupeptin	Sigma-Aldrich Chemie GmbH, Taufkirchen
Pepstatin A	Biomol GmbH, Hamburg
Phenylmethylsulfonyl fluoride	Sigma-Aldrich Chemie GmbH, Taufkirchen
Protease inhibitor cocktail (PIC)	Sigma-Aldrich Chemie GmbH, Taufkirchen
RNAse AWAY	Carl Roth GmbH, Karlsruhe
RNAse inhibitor	Life Technologies, Darmstadt
Triacsin C	Enzo Life Science GmbH, Farmingdale

5.10. Chemicals

Table 5.24.: Chemicals

Name	Company
100x BSA (Bovine serum albumin for restriction enzymes)	New England Biolabs GmbH, Ipswich (USA)
10x MungBean nuclease buffer	New England Biolabs GmbH, Ipswich (USA)
10x T4-Ligase Buffer	ThermoFisher Bioscience, Darmstadt
10x Taq Buffer KCl	ThermoFisher Bioscience, Darmstadt
25 mM $MgCl_2$ (PCR)	ThermoFisher Bioscience, Darmstadt
2-Mercaptoethanol	Sigma-Aldrich Chemie GmbH, Taufkirchen
5x Phusion HF buffer	ThermoFisher Bioscience, Darmstadt
6-Aminocaproic acid	Sigma-Aldrich Chemie GmbH, Taufkirchen
6x DNA loading dye	ThermoFisher Bioscience, Darmstadt
Acetic acid	AppliChem GmbH, Darmstadt
Acrylamide solution (30%) - Mix 37.5	AppliChem GmbH, Darmstadt
Adenosine triphosphate (ATP)	AppliChem GmbH, Darmstadt
Agar bacteriology grade	AppliChem GmbH, Darmstadt
Agarose basic	AppliChem GmbH, Darmstadt
Albumin from bovine serum	Sigma-Aldrich Chemie GmbH, Taufkirchen

Ammonium chloride	Sigma-Aldrich Chemie GmbH, Taufkirchen
Ampicillin	AppliChem GmbH, Darmstadt
APS (Ammonium persulfate)	AppliChem GmbH, Darmstadt
ATP (Adenosine triphosphate)	AppliChem GmbH, Darmstadt
Bacto-trypton	AppliChem GmbH, Darmstadt
Bis-Tris	Sigma-Aldrich Chemie GmbH, Taufkirchen
Blasticidin S	AppliChem GmbH, Darmstadt
Bovine albumin (fatty acid free)	Sigma-Aldrich Chemie GmbH, Taufkirchen
Bromophenol blue	AppliChem GmbH, Darmstadt
Calcium chloride ($CaCl_2$)	AppliChem GmbH, Darmstadt
Chloroform	AppliChem GmbH, Darmstadt
Chloroquine diphosphate	Sigma-Aldrich Chemie GmbH, Taufkirchen
Coomassie brilliant blue G	Sigma-Aldrich Chemie GmbH, Taufkirchen
D(+)-Glucose monohydrat	AppliChem GmbH, Darmstadt
Dimethyl sulfoxide (DMSO)	AppliChem GmbH, Darmstadt
di-potassium hydrogen phosphate (K_2HPO_4)	AppliChem GmbH, Darmstadt
Disodium phosphate (Na_2HPO_4)	AppliChem GmbH, Darmstadt
dNTP Mix 10 mM	ThermoFisher Bioscience, Darmstadt
Dodecyl sulfate sodium salt	AppliChem GmbH, Darmstadt
Dulbecco's modified eagle medium (High glucose) (Gibco)	ThermoFisher Bioscience, Darmstadt
Dulbecco's phosphate buffered saline (DPBS)	Sigma-Aldrich Chemie GmbH, Taufkirchen
ECL lumi-light western blotting substrate	Hoffmann-la Roche, Basel (Switzerland)
EDTA	AppliChem GmbH, Darmstadt
EtBr (Ethidium bromide)	AppliChem GmbH, Darmstadt
Ethanol	Geyer Th. GmbH & Co.KG, Renningen
Ethanol absolute (used for RNA isolation)	AppliChem GmbH, Darmstadt
Ethanol ROTIPURAN 99,8%	Roth GmbH + Co. KG, Karlsruhe
Fetal Calf Serum (FCS)	Biochrom AG, Berlin
Formaldehyde - Solution 37%	AppliChem GmbH, Darmstadt

G418 disulfate	AppliChem GmbH, Darmstadt
GlutaMAX 100x (Gibco)	ThermoFisher Bioscience, Darmstadt
Glutathione	AppliChem GmbH, Darmstadt
Glycerol anhydrous	AppliChem GmbH, Darmstadt
Glycine	AppliChem GmbH, Darmstadt
HEPES	Sigma-Aldrich Chemie GmbH, Taufkirchen
Hydrogen chloride	AppliChem GmbH, Darmstadt
Hydrogen peroxide 10%	AppliChem GmbH, Darmstadt
Isopropanol	AppliChem GmbH, Darmstadt
Isopropanol (used for RNA isolation)	Sigma-Aldrich Chemie GmbH, Taufkirchen
Magnesium chloride	AppliChem GmbH, Darmstadt
Methanol (MeOH)	AppliChem GmbH, Darmstadt
MG132	Merck, Darmstadt
Monopotassium phosphate (KH_2PO_4)	AppliChem GmbH, Darmstadt
n-Dodecyl β-D-maltoside	Sigma-Aldrich Chemie GmbH, Taufkirchen
Nonfat dried milk powder	AppliChem GmbH, Darmstadt
Nonidet-P40	AppliChem GmbH, Darmstadt
Nuclease-free water	ThermoFisher Bioscience, Darmstadt
Oleic acid	Sigma-Aldrich Chemie GmbH, Taufkirchen
OptiMEM (Gibco)	ThermoFisher Bioscience, Darmstadt
OptiPREP (60% Iodixanol)	Sigma-Aldrich Chemie GmbH, Taufkirchen
Palmitic acid [1-14C]	Hartmann Analytic GmbH, Braunschweig
Paraformaldehyde (PFA)	AppliChem GmbH, Darmstadt
Penicillin/Streptomycin 100x	Sigma-Aldrich Chemie GmbH, Taufkirchen
Phenole-Chloroform-Isoamyl alcohol (25:24:1 vol/vol/vol)	AppliChem GmbH, Darmstadt
Phenylmethylsulfonyl fluoride (PMSF)	AppliChem GmbH, Darmstadt
Polybrene (Hexadimethrine bromide)	Sigma-Aldrich Chemie GmbH, Taufkirchen
Polyethylene glycol (PEG) - 8000	AppliChem GmbH, Darmstadt
Potasium dihydrogen phosphate	AppliChem GmbH, Darmstadt
Potassium acetate	AppliChem GmbH, Darmstadt
Potassium chloride (KCl)	AppliChem GmbH, Darmstadt

Potassium hydrogen phosphate	AppliChem GmbH, Darmstadt
Potassium hydroxide (KOH)	AppliChem GmbH, Darmstadt
Potassium phosphate	AppliChem GmbH, Darmstadt
Puromycin	Geyer Th. GmbH & Co.KG, Renningen
Random Hexamer	QIAGEN, Hilden
RNase Away	ThermoFisher Bioscience, Darmstadt
RNAse free water (Ambion)	ThermoFisher Bioscience, Darmstadt
Rotiszint®eco plus	Roth GmbH + Co. KG, Karlsruhe
Silver nitrate ($AgNO_3$)	AppliChem GmbH, Darmstadt
Sodium acetate ($C_2H_3NaO_2$) 3 M pH 5.2	AppliChem GmbH, Darmstadt
Sodium carbonate (Na_2CO_3)	AppliChem GmbH, Darmstadt
Sodium chloride (NaCl)	AppliChem GmbH, Darmstadt
Sodium desoxycholate	AppliChem GmbH, Darmstadt
Sodium dodecyl sulfate (SDS)	AppliChem GmbH, Darmstadt
Sodium hydroxide	AppliChem GmbH, Darmstadt
Sodium hypochlorite	Merck, Darmstadt
Sodium palmitate	Sigma-Aldrich Chemie GmbH, Taufkirchen
Sodium thiosulfate ($Na_2S_2O_3$)	AppliChem GmbH, Darmstadt
Sucrose	AppliChem GmbH, Darmstadt
SuperSignal West Femto	ThermoFisher Bioscience, Darmstadt
TEMED (Tetramethylethylenediamine)	AppliChem GmbH, Darmstadt
TRI Reagent	Sigma-Aldrich Chemie GmbH, Taufkirchen
Tris ultrapure (Tris-base)	AppliChem GmbH, Darmstadt
Tris-HCl	AppliChem GmbH, Darmstadt
Triton X-100	AppliChem GmbH, Darmstadt
Trypan Blue Stain (0.4%) for Countess Automated Cell Counter	Life Technolgies GmbH, Darmstadt
Trypsin/EDTA (0,05% / 0,02% w/v) (Gibco)	ThermoFisher Bioscience, Darmstadt
Tryptone	AppliChem GmbH, Darmstadt
Tween 20 molecular biology grade	AppliChem GmbH, Darmstadt
Water nuclease-free	ThermoFisher Bioscience, Darmstadt

Water Rotisolv HPLC grade	Roth GmbH + Co. KG, Karlsruhe
Yeast extract	AppliChem GmbH, Darmstadt
β-Mercaptoethanol	Sigma-Aldrich Chemie GmbH, Taufkirchen

5.11. Kits

Table 5.25.: Kits

Name	Company
CellTiter 96® AQueous One Solution Reagent	Promega Corporation, Mannheim
DC Protein Assay	BioRad GmbH, Munich
DNA-free DNA removal kit (Ambion)	ThermoFisher Bioscience, Darmstadt
Luciferase Reporter Assay System	Promega Corporation, Mannheim
HCV Core ELISA	BioCat GmbH, Heidelberg
Infinity Triglyceride Reagent	ThermoFisher Bioscience, Darmstadt
Maxima SYBR Green qPCR Master Mix	Life Technologies, Darmstadt
Megascript T7 Transcription Kit	Life Technologies, Darmstadt
NEFA-HR	WAKO Chemicals, Neuss
NEFA-Standard	WAKO Chemicals, Neuss
NucleoBond® XtraMaxi Kit	Macherey-Nagel GmbH + Co KG, Düren
Nucleospin RNA® Virus	Macherey-Nagel GmbH + Co KG, Düren
NucleoSpin® Gel and PCR Clean-Up Kit	Macherey-Nagel GmbH + Co KG, Düren
NucleoSpin® Plasmid Kit	Macherey-Nagel GmbH + Co KG, Düren

5.12. Consumables

Table 5.26.: Consumables

Name	Company
5 Prime Phase-Lock Tube	5Prime GmbH, Hilden
μ-Dish 35 mm, high, Glass Bottom	IBIDI GmbH, Planegg
1.5 ml-reaction tubes RNAse free	Sarstedt AG & Co KG, Nümbrecht
4–20% Mini-PROTEAN® TGX Stain-Free™ protein gels	Biorad GmbH, Munich
15 ml- and 50 ml-tubes (conical)	Greiner GmbH, Frickenhausen
12% Mini-PROTEAN® TGX Stain-Free™ protein gels	Biorad GmbH, Munich
96 Fast PCR Plate half skirt	Sarstedt AG & Co KG, Nümbrecht
96-well micro test plate conical bottom	Sarstedt AG & Co KG, Nümbrecht
Adhesive qPCR seal	Sarstedt AG & Co KG, Nümbrecht
Amersham Hyperfilm ECL	Geyer Th. GmbH & Co.KG, Renningen
Amersham Protran Premium Nitrocellulose membrane	Geyer Th. GmbH & Co.KG, Renningen
Beckmann Ultra-clear tube	Beckman Coulter GmbH, Krefeld
Biosphere Filter Tips	Sarstedt AG & Co KG, Nümbrecht
Blunt-end cannula	Kleiser Medical GmbH, Messkirch
Cannula	Sarstedt AG & Co KG, Nümbrecht
Cell culture dishes	Sarstedt AG & Co KG, Nümbrecht
Cell culture flasks	Sarstedt AG & Co KG, Nümbrecht
Cell culture plates	Sarstedt AG & Co KG, Nümbrecht
Cell scraper	VWR International GmbH, Darmstadt
Cellstar serological pipettes	Greiner GmbH, Frickenhausen
Centrifuge tube, thinwall ultraclear	Beckman Coulter GmbH, Krefeld
Combitips advanced	VWR International GmbH, Darmstadt
Cover slips	VWR International GmbH, Darmstadt
Cryo tubes	Sarstedt AG & Co KG, Nümbrecht
Electroporation cuvette 0.2 mm	VWR International GmbH, Darmstadt
Electroporation cuvette 0.4 mm	VWR International GmbH, Darmstadt
Eppendorf Research plus pipettes	Eppendorf AG, Hamburg

Erlenmeyer flask	VWR International GmbH, Darmstadt
Glass flask	VWR International GmbH, Darmstadt
Glass slides	VWR International GmbH, Darmstadt
Glass-Pistill (Dounce), 7 ml	ThermoFisher Bioscience, Darmstadt
Homogenisator for Douncing, 7 ml	ThermoFisher Bioscience, Darmstadt
Luer-Lok syringe	BD Plastipak, Heidelberg
Microtest plate	Sarstedt AG & Co KG, Nömbrecht
Nunc-Immuno MicroWell 96 well polystyrene plates (white)	ThermoFisher Bioscience, Darmstadt
Parafilm	Bemis, Oshkosh (USA)
PCR plates	Sarstedt AG & Co KG, Nümbrecht
PCR tubes	Sarstedt AG & Co KG, Nümbrecht
Pipette tips	VWR International GmbH, Darmstadt
Pipette tips RNAse free	Sarstedt AG & Co KG, Nümbrecht
Pipettes	Sarstedt AG & Co KG, Nümbrecht
RNAse free microfuge tubes	Life Technologies, Darmstadt
SafeSeal 1.5 ml-reaction tube	Sarstedt AG & Co KG, Nümbrecht
SafeSeal 2 ml-reaction tube	Sarstedt AG & Co KG, Nümbrecht
Steriflip 0.22 μm	Merck Millipore, Darmstadt
Sterile filter 0.22 μm	ThermoFisher Bioscience, Darmstadt
Sterile filter 0.45 μm	ThermoFisher Bioscience, Darmstadt
Syringe	neoLab GmbH, Heidelberg
Tissue culture dishes	Sarstedt AG & Co KG, Nümbrecht
Tissue culture flasks	Sarstedt AG & Co KG, Nümbrecht
Tissue culture plates	Sarstedt AG & Co KG, Nümbrecht
Whatman paper	GE Healthcare, München
PVDF transfer membrane	GE Healthcare, Munich

5.13. Devices

Table 5.27.: Devices

Device	Company
Andor iXON 888	Andor, Belfast (UK)
100x, NA 1.49 CFI Apo TIRF	Nikon, Düsseldorf
405, 488, 561, 647 nm lasers	Andor, Belfast (UK)
7500 fast real time PCR system	Applied Biosystems, Darmstadt
Agarose casting stand	Biorad GmbH, Munich
Agarose gel chamber comb	Biorad GmbH, Munich
Centrifuge 5424R	Eppendorf AG, Hamburg
Centrifuge 5810R	Eppendorf AG, Hamburg
Centrifuge Multifuge 3 SR	ThermoFisher Bioscience, Darmstadt
Centrifuge Sorvall RC5C Plus	ThermoFisher Bioscience, Darmstadt
Dual-camera W2 spinning disk confocal scan head	Yokogawa, Ratingen
GelDoc	Biorad GmbH, Munich
Gene Pulser Xcell electroporation system	Biorad GmbH, Munich
GeneAmp PCR system 9700	Applied Biosystems, Darmstdt
Hera freezer	ThermoFisher Bioscience, Darmstadt
HERAsafe incubator	ThermoFisher Bioscience, Darmstadt
Herasafe sterile bench	ThermoFisher Bioscience, Darmstadt
Infinite M200 plate reader	Tecan Group Ltd, Männedorf
Innova 43 inkubator	New Brunswick Scientific, Hamburg
Leica DMIL microscope	Leica Camera AG, Wetzlar
LS 6500 Scintillation Counter	Beckman Coulter GmbH, Krefeld
LSR Fortessa flow cytometer	BD Bioscience, Heidelberg
Magnetic stirrer heating plate IKA RH basic	IKA®-Werke GmbH & CO. KG, Staufen
Micro centrifuge	Carl Roth GmbH, Karlsruhe
Mini Protean Tetra system	Biorad GmbH, Munich
Multipipette plus	Eppendorf AG, Hamburg
Nanodrop 1000 Spectrophotometer	Peqlab Biotechnologie GmbH, Erlangen

Neubauer Counting Chamber	Cellomics Technology, Halethopre (MD)
Optima L-90K ultracentrifuge	Beckman Coulter GmbH, Krefeld
Pipette boy	VWR International GmbH, Darmstadt
Pipettes Research plus	Eppendorf AG, Hamburg
Sonifier B-12	Danbury, Connecticut (USA)
Thermomixer comfort	Eppendorf AG, Hamburg
UV Illuminator	VWR International GmbH, Darmstadt
Vortex-Genie 2	VWR International GmbH, Darmstadt
Water bath WBT-series	LTF Labortechnik, Wasserburg
Wide Mini Sub Cell GT	Biorad GmbH, Munich

5.14. Software

Table 5.28.: Software

Software	Company
7500 Software v2.3	AB Applied Biosystems, Darmstadt
AutoQuant X2	Media Cybernetics, Cambridge (UK)
BD FACSDiva 8.0.1	BD Science, Heidelberg
Fiji/ ImageJ 1.48t	Wayne Resband, National Institutes of Health (USA)
FlowJo	Treestar Inc., Ashland (USA)
GraphPad Prism (5.03)	Graphpad, La Jola (USA)
Image J	Wayne Resband, National Institutes of Health (USA)
Imaris 7.6.4	Bitplane AG, Zurich (Switzerland)
NIS-Elements	Nikon, Düsseldorf
NIS-Elemetns Ar 4.3	Nikon, Düsseldorf
R Studio	R Studio.Ink, Boston (USA)
Serial Cloner 2.6.1	Softpedia staff, Bucharest (Romania)

6. Methods

6.1. Molecular biochemical methods

6.1.1. Cultivation of bacteria

DH5α and Stbl2 bacteria were cultured in LB media under constant shaking or on LB agar plates at 37 °C. The plasmids carried an ampicillin resistance gene marker enabling to select for the transformed bacteria with LB media supplemented with 100 μg/ml of the antibiotic.

6.1.2. Glycerolstock

Bacteria were cultured overnight in 300–500 ml LB medium supplemented with 100 μg/ml ampicillin under constant shaking at 37 °C. 700 μl of bacteria were mixed with 300 μl 100% glycerol and stored at -80 °C.

6.1.3. Isolation of plasmid DNA

For the isolation of plasmid DNA, the Nucleospin Mini kit or the Nucleobond Xtra Maxi kit was used according to manufactures' instructions. The isolated DNA from the large-scale preparation was resuspended in TE-buffer, pH 7.2. DNA concentration and purity was determined photometrically (NanoDrop).

6.1.4. Phenol-Chloroform extraction

To purify plasmid DNA, a phenol-chloroform-isoamyl alcohol extraction was performed. Therefore, 1 volume of the plasmid DNA was transferred into phase-lock tubes and the 1 volume phenol-chloroform-isoamyl alcohol (25:24:1 vvol/vol/vol) was added. The tubes inverted and centrifuged at 12,000 x g for 15 min at RT. Afterwards, 100 μl chloroform was added and the second centrifugation step for 5 min at the same speed was performed. The aqueous phase was transferred into a new tube and the DNA was precipitated overnight at -20 °C by adding 1/10 volume 3 M NaAc and 2.5 volume 99.5% ethanol. Then, the DNA was pelleted at 12,000 x g for 20 min at 4 °C. The supernatant was discarded and the pellet was washed with 500 μl 70% ethanol. After another centrifugation step at 12,000 x g for 20 min at 4 °C, the pellet was air dried and resuspended in the appropriate volume of nuclease-free water.

6.1.5. Cloning

Polymerase chain reaction (PCR)

DNA fragments were amplified by PCR using a forward and reverse primer specific for the fragment of interest. Standard reaction mixture and PCR conditions are listed below.

Table 6.1.: PCR mixture

Component	Volume
5x Phusion HF buffer 6	10 μl
10 mM dNTPs	1 μl
10 μM Primer fw	2.5 μl
10 μM Primer rev	2.5 μl
Template DNAs	100 ng
Phusion DNA polymerase	0.5 μl
dH$_2$O	up to 50

Table 6.2.: PCR conditions

Cycles	Time	Temperature	Description
1 x	2 min	98 °C	initial denaturation
25 x	10 s	98 °C	denaturation
	30 s	60 °C	annealing
	1 min	72 °C	elongation
1 x	10 min	72 °C	final elongation
	∞	4 °C	

The PCR product was analyzed by agarose gel electrophoresis on a 1% agarose gel and purified using the Nucleospin PCR & Gel clean up kit according to the manufacturers' instructions.

Restriction endonuclease digest

Insertion of the PCR amplified product into a vector plasmid was performed by cutting the plasmid with restriction enzymes creating the same nucleotides overhangs of the amplified PCR product. A standard restriction protocol is listed below. The insert can also be a product of the restriction digest of a donor plasmid DNA.

Table 6.3.: Restriction digest

Component	Volume/Concentration
DNA	1 μg
Restriction endonuclease I	1 μl
Restriction endonuclease II	1 μl
10x Buffer	2 μl
dH$_2$O	up to 20 μl

Buffer conditions were selected specifically for the needs of the enzyme mixture according to manufacturers' recommendations. The digest of the plasmids or the insert was performed for at least 1 h at 37 °C. Prior to ligation of vector and insert, the vector plasmid was de-phosphorylated to avoid re-ligation of the vector. A standard protocol for de-phosphorylation is listed below and was added to the restriction digest at the end of the incubation time.

Table 6.4.: De-phosphorylation of the vector

Component	Volume/Concentration	Time and Temperature
Vector digest mixture	20 μl	
CIP	1 μl	30 min, 37 °C
10x CutSmart buffer	2.5 μl	
dH$_2$O	up to 25 μl	

Products of the endonuclease restriction digest were checked by agarose gel electrophoresis on a 1% agarose gel and purified using the Nucleospin PCR & Gel clean up kit according to the manufacturers' instructions.

Phosphorylation and annealing of oligonucleotides

Another method for the generation of an insert for ligation into the vector, is the annealing of primers. First, the forward and the reverse primers have to be phosphorylated. The protocol for the phosphorylation mixture is listed below. The reaction was performed for 45 min at 37 °C followed by an incubation for 20 min at 65 °C to inactivate the PNK.

Table 6.5.: Phosphorylation of primer

Component	Volume	Time and Temperature
100 μM Primer	2 μl	
T4 PNK	0.4 μl	45 min, 37 °C
T4 Ligation buffer	1 μl	20 min, 65 °C
dH$_2$O	6.6 μl	

The phosphorylated primers were annealed as described below. After an initial incubation time for 5 min at 95 °C, the temperature dropped 1 °C every minute for 88 min.

Table 6.6.: Annealing of primer

Component	Volume
Phoshorylated primer fw	5 μl
Phoshorylated primer rev	5 μl
Annealing buffer	25 μl
dH$_2$O	15 μl

Ligation

The amplified PCR product or the annealed primers were ligated as described below. The mixture was incubated for 20 s at 28 °C followed by an incubation for 20 s at 4 °C. This step was repeated 49 times before the ligation mixture was transformed into DH5α.

Table 6.7.: Ligation mixture

Component	Volume
Vector	2 μl
Annealed primer	1 μl
Ligase buffer	1 μl
T4 Ligase	0.5
dH$_2$O	5.5 μl

Overlap extension PCR

The overlap extension PCR was used to generate the shRNA-resistant mutant of PLIN2 for overexpression. In a first reaction, two fragments with a complementary overhang were generated. The overlap product contained the silent mutation with or without an HA-TAG. The initial PCR products were then hybridized and amplified in a third PCR reaction (overlap PCR) followed by a purification step. A scheme of the overlap PCR, PCR conditions and reaction mixture are listed below.

Figure 6.1.: Scheme of the overlap PCR principle

Table 6.8.: PCR reaction mixture

Component	Volume
100 ng Template DNA	x μl
10 mM dNTPs	1 μl
100 μM Primer (1,3) fw	2.5 μl
100 μM Primer (2,4) rev	2.5 μl
Phusion DNA polymerase	0.5 μl
5x Phusion DNA polymerase buffer	10 μl
H_2O	x μl

Table 6.9.: PCR conditions

Cycles	Time	Temperature	Description
1 x	2 min	98 °C	initial denaturation
25 x	10 s	98 °C	denaturation
	30 s /kb	60 °C	annealing
	1 min	72 °C	elongation
1 x	10 min	72 °C	final elongation
	∞	4 °C	

The PCR products were analyzed by agarose gel electrophoresis on a 1% agarose gel. The bands with the expected kb size were excised from the gel and purified using the Nucleospin

PCR & Gel clean up kit according to the manufacturers' instructions. Then, the two complementary products were mixed in equimolar amounts, hybridized and amplified as described below.

Table 6.10.: Hybridisation mixture

Component	Volume
Product primer 1+3	x μl
Product primer 2+4	x μl
5x Phusion HF buffer	10 μl
10 mM dNTPs	1 μl
Phusion DNA-Polymerase	0.5 μl
dH$_2$O	x μl
Total volume	45 μl

Table 6.11.: PCR conditions for the elongation reaction

Cycles	Time	Temperature	Description
1 x	2 min	98 °C	initial denaturation
15 x	10 s	98 °C	denaturation
	30 s /kb	60 °C	annealing
	1 min	72 °C	elongation

To amplify and purify the product, 2.5 μl of the sense primer of the primer product 1+3 and 2.5 μl of the antisense primer of primer product 2+4 were added and the final PCR was performed under following conditions:

Table 6.12.: Purification PCR conditions

Cycles	Time	Temperature	Description
1 x	2 min	98°C	initial denaturation
20 x	10 s	98 °C	denaturation
	30 s /kb	60 °C	annealing
	1 min	72 °C	elongation
1 x	10 min	72 °C	final elongation
	∞	4 °C	

Ligation independent cloning

A powerful tool to insert a PCR product into a plasmid is the ligation independent cloning method. This method is dependent on the DNA self-repair mechanism of the bacteria in which the PCR product and the plasmid is transformed. Therefore, the PCR product and the digested plasmids must have complementary overhangs. Then, the purified PCR product and the vector plasmid (without de-phosphorylation) are digested with the T4 DNA Polymerase without NTPs (3' 5' exonuclease activity) to create single stranded overhangs. The digestion mixture is described below. The mixture was incubated for 30 min at 22 °C followed by an incubation for 20 min at 75 °C to inactivate the T4 polymerase.

Table 6.13.: T4 DNA polymerase digestion mixture

Component	Amount
PCR product or vector plasmid	50 ng
10x T4 DNA polymerase buffer	2
T4 DNA polymerase (LIC-qualified)	0.4 μl
100 mM DTT	1 μl
dH$_2$O	add 20 μL

Afterwards, the PCR product and plasmids were annealed as described below and transformed into chemical competent bacteria.

Table 6.14.: Annealing of primer and vector

Component	Volume	Temperature and Time
primer	4 μl	30 sec, 70 °C
vector	2 μl	5 min, RT

Transformation into bacteria

20–100 ng plasmid or 5 μl of the ligation product were incubated with 50 μl bacteria for 30 min on ice. Transformation was performed by heat shock for 30 s at 42 °C following a 2 min incubation time on ice. 200 μl of LB medium without antibiotics was added and the bacteria were incubated for 30–90 min at 37 °C with constant mixing on a thermomixer. Finally, the bacteria were plated on agar plates containing the respective antibiotics for selective pressure and were cultured overnight at 37 °C. Bacterial clones were further investigated by colony PCR and positive clones were cultured to isolate plasmid DNA. Plasmid DNA was further investigated by endonuclease restriction digest and sequencing.

Colony PCR

To analyze whether the bacteria colony harbors the plasmid of interest, a PCR reaction was performed. Therefore, the colony was picked and cultivated on an LB-agar plate. The bacteria were then added to the PCR reaction mixture as described below. Positive clones were further cultivated for the isolation of plasmid DNA and send out for sequencing.

Table 6.15.: PCR reaction mixture per bacterial clone

Component	Volume
10x Taq buffer KCl	2 μl
10mM dNTP	0.4 μl
10μM Primer fw	1 μl
10μM Primer rev	1 μl
25mM MgCl$_2$	1.6 μl
Taq polymerase	0.1 μl
dH$_2$O	13.9 μl

Table 6.16.: PCR conditions

Cycles	Time	Temperature	Description
1 x	10 min	98 °C	initial denaturation
25 x	10 s	98 °C	denaturation
	30 s /kb	60 °C	annealing
	1 min	72 °C	elongation
1 x	10 min	72 °C	final elongation
	∞	4 °C	

Sequencing

DNA plasmids were sequenced at GATC.

6.1.6. RNA *in vitro* transcription

16 μg plasmids encoding the different HCV strains were linearized overnight at 37 °C with SspI or MluI. In case for MluI digestion, the reaction was incubated with 2 μl of MungBean nuclease, 5 μl of 10x MungBean nuclease buffer, and 45 μl digested plasmid for 30 min at 30 °C to remove sticky ends. The plasmid was purified by phenol-chloroform extraction and the digestion was confirmed by electrophoresis on a 1% agarose gel. *In vitro* transcription was performed using the MegaScript T7 kit according to the manufacturers' instructions. RNA quality was analyzed by electrophoresis on a 1% agarose gel and the concentration was determined photometrically (NanoDrop). 10 μg RNA aliquots were stored at -80 °C.

6.2. Cell-biological methods

6.2.1. Freezing and thawing of eukaryotic cells

Cells were thawn in a 37 °C water bath and diluted with pre-warmed medium. Cells were transferred in a T75 flask and cultured in 10 ml DMEM medium. After attachment of the cells, the medium was replaced to remove dead cells. For long-term storage of cell lines, a confluent T175 flask of adherent cells was washed with PBS, trypsinized and resuspended in medium. Cells were transferred into a 50 ml tube, the cell number was determined and cells were centrifuged at 200 x g for 5 min at RT. The collected cells were resuspended in approximately $5*10^6$ cells/ml in FCS containing 10% DMSO to avoid ice crystallization and dehydration of the cells. Cells were transferred to cryo vials and cooled down in a Cool Boy to ensure controlled freezing of cells with a freezing rate of -1°C/min in a -80 °C freezer. The day after, the cells were placed in a liquid nitrogen tank for long-time storage.

6.2.2. Cultivation of eukaryotic cells

All cell lines were cultured in DMEM medium at 37 °C in a humidified air chamber containing 5% CO_2. For passaging, every 2-3 days cells were washed with PBS, and detached by treatment with trypsin/EDTA. Depending on the cell line, the splitting ratio varied between 1:4 to 1:8. If necessary, the cell number was determined via Neubauer Cell Counter and cells were seeded at desired cell number.

6.2.3. Production of lentivirus pseudoparticles and transduction

Lentiviral particles are used for gene transfer in various cell lines (Vigna et al., 2000) and are generated by transient transfection with the help of three different plasmids encoding specific genes necessary for infectious particle production. The system is based on the packing plasmid pCMV delta R8.91 plasmid expressing the Gag-Pol, Tat and Ref Genes of HIV virus type 1, an envelope plasmid pMD.G encoding the G protein from vesicular stomatitis virus (VSV-G) and a third transfer plasmid carrying the insert of interest flanked by HIV-LTR regions. The plasmid carries different fluorescent markers or resistance genes to monitor transduction. The transfection was carried out in 293T cells, carrying the SV40 T-antigen, which is a highly transfectable derivate of the 293 cell line. The cells were seeded in 150 cm^2 dishes at a density of approximately 5x10^6 cells a day before transfection. Then, 20 μg packaging plasmid, 15 μg transfer plasmid and 6 μg envelope plasmid were mixed, filled up with water to 450 μL and 50 μL of 2.5 M $CaCl_2$ were added to facilitate the binding of the DNA and to co-precipitate to the cell surface. The solution was transferred into a 15 ml tube containing the same volume of 2x HBS and was incubated for approximately 30 min at RT. Before adding the transfection mixture, the medium of the cells was exchanged with medium containing 25 μM chloroquine, an inhibitor of lysosomal degradation that protects the foreign DNA. After 6-8 h incubation, the medium was replaced to DMEM due to toxicity of the chloroquine and the transfection mix. The produced

virus was harvested after 72 h by filtration of the supernatant through an 0.45 μm filter and if necessary, concentrated by ultracentrifugation at 100,000 x g for 2 h at 4 °C. The virus was aliquoted and stored at -80 °C. Transduction of cells with the virus was performed overnight in the presence of 4 μg/ml polybrene in the culture medium. The transduction efficacy of the produced lentiviral particles was determined by titration on naïve Huh7.5 cells and further analyzed by measuring the percentage and the mean fluorescence intensity of the fluorescent reporter by flow cytometry. If the cells carried an antibiotic resistance gene, the virus was titrated on naïve Huh7.5 cells and selected for at least one week with the corresponding antibiotic.

6.2.4. Production of HCV viral stocks and infection of naïve cells

Huh7.5 cells were transfected with *in vitro* transcribed (+) ssRNA by electroporation (Kato et al., 2006). Therefore, cells were trypsinized, washed with OptiMEM and 4*10^6 cells were resuspended in 400 μl cytomix containing 8 μL 0.1 M ATP and 20 μL 0.1M Glutathione. 10 μg RNA were added and the cell suspension was transferred into a 4 mm electroporation cuvette. Transfection was performed at 260 V and 950 μF using the Gene Pulser II. The cells were diluted with DMEM and plated in a T75 flask. After 3–4 h the media was exchanged and the cells were transferred into the BSL3** lab for further cultivation. After three days the supernatant was used to infected naïve cells. The medium of the infected cells was collected for 1 to 2 weeks, filtered, aliquoted and stored at -80 °C. Supernatant of low replicating virus was concentrated by PEG8000 precipitation. The viral titer was determined by TCID$_{50}$ titration on Huh7.5-RFP-NLS-IPS cells (Jones et al., 2010).

Naïve cells were infected by inoculation with viral supernatant or concentrated stock for 4–24 h. The medium was changed and in case of a selection marker in the HCV strain, the corresponding antibiotic was added to the culture media.

6.2.5. Concentration of HCV viral stocks

Supernatant of low replicating virus was incubated overnight with PEG8000 in a 50 ml tube to a final concentration of 10% at 4 °C. The next day, the virus was pelleted by centrifugation at 4 °C and 1,300 x g for at least 1 h. The supernatant was removed and the virus was resuspended in 1 ml DMEM per 50 ml viral supernatant. The viral stock was aliquoted and stored at -80 °C.

6.2.6. Determination of the tissue culture infectious dose (TCID$_{50}$) of HCV viral stocks

The tissue culture infectious dose (TCID$_{50}$) of viral particles was calculated using the Reed and Munch method (Reed LJ, 1938). Therefore, Huh7.5 cells carrying the RFP-NLS-IPS reporter construct (Jones et al., 2010) were used. The cells were seeded in a 96-well plate and infected with serial dilutions of either viral supernatant or concentrated viral stocks. After 2–3 days the cells were fixed with PFA to a final concentration of 2% PFA. Foci of infected cells were detected by the translocation of the RFP-NLS into the nucleus.

6.2.7. HCV spreading infection assay

Cells were infected with an HCV reporter strain carrying EGFP with a MOI of 0.01. After 24 h, the cells were seeded into a 6-well plate and harvested after two, four, and six days. Viral spreading was measured by monitoring the fluorescent marker via flow cytometry.

6.2.8. HCV replicon assays with antibiotic selection

For subgenomic replicon assays with construct carrying an antibiotic resistance gene, cells were electroporated with *in vitro* transcribed replicon RNA as described before. The cells were seeded in 10 cm^2 cell culture dishes and selected with 1 mg/ml G418. As a negative control, naïve cells were seeded at the same density in a 10 cm^2 dish and selected with the same antibiotic. After 2–3 weeks of selection, the cells were fixed with 2% PFA for 20 min and surviving, e.g. HCV replicating cell colonies, were stained with crystal violet.

6.2.9. Luciferase HCV replicon assays

Huh7.5 cells were electroporated with *in vitro* transcribed subgenomic Jc1△E1E2$^{NS5AB-Luc}$ RNA as described before. Cells were resuspended in 13 ml DMEM and seeded in a 12-well plate at a density of 1.5*10^{5}c/well. To analyze the transfection efficiency as well as viral RNA replication, the cells were harvested after 4h, 24 h, 48 h, and 72 h post transfection. Therefore, the cells were washed once with PBS, lysed with 150 μl 1x cell culture lysis buffer and stored at -20 °C until all samples were harvested. Afterwards, samples were transferred into a 96-well plate and centrifuged for 5 min at 300 x *g* at to remove cell debris. The supernatant was transferred into a new 96-well plate. To measure the firefly luciferase activity, the luciferase assay system (Promega) was used. 20 μl of sample were mixed with 100 μl of luciferase assay reagent and the absorbance was measured at 595 nm using the Tecan Infinite M200 plate reader. The relative light units of the luciferase assay were normalized to the protein amount and to the transfection efficiency measured after 4 h.

6.2.10. Cell viability assay

Viability of transduced cells was analyzed using CellTiter 96 AQueous One Solution Reagent (Promega) according to manufacturer's instructions.

6.2.11. Flow cytometry analysis

The cells were trypsinized, resuspended in DMEM and transferred in a 1.5 ml tube. After centrifugation for 5 min at 300 x *g* at room temperature, the supernatant was discarded and the cell pellet was resuspended in PBS containing 2% PFA to fix the cells.

6.2.12. Cell surface staining

Cells were washed once with PBS, detached with 0.5 mM EDTA/PBS at 37 °C and transferred in a 1.5 ml tube. To collect the cells, a centrifugation step was performed for 5 min at 300 x *g* at room temperature. The cells were washed once in PBS containing 1% FCS. To label the cells with different primary antibodies, the cells were resuspended in 100 μl antibody solution containing 1% FCS and incubated for 15 min at room temperature. Afterwards, the cells washed once with PBS/1% FCS and resuspended in secondary antibody solution. After a second incubation for the same time in the dark, cells were centrifuged and resuspended in PBS / 1% FCS containing 2% PFA to fix the cells.
All samples were measured on the LSR Fortessa (BD Bioscience) flow cytometer and analyzed using FlowJo software (Treestar).

6.2.13. Immunofluorescence staining and lipid droplets staining

For immunofluorescence studies, cells were seeded on coverslips and, after fixation with 2% PFA, the cells were permeabilized with 0.1% triton X-100 for 5 min at RT. Following a 1 h incubation with IF blocking solution, the cells were incubated with antibodies in IF blocking solution overnight at 4 °C. Afterwards, the cells were washed and incubated with the secondary antibody in IF blocking solution. To visualize the lipid droplets and/or the nuclei, the cells were washed and incubated with Bodipy650/665 and Hoechst diluted in PBS for 1 h at RT. Then, the coverslips were embedded in Mowiol mounting medium (Longin et al., 1993). For imaging a spinning disk confocal microscope was used. The microscope is equipped with an 100x, NA 1.49 CFI Apo TIRF Nikon and a dual-camera Yokogawa W2 Spinning disk confocal scan head and Andor iXON 888 cameras. An Andor Borealis System ensured Illumination flatness of 405, 488, 561, 647 nm lasers. For colocalization analysis, the coloc2 plugin of Fiji (Schindelin et al., 2012) was used to determine the Manders' overlap coefficient. To analyze the lipid droplet morphology, Huh7.5 cells stably expressing the HCV reporter RFP-NLS-IPS were used. Cells were infected with HCV, seeded on μ-Dishes (IBIDI) and fixed with 2% PFA prior to the lipid droplet and nuclei staining using Bodipy493/503 and Hoechst, respectively. A spinning disk confocal microscope was used to record z-stacks. The images were deconvoluted with 75 iterations

and a high noise level using the AutoQuant X2 software. The intensity threshold was reduced to 1/5 of the highest intensity and volumetric analysis of the recorded z-stacks was performed using the 3D objects counter function of Fiji (Bolte et al., 2006). The 3D reconstruction was visualized using the Imaris Bitplane software. Objects below the resolution of the microscope and the acquisition settings were excluded from the analysis ($0.028~\mu m^3$).

6.2.14. Lipid droplet isolation

For the isolation of lipid droplets, approximately 1–2 x10^6 cells were seeded in a 150 cm^2 cell culture dish. After two to five days, the cells were washed with cold PBS, scraped and collected in a 50 ml tube. After centrifugation at 300 x *g* for 5 min at 4 °C, the supernatant was removed and the pellet was resuspended in 4 ml sucrose buffer containing protease inhibitors. Cells were destroyed with a tight-fitting Dounce homogenizer and cell nuclei were collected by centrifugation at 1,000 x *g* for 10 min at 4 °C. The post-nuclear supernatant was transferred in SW41 Ti centrifuge tubes and overlaid with an isotonic potassium phosphate buffer. To separate lipid droplets, an ultracentrifugation step was performed in a SW41 Rotor at 36,000 x *g* for 2 h at 4 °C. The upper phase containing the purified lipid droplets was collected with a gauge needle and transferred in a 1.5 ml tube. To concentrate the lipid droplets fraction, a centrifugation step was performed at 21,000 x *g* for 20 min at 4 °C. The aqueous phase was reduced with a gauge needle and the protein concentration was determined with a DC Protein Assay according to manufacturer's recommendations. For western blot analysis, lipid droplets were denaturized in 6x Laemmli buffer followed by SDS-PAGE and western blotting.

6.2.15. Lipid droplet isolation for *in vitro* self-digestion

Lipid droplets were isolated with a slightly modified protocol as described above: Instead of a protease inhibitor cocktail, the protease inhibitors leupeptin (20 μg/ml), antipain (2 μg/ml) and pepstatin (1 μg/ml) were used. The pH of the sucrose buffer was adjusted to 7.2. Cells were destroyed mechanically; cell nuclei were removed and the supernatant was placed onto a SW41 Ti centrifuge tube and overlaid with an isotonic potassium phosphate buffer. The floating lipid droplet fraction was harvested, concentrated by centrifugation, sonicated and further processed to determine the lipid droplet associated lipase activity as described in 6.3.8.

6.2.16. Inhibition of the lysosomal and proteasomal degradation pathway

For the analysis of the ApoE degradation pathway, 4 x 10^5 cells were seeded in a 6-well plate. The cells were either treated for 12–16 h with 2 μg/ml of the proteasomal inhibitor MG132 or for 6 h with 100 μg/ml leupeptin, 200 μM Chloroquine or 10 mM NH$_4$Cl as lysosomal inhibitors. Then, the cell lysates were harvested for SDS-PAGE followed by western blot analysis. Band intensities were quantified using the densitometric quantification function of Fiji.

6.3. Biochemical Methods

6.3.1. SDS-Polyacrylamide-Electrophoresis (SDS-PAGE) and western blotting

Cells were lysed under denaturing conditions using RIPA buffer supplemented with protease inhibitors. The SDS-PAGE usually consists of two different gel matrices: a stacking gel with a neutral pH and 4% acrylamide where all proteins are concentrated before running into the separation gel with a basic pH. According to the expected size of the protein, different concentrations of acrylamide in the separation gel were used (Laemmli, 1970). Proteins bigger than 200 kDa were run on a gel without separation gel to avoid sticking of protein in the stacking gel. Prior to loading, the sample was mixed with 6x Laemmli buffer in the ratio 1:6 and boiled at 95 °C for at least 5 min. The samples were loaded on the gel and electrophoresis was performed in running buffer at constant voltage of 200 V for approximately 45 min. A protein standard was run on the same gel for the estimation of the size of the protein. The gel was blotted on a nitrocellulose membrane in blotting buffer for 90 min at 80 V. The membrane was blocked in blocking solution for 1 h at RT prior to the overnight incubation with the primary antibody at 4 °C. Then, the membrane was washed 3 x in 1x TBS-T and incubated with the secondary antibody for 1 h at RT. Afterwards, another washing step (3 x in 1x TBS-T) was performed. To visualize the proteins, the chemiluminescence substrate Lumi-Light or SuperSignal West Femto was used. The HRP catalyzes the oxidation of luminol under the presences of H_2O_2 by emitting light. The emitted light was detected on an ECL Hyperfilm (Amersham). The sensitivity of the ECL-Lumi-Light system is in the range of 10-50 pg antigen. For the detection of proteins in the femtogram range, the SuperSignal West Femto Maximum Sensitivity Substrate (Thermo Fisher) was used.

6.3.2. 2D blue native PAGE of cell lysates

For the analysis of the formation of core complexes, the cells were transfected with HCV Jc1[NS5AB-EGFP] RNA. Three days post electroporation, same amounts of cells were trypsinized, centrifuged for 3 min at 300 x g and resuspended in 80 μl native PAGE buffer. 15 μl 10% n-dodecyl-β-D-maltopyranoside were added and the samples were lysed on ice for 30 min under non-denaturing conditions. Cell nuclei were removed by centrifugation at 16,000 x g and 4 °C for 30 min. To the post-nuclear fractions 20 μg/ml leupeptin, 2 μg/ml antipain and 1 μg/ml pepstatin as protease inhibitors were added. Then, the samples were mixed with the same volume of 2x non-reducing sample buffer before 10 μl 5% Coomassie Brilliant Blue G were added. 40 μl of the sample was loaded on a 4–20% polyacrylamide precast gradient gel. A constant voltage of 200 V was applied for 5 min and the separation of the proteins by charge in the first dimension was performed at 150 V for 2 h. For the 2nd dimension the gel was incubated in 2x SDS sample buffer for 1 h. Sample lanes of the blue native PAGE were sliced out and applied horizontally on a 15% polyacrylamide SDS gel and electrophoresis was performed in SDS running buffer as described above. To analyze core complex formation by western blotting the proteins were transferred onto a PVDF membrane.

6.3.3. 2D blue native PAGE of cell compartments

To obtain the microsomal- and the lipid droplet fraction, Jc1[NS5AB-EGFP] infected cells were lysed mechanically as described in 6.2.14. The sucrose buffer contained the protease inhibitors 20 μg/ml leupeptin, 2 μg/ml antipain, and 1 μg/ml pepstatin instead of the protease inhibitor cocktail. Post-nuclear fractions were centrifuged 3 x for 10 min at 10,200 x g at 4 °C to remove mitochondria. Lipid droplets and ER were separated from the supernatant by centrifugation for 1 h at 100,000 x g at 4 °C. The samples were adjusted to the same protein concentrations in native PAGE buffer. The supernatant was mixed with Coomassie blue G to a final concentration of 0.5% and used for 2D blue native PAGE as described above.

6.3.4. Silver staining

The samples were loaded on a SDS gel and separated by electrophoresis as described above. The gel was fixed in fixation solution for at least 1 h. Then, the gel was washed three times with washing solution followed by incubation for 60 sec in pretreatment solution. The gel was washed 2x in dH$_2$O prior to 20 min incubation in impregnate solution. Afterwards, the gel was washed 2x in dH$_2$O and the development solution was added for 1–3 min until the first bands appear. The reaction was stopped by washing twice with dH$_2$O following 10 min incubation in stopping solution. Images of the gel were acquired on a BioRad Gel Doc.

6.3.5. Triglyceride extraction using the Bligh and Dyer method

Cells were grown until 90% confluence in a 6-well plate. Then, the cells were washed with PBS and detached in 600 μl methanol using a cell scraper, transferred into 2 ml tubes. To each sample 300 μl chloroform were added and incubated for 1 h at RT under constant shaking in a thermomixer. Afterwards, 300 μl HPLC-grade H$_2$O was added, samples were mixed and incubated for another 30 min at RT under constant shaking on a thermomixer. Next, the samples were centrifuged at 17,000 x g for 30 min at 4 °C to separate the organic phase from the inter-/water phase. The organic phase (bottom) was transferred to a 2 ml tube. A second extraction step was performed by adding 300 μl chloroform to the remaining inter-/water phase. Then, the samples were incubated and separated by centrifugation as described above. The organic phase was pooled with the first organic phase and supplemented with 5% triton X-100. The solvent was evaporated under a nitrogen stream and the resulting lipids were resuspended in water (to a final triton X-100 concentration of 2.5%). The quantification of the triglycerides was performed using the infinity triglyceride reagent (Thermo Fisher). Therefore, 25–30 μl of the sample were incubated with 150 μl infinity triglyceride reagent solution in a 96-well plate for 30 min at 37 °C. In addition, a glycerol standard (0.0625 mg/ml to 2.5 mg/ml in dH$_2$O) was used in parallel allowing calculating the triglyceride concentration of the samples. The absorbance was measured at 570 nm using the Tecan Infinite M200 plate reader.

6.3.6. Proteinase K protection assay

The proteinase K protection assay allows to analyze the envelopment of membrane proteins (Gentzsch et al., 2013). Therefore, cells were electroporated with HCV Jc1[NS5AB-EGFP] RNA and seeded in a 6-well plate. 48 h post electroporation cells were either resuspended in 150 μl proteinase K buffer or prepared for flow cytometry analysis to verify equal transfection rates. For the protection assay, cells were lysed by five freeze and thaw cycles. Afterwards, the cells were divided into three equal aliquots and were left either untreated, treated with 100 μg/ml proteinase K or with 1% triton X-100 and proteinase K as control for digestion. The digestion of membrane proteins was stopped by adding 5 mM phenylmethanesulfonyl fluoride. Proteinase K digestion was analyzed by SDS-PAGE followed by western blotting. Band intensities were quantified using the densitometric quantification function of Fiji.

6.3.7. Measurement of Apolipoprotein expression and secretion

For the analysis of ApoE and B expression and secretion, 4 x 10^5 cells were seeded in a 6-well plate. The day after, the medium was replaced to OptiMEM to avoid cross-reactivity with the serum proteins and the antibodies used for the detection of ApoB. The next day, the cells lysates and the supernatant was harvested. Same proteine amounts of the cell lysates and the same volume of the supernatant were used for SDS-PAGE following western blot analysis. Band intensities were quantified using the densitometric quantification function of Fiji.

6.3.8. Lipid droplet–associated lipase activity assay

The triglyceride concentration of the isolated lipid droplets was measured using the Infinity Triglyceride Kit (Thermo Fisher). Depending on the yield, between 0.4 to 1 mM of the triglycerides were used for self-digestion with 1% BSA (FA-free, Sigma) as a carrier at 37 °C with continuous shaking on a thermomixer for 1 h. To solubilize the released FFA, triton X-100 was added to final concentration of 1%, incubated for 10 min at RT and, following centrifugation for 30 min at 20,000 x g at RT, the FFA concentration of the underlying solution was determined with a NEFA kit (WAKO chemicals). The amount of released FFA reflects the lipid droplet–associated lipase activity.

6.3.9. Rate of mitochondrial β-oxidation

Free fatty acids can be oxidized in the mitochondria by multiple steps called β-oxidation (Huynh et al., 2014). The resulting acetyl-CoA enters the TCA cycle and can be further oxidized to CO_2. To measure the amount of β-oxidation, the cells were plated in a 24-well plate and were grown to 80% confluency. To inhibit the synthesis of lipid droplets, a DGAT1 inhibitor to a final concentration of 20 μM were added to the cells 12 h before the assay was performed. As a control, cells were treated with DMSO. The next day, the culture media was replaced by 0.5 ml of 0.3% BSA/ 100 μM palmitate/0.4 μCi/ml ^{14}C-palmitate mixture containing 1 mM

L-carnitine. After 3 h incubation at 37 °C and 5% CO_2, the supernatant was transferred into tubes prefilled with 200 μl of 1 M perchloric acid. Inside the cap of the tubes, a paper disc soaked with 1 M NaOH was placed to capture the released $^{14}CO_2$. These tubes were incubated for 1 h at RT under constant shaking. The paper discs were removed and transferred into a scintillation vial containing 4 ml of scintillation solution. To measure the acid soluble metabolites, the supernatant was centrifuged at 14,000 x g for 10 min and the supernatant was transferred into a scintillation vial. All measurements were performed in technical replicates. Read out of the radioactive ^{14}C was performed on the LS 6500 Scintillation Counter. The rate of converted ^{14}C was normalized to the protein amount of the cells.

6.3.10. RNA isolation of cell lysates

The cells were seeded in a 6-well plate and grown to ~80% confluence before the lysates were harvested. Therefore, the medium was removed; 1 ml TriReagent was added and mixed by pipetting. The lysates were transferred to a 1.5 ml tube and stored at -80 °C or immediately used for extraction. For the extraction, 200 μl chloroform were added and tubes were inverted for 15 sec. After 3 min incubation time at RT, the samples were centrifuged for 15 min at 12,000 x g and 4 °C. The upper phase was transferred into a new 1.5 ml-reaction tube. 500 μl isopropanol were added, and gently mixed by inverting following 10 min incubation at RT. A centrifugation step for 10 min at 1,200 x g and 4 °C was performed to remove the supernatant. The pellet was washed once with 1 ml 75% ethanol and centrifuged for 5 min at 7,500 x g and 4 °C. The supernatant was removed and the pellet was resuspended in 18 μl dH$_2$O. To remove DNA, 1.8 μl 10x rDNase buffer and 1 μl rDNaseI were added and incubated for 30 min at 37 °C. To inactivate the enzyme, 1.8 μl DNase inactivator was added and samples were incubated for 2 min at room temperature following a centrifugation step for 1.5 min at 10,000 x g at RT. The supernatant was transferred into a fresh 1.5 ml-reaction tube and the concentration was measured with a NanoDrop. The RNA was stored at -80 °C.

6.3.11. Isolation of viral RNA of the supernatant

Viral RNA of the supernatant was isolated using Nucleo-Spin RNA Virus kit (Macherey Nagel) according to manufacturer's recommendations.

6.3.12. cDNA synthesis

1 μg of the isolated RNA was reverse transcribed into cDNA using Superscript III reverse transcriptase (Invitrogen) with random hexamer primers (Qiagen) and RNaseOut (17,500 U, Thermo Fisher).

6.3.13. Preparation of the HCV Standard

To prepare a qPCR standard, 1 μg of *in vitro* transcribed Jc1 RNA was synthesized into cDNA as described above. The cDNA standard was diluted from 1:10^2 to 1:10^8. 1 μl of each dilution was used as a template for qRT-PCR corresponding to 0.01-10,000 pg RNA per qRT-PCR reaction.

6.3.14. Quantitative real-time PCR (qRT-PCR)

The synthesized cDNA was subjected to qPCR using the Maxima SYBR green master mix (Thermo Fisher) on a 7900HT Fast Real-time PCR System (Applied Biosystems). The qRT-PCR reaction mixture and PCR program is listed above. For gene expression analysis, the samples were either normalized to 18S rRNA and to control cells and shown as $2^{-\Delta\Delta Ct}$ or normalized to 18S rRNA and shown as $2^{-\Delta Ct}$.

Table 6.17.: qRT-PCR mixture

Component	Volume
2x SYBR green	10 μl
ROX (5 μm)	0.04 μl
PCR primer mix	0.6 μl
cDNA	1 μl
dH$_2$O	8.24 μl

Table 6.18.: qRT PCR conditions

Cycles	Time	Temperature	Description
1 x	10 min	95°C	initial denaturation
40 x	15 s	95°C	denaturation
	1 min	60°C	annealing/extension

6.4. Statistical analysis

For statistical analysis, R (R Core Team, 2015), RStudio (Team, 2015), and GraphPadPrism (GraphPad Software, Inc) were used. Statistical analysis was performed using unpaired two-tailed Welch's t-test and in case of normalized data one sample t-test. For the analysis of the lipid droplet volume, the Wilcoxon-Mann-Whitney-Test was used.

7. Danksagung

8. Eidesstattliche Versicherung

Hiermit versichere ich an Eides statt, die vorliegende Dissertation selbst verfasst und keine anderen als die angegebenen Hilfsmittel benutzt zu haben. Die eingereichte schriftliche Fassung entspricht der auf dem elektronischen Speichermedium. Ich versichere, dass diese Dissertation nicht in einem früheren Promotionsverfahren eingereicht wurde.

Hamburg, den

Bibliography

Abid, K., V. Pazienza, A. de Gottardi, L. Rubbia-Brandt, B. Conne, P. Pugnale, C. Rossi, A. Mangia, and F. Negro (2005). "An in vitro model of hepatitis C virus genotype 3a-associated triglycerides accumulation". In: *J Hepatol 42(5): p. 744-51*.

Ai, L. S., Y. W. Lee, and S. S. Chen (2009). "Characterization of hepatitis C virus core protein multimerization and membrane envelopment: revelation of a cascade of core-membrane interactions". In: *J Virol 83: 9923-39*.

Amako, Y., T. Munakata, M. Kohara, A. Siddiqui, C. Peers, and M. Harris (2015). "Hepatitis C virus attenuates mitochondrial lipid beta-oxidation by downregulating mitochondrial trifunctional-protein expression". In: *J Virol 89(8): 4092-4101*.

Andre, P., F. Komurian-Pradel, S. Deforges, M. Perret, J. L. Berland, M. Sodoyer, S. Pol, C. Brechot, G. Paranhos-Baccala, and V. Lotteau (2002). "Characterization of low- and very-low-density hepatitis C virus RNA-containing particles". In: *J Virol 76(14): p. 6919-28*.

Appel, N., T. Pietschmann, and R. Bartenschlager (2005). "Mutational analysis of hepatitis C virus nonstructural protein 5A: potential role of differential phosphorylation in RNA replication and identification of a genetically flexible domain". In: *J Virol 79(5): p. 3187-94*.

Ariumi, Y., M. Kuroki, M. Maki, M. Ikeda, H. Dansako, T. Wakita, and N. Kato (2011). "The ESCRT System Is Required for Hepatitis C Virus Production". In: *PLoS ONE 6(1): p. e14517*.

Bankwitz, D.and others (2014). "Role of hypervariable region 1 for the interplay of hepatitis C virus with entry factors and lipoproteins". In: *J Virol 88(21): p. 12644-55*.

Barbosa, A.D., D.B. Savage, and S. Siniossoglou (2015). "Lipid droplet-organelle interactions: emerging roles in lipid metabolism". In: *Curr Opin Cell Biol 35: p. 91-7*.

Bartenschlager, R., M. Frese, and T. Pietschmann (2004). "Novel insights into hepatitis C virus replication and persistence". In: *Adv Virus Res 63: p. 71-180*.

Bartenschlager, R., F. Penin, V. Lohmann, and P. Andre (2011). "Assembly of infectious hepatitis C virus particles". In: *Trends Microbiol 19(2): p. 95-103*.

Bell, M., H. Wang, H. Chen, J. C. McLenithan, D. W. Gong, R. Z. Yang, D. Yu, S. K. Fried, M. J. Quon, C. Londos, and C. Sztalryd (2008). "Consequences of lipid droplet coat protein downregulation in liver cells: abnormal lipid droplet metabolism and induction of insulin resistance". In: *Diabetes 57(8): p. 2037-45*.

Benova, L., Y. A. Mohamoud, C. Calvert, and L. J. Abu-Raddad (2014). "Vertical transmission of hepatitis C virus: systematic review and meta-analysis". In: *Clin Infect Dis 59(6): p. 765-73*.

Bickel, P.E., J.T. Tansey, and M.A. Welte (2009). "PAT proteins, an ancient family of lipid droplet proteins that regulate cellular lipid stores". In: *Biochim Biophys Acta 1791(6): p. 419-40*.

Bidell, M. R., M. McLaughlin, J. Faragon, C. Morse, and N. Patel (2016). "Desirable Characteristics of Hepatitis C Treatment Regimens: A Review of What We Have and What We Need". In: *Infect Dis Ther 5(3): p. 299-312*.

Blight, K.J., A.A. Kolykhalov, and C.M. Rice (2000). "Efficient initiation of HCV RNA replication in cell culture". In: *Science 290(5498): p. 1972-1974*.

Bolte, S. and F.P. Cordelieres (2006). "A guided tour into subcellular colocalization analysis in light microscopy". In: *J Microsc 224(Pt 3): p. 213-32*.

Bosma, M., M. K. Hesselink, L. M. Sparks, S. Timmers, M. J. Ferraz, F. Mattijssen, D. van Beurden, G. Schaart, M. H. de Baets, F. K. Verheyen, S. Kersten, and P. Schrauwen (2012). "Perilipin 2 improves insulin sensitivity in skeletal muscle despite elevated intramuscular lipid levels". In: *Diabetes, 61: 2679-90*.

Bosma, M., R. Minnaard, L. M. Sparks, G. Schaart, M. Losen, M. H. de Baets, H. Duimel, S. Kersten, P. E. Bickel, P. Schrauwen, and M. K. Hesselink (2012a). "The lipid droplet coat protein perilipin 5 also localizes to muscle mitochondria". In: *Histochem Cell Biol 137(2): p. 205-16*.

Boulant, S., R. Montserret, R. G. Hope, M. Ratinier, P. Targett-Adams, J. P. Lavergne, F. Penin, and J. McLauchlan (2006). "Structural determinants that target the hepatitis C virus core protein to lipid droplets". In: *J Biol Chem 281(31): p. 22236-47*.

Boulant, S., M. W. Douglas, L. Moody, A. Budkowska, P. Targett-Adams, and J. McLauchlan (2008). "Hepatitis C virus core protein induces lipid droplet redistribution in a microtubule- and dynein-dependent manner". In: *Traffic 9(8): 1268-1282*.

Branche, E., S. Conzelmann, C. Parisot, L. Bedert, P. L. Levy, B. Bartosch, S. Clement, and F. Negro (2016). "Hepatitis C Virus Increases Occludin Expression via the Upregulation of Adipose Differentiation-Related Protein." In: *PLoS One 11(1): e0146000*.

Brasaemle, D. L., T. Barber, A. R. Kimmel, and C. Londos (1997). "Post-translational regulation of perilipin expression. Stabilization by stored intracellular neutral lipids". In: *J Biol Chem 272(14): p. 9378-87*.

Brasaemle, D. L., V. Subramanian, A. Garcia, A. Marcinkiewicz, and A. Rothenberg (2008). "Perilipin A and the control of triacylglycerol metabolism". In: *Mol Cell Biochem*.

Bulankina, A. V., A. Deggerich, D. Wenzel, K. Mutenda, J. G. Wittmann, M. G. Rudolph, K. N. Burger, and S. Honing (2009). "TIP47 functions in the biogenesis of lipid droplets". In: *J Cell Biol 185(4): p. 641-55*.

Burguete, A.S., U. Sivars, and S. Pfeffer (2005). "Purification and analysis of TIP47 function in Rab9-dependent mannose 6-phosphate receptor trafficking". In: *Methods Enzymol 403: p. 357-66*.

Bussell R., Jr. and D. Eliezer (2003). "A structural and functional role for 11-mer repeats in alpha-synuclein and other exchangeable lipid binding proteins". In: *J Mol Biol 329(4): p. 763-78*.

Camus, G., E. Herker, A. A. Modi, J. T. Haas, H. R. Ramage, Jr. R. V. Farese, and M. Ott (2013). "Diacylglycerol acyltransferase-1 localizes hepatitis C virus NS5A protein to lipid droplets and enhances NS5A interaction with the viral capsid core". In: *J Biol Chem 288(14): p. 9915-23*.

Camus, G., M. Schweiger, E. Herker, C. Harris, A. S. Kondratowicz, C. L. Tsou, R. V. Farese, K. Herath Jr., S. F. Previs, T. P. Roddy, S. Pinto, R. Zechner, and M. Ott (2014). "The hepatitis C virus core protein inhibits adipose triglyceride lipase (ATGL)-mediated lipid mobilization and enhances the ATGL interaction with comparative gene identification 58 (CGI-58) and lipid droplets". In: *J Biol Chem 289(52): 35770-35780*.

Cao, X., Q. Ding, J. Lu, W. Tao, B. Huang, Y. Zhao, J. Niu, Y. J. Liu, and J. Zhong (2015). "MDA5 plays a critical role in interferon response during hepatitis C virus infection". In: *J Hepatol 62(4): p. 771-8*.

Catanese, M. T., K. Uryu, M. Kopp, T. J. Edwards, L. Andrus, W. J. Rice, M. Silvestry, R. J. Kuhn, and C. M. Rice (2013). "Ultrastructural analysis of hepatitis C virus particles". In: *Proc Natl Acad Sci U S A 110(23): p. 9505-10*.

Chang, B. H., L. Li, A. Paul, S. Taniguchi, V. Nannegari, W. C. Heird, and L. Chan (2006). "Protection against fatty liver but normal adipogenesis in mice lacking adipose differentiation-related protein". In: *Mol Cell Biol 26(3): p. 1063-76*.

Chang, K. S., J. Jiang, Z. Cai, and G. Luo (2007). "Human apolipoprotein e is required for infectivity and production of hepatitis C virus in cell culture". In: *J Virol 81: 13783-93*.

Chassey, B. de et al. (2008). "Hepatitis C virus infection protein network". In: *Mol Syst Biol 4: p. 230*.

Chen, E., T. H. Tsai, L. Li, P. Saha, L. Chan, and B. H. Chang (2017). "PLIN2 is a Key Regulator of the Unfolded Protein Response and Endoplasmic Reticulum Stress Resolution in Pancreatic beta Cells". In: *Sci Rep 7: p. 40855*.

Choi, J., K. J. Lee, Y. Zheng, A. K. Yamaga, M. M. Lai, and J. H. Ou (2004). "Reactive oxygen species suppress hepatitis C virus RNA replication in human hepatoma cells". In: *Hepatology 39(1): p. 81-9*.

Choudhary, V., N. Ojha, A. Golden, and W. A. Prinz (2015). "A conserved family of proteins facilitates nascent lipid droplet budding from the ER". In: *J Cell Biol 211(2): p. 261-71*.

Chu, Q., A. Rathore, J. K. Diedrich, C. J. Donaldson, 3rd J. R. Yates, and A. Saghatelian (2017). "Identification of Microprotein-Protein Interactions via APEX Tagging". In: *Biochemistry, 56: 3299-306*.

Cohen, A. W., R. Hnasko, W. Schubert, and M. P. Lisanti (2004). "Role of caveolae and caveolins in health and disease". In: *Physiol Rev 84(4): p. 1341-79*.

Cole, N. B., D. D. Murphy, T. Grider, S. Rueter, D. Brasaemle, and R. L. Nussbaum (2002). "Lipid droplet binding and oligomerization properties of the Parkinson's disease protein alpha-synuclein". In: *J Biol Chem 277(8): p. 6344-52*.

Conte M., C. Franceschi M. Sandri and S. Salvioli (2016). "Perilipin 2 and Age-Related Metabolic Diseases: A New Perspective". In: *Trends Endocrinol Metab 27(12): 893-903*.

Counihan, N.A., S.M. Rawlinson, and B.D. Lindenbach (2011). "Trafficking of hepatitis C virus core protein during virus particle assembly". In: *PLoS Pathog 7(10): p. e1002302*.

Da Poian, A.T., T. El-Bacha, and M. R.M.P. Luz (2010). "Nutrient Utilization in Humans: Metabolism Pathways". In: *Nature Education 3((9):11)*.

Daemen, S., M. A. van Zandvoort, S. H. Parekh, and M. K. Hesselink (2016). "Microscopy tools for the investigation of intracellular lipid storage and dynamics". In: *Mol Metab, 5: 153-63*.

Deng, J., V. Rudick, and L. Dory (1995). "Lysosomal degradation and sorting of apolipoprotein E in macrophages". In: *J Lipid Res 36: 2129-40*.

Diaz, E. and S.R. Pfeffer (1998). "TIP47: a cargo selection device for mannose 6-phosphate receptor trafficking". In: *Cell 93(3): p. 433-43*.

Ding, Q., M. von Schaewen, and A. Ploss (2014). "The impact of hepatitis C virus entry on viral tropism". In: *Cell Host Microbe 16(5): p. 562-568*.

Dong, H. and M. J. Czaja (2011). "Regulation of lipid droplets by autophagy". In: *Trends Endocrinol Metab, 22: 234-40*.

DuBridge, R. B., P. Tang, H. C. Hsia, P. M. Leong, J. H. Miller, and M. P. Calos (1987). "Analysis of mutation in human cells by using an Epstein-Barr virus shuttle system". In: *Mol Cell Biol 7(1): p. 379-87*.

Duelund, L., G. V. Jensen, H. K. Hannibal-Bach, C. S. Ejsing, J. S. Pedersen, K. I. Pakkanen, and J. H. Ipsen (2013). "Composition, structure and properties of POPC-triolein mixtures. Evidence of triglyceride domains in phospholipid bilayers". In: *Biochim Biophys Acta 1828(8): p. 1909-17*.

Dusheiko, G. (1997). "Side effects of alpha interferon in chronic hepatitis C". In: *Hepatology 26(3 Suppl 1): p. 112S-121S*.

Egger, D., B. Wolk, R. Gosert, L. Bianchi, H. E. Blum, D. Moradpour, and K. Bienz (2002). "Expression of hepatitis C virus proteins induces distinct membrane alterations including a candidate viral replication complex". In: *J Virol 76(12): p. 5974-84*.

Eggert, D., K. Rosch, R. Reimer, and E. Herker (2014). "Visualization and analysis of hepatitis C virus structural proteins at lipid droplets by super-resolution microscopy". In: *PLoS One 9(7): p. e102511*.

Eichmann, T. O., M. Kumari, J. T. Haas, Jr. R. V. Farese, R. Zimmermann, A. Lass, and R. Zechner (2012). "Studies on the substrate and stereo/regioselectivity of adipose triglyceride lipase, hormone-sensitive lipase, and diacylglycerol-O-acyltransferases". In: *J Biol Chem 287(49): 41446-41457*.

Fagerberg, L. et al. (2014). "Analysis of the human tissue-specific expression by genome-wide integration of transcriptomics and antibody-based proteomics". In: *Mol Cell Proteomics 13(2): p. 397-406*.

Farese R.V., Jr. and T.C. Walther (2009). "Lipid droplets finally get a little R-E-S-P-E-C-T". In: *Cell 139(5): p. 855-60*.

Farnik, H., C. M. Lange, C. Sarrazin, B. Kronenberger, S. Zeuzem, and E. Herrmann (2010). "Meta-analysis shows extended therapy improves response of patients with chronic hepatitis C virus genotype 1 infection". In: *Clin Gastroenterol Hepatol 8(10): p. 884-90*.

Feng, Y. Z., J. Lund, Y. Li, I. K. Knabenes, S. S. Bakke, E. T. Kase, Y. K. Lee, A. R. Kimmel, G. H. Thoresen, A. C. Rustan, and K. T. Dalen (2017). "Loss of perilipin 2 in cultured myotubes enhances lipolysis and redirects the metabolic energy balance from glucose oxidation towards fatty acid oxidation". In: *J Lipid Res*.

Fernandez-Sanles, A., P. Rios-Marco, C. Romero-Lopez, and A. Berzal-Herranz (2017). "Functional Information Stored in the Conserved Structural RNA Domains of Flavivirus Genomes". In: *Front Microbiol 8: p. 546*.

Fields, B.N., D.M. Knipe, and P.M. Howley (2007). "Fields' virology. 5th ed ed, ed." In: *Philadelphia: Wolters kluwer/Lippincott Williams & Wilkins*.

Friebe, P., J. Boudet, J. P. Simorre, and R. Bartenschlager (2005). "Kissing-loop interaction in the 3' end of the hepatitis C virus genome essential for RNA replication". In: *J Virol 79(1): p. 380-92*.

Fritzsching, B., B. Schwer, J. Kartenbeck, A. Pedal, V. Horejsi, and M. Ott (2002). "Release and intercellular transfer of cell surface CD81 via microparticles". In: *J Immunol 169(10): 5531-5537*.

Fujimoto, T. and R.G. Parton (2011). "Not just fat: the structure and function of the lipid droplet". In: *Cold Spring Harb Perspect Biol 3(3)*.

Fujimoto, Y., H. Itabe, J. Sakai, M. Makita, J. Noda, M. Mori, Y. Higashi, S. Kojima, and T. Takano (2004). "Identification of major proteins in the lipid droplet-enriched fraction isolated from the human hepatocyte cell line HuH7". In: *Biochim Biophys Acta 1644(1): 47-59*.

Ganley, I. G., K. Carroll, L. Bittova, and S. Pfeffer (2004). "Rab9 GTPase regulates late endosome size and requires effector interaction for its stability". In: *Mol Biol Cell 15(12): p. 5420-30*.

Gao, Q. and J. M. Goodman (2015). "The lipid droplet-a well-connected organelle". In: *Front Cell Dev Biol, 3: 49*.

Gastaminza, P., G. Cheng, S. Wieland, J. Zhong, W. Liao, and F. V. Chisari (2008). "Cellular determinants of hepatitis C virus assembly, maturation, degradation, and secretion". In: *J Virol 82(5): p. 2120-9*.

Gastaminza, P., K. A. Dryden, B. Boyd, M. R. Wood, M. Law, M. Yeager, and F. V. Chisari (2010). "Ultrastructural and biophysical characterization of hepatitis C virus particles produced in cell culture". In: *J Virol 84(21): p. 10999-1009*.

Gautam P., A. Recino R. D. Foale J. Zhao S. U. Gan M. Wallberg R. Calne and A. M. Lever (2016). "Promoter optimisation of lentiviral vectors for efficient insulin gene expression in canine mesenchymal stromal cells: potential surrogate beta cells". In: *J Gene Med, 18: 312-21*.

Gentzsch, J., C. Brohm, E. Steinmann, M. Friesland, N. Menzel, G. Vieyres, P. M. Perin, A. Frentzen, L. Kaderali, and T. Pietschmann (2013). "Hepatitis c Virus p7 is critical for capsid assembly and envelopment". In: *PLoS Pathog 9(5): p. e1003355*.

Germi, R., J. M. Crance, D. Garin, J. Guimet, H. Lortat-Jacob, R. W. Ruigrok, J. P. Zarski, and E. Drouet (2012). "Cellular glycosaminoglycans and low density lipoprotein receptor are involved in hepatitis C virus adsorption". In: *J Virol 86(13): p. 7256-67*.

Gong, J., Z. Sun, L. Wu, W. Xu, N. Schieber, D. Xu, G. Shui, H. Yang, R. G. Parton, and P. Li (2011). "Fsp27 promotes lipid droplet growth by lipid exchange and transfer at lipid droplet contact sites". In: *J Cell Biol 195(6): p. 953-63*.

Gower, E., C. Estes, S. Blach, K. Razavi-Shearer, and H. Razavi (2014). "Global epidemiology and genotype distribution of the hepatitis C virus infection". In: *J Hepatol 61(1 Suppl): p. S45-57*.

Greenberg, A. S., R. A. Coleman, F. B. Kraemer, J. L. McManaman, M. S. Obin, V. Puri, Q. W. Yan, H. Miyoshi, and D. G. Mashek (2011). "The role of lipid droplets in metabolic disease in rodents and humans". In: *J Clin Invest 121(6): p. 2102-10*.

Gregan, Juraj, Christian G. Riedel, Mark Petronczki, Lubos Cipak, Cornelia Rumpf, Ina Poser, Frank Buchholz, Karl Mechtler, and Kim Nasmyth (2007). "Tandem affinity purification of functional TAP-tagged proteins from human cells". In: *Nature protocols, 2: 1145-51*.

Guedj, J., H. Dahari, L. Rong, N. D. Sansone, R. E. Nettles, S. J. Cotler, T. J. Layden, S. L. Uprichard, and A. S. Perelson (2013). "Modeling shows that the NS5A inhibitor daclatasvir has two modes of action and yields a shorter estimate of the hepatitis C virus half-life". In: *Proc Natl Acad Sci U S A 110(10): p. 3991-6*.

Guevin, C., A. Lamarre, and P. Labonte (2009). "Novel HCV replication mouse model using human hepatocellular carcinoma xenografts." In: *Antiviral Res 84(1): 14-22*.

Harris, C., E. Herker, Jr. R. V. Farese, and M. Ott (2011). "Hepatitis C virus core protein decreases lipid droplet turnover: a mechanism for core-induced steatosis". In: *J Biol Chem 286(49): 42615-42625*.

Herker, E., C. Harris, C. Hernandez, A. Carpentier, K. Kaehlcke, A. R. Rosenberg, Jr. R. V. Farese, and M. Ott (2010). "Efficient hepatitis C virus particle formation requires diacylglycerol acyltransferase-1". In: *Nat Med 16(11): p. 1295-8*.

Herker, E. and M. Ott (2011). "Unique ties between hepatitis C virus replication and intracellular lipids". In: *Trends Endocrinol Metab 22(6): p. 241-8*.

Herker, E. and M. Ott (2012). "Emerging role of lipid droplets in host/pathogen interactions". In: *J Biol Chem 287(4): p. 2280-7*.

Hickenbottom, S. J., A. R. Kimmel, C. Londos, and J. H. Hurley (2004). "Structure of a lipid droplet protein; the PAT family member TIP47". In: *Structure 12(7): p. 1199-207*.

Hoofnagle, J.H. (1997). "Hepatitis C: the clinical spectrum of disease". In: *Hepatology 26(3 Suppl 1): p. 15S-20S*.

Hueging, K., M. Doepke, G. Vieyres, D. Bankwitz, A. Frentzen, J. Doerrbecker, F. Gumz, S. Haid, B. Wolk, L. Kaderali, and T. Pietschmann (2014). "Apolipoprotein E codetermines tissue

tropism of hepatitis C virus and is crucial for viral cell-to-cell transmission by contributing to a postenvelopment step of assembly". In: *J Virol 88(3): p. 1433-46*.

Hung, V., N. D. Udeshi, S. S. Lam, K. H. Loh, K. J. Cox, K. Pedram, S. A. Carr, and A. Y. Ting (2016). "Spatially resolved proteomic mapping in living cells with the engineered peroxidase APEX2". In: *Nat Protoc, 11: 456-75*.

Huynh, F. K., M. F. Green, T. R. Koves, and M. D. Hirschey (2014). "Measurement of fatty acid oxidation rates in animal tissues and cell lines". In: *Methods Enzymol 542: p. 391-405*.

Imai, Y., S. Boyle, G. M. Varela, E. Caron, X. Yin, R. Dhir, R. Dhir, M. J. Graham, and R. S. Ahima (2012). "Effects of perilipin 2 antisense oligonucleotide treatment on hepatic lipid metabolism and gene expression". In: *Physiol Genomics 44(22): p. 1125-31*.

Imamura, T. Inoguchi M., S. Ikuyama, S. Taniguchi, andN. Nakashima K. Kobayashi, and H. Nawata (2002). "ADRP stimulates lipid accumulation and lipid droplet formation in murine fibroblasts". In: *Am J Physiol Endocrinol.Metab 283(4): E775-E783*.

Itabe, H., T. Yamaguchi, S. Nimura, and N. Sasabe (2017). "Perilipins: a diversity of intracellular lipid droplet proteins". In: *Lipids Health Dis 16(1): p. 83*.

Ivashkina, N., B. Wolk, V. Lohmann, R. Bartenschlager, H. E. Blum, F. Penin, and D. Moradpour (2002). "The hepatitis C virus RNA-dependent RNA polymerase membrane insertion sequence is a transmembrane segment". In: *J Virol 76(24): p. 13088-93*.

Jiang, J. and G. Luo (2009). "Apolipoprotein E but not B is required for the formation of infectious hepatitis C virus particles". In: *J Virol 83(24): p. 12680-91*.

Jiang, J., W. Cun, X. Wu, Q. Shi, H. Tang, and G. Luo (2012). "Hepatitis C virus attachment mediated by apolipoprotein E binding to cell surface heparan sulfate". In: *J Virol 86(13): p. 7256-67*.

Jones, C. T., M. T. Catanese, L. M. Law, S. R. Khetani, A. J. Syder, A. Ploss, T. S. Oh, J. W. Schoggins, M. R. MacDonald, S. N. Bhatia, and C. M. Rice (2010). "Real-time imaging of hepatitis C virus infection using a fluorescent cell-based reporter system". In: *Nat Biotechnol 28(2): p. 167-71*.

Jopling, C. L., M. Yi, A. M. Lancaster, S. M. Lemon, and P. Sarnow (2005). "Modulation of hepatitis C virus RNA abundance by a liver-specific MicroRNA". In: *Science 309(5740): p. 1577-81*.

Kao, C.C., G. Yi, and H.C. Huang (2016). "The core of hepatitis C virus pathogenesis". In: *Curr Opin Virol 17: p. 66-73*.

Kato, T., T. Date, A. Murayama, K. Morikawa, D. Akazawa, and T. Wakita (2006). "Cell culture and infection system for hepatitis C virus". In: *Nat Protoc 1(5): p. 2334-9*.

Kaushik, S. and A.M. Cuervo (2015). "Degradation of lipid droplet-associated proteins by chaperone-mediated autophagy facilitates lipolysis". In: *Nat Cell Biol 17(6): p. 759-70*.

Kaushik, S. and A. M. Cuervo (2016). "AMPK-dependent phosphorylation of lipid droplet protein PLIN2 triggers its degradation by CMA". In: *Autophagy 12(2): 432-438*.

Keum, S. J., S. M. Park, J. H. Park, J. H. Jung, E. J. Shin, and S. K. Jang (2012). "The specific infectivity of hepatitis C virus changes through its life cycle". In: *Virology 433(2): 462-470*.

Kimmel, A. R., D. L. Brasaemle, M. McAndrews-Hill, C. Sztalryd, and C. Londos (2010). "Adoption of PERILIPIN as a unifying nomenclature for the mammalian PAT-family of intracellular lipid storage droplet proteins". In: *J Lipid Res 51(3): p. 468-71*.

King, N.J., E.J. Delikatny, and K.T. Holmes (1994). "1H magnetic resonance spectroscopy of primary human and murine cells of the myeloid lineage". In: *Immunomethods 4(2): p. 188-98*.

Kohli, A., R. Kapoor, Z. Sims, A. Nelson, S. Sidharthan, B. Lam, R. Silk, C. Kotb, C. Gross, G. Teferi, K. Sugarman, P. S. Pang, A. Osinusi, M. A. Polis, V. Rustgi, H. Masur, and S. Kottilil (2015). "Ledipasvir and sofosbuvir for hepatitis C genotype 4: a proof-of-concept, single-centre, open-label phase 2a cohort study". In: *Lancet Infect Dis 15(9): p. 1049-54*.

Kornfeld, S. (1992). "Structure and function of the mannose 6-phosphate/insulinlike growth factor II receptors". In: *Annu Rev Biochem 61: p. 307-30*.

Krahmer, N., Y. Guo, F. Wilfling, M. Hilger, S. Lingrell, K. Heger, H. W. Newman, M. Schmidt-Supprian, D. E. Vance, M. Mann, Jr. R. V. Farese, and T. C. Walther (2011). "Phosphatidylcholine synthesis for lipid droplet expansion is mediated by localized activation of CTP:phosphocholine cytidylyltransferase". In: *Cell Metab 14(4): p. 504-15*.

Kuang, W. F., Y. C. Lin, F. Jean, Y. W. Huang, C. L. Tai, D. S. Chen, P. J. Chen, and L. H. Hwang (2004). "Hepatitis C virus NS3 RNA helicase activity is modulated by the two domains of NS3 and NS4A". In: *Biochem Biophys Res Commun 317(1): p. 211-7*.

Kuramoto, K.and T. Okamura, T. Yamaguchi, T. Y. Nakamura, S. Wakabayashi, H. Morinaga, M. Nomura, T. Yanase, K. Otsu, N. Usuda, S. Matsumura, K. Inoue, T. Fushiki, Y. Kojima, T. Hashimoto, F. Sakai, F. Hirose, and T. Osumi (2012). "Perilipin 5, a lipid droplet-binding protein, protects heart from oxidative burden by sequestering fatty acid from excessive oxidation". In: *J Biol Chem 287(28): p. 23852-63*.

Laemmli, U.K. (1970). "Cleavage of structural proteins during the assembly of the head of bacteriophage T4". In: *Nature 227(5259): p. 680-685*.

Laffel, L. (1999). "Ketone bodies: a review of physiology, pathophysiology and application of monitoring to diabetes". In: *Diabetes Metab Res Rev 15(6): p. 412-26*.

Lavie, M., A. Goffard, and J. Dubuisson (2006). "HCV Glycoproteins: Assembly of a Functional E1-E2 Heterodimer, in Hepatitis C Viruses: Genomes and Molecular Biology". In: *S.L. Tan, Editor: Norfolk (UK)*.

Lee, J. Y., E. G. Acosta, I. K. Stoeck, G. Long, M. S. Hiet, B. Mueller, O. T. Fackler, S. Kallis, and R. Bartenschlager (2014). "Apolipoprotein E likely contributes to a maturation step of infectious hepatitis C virus particles and interacts with viral envelope glycoproteins". In: *J Virol 88(21): p. 12422-37*.

Lehner, R., J. Lian, and A. D. Quiroga (2012). "Lumenal lipid metabolism: implications for lipoprotein assembly". In: *Arterioscler Thromb Vasc Biol 32(5): 1087-1093*.

Li, X. D., L. Sun, R. B. Seth, G. Pineda, and Z. J. Chen (2005). "Hepatitis C virus protease NS3/4A cleaves mitochondrial antiviral signaling protein off the mitochondria to evade innate immunity". In: *Proc Natl Acad Sci U S A 102(49): p. 17717-22*.

Libby, A. E., E. Bales, D. J. Orlicky, and J. L. McManaman (2016). "Perilipin-2 Deletion Impairs Hepatic Lipid Accumulation by Interfering with Sterol Regulatory Element-binding Protein (SREBP) Activation and Altering the Hepatic Lipidome". In: *J Biol Chem 291(46): p. 24231-24246*.

Liefhebber, J. M., C. V. Hague, Q. Zhang, M. J. Wakelam, and J. McLauchlan (2014). "Modulation of triglyceride and cholesterol ester synthesis impairs assembly of infectious hepatitis C virus". In: *J Biol Chem 289(31): 21276-21288*.

Lindenbach, B. D., M. J. Evans, A. J. Syder, B. Wolk, T. L. Tellinghuisen, C. C. Liu, T. Maruyama, R. O. Hynes, D. R. Burton, J. A. McKeating, and C. M. Rice (2005). "Complete replication of hepatitis C virus in cell culture". In: *Science 309(5734): 623-626*.

Lindenbach, B.D. (2013b). "Virion assembly and release". In: *Curr Top Microbiol Immunol 369: p. 199-218*.

Lindenbach, B.D. and C.M. Rice (2013a). "The ins and outs of hepatitis C virus entry and assembly". In: *Nat Rev Microbiol 11(10): p. 688-700*.

Listenberger, L. L., A. G. Ostermeyer-Fay, E. B. Goldberg, W. J. Brown, and D. A. Brown (2007). "Adipocyte differentiation-related protein reduces the lipid droplet association of adipose triglyceride lipase and slows triacylglycerol turnover". In: *J Lipid Res 48(12): p. 2751-61*.

Lohmann, V. (2013). "Hepatitis C virus RNA replication". In: *Curr Top Microbiol Immunol 369: p. 167-98*.

Londos, C., D. L. Brasaemle, C. J. Schultz, J. P. Segrest, and A. R. Kimmel (1999). "Perilipins, ADRP, and other proteins that associate with intracellular neutral lipid droplets in animal cells". In: *Semin Cell Dev Biol 10(1): p. 51-8*.

Londos, C., C. Sztalryd, J. T. Tansey, and A. R. Kimmel (2005). "Role of PAT proteins in lipid metabolism". In: *Biochimie 87(1): p. 45-9*.

Long, A. P., A. K. Manneschmidt, B. VerBrugge, M. R. Dortch, S. C. Minkin, K. E. Prater, J. P. Biggerstaff, J. R. Dunlap, and P. Dalhaimer (2012). "Lipid droplet de novo formation and fission are linked to the cell cycle in fission yeast". In: *Traffic 13(5): p. 705-14*.

Longin, A., C. Souchier, M. Ffrench, and P. A. Bryon (1993). "Comparison of anti-fading agents used in fluorescence microscopy: image analysis and laser confocal microscopy study". In: *J Histochem Cytochem 41(12): p. 1833-40*.

Lu, X., J. Gruia-Gray, N. G. Copeland, D. J. Gilbert, N. A. Jenkins, C. Londos, and A. R. Kimmel (2001). "The murine perilipin gene: the lipid droplet-associated perilipins derive from tissue-specific, mRNA splice variants and define a gene family of ancient origin". In: *Mamm.Genome 12(9): p. 741-749*.

Majeau, N., R. Fromentin, C. Savard, M. Duval, M. J. Tremblay, and D. Leclerc (2009). "Palmitoylation of hepatitis C virus core protein is important for virion production". In: *J Biol Chem 284(49): p. 33915-25*.

Mak, K. M., C. Ren, A. Ponomarenko, Q. Cao, and C. S. Lieber (2008). "Adipose differentiation-related protein is a reliable lipid droplet marker in alcoholic fatty liver of rats". In: *Alcohol Clin Exp Res 32(4): p. 683-9*.

Manns, M.P., H. Wedemeyer, and M. Cornberg (2006). "Treating viral hepatitis C: efficacy, side effects, and complications". In: *Gut 55(9): p. 1350-9*.

Martin, D.N. and S.L. Uprichard (2013). "Identification of transferrin receptor 1 as a hepatitis C virus entry factor". In: *Proc Natl Acad Sci U S A 110(26): p. 10777-82*.

Martin, S. and R.G. Parton (2006). "Lipid droplets: a unified view of a dynamic organelle". In: *Nat Rev Mol Cell Biol 7(5): p. 373-8*.

Martinez-Vicente, M., Z. Talloczy, E. Wong, G. Tang, H. Koga, S. Kaushik, R. de Vries, E. Arias, S. Harris, D. Sulzer, and A. M. Cuervo (2010). "Cargo recognition failure is responsible for inefficient autophagy in Huntington's disease". In: *Nat Neurosci 13(5): p. 567-76*.

Mason, R. R., R. Mokhtar, M. Matzaris, A. Selathurai, G. M. Kowalski, N. Mokbel, P. J. Meikle, C. R. Bruce, and M. J. Watt (2014). "PLIN5 deletion remodels intracellular lipid composition and causes insulin resistance in muscle". In: *Mol Metab 3(6): p. 652-63*.

McIntosh, A. L., S. Senthivinayagam, K. C. Moon, S. Gupta, J. S. Lwande, C. C. Murphy, S. M. Storey, and B. P. Atshaves (2012). "Direct interaction of Plin2 with lipids on the surface of lipid droplets: a live cell FRET analysis". In: *Am J Physiol Cell Physiol 303(7): p. C728-42*.

McLauchlan, J. (2000). "Properties of the hepatitis C virus core protein: a structural protein that modulates cellular processes". In: *J Viral Hepat 7(1): p. 2-14*.

McLauchlan, J., M. K. Lemberg, G. Hope, and B. Martoglio (2002). "Intramembrane proteolysis promotes trafficking of hepatitis C virus core protein to lipid droplets". In: *EMBO Journal 21(15): p. 3980-3988*.

Meex, S. J., U. Andreo, J. D. Sparks, and E. A. Fisher (2011). "Huh-7 or HepG2 cells: which is the better model for studying human apolipoprotein-B100 assembly and secretion?" In: *J Lipid Res 52(1): p. 152-8*.

Menzel, N., W. Fischl, K. Hueging, D. Bankwitz, A. Frentzen, S. Haid, J. Gentzsch, L. Kaderali, R. Bartenschlager, and T. Pietschmann (2012). "MAP-kinase regulated cytosolic phospholipase A2 activity is essential for production of infectious hepatitis C virus particles". In: *PLoS Pathog 8(7): p. e1002829*.

Merz, A., G. Long, M. S. Hiet, B. Brugger, P. Chlanda, P. Andre, F. Wieland, J. Krijnse-Locker, and R. Bartenschlager (2011). "Biochemical and morphological properties of hepatitis C virus particles and determination of their lipidome". In: *J Biol Chem 286(4): p. 3018-32*.

Messina, J. P., I. Humphreys, A. Flaxman, A. Brown, G. S. Cooke, O. G. Pybus, and E. Barnes (2015). "Global distribution and prevalence of hepatitis C virus genotypes". In: *Hepatology 61(1): p. 77-87*.

Meyers, A., T.M. Weiskittel, and P. Dalhaimer (2017). "Lipid Droplets: Formation to Breakdown". In: *Lipids 52(6): p. 465-475*.

Micallef, J.M., J.M. Kaldor, and G.J. Dore (2006). "Spontaneous viral clearance following acute hepatitis C infection: a systematic review of longitudinal studies". In: *J Viral Hepat 13(1): p. 34-41*.

Miyanari, Y., K. Atsuzawa, N. Usuda, K. Watashi, T. Hishiki, M. Zayas, R. Bartenschlager, T. Wakita, M. Hijikata, and K. Shimotohno (2007). "The lipid droplet is an important organelle for hepatitis C virus production". In: *Nat Cell Biol 9(9): 1089-1097*.

Miyoshi, H., 2nd J. W. Perfield, S. C. Souza, W. J. Shen, H. H. Zhang, Z. S. Stancheva, F. B. Kraemer, M. S. Obin, and A. S. Greenberg (2007). "Control of adipose triglyceride lipase action by serine 517 of perilipin A globally regulates protein kinase A-stimulated lipolysis in adipocytes". In: *J Biol Chem 282(2): p. 996-1002*.

Moradpour, D. and F. Penin (2013). "Hepatitis C Virus Proteins: From Structure to Function, in Hepatitis C Virus: From Molecular Virology to Antiviral Therapy". In: *R. Bartenschlager, Editor Springer Berlin Heidelberg: Berlin, Heidelberg. p. 113-142*.

Morikawa, K., C. M. Lange, J. Gouttenoire, E. Meylan, V. Brass, F. Penin, and D. Moradpour (2011). "Nonstructural protein 3-4A: the Swiss army knife of hepatitis C virus". In: *J Viral Hepat 18(5): p. 305-15*.

Muoio, D. M., T. M. Lewin, P. Wiedmer, and R. A. Coleman (2000). "Acyl-CoAs are functionally channeled in liver: potential role of acyl-CoA synthetase." Am J Physiol Endocrinol Metab 279(6): E1366-1373". In: *Am J Physiol Endocrinol Metab 279(6): E1366-1373*.

Najt, C. P., J. S. Lwande, A. L. McIntosh, S. Senthivinayagam, S. Gupta, L. A. Kuhn, and B. P. Atshaves (2014). "Structural and functional assessment of perilipin 2 lipid binding domain(s)". In: *Biochemistry 53(45): p. 7051-66*.

Nakabayashi, H., K. Taketa, K. Miyano, T. Yamane, and J. Sato (1982). "Growth of human hepatoma cells lines with differentiated functions in chemically defined medium". In: *Cancer Res 42(9): p. 3858-63*.

Naldini, L., U. Blomer, P. Gallay, D. Ory, R. Mulligan, F. H. Gage, I. M. Verma, and D. Trono (1996). "In vivo gene delivery and stable transduction of nondividing cells by a lentiviral vector". In: *Science 272(5259): p. 263-7*.

Neufeldt, C. J., M. A. Joyce, A. Levin, R. H. Steenbergen, D. Pang, J. Shields, D. L. Tyrrell, and R. W. Wozniak (2013). "Hepatitis C virus-induced cytoplasmic organelles use the nuclear transport machinery to establish an environment conducive to virus replication". In: *PLoS Pathog 9(10): p. e1003744*.

Neumann-Haefelin, C. and R. Thimme (2013). "Adaptive immune responses in hepatitis C virus infection". In: *Curr Top Microbiol Immunol 369: p. 243-62*.

Neveu, G., R. Barouch-Bentov, A. Ziv-Av, D. Gerber, Y. Jacob, and S. Einav (2012). " Identification and Targeting of an Interaction between a Tyrosine Motif within Hepatitis C Virus Core Protein and AP2M1 Essential for Viral Assembly". In: *PLoS Pathogens 8(8): p. e1002845*.

Ohsaki, Y., J. Cheng, M. Suzuki, A. Fujita, and T. Fujimoto (2008). "Lipid droplets are arrested in the ER membrane by tight binding of lipidated apolipoprotein B-100". In: *J Cell Sci, 121: 2415-22*.

Okumura, T. (2011). "Role of lipid droplet proteins in liver steatosis". In: *J Physiol Biochem 67(4): p. 629-36*.

Palumbo, E. (2011). "Pegylated interferon and ribavirin treatment for hepatitis C virus infection". In: *Ther Adv Chronic Dis 2(1): p. 39-45*.

Ploen, D., M. L. Hafirassou, K. Himmelsbach, S. A. Schille, M. L. Biniossek, T. F. Baumert, C. Schuster, and E. Hildt (2013a). "TIP47 is associated with the hepatitis C virus and its interaction with Rab9 is required for release of viral particles". In: *Eur J Cell Biol, 92: 374-82*.

Ploen, D., M. L. Hafirassou, K. Himmelsbach, D. Sauter, M. L. Biniossek, T. S. Weiss, T. F. Baumert, C. Schuster, and E. Hildt (2013b). "TIP47 plays a crucial role in the life cycle of hepatitis C virus". In: *J Hepatol 58: 1081-8*.

Pol, A., S.P. Gross, and R.G. Parton (2014). "Review: biogenesis of the multifunctional lipid droplet: lipids, proteins, and sites". In: *J Cell Biol 204(5): p. 635-46*.

Popescu, C. I., N. Callens, D. Trinel, P. Roingeard, D. Moradpour, V. Descamps, G. Duverlie, F. Penin, L. Heliot, Y. Rouille, and J. Dubuisson (2011). "NS2 protein of hepatitis C virus interacts with structural and non-structural proteins towards virus assembly". In: *PLoS Pathog 7(2): p. e1001278*.

Quinkert, D., R. Bartenschlager, and V. Lohmann (2005). "Quantitative analysis of the hepatitis C virus replication complex". In: *J Virol 79(21): p. 13594-605*.

Quiroga, A.D. and R. Lehner (2012). "Liver triacylglycerol lipases". In: *Biochim Biophys Acta 1821(5): p. 762-9*.

R Core Team, R (2015). "A Language and Environment for Statistical Computing". In: *R Foundation for Statistical Computing, http://www.R-project.org*.

Reed LJ, M.H. (1938). "A simple method of estimating fifty per cent endpoints". In: *Am J Hyg. (27): p. 493-497*.

Ridgway, N. (2015). "Biochemistry of Lipids, Lipoproteins and Membranes". In: *6. Aufl. ed, ed. R. McLeod s.l.: Elsevier Reference Monographs*.

Romero-Brey, I., A. Merz, A. Chiramel, J. Y. Lee, P. Chlanda, U. Haselman, R. Santarella-Mellwig, A. Habermann, S. Hoppe, S. Kallis, P. Walther, C. Antony, J. Krijnse-Locker, and R. Bartenschlager (2012). "Three-dimensional architecture and biogenesis of membrane structures associated with hepatitis C virus replication". In: *PLoS Pathog 8(12): p. e1003056*.

Rosch, K., M. Kwiatkowski, S. Hofmann, A. Schobel, C. Gruttner, M. Wurlitzer, H. Schluter, and E. Herker (2016). "Quantitative Lipid Droplet Proteome Analysis Identifies Annexin A3 as a Cofactor for HCV Particle Production". In: *Cell Rep 16(12): 3219-3231*.

Roux, K. J., D. I. Kim, and B. Burke (2013). "BioID: a screen for protein-protein interactions". In: *Curr Protoc Protein Sci, 74: Unit 19 23*.

Rowe, E. R., M. L. Mimmack, A. D. Barbosa, A. Haider, I. Isaac, M. M. Ouberai, A. R. Thiam, S. Patel, V. Saudek, S. Siniossoglou, and D. B. Savage (2016). "Conserved Amphipathic Helices Mediate Lipid Droplet Targeting of Perilipins 1-3". In: *J Biol Chem 291(13): p. 6664-78*.

Russo, M.W. and M.W. Fried (2003). "Side effects of therapy for chronic hepatitis C". In: *Gastroenterology 124(6): p. 1711-9*.

Sainz B., Jr., N. Barretto, D. N. Martin, N. Hiraga, M. Imamura, S. Hussain, K. A. Marsh, X. Yu, K. Chayama, W. A. Alrefai, and S. L. Uprichard (2012). "Identification of the Niemann-Pick

C1-like 1 cholesterol absorption receptor as a new hepatitis C virus entry factor". In: *Nat Med 18(2): p. 281-5*.

Santolini, E., G. Migliaccio, and N. La Monica (1994). "Biosynthesis and biochemical properties of the hepatitis C virus core protein". In: *J Virol 68(6): p. 3631-41*.

Sapiro, J. M., M. T. Mashek, A. S. Greenberg, and D. G. Mashek (2009). "Hepatic triacylglycerol hydrolysis regulates peroxisome proliferator-activated receptor alpha activity". In: *J Lipid Res 50(8): 1621-1629*.

Sato, C., T. Saito, K. Misawa, T. Katsumi, K. Tomita, R. Ishii, H. Haga, K. Okumoto, Y. Nishise, H. Watanabe, Y. Ueno, and S. Kawata (2013). "'Impaired mitochondrial beta-oxidation in patients with chronic hepatitis C: relation with viral load and insulin resistance". In: *BMC Gastroenterol, 13: 112*.

Scheel, T.K. and C.M. Rice (2013). "Understanding the hepatitis C virus life cycle paves the way for highly effective therapies". In: *Nat Med 19(7): p. 837-49*.

Schindelin, J., I. Arganda-Carreras, E. Frise, V. Kaynig, M. Longair, T. Pietzsch, S. Preibisch, C. Rueden, S. Saalfeld, B. Schmid, J. Y. Tinevez, D. J. White, V. Hartenstein, K. Eliceiri, P. Tomancak, and A. Cardona (2012). "Fiji: an open-source platform for biological-image analysis". In: *Nat Methods 9(7): p. 676-82*.

Schweiger, M., R. Schreiber, G. Haemmerle, A. Lass, C. Fledelius, P. Jacobsen, H. Tornqvist, R. Zechner, and R. Zimmermann (2006). "Adipose triglyceride lipase and hormone-sensitive lipase are the major enzymes in adipose tissue triacylglycerol catabolism". In: *J Biol Chem 281(52): p. 40236-41*.

Schwer, B., S. Ren, T. Pietschmann, J. Kartenbeck, K. Kaehlcke, R. Bartenschlager, T. S. Yen, and M. Ott (2004). "Targeting of hepatitis C virus core protein to mitochondria through a novel C-terminal localization motif". In: *J Virol 78(15): 7958-7968*.

Seeff, L.B. (2009). "The history of the "natural history" of hepatitis C (1968-2009)". In: *Liver Int 29 Suppl 1: p. 89-99*.

Sharma, N. R., G. Mateu, M. Dreux, A. Grakoui, F. L. Cosset, and G. B. Melikyan (2011). "Hepatitis C virus is primed by CD81 protein for low pH-dependent fusion". In: *J Biol Chem 286(35): p. 30361-76*.

Shavinskaya, A., S. Boulant, F. Penin, J. McLauchlan, and R. Bartenschlager (2007). "The lipid droplet binding domain of hepatitis C virus core protein is a major determinant for efficient virus assembly". In: *J Biol Chem 282(51): p. 37158-69*.

Shi, S. T., S. J. Polyak, H. Tu, D. R. Taylor, D. R. Gretch, and M. M. Lai (2002). "Hepatitis C virus NS5A colocalizes with the core protein on lipid droplets and interacts with apolipoproteins". In: *Virology 292: 198-210*.

Singh, R., S. Kaushik, Y. Wang, Y. Xiang, I. Novak, M. Komatsu, K. Tanaka, A. M. Cuervo, and M. J. Czaja (2009). "Autophagy regulates lipid metabolism". In: *Nature 458(7242): p. 1131-5*.

Singh, R. and A.M. Cuervo (2012). "Lipophagy: Connecting Autophagy and Lipid Metabolism". In: *Int J Cell Biol: p. 12*.

Smith, D. B., J. Bukh, C. Kuiken, A. S. Muerhoff, C. M. Rice, J. T. Stapleton, and P. Simmonds (2014). "Expanded classification of hepatitis C virus into 7 genotypes and 67 subtypes: updated criteria and genotype assignment web resource". In: *Hepatology 59(1): p. 318-27*.

Smith, D. B., P. Becher, J. Bukh, E. A. Gould, G. Meyers, T. Monath, A. S. Muerhoff, A. Pletnev, R. Rico-Hesse, J. T. Stapleton, and P. Simmonds (2016). "Proposed update to the taxonomy of the genera Hepacivirus and Pegivirus within the Flaviviridae family". In: *J Gen Virol 97(11): p. 2894-2907*.

Sourisseau, M., M. L. Michta, C. Zony, B. Israelow, S. E. Hopcraft, C. M. Narbus, A. Parra Martin, and M. J. Evans (2013). "Temporal analysis of hepatitis C virus cell entry with occludin directed blocking antibodies". In: *PLoS Pathog 9(3): p. e1003244*.

Stapleton, J. T., S. Foung, A. S. Muerhoff, J. Bukh, and P. Simmonds (2011). "The GB viruses: a review and proposed classification of GBV-A, GBV-C (HGV), and GBV-D in genus Pegivirus within the family Flaviviridae". In: *J Gen Virol 92(Pt 2): p. 233-46*.

Steinmann, E., F. Penin, S. Kallis, A. H. Patel, R. Bartenschlager, and T. Pietschmann (2007). "Hepatitis C virus p7 protein is crucial for assembly and release of infectious virions". In: *PLoS Pathog 3(7): p. e103*.

Straub, B. K., P. Stoeffel, H. Heid, R. Zimbelmann, and P. Schirmacher (2008). "Differential pattern of lipid droplet-associated proteins and de novo perilipin expression in hepatocyte steatogenesis". In: *Hepatology 47(6): p. 1936-46*.

Syed, G. H., M. Khan, S. Yang, and A. Siddiqui (2017). "Hepatitis C Virus Lipoviroparticles Assemble in the Endoplasmic Reticulum (ER) and Bud off from the ER to the Golgi Compartment in COPII Vesicles". In: *J Virol 91(15)*.

Sztalryd, C., M. Bell, X. Lu, P. Mertz, S. Hickenbottom, B. H. Chang, L. Chan, A. R. Kimmel, and C. Londos (2006). "Functional compensation for adipose differentiation-related protein (ADFP) by Tip47 in an ADFP null embryonic cell line". In: *J Biol Chem, 281: 34341-8*.

Takahashi, Y., A. Shinoda, H. Kamada, M. Shimizu, J. Inoue, and R. Sato (2016). "Perilipin2 plays a positive role in adipocytes during lipolysis by escaping proteasomal degradation". In: *Sci Rep 6: p. 20975*.

Tanaka, Naoki, Kyoji Moriya, Kendo Kiyosawa, Kazuhiko Koike, Frank J. Gonzalez, and Toshifumi Aoyama (2008). "PPARα activation is essential for HCV core protein–induced hepatic steatosis and hepatocellular carcinoma in mice". In: *J Clin Invest 118: 683-94*.

Tanaka, T., N. Kato, M. J. Cho, and K. Shimotohno (1995). "A novel sequence found at the 3' terminus of hepatitis C virus genome". In: *Biochem Biophys Res Commun 215(2): p. 744-9*.

Tauchi-Sato, K., S. Ozeki, T. Houjou, R. Taguchi, and T. Fujimoto (2002). "The surface of lipid droplets is a phospholipid monolayer with a unique Fatty Acid composition". In: *J Biol Chem, 277: 44507-12*.

Team, RStudio (2015). "Integrated Development Environment for R". In: *RStudio*.

Terrault, N. A., J. L. Dodge, E. L. Murphy, J. E. Tavis, A. Kiss, T. R. Levin, R. G. Gish, M. P. Busch, A. L. Reingold, and M. J. Alter (2013). "Sexual transmission of hepatitis C virus

among monogamous heterosexual couples: the HCV partners study". In: *Hepatology 57(3): p. 881-9*.

Thiam, A.R., Jr. R.V. Farese, and T.C. Walther (2013). "The biophysics and cell biology of lipid droplets". In: *Nat Rev Mol Cell Biol 14(12): p. 775-86*.

Thomssen, R., S. Bonk, C. Propfe, K. H. Heermann, H. G. Kochel, and A. Uy (1992). "Association of hepatitis C virus in human sera with beta-lipoprotein". In: *Med Microbiol Immunol 181(5): p. 293-300*.

Tsai, T. H., E. Chen, L. Li, P. Saha, H. J. Lee, L. S. Huang, G. S. Shelness, L. Chan, and B. H. Chang (2017). "The constitutive lipid droplet protein PLIN2 regulates autophagy in liver". In: *Autophagy: p. 1-15*.

Uzbekov, R. and P. Roingeard (2013). "Nuclear lipid droplets identified by electron microscopy of serial sections". In: *BMC Res Notes 6: p. 386*.

Varela, G. M., D. A. Antwi, R. Dhir, X. Yin, N. S. Singhal, M. J. Graham, R. M. Crooke, and R. S. Ahima (2008). "Inhibition of ADRP prevents diet-induced insulin resistance". In: *Am J Physiol Gastrointest Liver Physiol 295(3): p. G621-8*.

Vermehren, J. and C. Sarrazin (2011). "New HCV therapies on the horizon". In: *Clin Microbiol Infect 17(2): p. 122-34*.

Vieyres, G., X. Thomas, V. Descamps, G. Duverlie, A. H. Patel, and J. Dubuisson (2010). "Characterization of the envelope glycoproteins associated with infectious hepatitis C virus". In: *J Virol 84(19): p. 10159-68*.

Vigna, E. and L. Naldini (2000). "Lentiviral vectors: excellent tools for experimental gene transfer and promising candidates for gene therapy". In: *J Gene Med 2(5): p. 308-16*.

Villanueva, C. J., M. Monetti, M. Shih, P. Zhou, S. M. Watkins, S. Bhanot, and Jr. R. V. Farese (2009). "Specific role for acyl CoA:Diacylglycerol acyltransferase 1 (Dgat1) in hepatic steatosis due to exogenous fatty acids". In: *Hepatology*.

Vogt, D. A., G. Camus, E. Herker, B. R. Webster, C. L. Tsou, W. C. Greene, T. S. Yen, and M. Ott (2013). "Lipid droplet-binding protein TIP47 regulates hepatitis C Virus RNA replication through interaction with the viral NS5A protein". In: *PLoS Pathog 9(4): p. e1003302*.

Voisset, C. and J. Dubuisson (2004). "Functional hepatitis C virus envelope glycoproteins". In: *Biol Cell 96(6): p. 413-20*.

Walther, T.C., J. Chung, and Jr. R.V. Farese (2017). "Lipid Droplet Biogenesis". In: *Annu Rev Cell Dev Biol, 2017*.

Wanders, R. J., P. Vreken, S. Ferdinandusse, G. A. Jansen, H. R. Waterham, C. W. van Roermund, and E. G. Van Grunsven (2001). "Peroxisomal fatty acid alpha- and beta-oxidation in humans: enzymology, peroxisomal metabolite transporters and peroxisomal diseases". In: *Biochem Soc Trans 29(Pt 2): p. 250-67*.

Wang, H., D. Gilham, and R. Lehner (2007). "Proteomic and lipid characterization of apolipoprotein B-free luminal lipid droplets from mouse liver microsomes: implications for very low density lipoprotein assembly". In: *J Biol Chem 282(45): p. 33218-26*.

Wang, H., M. Bell, U. Sreenivasan, H. Hu, J. Liu, K. Dalen, C. Londos, T. Yamaguchi, M. A. Rizzo, R. Coleman, D. Gong, D. Brasaemle, and C. Sztalryd (2011). "Unique regulation of adipose triglyceride lipase (ATGL) by perilipin 5, a lipid droplet-associated protein". In: *J Biol Chem 286(18): p. 15707-15*.

Wang, H. et al. (2016). "Seipin is required for converting nascent to mature lipid droplets". In: *eLife 5: p. e16582*.

Weber, K., U. Bartsch, C. Stocking, and B. Fehse (2008). "A multicolor panel of novel lentiviral "gene ontology" (LeGO) vectors for functional gene analysis". In: *Mol Ther 16(4): 698-706*.

Webster, B., M. Ott, and W.C. Greene (2013). "Evasion of superinfection exclusion and elimination of primary viral RNA by an adapted strain of hepatitis C virus". In: *J Virol 87(24): p. 13354-69*.

Welte, M.A. (2015). "Expanding roles for lipid droplets". In: *Curr Biol 25(11): p. R470-81*.

WHO (2017). "WHO Guidelines on Hepatitis B and C Testing". In: *2017: Geneva*.

Wilfling, F., A. R. Thiam, M. J. Olarte, J. Wang, R. Beck, T. J. Gould, E. S. Allgeyer, F. Pincet, J. Bewersdorf, Jr. R. V. Farese, and T. C. Walther (2014a). "Arf1/COPI machinery acts directly on lipid droplets and enables their connection to the ER for protein targeting". In: *eLife 3: p. e01607*.

Wilfling, F., J. T. Haas, T. C. Walther, and Jr. R. V. Farese (2014b). "Lipid droplet biogenesis". In: *Curr Opin Cell Biol 29: p. 39-45*.

Wissing, S., M. Montano, J. L. Garcia-Perez, J. V. Moran, and W. C. Greene (2011). "Endogenous APOBEC3B restricts LINE-1 retrotransposition in transformed cells and human embryonic stem cells". In: *J Biol Chem 286(42): p. 36427-37*.

Wolins, N. E., J. R. Skinner, M. J. Schoenfish, A. Tzekov, K. G. Bensch, and P. E. Bickel (2003). "Adipocyte protein S3-12 coats nascent lipid droplets". In: *J Biol Chem 278(39): p. 37713-21*.

Wolins, N. E., B. K. Quaynor, J. R. Skinner, M. J. Schoenfish, A. Tzekov, and P. E. Bickel (2005). "S3-12, Adipophilin, and TIP47 package lipid in adipocytes". In: *J Biol Chem 280(19): p. 19146-55*.

Wolins, N. E., B. K. Quaynor, J. R. Skinner, A. Tzekov, M. A. Croce, M. C. Gropler, V. Varma, A. Yao-Borengasser, N. Rasouli, P. A. Kern, B. N. Finck, and P. E. Bickel (2006). "OXPAT/PAT-1 is a PPAR-induced lipid droplet protein that promotes fatty acid utilization". In: *Diabetes 55(12): p. 3418-3428*.

Wolins, N.E., B. Rubin, and D.L. Brasaemle (2001). "TIP47 associates with lipid droplets". In: *J Biol Chem 276(7): p. 5101-8*.

Wozniak, A. L., S. Griffin, D. Rowlands, M. Harris, M. Yi, S. M. Lemon, and S. A. Weinman (2010). "Intracellular proton conductance of the hepatitis C virus p7 protein and its contribution to infectious virus production". In: *PLoS Pathog 6(9): p. e1001087*.

Wu, J. W., S. P. Wang, F. Alvarez, S. Casavant, N. Gauthier, L. Abed, K. G. Soni, G. Yang, and G. A. Mitchell (2011). "Deficiency of liver adipose triglyceride lipase in mice causes progressive hepatic steatosis". In: *Hepatology 54(1): p. 122-32*.
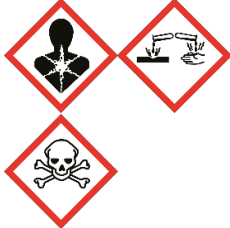
Xu, G., C. Sztalryd, X. Lu, J. T. Tansey, J. Gan, H. Dorward, A. R. Kimmel, and C. Londos (2005). "Post-translational regulation of adipose differentiation-related protein by the ubiquitin/proteasome pathway". In: *J Biol Chem 280(52): p. 42841-7*.

Yamaguchi, T., S. Matsushita, K. Motojima, F. Hirose, and T. Osumi (2006). "MLDP, a novel PAT family protein localized to lipid droplets and enriched in the heart, is regulated by peroxisome proliferator-activated receptor alpha". In: *J Biol Chem 281(20): p. 14232-40*.

Yan, S., X. F. Yang, H. L. Liu, N. Fu, Y. Ouyang, and K. Qing (2015). "Long-chain acyl-CoA synthetase in fatty acid metabolism involved in liver and other diseases: an update". In: *World J Gastroenterol 21(12): p. 3492-8*.

Ye, S. Q., C. A. Reardon, and G. S. Getz (1993). "Inhibition of apolipoprotein E degradation in a post-Golgi compartment by a cysteine protease inhibitor". In: *J Biol Chem, 268: 8497-502*.

Zechner R., F. Madeo and D. Kratky (2017). "Cytosolic lipolysis and lipophagy: two sides of the same coin". In: *Nat Rev Mol Cell Biol 18(11): 671-684*.

Zierler, K.A., R. Zechner, and G. Haemmerle (2014). "Comparative gene identification-58/alpha/beta hydrolase domain 5: more than just an adipose triglyceride lipase activator?" In: *Curr Opin Lipidol 25(2): p. 102-9*.
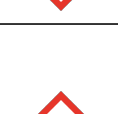
A. Appendix A
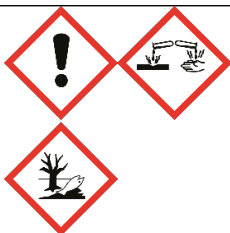
A.1. Chemicals

Chemical	GHS hazard pictogram	GHS hazard statements	GHS precautionar statements
1,4-Dithiothreitol (DTT)		H302-H315-H319	P302+P350-P305+P351+P338
2-Propanol		H225-H319-H336	P210-P233-P305+P351+P338
Acetic acid		H314	P301+P330+P331-P303+P361+P353-P305+P351+P338-P313
Acrylamide solution (30%) - Mix 37.5		H301-H312+H332-H315-H317-H319-H340-H350-H361f-H372	P201-P280-P302+P352-P305+P351+P338
AgNO$_3$ (Silver nitrate)		H272-H314-H410	P273-P280-P301+P330+P331-P305+P351+P338
Ammonium acetate		H303, H316, H320, H333	P281, P335
Ammonium chloride		H302, H319	P305+351+338
Ampicillin		H317-H334	P261-P280-P342+P311

APS (Ammonium persulfate)		H272-H302-H315-H317-H319-H334-H335	P220-P261-P280-P305 + P351 + P338-P342 + P311
Blasticidin S		H300	P264 P301 + P310
$CaCl_2$ (Calciumchloride)		H319	P264-P280-P305+P351+P338-P337+P313
Chloroform		H302-H315-H319-H331-H351-H361d-H372	P281-P302+P352-P304+P340-P305+P351+P338-P308-P310
Chloroquine diphosphate		H302	
Crystal violet		H351 H302 H318 H410	P273 P280 P305 + P351 + P338 P501
DAPCO		H228-H302-H315-H319-H412	P273-P280-P305 + P351 + P338-P332 + P313
DNase I Buffer (10x)		H316	P332 + P313
DNase Inactivation Reagent		H315-H335-H318	P280 P305 + P351 + P338
Dodecyl sulfate sodium salt		H228 H302 + H332 H315 H318 H335 H412	P210 P261 P273 P305 + P351 + P338
EDTA		H319-H332-H373	P260-P261-P271-P304+P340-P305+P351+P338-P312

EtBr (Ethidiumbromide)		H302-H330-H341	P281-P302+P352-P304+P340-P305+P351+P338-P309-P310
Ethanol		H225	P210
Formaldehyde		H301+H311+H331-H314-H317-H335-H341-H350	P301+P330+P331-P302+P352-P305+P351+P338-P309-P310
G413		H317 H334 H316	P285 P304 + P341 P305 + P351 + P338 P332 + P313 P261 P280
Hoechst		H302-H315-H319	P280-P305+P351+P338-P313
Hydrochloric acid (HCl)		H290-H314-H335	P280-P301+P330+P331-P305+P351+P338
KOH (Potassium hydroxide)		H290-H302-H314	P280-P301+P330+P331-P305+P351+P338
Methanol (MeOH)		H225-H301+H311+H331-H370	P210-P233-P280-P302+P352-P309-P310-P501
Na_2CO_3 (Sodium carbonate)		H319	P260-P305+P351+P338
Nonidet-P40		H302-H318-H411	P280-P301+P312-P305+P351+P338

Palmitate		H319	P305+351+338
Paraformaldehyde (PFA)		H228-H302-H315-H317-H319-H335-H351	P281-P302+P352-P304+P340-P305+P351+P338-P308+P313
Passive Lysis Buffer 5x		H360	P201-P202-P280-P308+P313-P405-P501
Perchlorid acid		H271-H290-H302-H314-H373	P210-P280-P303 + P361 + P353-P304 + P340 + P310-P305 + P351 + P338-P371 + P380 + P375
Phenol-Chloroform-Isoamyl alcohol (25:24:1 vol/vol/vol)		H301+H311+H331-H314-H341-H351-H361d-H372	P280b-P301+P330+P331-P305+P351+P338-P309+P311
Phenylmethylsulfonyl fluoride (PMSF)		H301-H314	P280-P305+P351+P338-P310
Polybrene (Hexadimethrinbromid)		H302	
Potassium hydroxide		H290 H302 H314	P280 P305 + P351 + P338 P313
Proteinase K		H334	P304 + P340 P342 + P311 P284
RNAse Away		H315 H319	P280 P332 + P313 P305 + P351 + P338 P362 P264 P337 + P313

Scintillation cocktail		H226-H302-H304-H318-H411	P210-P280-P301 + P310-P305 + P351 + P338 + P310-P331-P370 + P378
Sodium deoxycholate		H302	P261
Sodium dodecyl sulfate (SDS)		H228-H302+H332-H315-H318-H335-H412	P210-P280-P302+P352-P304+P341-P305+P351+P338
Sodium hydroxide		H290-H314	P280-P301+P330+P331-P305+P351+P338
Sodium hypochlorite		EUH031-H315-H319	P264-P280-P302+P352-P305+P351+P338-P321-P501
TEMED (Tetram-ethylethylenediamine)		H225-H302+H332-H314	P210-P233-P280-P301+P330+P331-P305+P351+P338
TRI Reagent		H301+ H311+ H331-H314-H341-H373-H411	P201-P261-P280-P301 + P310 + P330-P303 + P361 + P353-P305 + P351 + P338
Tris ultrapure (Tris-base)		H315-H319	P302+P352-P305+P351+P338
Triton X-100		H302-H318-H411	P273-P280-P305+P351+P338-P310

Trypan blue solution 0,4%		H350	P201-P308+P313
ß-Mercaptoethanol		H301+H331-H310-H315-H317-H318-H373-H410	P273-P280-P302+P352-P304+P341-P305+P351+P338

A.2. Definition Chemicals

	Acute Toxic	Identifies chemicals with the following hazards: Irritant, skin sensitizer, acute toxicity (harmful), narcotic effects, respiratory tract infection, hazardous ozone layer
	Severe Toxic	Identifies chemicals with the following hazards: Acute toxicity (fatal or toxic)
	Health Hazard	Identifies chemicals with the following hazards: Carcinogen, mutagenicity, reproductive toxicity, respiratory sensitizer, target organ toxicity, aspiration toxicity.
	Environmental Hazard	Identifies chemicals with the following hazards: Aquatic toxicity.
	Corrosive	Identifies chemicals with the following hazards: Skin corrosion, eye damage, corrosive metals.
	Flame	Flammables, pyrophorics, self-heating, emits flammable gas, self-reactives, organic peroxides
	Oxidizing	Identifies chemicals with the following hazards: Oxidizers

A.3. GHS hazard statements

H Codes	H Phrases
H200	Unstable explosives.
H201	Explosive; mass explosion hazard.
H202	Explosive, severe projection hazard.
H203	Explosive; fire, blast or projection hazard.
H204	Fire or projection hazard.
H205	May mass explode in fire.
H220	Extremely flammable gas.
H221	Flammable gas.
H222	Extremely flammable aerosol.
H223	Flammable aerosol.
H224	Extremely flammable liquid and vapour.
H225	Highly flammable liquid and vapour.
H226	Flammable liquid and vapour.
H228	Flammable solid.
H229	Pressurised container: May burst if heated.
H230	May react explosively even in the absence of air.
H231	May react explosively even in the absence of air at elevated pressure and/or temperature.
H240	Heating may cause an explosion.
H241	Heating may cause a fire or explosion.
H242	Heating may cause a fire.
H250	Catches fire spontaneously if exposed to air.
H251	Self-heating: may catch fire.
H252	Self-heating in large quantities; may catch fire.
H260	In contact with water releases flammable gases which may ignite spontaneously.
H261	In contact with water releases flammable gases.
H270	May cause or intensify fire; oxidizer.
H271	May cause fire or explosion; strong oxidizer.
H272	May intensify fire; oxidizer.
H280	Contains gas under pressure; may explode if heated.
H281	Contains refrigerated gas; may cause cryogenic burns or injury.
H290	May be corrosive to metals.
H300	Fatal if swallowed.
H301	Toxic if swallowed.
H302	Harmful if swallowed.
H304	May be fatal if swallowed and enters airways.
H310	Fatal in contact with skin.
H311	Toxic in contact with skin.
H312	Harmful in contact with skin.

H314	Causes severe skin burns and eye damage.
H315	Causes skin irritation.
H317	May cause an allergic skin reaction.
H318	Causes serious eye damage. (not needed beside H314)
H319	Causes serious eye irritation.
H330	Fatal if inhaled.
H331	Toxic if inhaled.
H332	Harmful if inhaled.
H334	May cause allergy or asthma symptoms or breathing difficulties if inhaled.
H335	May cause respiratory irritation.
H336	May cause drowsiness or dizziness.
H340	May cause genetic defects <state route of exposure if it is conclusively proven that no other routes of exposure cause the hazard>.
H341	Suspected of causing genetic defects <state route of exposure if it is conclusively proven that no other routes of exposure cause the hazard>.
H350	May cause cancer <state route of exposure if it is conclusively proven that no other routes of exposure cause the hazard>.
H351	Suspected of causing cancer <state route of exposure if it is conclusively proven that no other routes of exposure cause the hazard>.
H360	May damage fertility or the unborn child <state specific effect if known > <state route of exposure if it is conclusively proven that no other routes of exposure cause the hazard>.
H361	Suspected of damaging fertility or the unborn child <state specific effect if known> <state route of exposure if it is conclusively proven that no other routes of exposure cause the hazard>.
H362	May cause harm to breast-fed children.
H370	Causes damage to organs <or state all organs affected, if known> <state route of exposure if it is conclusively proven that no other routes of exposure cause the hazard>.
H371	May cause damage to organs <or state all organs affected, if known> <state route of exposure if it is conclusively proven that no other routes of exposure cause the hazard>.
H372	Causes damage to organs <or state all organs affected, if known> through prolonged or repeated exposure <state route of exposure if it is conclusively proven that no other routes of exposure cause the hazard>.
H373	May cause damage to organs <or state all organs affected, if known> through prolonged or repeated exposure <state route of exposure if it is conclusively proven that no other routes of exposure cause the hazard>.

H300 + H310	Fatal if swallowed or in contact with skin.
H300 + H330	Fatal if swallowed or if inhaled.
H310 + H330	Fatal in contact with skin or if inhaled.
H300 + H310 + H330	Fatal if swallowed, in contact with skin or if inhaled.
H301 + H311	Toxic if swallowed or in contact with skin.
H301 + H331	Toxic if swallowed or if inhaled.
H311 + H331	Toxic in contact with skin or if inhaled.
H301 + H311 + H331	Toxic if swallowed, in contact with skin or if inhaled.
H302 + H312	Harmful if swallowed or in contact with skin.
H302 + H332	Harmful if swallowed or if inhaled.
H312 + H332	Harmful in contact with skin or if inhaled.
H302 + H312 + H332	Harmful if swallowed, in contact with skin or if inhaled.
H400	Very toxic to aquatic life.
H410	Very toxic to aquatic life with long lasting effects
H411	Toxic to aquatic life with long lasting effects.
H412	Harmful to aquatic life with long lasting effects.
H413	May cause long lasting harmful effects to aquatic life.
H420	Harms public health and the environment by destroying ozone in the upper atmosphere.

A.4. EUH Codes

EUH Code	EUH Phrases
EUH001	Explosive when dry
EUH014	Reacts violently with water.
EUH018	In use may form flammable/explosive vapour-air mixture.
EUH019	May form explosive peroxides.
EUH029	Contact with water liberates toxic gas.
EUH031	Contact with acids liberates toxic gas.
EUH032	Contact with acids liberates very toxic gas.
EUH044	Risk of explosion if heated under confinement.
EUH066	Repeated exposure may cause skin dryness or cracking.
EUH070	Toxic by eye contact
EUH071	Corrosive to the respiratory tract.
EUH201	Contains lead. Should not be used on surfaces liable to be chewed or sucked by children.
EUH201A	Warning! Contains lead.
EUH202	Cyanoacrylate. Danger. Bonds skin and eyes in seconds. Keep out of the reach of children.
EUH203	Contains chromium (VI). May produce an allergic reaction.
EUH204	Contains isocyanates. May produce an allergic reaction.

EUH205	Contains epoxy constituents. May produce an allergic reaction.
EUH206	Warning! Do not use together with other products. May release dangerous gases (chlorine).
EUH207	Warning! Contains cadmium. Dangerous fumes are formed during use. See information supplied by the manufacturer. Comply with the safety instructions.
EUH208	Contains (name of sensitising substance). May produce an allergic reaction. (EUH08 may be omitted if EUH204 or EUH205 has to be applied.)
EUH209	Can become highly flammable in use.
EUH209A	Can become flammable in use.
EUH210	Safety data sheet available on request
EUH401	To avoid risks to human health and the environment, comply with the instructions for use.

A.5. The EU-GHS precautionary statements

P Codes	P Phrases
P101	If medical advice is needed, have product container or label at hand.
P102	Keep out of reach of children.
P103	Read label before use.
P201	Obtain special instructions before use.
P202	Do not handle until all safety precautions have been read and understood.
P210	Keep away from heat, hot surfaces, sparks, open flames and other ignition sources. No smoking.
P211	Do not spray on an open flame or other ignition source.
P220	Keep away from clothing and other combustible materials.
P222	Do not allow contact with air.
P223	Do not allow contact with water.
P230	Keep wetted with c
P231	Handle and store contents under inert gas/ . . .
P232	Protect from moisture.
P233	Keep container tightly closed.
P234	Keep only in original packaging.
P235	Keep cool.
P240	Ground and bond container and receiving equipment.
P241	Use explosion-proof [electrical/ventilating/lighting/. . .] equipment.
P242	Use non-sparking tools.
P243	Take action to prevent static discharges.
P244	Keep valves and fittings free from oil and grease.

P250	Do not subject to grinding/shock/friction/...
P251	Do not pierce or burn, aven after use.
P260	Do not breathe dust/fume/gas/mist/vapours/spray.
P261	Avoid breathing dust/fume/gas/mist/vapours/spray.
P262	Do not get in eyes, on skin, or on clothing.
P263	Avoid contact during pregnancy and while nursing.
P264	Wash ... thoroughly after handling.
P270	Do no eat, drink or smoke when using this product.
P271	Use only outdoors or in a well-ventilated area.
P272	Contaminated work clothing should not be allowed out of the workplace.
P273	Avoid release to the environment.
P280	Wear protective gloves/protective clothing/eye protection/face protection.
P282	Wear cold insulating gloves and either face shield or eye protection.
P283	Wear fire resistant or flame retardant clothing.
P284	[In case of inadequate ventilation] wear respiratory protection.
P231+P232	Handle and store contents under inert gas/... Protect from moisture.
P301	IF SWALLOWED:
P302	IF ON SKIN:
P303	IF ON SKIN (or hair):
P304	IF INHALED:
P305	IF IN EYES:
P306	IF ON CLOTHING:
P308	IF exposed or concerned:
P310	Immediately call a POISON CENTER/doctor/...
P311	Call a POISON CENTER/doctor/....
P312	Call a POISON CENTER/doctor/... if you feel unwell.
P313	Get medical advice/attention.
P314	Get medical advice/attention if you feel unwell.
P315	Get immediate medical advice/attention.
P320	Specific treatment is urgent (see ... on this label).
P321	Specific treatment (see ... on this label).
P330	Rinse mouth.
P331	Do NOT induce vomiting.
P332	If skin irritation occurs:
P333	If skin irritation or rash occurs:
P334	Immerse in cool water [or wrap in wet bandages].
P335	Brush off loose particles from skin.
P336	Thaw frosted parts with lukewarm water. Do no rub affected area.
P337	If eye irritation persists:

P338	Remove contact lenses, if present and easy to do. Continue rinsing.
P340	Remove person to fresh air and keep comfortable for breathing.
P342	If experiencing respiratory symptoms:
P351	Rinse cautiously with water for several minutes.
P352	Wash with plenty of water/…
P353	Rinse skin with water [or shower].
P360	Rinse immediately contaminated clothing and skin with plenty of water before removing clothes.
P361	Take off immediately all contaminated clothing.
P362	Take off contaminated clothing.
P363	Wash contaminated clothing before reuse.
P364	And wash it before reuse.
P370	In case of fire:
P371	In case of major fire and large quantities:
P372	Explosion risk.
P373	DO NOT fight fire when fire reaches explosives.
P375	Fight fire remotely due to the risk of explosion.
P376	Stop leak if safe to do so.
P377	Leaking gas fire: Do not extinguish, unless leak can be stopped safely.
P378	Use … to extinguish.
P380	Evacuate area.
P381	In case of leakage, eliminate all ignition sources.
P390	Absorb spillage to prevent material damage.
P391	Collect spillage.
P301+P310	IF SWALLOWED: Immediately call a POISON CENTER/doctor/….
P301+P312	IF SWALLOWED: Call a POISON CENTER/doctor/… if you feel unwell.
P301+P330+P331	IF SWALLOWED: Rinse mouth. Do NOT induce vomiting.
P302+P334	IF ON SKIN: Immerse in cool water [or wrap in wet bandages].
P302+P335+P334	IF ON SKIN: Brush off loose particles from skin. Immerse in cool water [or wrap in wet bandages].
P302+P352	IF ON SKIN: Wash with plenty of water/…
P303+P361+P353	IF ON SKIN (or hair): Take off immediately all contaminated clothing. Rinse skin with water [or shower].
P304+P340	IF INHALED: Remove person to fresh air and keep comfortable for breathing.
P305+P351+P338	IF IN EYES: Rinse cautiously with water for several minutes. Remove contact lenses, if present and easy to do. Continue rinsing.

P306+P360	IF ON CLOTHING: rinse immediately contaminated clothing and skin with plenty of water before removing clothes.
P308+P311	IF exposed or concerned: Call a POISON CENTER/doctor/...
P308+P313	IF exposed or concerned: Get medical advice/attention.
P332+P313	If skin irritation occurs: Get medical advice/attention.
P333+P313	If skin irritation or rash occurs: Get medical advice/attention.
P336+P315	Thaw frosted parts with lukewarm water. Do not rub affected area. Get immediate medical advice/attention.
P337+P313	If eye irritation persists: Get medical advice/attention.
P342+P311	If experiencing respiratory symptoms: Call a POISON CENTER/doctor/...
P361+P364	Take off immediately all contaminated clothing and wash it before reuse.
P362+P364	Take off contaminated clothing and wash it before reuse.
P370+P376	In case of fire: Stop leak if safe to do so.
P370+P378	In case of fire: Use ... to extinguish.
P370+P372+P380+ P373	In case of fire: Explosion risk. Evacuate area. DO NOT fight fire when fire reaches explosives.
P370+P380+P375	In case of fire: Evacuate area. Fight fire remotely due to the risk of explosion.
P370+P380+P375 [+P378]	In case of fire: Evacuate area. Fight fire remotely due to the risk of explosion. [Use ... to extinguish].
371+P380+P375	In case of major fire and large quantities: Evacuate area. Fight fire remotely due to the risk of explosion.
P401	Store in accordance with...
P402	Store in a dry place.
P403	Store in a well–ventilated place.
P404	Store in a closed container.
P405	Store locked up.
P406	Store in a corrosion resistant/... container with a resistant inner liner.
P407	Maintain air gap between stacks or pallets.
P410	Protect from sunlight.
P411	Store at temperatures not exceeding ... °C/... °F.
P412	Do not expose to temperatures exceeding 50°C/ 122°F.
P413	Store bulk masses greater than ... kg/... lbs at temperatures not exceeding ... °C/... °F.
P420	Store separately.
P402+P404	Store in a dry place. Store in a closed container.
P403+P233	Store in a well—ventilated place. Keep container tightly closed.
P403+P235	Store in a well–ventilated place. Keep cool.
P410+P403	Protect from sunlight. Store in a well-ventilated place.

P410+P412   Protect from sunlight. Do not expose to temperatures
                   exceeding 50°C/ 122°F.
P501   Dispose of contents/container to . . .
P502   Refer to manufacturer or supplier for information on
                   recovery or recycling.

List of Figures

List of Tables